University of Alberta

FLOCCULATION MIXING BY MEANS OF VERTICALLY OSCILLATING GRIDS

BY

L. EDWIN LIEM ©

A thesis submitted to the Faculty of Graduate Studies and Research in partial fulfillment of the requirements for the degree of Doctor of Philosophy

in

ENVIRONMENTAL ENGINEERING

DEPARTMENT OF CIVIL AND ENVIRONMENTAL ENGINEERING

EDMONTON, ALBERTA

Fall, 1998

National Library of Canada

Acquisitions and Bibliographic Services

395 Wellington Street
Ottawa ON K1A 0N4
Canada

Bibliothèque nationale du Canada

Acquisitions et services bibliographiques

395, rue Wellington
Ottawa ON K1A 0N4
Canada

Your file Votre référence

Our file Notre référence

The author has granted a non-exclusive licence allowing the National Library of Canada to reproduce, loan, distribute or sell copies of this thesis in microform, paper or electronic formats.

L'auteur a accordé une licence non exclusive permettant à la Bibliothèque nationale du Canada de reproduire, prêter, distribuer ou vendre des copies de cette thèse sous la forme de microfiche/film, de reproduction sur papier ou sur format électronique.

The author retains ownership of the copyright in this thesis. Neither the thesis nor substantial extracts from it may be printed or otherwise reproduced without the author's permission.

L'auteur conserve la propriété du droit d'auteur qui protège cette thèse. Ni la thèse ni des extraits substantiels de celle-ci ne doivent être imprimés ou autrement reproduits sans son autorisation.

0-612-34802-4

Canada

University of Alberta

Library Release Form

Name of Author: L. Edwin Liem

Title of Thesis: Flocculation Mixing by means of Vertically Oscillating Grids

Degree: Doctor of Philosophy

Year of this Degree Granted: 1998

Permission is hereby granted to the University of Alberta Library to reproduce single copies of this thesis and to lend or sell such copies for private, scholarly, or scientific research purposes only.

The author reserves all other publication and other rights in association with the copyright in the thesis, and except as hereinbefore provided, neither the thesis nor any substantial portion thereof may be printed or otherwise reproduced in any material from whatever without the author's prior written permission.

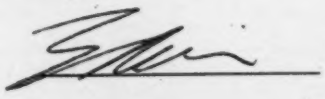

4242 49 St. Vegreville. AB
T9C - 1B5

Date: Aug 31, 1998

University of Alberta

Faculty of Graduate Studies and Research

The undersigned certify that they have read, and recommended to the Faculty of Graduate Studies and Research for acceptance, a thesis entitled **Flocculation Mixing by Means of Vertically Oscillating Grids** submitted by **L. Edwin Liem** in partial fulfilment of the requirement for the degree of Doctor of Philosophy in Environmental Engineering.

Dr. D. W. Smith

Dr. S. J. Stanley

Dr. I. Buchanan

Dr. K. Nandakumar

Dr. J. McCorquodale

Date: 31 August 98

ABSTRACT

A newly designed grid mixing has been used to produce flocculation mixing within a standard 2 L jar. Different solidity ratio and number of grids have been tried at different vertical grid speed. It has been found that the average root means square turbulent velocity q' is uniform both at the horizontal and vertical points of measurement; a condition that cannot be achieved in the case of impeller mixing. Constant macro length scales have also been found that basically verifies the data analysis. Due to the mixing uniformity, the average volume velocity gradient $\overline{G}$ may be applied as the surrogate mixing intensity parameter.

Particle removal study has also been completed at different flocculation time and mixing intensity, as well as different solidity ratio and number of grids. Kaolin has been used as the turbid particle, while alum is used as the chemical coagulant. The grid mixing provides an excellent particle removal, represented by the settled water turbidity. At the optimum mixing arrangement (triple high solidity ratio types of grids), a very stable flocculation performance in terms of low settled water turbidity at a wide range of $\overline{G}$ (20 to 76 s^{-1}) has been monitored. High agglomeration rate coefficient k_1 and low erosion rate coefficient k_2 have also been achieved.

It has also been found that the mixing intensity and flocculation performance can directly be controlled by the grid vertical speed, number of grids, and grid solidity ratio which is very important from a practical point of view.

In general, the grid mixing has shown an advantage over traditional impellers. A more uniform mixing environment and a more stable flocculation performance can be expected.

ACKNOWLEDGMENT

A great appreciation will be addressed to Dr. D. W Smith as supervisor and Dr. S. J. Stanley as co - supervisor. A great deal of help and guidance has been given throughout the research work. Research funding from the Natural Science and Engineering Research Council as well as Aqualta is also greatly appreciated.

Mr. N. Chernuka of the Department of Civil and Environmental Engineering maintained the equipment. Dr. I. D. Buchanan of the Department of Civil and Environmental Engineering, Dr. K. Nandakumar of the Department of Chemical and Materials Engineering, and Dr. J. A. McCorquedale of the University of New Orleans served as committee members.

Last but not least, a special thank you will be addressed to fellow students and technicians who have helped for completion of this research work.

TABLE OF CONTENTS

1.0 INTRODUCTION **01**

1.1 BACKGROUND 01

1.2 COAGULATION AND FLOCCULATION 06

1.2.1 Colloid Stability and Destabilization 07

1.2.2 Particle Transport Mechanism 12

1.3 MIXING REQUIREMENT 20

1.4 COAGULATION AND FLOCCULATION PERFORMANCE 22

1.5 SCALE UP EFFECT 24

1.6 SCOPE OF STUDY 25

1.7 THESIS LAYOUT 29

1.8 REFERENCES 30

2.0 TURBULENT PARAMETER STUDY **51**

2.1 INTRODUCTION 51

2.2 METHODS AND MATERIAL 54

2.3 EXPERIMENT RESULT AND ANALYSIS 55

2.4 VOLUME AVERAGE TURBULENT PARAMETERS 61

2.5 DISCUSSION 66

2.6 CONCLUSIONS 69

2.7 REFERENCES 70

3.0 PARTICLE REMOVAL STUDY **94**

3.1 INTRODUCTION..... 94

3.2 METHODS AND MATERIAL..... 97

3.3 TURBIDITY ANALYSIS..... 100

3.4 PARTICLE ANALYSIS..... 104

3.5 FLOC AGGREGATION AND EROSION COEFFICIENTS..... 106

3.6 CONCLUSIONS..... 112

3.7 REFERENCES..... 114

4.0 COMPARATIVE STUDY..... 133

4.1 INTRODUCTION..... 133

4.2 METHODS AND MATERIAL..... 136

4.3 RESULTS AND ANALYSIS..... 139

4.3.1 Turbulent Parameter Results and Analysis..... 139

4.3.2 Particle Reduction Results and Analysis..... 146

4.3.3 Standard Impeller Results and Analysis..... 153

4.4 CONCLUSIONS..... 154

4.7 REFERENCES..... 155

5.0 GENERAL DISCUSSION AND CONCLUSIONS..... 185

5.1 INTRODUCTION..... 185

5.2 HIGHLIGHTS OF STUDY..... 187

5.2.1 Turbulent Mixing Parameters..... 187

5.2.2 Particle Removal Study..... 189

5.2.3 General Relationships among Parameters..... 190

5.3 LIMITATIONS AND SUGGESTIONS..... 191

5.4 GENERAL CONCLUSIONS..... 195

5.5 REFERENCES..... 196

6.0 APPENDICES..... 200

LIST OF TABLES

Table 1.1a: Impeller Rapid Mixing Requirement..... 39

Table 1.1b: Impeller Slow Mixing Requirement..... 40

Table 1.1c: Temperature Correction Factor for $\overline{G}$ 41

Table 1.2: Selected Contaminant Limits..... 42

Table 2.1: Grid Characteristics and m (q'/GS)..... 74

Table 3.1: Grid Physical Characteristics..... 118

Table 3.2: Chemical Setup..... 119

Table 3.3: Range of $\overline{G}$ and $\overline{G}$ * Values..... 120

Table 4.1: m vs. d/M..... 159

Table 4.2: Range for $\overline{G}$ Values and $\overline{G}$ *..... 160

Table 4.3: Generalizing Factors..... 161

Table 4.4: Coefficient of Variation for Average Values..... 162

Table 4.5a: R^2 Values k_1 163

Table 4.5b: k_1 and k_2 vs. $\overline{G}$ 164

Table 5.1: Generalizing Factors..... 200

LIST OF FIGURES

Figure 1.1: Particle Sizes..... 43

Figure 1.2: Conventional Treatment Process Components..... 44

Figure 1.3: Reaction Schematics among Particles, $Al(OH)_q^{r+}$, and $Al(OH)_3$..... 45

Figure 1.4: Alum Coagulation Diagram..... 46

Figure 1.5a: Turbidity vs. Coagulant Dose..... 47

Figure 1.5b: Coagulant Dose vs. Particle Concentration..... 47

Figure 1.6a: Double Layer Compression..... 48

Figure 1.6b: Energies on Particles 48

Figure 1.7: Impeller Mixing Devices..... 49

Figure 1.8: Overall Grid Mixing Study..... 50

Figure 2.1a: Vertically Oscillating Grid Mixing Device..... 75

Figure 2.1b: Vertically Oscillating Grid Mixing Device..... 76

Figure 2.2: Vertical Levels of Measurement..... 77

Figure 2.3: Horizontal Points of Measurement..... 78

Figure 2.4: LDA System..... 79

Figure 2.5: Autocorrelation Correction..... 80

Figure 2.6: Isotropicity vs. Horizontal Points for Grid No. 9 at y = 0 mm..... 81

Figure 2.7: Average rms Turbulent Velocity vs. Horizontal Points for Grid No. 9 at y = 0 mm..... 82

Figure 2.8: Average rms Turbulent Velocity vs. Vertical Grid Speed..... 83

Figure 2.9: Slope vs. Solidity Ratio..... 84

Figure 2.10: Vertical Velocities vs. Vertical Grid Speed for Grid No. 9..... 85

Figure 2.11: Velocity Gradient vs. Vertical Grid Speed..... 86

Figure 2.12: Velocity Gradient vs. Reynolds Number..... 87

Figure 2.13: Macro Length Scale vs. Velocity Gradient..... 88

Figure 2.14: Dimensionless Length Scale vs. Solidity Ratio..... 89

Figure 2.15: Kolmogoroff Microscale vs. Vertical Grid Speed.....90

Figure 2.16: Range vs. Grid Types y = 0 mm..... 91

Figure 2.17: Coefficient of Variation vs. Grid Types y = 0 mm..... 92

Figure 2.18: Kolmogoroff Microscale vs. Velocity Gradient..... 93

Figure 3.1: Velocity Gradient vs. Vertical Grid Speed..... 121

Figure 3.2: Relative Turbidity vs. Flocculation Time for Grid No. 9..... 122

Figure 3.3: Relative Turbidity vs. Velocity Gradient for Grid No. 9..... 123

Figure 3.4: Optimum Velocity Gradient vs. Flocculation Time..... 124

Figure 3.5: Minimum Relative Turbidity vs. Flocculation Time..... 125

Figure 3.6: Minimum Relative Turbidity vs. Velocity Gradient * Flocculation Time..... 126

Figure 3.7: % Particle Count vs. Unflocculated Kaolin..... 127

Figure 3.8: Turbidity vs. Unflocculated Kaolin..... 128

Figure 3.9: Agglomeration Rate vs. Velocity Gradient..... 129

Figure 3.10: Erosion Rate vs. Velocity Gradient..... 130

Figure 3.11: k_2/k_1 vs. Velocity Gradient..... 131

Figure 3.12: Kolmogoroff Microscale vs. Velocity Gradient..... 132

Figure 4.1a: Vertical Levels of Sampling Points..... 165

Figure 4.1b: Horizontal Points of Measurement..... 166

Figure 4.2: Average rms Turbulent Velocity vs. Horizontal Points for Grid No. 9, n = 3..... 167

Figure 4.3a: Range Values..... 168

Figure 4.3b: Coefficient of Variation Values..... 169

Figure 4.4: Slope vs. Solidity Ratio..... 170

Figure 4.5: Velocity Gradient vs. Vertical Grid Speed..... 171

Figure 4.6: Velocity Gradient vs. Reynolds Number for Grid No. 9..... 172

Figure 4.7: Macro Length Scale vs. Vertical Grid Speed..... 173

Figure 4.8: Kolmogoroff Microscale vs. Vertical Grid Speed..... 174

Figure 4.9a: Relative Turbidity vs. Velocity Gradient for Grid No. 9..... 175

Figure 4.9b: Relative Turbidity vs. Flocculation Time for Grid No. 9..... 176

Figure 4.10: Optimum Velocity Gradient vs. Flocculation Time..... 177

Figure 4.11: Minimum Relative Turbidity vs. Optimum Velocity Gradient * Flocculation Time..... 178

Figure 4.12: Minimum Relative Turbidity vs. Flocculation Time..... 179

Figure 4.13a: Agglomeration Rate vs. Velocity Gradient..... 180

Figure 4.13b: Erosion Rate vs. Velocity Gradient..... 181

Figure 4.14: Relative Turbidity vs. Velocity Gradient (Flocculation Time = 20 min) 182

Figure 4.15a: Agglomeration Rate vs. Velocity Gradient..... 183

Figure 4.15b: Erosion Rate vs. Velocity Gradient..... 184

Figure 5.1: Oscillating Grid Mixing in a Continuous System..... 198

Figure 5.2: Generalizing Factors..... 199

NOMENCLATURE

$\overline{G}$	= average volume velocity gradient (s^{-1})
$\frac{dN}{dt}$	= rate of disappearance of the initial particle (min^{-1})
$\overline{U_R^2}$	= relative mean velocity between grid and fluid (mm/s)
$\overline{\varepsilon}$	= volume average energy dissipation rate (mm^2/s^3)
$\overline{G}$ *	= optimum $\overline{G}$ with respect to T/To* (s^{-1})
$\overline{G}$ *t_F	= $\overline{G}$ * multiplied by t_F
$\overline{q'}$	= average rms turbulent velocity
$\overline{U}$, $\overline{V}$, and $\overline{W}$	= mean velocities in x, y , and z directions (mm/s)
ρ	= fluid density (g/mm^3)
°C	= degree of Celsius
ν	= fluid kinematic viscosity (mm^2/s)
η	= Kolmogoroff microscale
A	= coefficient in the order of unity or constant for cosine series
α	= porosity
a	= power coefficient for d/M
Al	= aluminum
$Al(OH)_q^{r+}$	= aluminum hydrolysis

$Al_2(SO_4)_3$ 14 H_2O = alum

AO	= aesthetic objective
A_s	= grid solid area (mm^2)
b, b_1, and b_2	= power coefficients for $\overline{G}$
C	= coefficient for λ
Ca	= calcium
C_D	= grid drag coefficient
COV	= coefficient of variation
D	= particle diameter for each channel (μm)
d	= rod diameter (mm)
D(1,0)	= arithmetic mean particle diameter (μm)
d/M	= solidity ratio
DBP	= disinfection by product
d_i and d_j	= diameters for particles i and j
D_{ij}	= diffusion coefficient for perikinetic flocculation
d_{max}	= maximum particle diameter
ΔT	= time interval
ε	= energy dissipation rate (mm^2/s)
f	= frequency (s^{-1})
$f(Re_d)$	= function of Re_d
F_D	= drag force (g mm/s^2)
Fe	= iron

$Fe_2(SO_4)_3$	= ferric sulfate
g	= gram or gravity acceleration
γ	= water specific gravity
η	= Kolmogoroff microscale (mm)
H_2O	= water
HCl	= hydrochlorous acid
Hz	= hertz
IMAC	= interim maximum aceptable concentration
k_1 and k_2	= agglomeration and erosion rate coefficients (min^{-1})
K_s	= energy spectrum related coefficient
λ	= pressure loss coefficient
L	= liter or average macro length scale (mm)
LDA	= laser doppler anemometer
M	= mesh = center to center distance between two rods (mm)
m	= linear equation coefficient or number of vessels in series
M	= mesh = center to center distance between two rods (mm)
MAC	= maximum acceptable concentration
meq	= milliequivalent
Mg	= magnesium
mg	= milligram
MHz	= megahertz
min	= minute
mL	= milliliter

μm	= micrometer
mm	= millimeter
ν	= fluid kinematic viscosity (mm^2/s)
N	= impeller speed (rpm)
ν	= kinematic water viscosity
n	= number of grids
N	= number of particle
N/No	= relative particle removal
Na	= sodium
$NaHCO_3$	= sodium bicarbonate
NaOH	= sodium hydroxide
N_i and N_j	= concentration of particles i and j
N_i^I and N_i^E	= concentration of primary particles in the influent and effluent
N_o	= initial number of particles
N_s and N_l	= small scale and large scale impeller speed
NTU	= nephelemoetric turbidity unit
pH	= - log $[H^+]$
q'	= average rms turbulent velocity (mm/s)
r	= radial distance (mm)
$R(\tau)$	= time auto correlation function
R^2	= coefficient of determination
Re_d	= Reynolds number based on rod diameter

rms	= root mean square
rpm	= rotation per minute
S	= scaling factor
s	= second
Σ	= sum
SD	= standard deviation
Si	= silicon
t	= time (s or min)
τ	= time interval (s)
T	= turbidity (NTU)
T/T_o	= relative turbidity
T/T_o*	= minimum relative turbidity with at a given t_F
T/T_o**	= minimum relative turbidity with at a given v_{GS}
t_D	= detention time (min)
t_F	= flocculation time (min)
THM	= trihalomethane
TiO_2	= titanium oxide
T_o	= initial turbidity reading (NTU)
t_R	= rapid mixing time (min)
U and V	= instantaneous velocity in y and x directions (mm/s)
u, v, and w	= turbulent velocities in x, y, and z directions (mm/s)
u', v', and w'	= rms turbulent velocities for x, y, and z directions (mm/s)
V	= fluid volume (mm^3)

v	= velocity gradient (s^{-1})
v_{GS}	= vertical grid speed (mm/s)
x, y, and z	= first horizontal, vertical, and second horizontal distances (mm)
$X_p(OH)_q^{r+}$	= metal hydroxide
Ψ_R	= repulsive force

1. INTRODUCTION

1.1 BACKGROUND

The production of potable drinking water is the main goal of water treatment processes. As stated by Cotruvo and Vogt (1990), the term "potable" is defined as a condition where the water can be consumed in any desired amount without giving any adverse health effects to the consumer. Water must also be free from aesthetic concerns, such as excessive colour, taste, odour, and turbidity. Removal of small particles and dissolved materials causing impurity in water is therefore required in water treatment processes.

A major source of impurity in drinking water are particles smaller than 10 μm. with the majority smaller than 1.5 μm (Hudson 1965). These impurities can be classed as colloids and dissolved solids. Colloids are small particles that cannot be removed by standard filtration and sedimentation processes. While, dissolved solids are actually true solution in water which consist of various ions (Tchobanoglous and Schroeder 1985). Figure 1.1 shows particle characteristics with respect to their sizes and types of filters (Stumm 1977).

The presence of colloids and dissolved solids in water is very important in relation to the health and aesthetic concerns. Colloids can easily be found in water in the forms of microorganisms, inorganics, and organics. Protozoans such as Giardia lamblia and Crypotsporidium parvum, and enteric viruses have been identified to be

the main causes of numerous waterborne diseases in North America in recent years. Giardiasis followed by hepatitis A were the main identified types of waterborne sickness reported in the United States for the two year period of 1989 to 1990 (Herwaldt et al. 1992). Similar cases were reported for the following period of 1991 to 1992 with increasing reports of cryptosporidiosis (Moore et al. 1994). While, between 1993 and 1994, cryptosporidiosis outbreaks were very dominant (Kramer et al. 1996). These protozoan cysts are more difficult to be inactivated using ordinary disinfection processes (White 1992).

Clays and silts are the most common types of inorganic colloids found in water. These inorganics can cause aesthetic concerns such as turbidity and colour problems. In general, inorganic colloids do not cause direct harmful effects on human health. However, they can exert some health effects by adsorption, transport, and release of other colloids and toxic substances (O'Melia 1978). High levels of turbidity in water can protect microorganisms from disinfectants. Some types of turbidity causing materials can add nutrients for the growth of microorganisms (Health Canada 1996).

Some humic substances are colloidal sized organic molecules and can be found in all surface waters and many groundwaters. Humic substances may cause colour, taste, and odour. However, the most important concern is the possible reaction between humic substances and chemicals used to disinfect the water which may produce disinfection by - products (DBPs). Trihalomethanes (THMs) were the one of the first group of halogenated DBPs identified in finished drinking water (Bellar et al.

1974). These compounds were suspected to be carcinogenic to human. Other types of halogenated DBPs such as haloacetic acids were even reported to be more toxic than any of the trihalomethanes (Lykins et al. 1994). This situation becomes worse when an excessive amount of disinfectant is applied in order to inactivate newly recognized and more formidable types of microorganisms.

It is evident that the production of potable drinking water more efficiently and at a high quality requires a broader knowledge. A comprehensive health risk assessment for microbial and chemical contamination is necessary in order to improve the current health risk reduction effort (Sobsey et al. 1993). Putnam and Graham (1993) stated that any efforts to reduce a target risk in the water supply might introduce, either intentionally or unintentionally, a different risk to the population the so - called competing risk. One method of minimizing the risk is by reducing the amount of colloids in the treated water through conventional treatment processes. This will reduce not only the direct risk due to the microorganisms and other harmful particles but also the risk of possible chemical by - product formations.

Figure 1.2 shows a conventional treatment process train used in many public water treatment plants. As can be seen, one alternative to remove colloids from water is through the coagulation and flocculation process. In general, there are two process mechanisms involved, the chemical reactions due to the addition of chemical coagulants and particle transport generated by the mixing device. Colloids having the same surface charge are destabilized using chemical coagulants to allow them to interact. Subsequently, the colloids are brought together through mixing process

creating larger flocs. The agglomerated flocs can then be removed using separation processes such as sedimentation and filtration. In most cases, these treatment processes provide an excellent performance in a reasonable cost.

The coagulation and flocculation process gains a more important attention due to tighter regulations for drinking water. The surface water treatment rule (SWTR) gives credits to the conventional treatment process (coagulation / flocculation and rapid sand filtration) of 2.5 and 2.0 log reductions for giardia and viruses with the remaining reductions obtained from disinfection process, i.e. 0.5 and 2.0 log reductions (Bryant et al. 1992). The proposed disinfection / disinfection by - products rule also includes the enhanced coagulation process to reduce the amount of DBP precusors (measured by total organic carbon TOC) from water (Krasner and Amy 1995).

The coagulation and flocculation process optimization study is then necessary to achieve its best possible performance. The overall process performance can be observed by the treatment plant monitoring system. However, detailed investigations have traditionally been conducted through bench scale studies. Since first being performed by Langelier in 1921 (Hyde and Ludwig 1944), jar tests have been applied by many investigators using various water vessels and stirrers. Currently, 2L square jars and flat blade impellers as described by Hudson and Wagner (1981) are used in standard jar test procedures. From jar tests, it is possible to conduct detailed investigations for a specific process component while eliminating any variations for other components. General relations among the parameters of interest can be obtained

by applying different process treatment conditions from which an optimum condition can be identified.

Particle transport in one main process mechanism that requires a more detailed study. Clark et al. (1994) put a great deal of work to investigate overall full scale flocculation mixing performances involving several types of impellers. While, Stanley (1995) and Stanley and Smith (1995) emphasized the detailed mixing and scale - up characteristics of flocculation mixing in bench and pilot scales. In general, there have been concerns related to the use of average volume mixing parameters as the controlling parameter in the coagulation and flocculation process. This is mainly caused by the fact that ordinary impellers do not produce uniform flow within the water vessel. Variations in mixing intensities and forces acting on flocs have been monitored especially when considering the scale-up effect. These finally govern the size and characteristic of the agglomerated flocs. Creating more uniform mixing environment within the water vessel is then desirable. This may be achieved by applying a newly designed mixing device that provides the optimum mixing environment for floc aggregation. This is in accordance with the previous recommendation mentioned by Clark et al. (1994) and Stanley (1995) to conduct a detailed study of fluid flow patterns induced by different flocculator impellers.

In this study, a new design of grid mixing is employed to generate a uniform mixing environment within the vessel. A detailed flocculation mixing study can then be focused on the mixing characteristics created by the mixing device. Variations in mixing intensity can be observed along with their effects to the overall particle

removal performance. An optimum condition for the overall coagulation and flocculation process can then be identified.

1.2 COAGULATION AND FLOCCULATION

There have been many definitions given to the terms coagulation and flocculation. From the chemical engineering perspective, coagulation is defined as processes that reduce the total potential energy of interaction between the electrical double layers of two particles, while flocculation is aggregation processes of colloidal particles into floc networks by the formation of inter - particle bridges (La Mer 1964). More detailed definitions for these two terms with respect to environmental engineering practices are mentioned by Hudson and Wolfner (1967). Coagulation is defined as the processes of chemical addition and reaction of a coagulant and or polymer in water. Rapid but intense mixing is required to distribute the coagulant agent uniformly throughout the water to assure it makes contact with particles. Flocculation is defined as the process that groups and compacts coagulated particles into larger flocs. In this case, slow but prolonged mixing is necessary. In other words, the term coagulation includes the chemical process of particle destabilization, while flocculation applies only to the transport aspect of the overall process of coagulation (Amirtharajah and Tambo 1991). From now on, these definitions will be assumed in this study.

1.2.1 Colloid Stability and Destabilization

Coagulation and flocculation are processes to agglomerate small particles so that they can be removed using separation processes. However, natural particulates usually carry the same (negative) charge (Niehof and Loeb 1972). This basically prevents the direct agglomeration process of the particles. Amirtharajah and O'Melia (1990) explained the origins of colloidal stability as the electrostatic and steric stabilizations.

The electrostatic stabilization occurs when surface groups on the colloids react with water and exchange ions or they react in water with solutes other than ions. In these two cases, surface charge depends on the concentration of ionized atoms or molecules and pH. The electrostatic stabilization can also arise from imperfections within the particle structure. This is commonly found in the case of some clay minerals where Al(III) ions are exchanged for Si(II) ions or other divalent cations (such as Mg(II) and Fe(II)) during the formation of the lattice structure. A negative charge will be formed from these processes. While, a positive surface charge may be formed in different conditions.

The steric stabilization can result from the adsorption of polymers at particulate - water interfaces. Adsorbed polymers can either stabilize or destabilize the particulate surface charge. This depends on the amount of polymer added, its affinity to the solid and water, and many other factors. Polymers that cause charge stabilization have a high affinity to solid and have hydrophilic groups that are left unattached in water. As mentioned by Gregory (1978), two polymer - coated particulates interacting at a close

distance can cause a repulsion as the volume available for the adsorbed molecules is reduced that restricts the movement of the polymers. The repulsion can also result from the increased concentration of strongly hydrophilic polymer segments in the overlapping region.

In order to make the particle aggregation possible, it is therefore necessary to destabilize the particles using certain types of coagulants or coagulant aids. These chemicals enhance the aggregation and attachment tendency. Alum ($Al_2(SO_4)_3$ 14 H_2O) and ferric salts ($Fe_2(SO_4)_3$ and $FeCl_3$) are the most common types of inorganic coagulants applied in water treatment practices (AWWA, 1990). They form polynuclear hydrolysis products $X_a(OH)_b^{c+}$ (where X is the metal ion Al or Fe) which are readily adsorbed at particulate - water interfaces (Stumm 1977). Recalling the definition above, this step is known as the coagulation process. As explained by Amirtharajah and Tambo (1991), there are two main mechanisms of the particle destabilization process using inorganic salts.

The first mechanism is the charge neutralization due to the adsorption of hydrolysis species (Al(III) and Fe(III)) carrying a positive charge on the colloid surfaces. These following chemical reactions show how some variations of Al hydrolysis may be formed (Amirtharajah and Mills 1982):

$$Al_2(SO_4)_3 14\ H_2O \ <==>\ Al(H_2O)_6^{3+} + 3\ SO_4^{2-} + 2\ H_2O$$

$$Al(H_2O)_6^{3+} + H_2O \ <==>\ Al(H_2O)_5(OH)^{2+} + H_3O^+$$

$$Al(H_2O)_5(OH)^{2+} + H_2O \ <==>\ Al(H_2O)_4(OH)_2^+ + H_3O^+$$

$$Al(H_2O)_4(OH)_2^+ + H_2O <==> Al(H_2O)_3(OH)_3 \text{ (solid)} + H_3O^+ \quad 1.1)$$

For the sake of simplicity, H_2O ligands attached to the Al ions can be omitted and $Al(H_2O)_5(OH)^{2+}$ can be written as $Al(OH)^{2+}$ for example. Reactions for the hydrolysis products with a positive charge occur very fast within microseconds, while formation of the hydroxide precipitate ($Al(OH)_3$) is relatively slow (1 to 7 seconds). In general, the ability of a coagulant to destabilize colloids is a combination of many reactions: colloid - solvent, coagulant - solvent, and coagulant - colloid. This mainly depends on the characteristics of the coagulant such as the surface active or non - surface active type of coagulant. In the case of the hydrolysis of an aluminum ion coagulant, the charge neutralization usually occurs from chemical reactions between coagulant and colloids (Amirtharajah and O'Melia 1990).

The second mechanism is the enmeshment or sweep flocculation in which the colloids interact with the hydroxide precipitates such as $Al(OH)_3$ (see the chemical reactions above). This can be achieved when treated water is supersaturated by three to four orders of magnitude; a condition where the hydroxide is quickly formed. In this case, the chemical condition for rapid hydroxide precipitation followed by colloid flocculation is more important than the transport interaction between the hydrolysis product and the colloid during destabilization process (Amirtharajah and Tambo 1991).

Figure 1.3 shows the reaction schematic for both charge neutralization and sweep flocculation mechanisms. Amirtharajah and Mills (1982) showed relations

between pH of mixed solution and alum concentration. Figure 1.4 shows areas for charge neutralization and sweep flocculation mechanisms. As shown in this figure, the optimum charge neutralization and sweep flocculation occur at pH of about 5 and 7, at alum concentrations of about 3 and 30 mg/L, respectively. A relation between the coagulant dose and residual turbidity was also obtained. Stumm and O'Melia (1968) explained this relation by separating the coagulant dose versus residual turbidity diagram into four zones (see Figure 1.5a). Zone 1 is the area when insufficient dose of coagulant is applied resulting in no destabilization. In zone 2, the coagulant is increased causing particle destabilization. However, increasing the coagulant dose which means covering the particle surface with an excessive amount of coagulant will restabilize the particles (zone 3). Finally, in zone 4, a sufficient degree of supersaturation occurs for the precipitation of metal hydroxides. In each case there are four possibilities depending on the colloid concentration. Figure 1.5b depicts the relation between the coagulant dosage and particle concentration. These two diagrams were developed for alum and ferric salt coagulants at a constant pH value.

Amirtharajah and O'Melia (1990) mentioned two more destabilization mechanisms. The double layer compression mechanism can be explained using Figure 1.6a. The figure shows how a negatively charged colloid has a layer of negative ions on its surface. Ions with the opposite (positive) charge accumulate in the interfacial region. These two opposite charge ions form an electrical double layer surrounding the particle. The net negative charge potential on the particle surface is termed as the nernst potential. While, the zeta potential is an electrical potential associated with the

shear force required to move the particle together with its rigid layer relative to the balanced charge of the surrounding fluid. The stern layer is the rigid layer attached to the particle with a potential equal to the difference of nernst and zeta potentials. The mathematical treatment of the double layer is known as the Gouy - Chapman model. Diffuse layers of two similar colloids will interact when the particles approach each other. This results a repulsive force (ψ_R) between them which increases as the distance between two particles decreases. On the other hand, an attractive force exists when two particles approach each other. This is termed as the van der Waals force which decreases with increasing distance between two particles. This becomes the attractive potential energy (ψ_A) whose summation with the repulsive energy (ψ_R) yields the net interaction energy between two colloids. A high concentration of electrolyte in solution, such as high ionic strength or high total dissolved solids, produces high concentrations of counter ions in the diffuse layer. The volume of the diffused layer decreases and so does the effective thickness of the layer. The range of the repulsive energy (ψ_R) between two colloids decreases and the attractive van der Waals (ψ_A) becomes dominant. Furthermore, the electrostatic stabilization can be reduced or even eliminated. This kind of colloid destabilization can be achieved using Al^{3+}, Ca^{2+}, and Na^{+} as the chemical coagulants (Amirtharajah and O'Melia 1990). Figure 1.6b shows schematic presentations of the diffuse double layer, layer potential, and two cases of particle interactions.

The last destabilization mechanism is the interparticle bridging. This mechanism occurs when segments of a polymer chain absorb on more than one

particle linking them together. As mentioned by Gregory (1978), when a polymer molecule comes in contact with colloids, some parts of the molecules might extend into the solution. This portion will attach to other colloids with some vacant adsorption sites on their surfaces. The effective mechanism occurs when the polymer extends far enough from the first colloid attaching to other colloids. However when an excess of polymer is added and adsorbed on the colloid surfaces, the particles can be restabilized by surface saturation. This is called as the steric stabilization as has been explained above.

1.2.2 Particle Transport Mechanism

There are three known particle transport mechanisms. Perikenetic flocculation is a transport mechanism of small colloidal particles. This mechanism is caused by Brownian diffusion, i. e. a random motion of particles due to the movement of the surrounding fluid molecules which is caused by the thermal energy of the fluid.

Orthokinetic flocculation is a transport mechanism for larger particles which is caused by fluid shear or velocity gradient in either laminar or turbulent fluid flow conditions. Velocity gradient can be represented as the change of velocity with distance ($\frac{du}{dz}$) in the case of laminar flow. In the case of turbulent flow, velocity gradient is represented by the average volume velocity gradient $\overline{G}$:

$$\overline{G} = \left(\frac{\varepsilon}{\nu}\right)^{1/2} \qquad 1.2)$$

where ε is the energy dissipation rate and ν is the water kinematic viscosity. The energy dissipation rate can be calculated based on:

$$\varepsilon = A\frac{u'^3}{L} \qquad 1.3)$$

where A is an empirical coefficient in the order of unity, u' is the root mean square (rms) turbulent velocity in the main velocity direction, and L is the macro length scale which is proportional to the size of mixing device. This dimensional relationship as described by Tennekes and Lumley (1972) is one method of developing this equation. The rms turbulent velocity can be calculated as:

$$U = \overline{U} + u \qquad 1.4)$$

$$\overline{U} = \frac{1}{\Delta T}\int_0^{\Delta T} U\,dt \qquad 1.5)$$

$$u' = \sqrt{\frac{1}{\Delta T}\int_0^{\Delta T}(U - \overline{U})^2 dt} \qquad 1.6)$$

where U, $\overline{U}$, and u are the instantaneous, mean, and turbulent velocities, respectively. While t and ΔT are the time and time measurement interval. Orthokinetic flocculation is sometimes called the physical flocculation as the velocity gradient is established by physical agitation.

The last transport mechanism is the differential settling. This type of mechanism is caused by gravity with the settling velocity of the particle becomes the controlling parameter (TeKippe and Ham 1971 and Amirtharajah and O'Melia 1990).

Perikinetic and orthokinetic transport mechanisms can be described using these two following equations originally derived by Smoluchowski (Camp and Stein 1943; TeKippe and Ham 1971; and Amirtharajah and O'Melia 1990) as:

$$\frac{dN_{ii}}{dt} \sim \frac{(d_i+d_j)^2}{d_i d_j} N_i N_j D_{ij} \qquad \text{for perikinetic} \qquad 1.7)$$

$$\frac{dN_{ii}}{dt} \sim (d_i+d_j)^3 N_i N_j \frac{du}{dz} \qquad \text{for orthokinetic} \qquad 1.8)$$

where $\frac{dN_{ij}}{dt}$ is the contact rate between particles i and j; d_i and d_j are diameters for particles i and j; N_i and N_j are number concentration of particles i and j; and D_{ij} is the diffusion coefficient for perikinetic flocculation (a function of temperature).

In the case of orthokinetic flocculation, the physical agitation produces turbulent shear that not only helps particles to collide but also creates forces that may cause the agglomerated flocs to break apart. The models have been developed in two regimes, known as the inertial (when particles > Kolmogoroff microscale η) and viscous (when particles < η) turbulent regimes. By definition, Kolmogoroff microscale is the smallest sustainable eddy that can be expressed as:

$$\eta = (\frac{\nu^3}{\varepsilon})^{1/4} \qquad 1.9)$$

In the inertial turbulent regime, eddies created by turbulent mixing produce turbulent shear and forces on particles. However, in the viscous turbulent regime, eddies tend to entrain particles providing only laminar shear with little surface stress.

Spielman (1978) used the Saffman and Turner (1956) theory assuming the collision rate to occur by a turbulent flow and colloidal spheres with diameters of d_i and d_j:

$$\frac{dN_{ij}}{dt} \sim (d_i+d_j)^3 N_i N_j \overline{G} \qquad 1.10)$$

This model has commonly been used for flocculation study due to the use of simple mixing parameter $\overline{G}$. However, this equation was originally developed based on the viscous turbulent regime. Delichatsios and Probstein (1975) developed a model for the inertial turbulent regime:

$$\frac{dN_{ij}}{dt} \sim (d_i+d_j)^3 N_i N_j \varepsilon^{1/3} \qquad 1.11)$$

The above equation was criticized by Cleasby (1986) who suggested the use of $\varepsilon^{2/3}$ factor instead of $\varepsilon^{1/3}$. This argument was made based on Schwartzerberg and Treybal (1968) investigation. Argaman and Kaufman (1970) developed a model based on the assumption that particles moved in a random motion. This can be expressed in terms of the turbulent energy spectrum:

$$\frac{dN_{ij}}{dt} \sim (d_i+d_j)^3 N_i N_j K_s u'^2 \qquad 1.12)$$

where notations i and j represent the initial and flocculated particles (therefore $d_i >> d_j$), while K_s is a turbulent energy related coefficient.

Floc break up is the opposing process that balances the particle collision process. Argaman and Kaufman (1970) and Parker et al. (1972) assumed that the floc

erosion was proportional to the shear stress and the surface area of the floc. The overall removal rate in the case of monosized colloid can be expressed as:

$$\frac{dN_i}{dt} = -k_1 N_i + k_2 \qquad 1.13)$$

where $\frac{dN_i}{dt}$ is the rate of disappearance of main particle of size i, while k_1 and k_2 are the agglomeration and erosion rate coefficients. The erosion rate coefficient can be expressed as:

$$k_2 \sim \frac{d_j^2}{d_i^2} N_j u'^2 \qquad 1.14)$$

where notations i and j in this case are related to the initial and flocculated particles, respectively. k_2 can also be obtained experimentally as follows:

$$k_2 = k_B \overline{G}^4 \quad \text{for inertial turbulent regime} \qquad 1.15)$$

$$= k_B \overline{G}^2 \quad \text{for viscous turbulent regime} \qquad 1.16)$$

where k_B is the erosion rate coefficient.

Amirtharajah and O'Melia (1990) presented Equation 1.13 above by incorporating $\overline{G}$ as the mixing variable:

$$\frac{dN_i}{dt} = -k_A \overline{G} N_i + k_B \overline{G}^b \qquad 1.17)$$

where k_A is the agglomeration rate coefficient and b is a power constant depending on the turbulent regime (see Equations 1.15 and 1.16). When analyzing the particle agglomeration rate coefficient, $\overline{G}$ has been used as the mixing parameter indicating that this equation follows Spielman's assumption as shown in Equation 1.10 above. Equation 1.17 has commonly been used to analyze the particle agglomeration and break up processes due to the simple mixing parameter $\overline{G}$.

Subsequently, Argaman and Kaufman (1970) and Argaman (1971) investigated the performance of a series of complete mixed reactors. They found the following relationship:

$$\frac{N_i^I}{N_i^E} = \frac{1 + k_B \overline{G}^2 \frac{t_D}{m} \sum_0^{n=m-1} [1 + k_B \overline{G} \frac{t_D}{m}]^n}{[1 + k_B \overline{G} \frac{t_D}{m}]^m} \qquad 1.18)$$

where N_i^I and N_i^E are the concentrations of primary particles in the influent and effluent of the reactor, respectively, m is the number of complete mixed reactors in

series, and t_D is the detention time (= volume / incoming flow). This equation shows that the larger the number of reactors the better the performance.

Furthermore, the maximum floc diameter can be related to $\overline{G}$ as:

$$d_{max} \sim \overline{G}^{-b} \qquad 1.19)$$

The same expression but different values of b were given by Thomas (1964), Parker (1972), Tambo and Hozumi (1979) and Tomi and Bagster (1978). b values were found in the range of 0.6 to 5 in the case of inertial turbulent regime and 0 to 1 for viscous turbulent regime.

Differential settling is the third type of transport mechanism. This occurs when particles with diameter d_i coalesce with slower settling particles with diameter d_j. Camp (1946) derived an expression for this situation, and with the incorporation of the Stokes' settling velocity, yields:

$$\frac{dN_{ij}}{dt} \sim (d_i+d_j)^3 (d_i-d_j) N_i N_j g (\gamma-1) \qquad 1.20)$$

where g is the gravity acceleration, and γ is the specific gravity of the particles.

1.3 MIXING REQUIREMENT

Rapid mixing is required to ensure a complete homogeneous coagulation process. The main characteristic of rapid mixing is that an added material is dispersed throughout the receiving liquid in a relatively short period of time. The length of time for complete mixing must be rapid enough to insure that the coagulant is uniformly distributed in water and makes contact with all colloids before the reaction is complete. In the absence of proper mixing, some parts of water are over treated with coagulant while other parts are under treated or may not be treated at all. There are some studies investigating the intense and period of rapid mixing. In the case of charge neutralization destabilization mechanism, rapid mixing has a very important role. There should be collisions between the colloids and the incipiently forming hydrolysis products. Amirtharajah and Trussell (1986) found a correlation between $\overline{G}$ and the charge properties of the colloids at different colloid diameters. However as shown by Amirtharajah and Mills (1982), rapid mixing did not seem to have major effects in the case of sweep flocculation mechanism. In this case, the water is supersaturated and the hydroxide precipitates are formed quickly. Therefore as long as the mixing is rapid enough to disperse the chemicals, only the precipitation reactions and the transport aspect are important. As it was found in their study, $\overline{G}$ values from 300 to 16,000 s^{-1} gave almost the same residual turbidity readings.

Slow mixing is required to allow the newly formed flocs to agglomerate. There should be enough energy in a longer period of mixing time to allow the aggregation

but not too excessive to break up the flocs. The optimum $\overline{G}$ and its related flocculation time for each condition have traditionally been obtained based on the residual turbidity reading through bench scale tests (Hudson and Wolfner, 1967; Andreu - Villegas and Letterman, 1976; and many others). Andreu - Villegas and Letterman (1976) found a practical relationship between the optimum $\overline{G}$ ($\overline{G}$ *) and flocculation time (t_F) as:

$$(\overline{G}\,^*)^b t_F = \text{constant} \qquad 1.21)$$

where b is a constant depending on the coagulant dose and type of impeller.

There have been many suggestions given for $\overline{G}$ and t_F applied in full scale treatment systems. Tables 1.1a and 1.1b show suggested values for rapid mixing and slow mixing, while Table 1.1c provides temperature correction factors for $\overline{G}$.

Both rapid and slow mixing can be achieved using many methods such as weirs, hydraulic jumps, dissipation plates, pipe discharges or jet nozzles, air mixing, static mixers, and mechanical mixing. However, mechanical mixing which involves moving devices is the most common type of mixing mechanism applied in practices. Flat blades and Rushton types of impellers produce radial flow, while pitched blades and marine propellers produce axial flow. Rake or gate impellers provide relatively a

uniform gentle mixing environment across the whole fluid region. Figure 1.7 shows the configuration of many types of impellers.

1.4 COAGULATION AND FLOCCULATION PERFORMANCE

As has been shown above, coagulation and flocculation performance are affected by numerous factors. pH and coagulant dose as can be seen in Figure 1.4 govern the optimum colloid destabilization condition. Figures 1.4 and 1.5 show the effect of colloid concentration and coagulant dose to the residual turbidity reading. Temperature plays a significant role in coagulation with alum as shown by Morris and Knocke (1984). The lower the temperature the greater the decreased the efficiency from the reference temperature. Cold temperatures increase water viscosity affecting the sedimentation process of flocs, decrease the hydrolysis and precipitation rates, and change smaller aggregate structures. Temperature also affected the mixing intensity as has been explained above. Specific anions such as sulfates are able to suppress the charge reversal and accelerate the precipitation of $Al(OH)_3$. Divalent cations have significant effects on coagulation by compressing the double layer and reducing the repulsive forces (Black et al. 1965).

The process efficiency is traditionally assessed based on the apparent particle removal through the turbidity reduction in the treated water. Gravimetric analysis is one accurate method which is very time consuming and not practical for real process control work. Particle size and distribution is also very accurate and sensitive especially for measuring the concentration of particles greater than 1 μm in size (Beard

and Tanaka, 1977). However, turbidity is the most practical and common method applied in water work practices. The measurement is based upon the property possessed by particulates of scattering light incident upon it (see Black and Hannah 1965 for more detailed explanations). As cited by Hudson (1962), turbidity reduction may accompany a parallel removal of microorganisms and other particulates. A qualitative description of the turbidity reduction performance can be described as: rapid, slow, and no flocculation with reductions in turbidity of greater than 85%, about 50%, and less than 10%, respectively (McCooke and West 1978).

O'Melia (1978) identified four types of turbid waters which can be treated by the coagulation and flocculation process: high turbidity and high alkalinity, high turbidity and low alkalinity, low turbidity and high alkalinity, and low turbidity and low alkalinity. The first type is the easiest case to be treated using ordinary coagulants by adjusting the pH value. The last type is the most difficult to be treated. Along with ordinary coagulants, additional turbidity particles, certain types of polymers, and pH adjustment are necessary.

Many regulations and guidelines have set maximum acceptable concentration values for turbidity for the final treated water of 1 or even 0.5 NTU (nephelometric turbidity unit). For aesthetic or appearance concern, turbidity values of less than 5 NTU are required (World Health Organization, 1993; Pontius, 1996; and Health Canada, 1996). Table 1.2 shows regulatory requirements for turbidity as well as other selected contaminants according to the Guidelines for Canadian Drinking Water Quality (Health Canada 1996).

1.5 SCALE - UP EFFECT

Most theoretical findings for coagulation and flocculation processes have been generated through bench scale or jar tests. Traditionally, results obtained from jar tests have been assumed to hold for larger scales, both pilot and full scale systems. This can be made through dimensional analysis as explained by Rushton (1951) and Clark and Fiessinger (1991):

$$\overline{G}_l \sim S^2 \qquad 1.22)$$

$$S = \frac{N_s}{N_l} \qquad 1.23)$$

where the subscripts l and s denote large and small scales, while N is the impeller speed and S is the scaling parameter. Both equations are valid at a constant temperature.

Even though there have been many critics addressed based on field practices. not many detailed studies have been completed to observe the scale - up effects from small to large scales. Oldshue and Mady (1978) and Clark and Fiessinger (1991) found that in the case of impeller mixing, optimum average volume velocity gradient $\overline{G}$ * (based on the settled water turbidity) decreases with increasing scale. One concern is related to the fact that impellers do not provide uniform mixing environment. This has been proven by many investigators such as Tomi and Bagster (1978), Wu and

Patterson (1989), Kresta and Wood (1993), Stanley (1995), and Stanley and Smith (1995). They have shown that the turbulent intensity, represented by the energy dissipation rate ε and velocity gradient G, in the impeller region is much higher than that in the bulk region. Another concern is related to the occurrence of a jet like flow created by the impeller movement. The jet drives the agglomerated flocs to the vessel wall before recirculating back to the impeller region. This creates local high shear regions that finally govern the overall floc agglomeration process (Stanley 1995 and Stanley and Smith 1995).

This indicates that forces acting on the flocs vary within the vessel. This may explain some difficulties in scaling - up mixing for flocculation. Average volume mixing parameters, such as $\overline{\varepsilon}$ and $\overline{G}$, may not the appropriate mixing parameters especially when they are used in scaling - up process as they do not represent local forces acting on flocs.

1.6 SCOPE OF STUDY

The main objective of this study is to investigate the use of grids to achieve a uniform environment within the vessel that may provide the optimum mixing for floc aggregation. A different type of mixing device, i. e. the vertically oscillating grid mixing device, is applied for this purpose. The grid mixing device can be considered as a novel flocculation mixing device that can be applied in water treatment practices. This mixing device applies a different approach to create uniform slow mixing in the vessel. Instead of having a rotating impeller, the grid mixing device applies a cam that

produces a constant vertical speed. A long stroke at low frequency of mixing creates a gentle mixing environment across the entire mixing region. Many combinations of mixing characteristics can be generated by adjusting the vertical grid speed, vertical stroke length, and grid physical characteristics.

The use of vertically oscillating grid system for slow or flocculation mixing is supported by the fact that grid mixing has traditionally been used to create what is called grid turbulence mixing in which homogeneous isotropic turbulence can be achieved (Taylor 1935a and 1935b; and Batchelor and Townsend 1948). Past studies of grid turbulence were conducted in wind or fluid tunnels where a single grid was placed in the flow path. The investigations were usually conducted at various points behind the grids in the middle part of the tunnel. It was mentioned that the isotropic condition occurs after a certain distance from the grid depending on the grid characteristics and grid Reynolds number (Morgan 1960 and Baines and Peterson 1951). The isotropic turbulence condition enabled the researchers to obtain several important parameters such as the turbulent intensity and energy decay downstream of the grid as summarized by Gad El Hak and Corrsin (1974) and Mohamed and LaRue (1994).

However, as found by Comte-Bellot and Corrsin (1966), the maximum isotropicity that could be achieved even in an improved grid turbulence system was less than 90%. This shows that a perfect isotropic turbulence is very difficult to be achieved in practice especially when a relatively small (narrow) channel is used due to the wall effect. This also indicates that the use of grids for flocculation mixing will

still unlikely to produce an isotropic turbulence condition. However, at least it can be expected that the grid is able to produce more uniform mixing environment than that of impellers.

Oscillating grid systems have also been studied by numerous investigators in the area of theoretical fluid mechanics. In this case, the grid is vertically oscillated in a small stroke but high frequency to simulate a line source of turbulent energy. The turbulent energy decays downstream as a function of the grid frequency and grid physical characteristics. The main application of this system is related to the stratified fluid interface mixing (Thompson and Turner 1975; Long 1978; Brumley and Jirka 1987; and Liu 1995).

The vertically oscillating grid mixing with a long stroke and low frequency can be found in Kostazos et al. (1990). However, turbulent mixing intensity measurement was not conducted, and neither was its application to flocculation. The investigation was focused on the chemical mixing properties. Another similar mixing concept can also be found in older references. The walking beam device applies a gentle vertical movement of a series of plates to promote floc aggregation (Monk and Trussell 1991 and Gemmel 1972). A brief experimental study of this mixing device can be found in Camp (1955). Two plates were vertically oscillated based on a circular disc that created a non uniform vertical movement. Note: this can be compared to the mixing device designed in this study that employs a cam giving a constant vertical movement. Power consumption was measured but not the turbulent mixing parameters. It can still be expected that the turbulent mixing intensity inside the vessel was not uniform.

Also, it may be difficult to investigate the effect of shape and size of the mixing plates. On the other hand, solidity ratio can simply be applied as the scaling factor in the case of grid mixing.

Static multiple porous plates as described by Watanabe et al. (1991) have also been applied to create a gentle mixing for floc aggregation. This system is known as the jet mixed separator. Larger flocs have been reported to settle due to the absence of large scale eddies. However, the mixing performance depends on the incoming flow which may be difficult to be controlled in water treatment plants. In the case of vertically oscillating grid mixing, the mixing environment can simply be controlled by adjusting the vertical grid speed or changing the grid physical characteristics.

The vertically oscillating grid mixing device can then be seen as an improvement to the previous mixing devices. This mixing device has been designed to produce the best mixing environment for floc aggregation. The mixing characteristics can also easily be controlled from the vertical grid speed, vertical stroke length, and grid physical characteristics.

The main objectives of this study are to show that:

1) the oscillating grid mixing device produces a uniform flocculation mixing environment throughout the mixing region,
2) the oscillating grid mixing device has an excellent flocculation performance in terms of turbidity reduction, and

3) the turbulent mixing intensity and flocculation performance parameters can easily be controlled by the grid movement, grid physical characteristics, and number of grids applied.

1.7 THESIS LAYOUT

This thesis has been written in a modified paper format. Each chapter, with the exception of chapters 1 and 5 which are the introduction and conclusions, contains different topics and different sets of experiment. The main thesis layout can be described as: Chapter 1: Introduction, Chapter 2: Turbulent Parameter Study, Chapter 3: Particle Removal Study, Chapter 4: Comparative Study, and Chapter 5: General Discussion and Conclusions. Appendices were added to provide complete experimental data.

Chapter 2 deals with the turbulent parameter measurement study using a laser doppler anemometer (LDA). This chapter shows results for the average root mean square (rms) turbulent velocity q' and horizontal and vertical mean velocities ($\overline{U}$ and $\overline{V}$). The average volume energy dissipation rate $\overline{\varepsilon}$ and velocity gradient $\overline{G}$ were also calculated as well as the macro length scale L.

Chapter 3 discusses the performance of the oscillating grid mixing device for particle removal. In this study, kaolin was used as the treated particles, alum was applied as the coagulant, and sodium bicarbonate was used as the pH buffer. Turbidity readings were obtained, subsequently the floc aggregation and erosion rate coefficients were calculated.

Chapter 4 compares three different grid mixing arrangements by applying single, double, and triple grids. In this study, double and triple grids were used for each case. A brief laboratory experiment using a standard flat blade impeller was also completed. Similar experimental works and analyses as those of two previous studies were conducted.

Chapter 5 provides a general discussion of results obtained from this study. Limitations of the study and some suggestions are also presented. This chapter is closed by conclusions.

Figure 1.8 shows the experimental setups for the three studies. Each study applied different number of grids, vertical mixing strokes, types of grids, and vertical grid speeds. However, physical (i.e. temperature) and chemical parameters were set constant for all cases.

1.8 REFERENCES

Amirtharajah, A. and Trussell, S. L. (1986). "Destabilization of Particles by Turbulent Rapid Mixing." *Journal of the Environmental Engineering*, 112 (10), 1085 - 1108.

Amirtharajah, A. (1978). "Design of rapid mixing units." *Water Treatment Plant Design*, R. L. Sanks, editor. Ann Arbor Science Inc., Ann Arbor, Michigan, 131 - 148.

Amirtharajah, A. and Mills, K. M. (1982). "Rapid - mix design for mechanisms of alum coagulation." *Journal AWWA*, 74 (4), 210 - 216.

Amirtharajah, A. and O'Melia, C. R. (1990). "Coagulation processes: Destabilization. mixing, and flocculation." *Water Quality and Treatment, 4th Edition*, F. W. Pontius, editor. McGraw - Hill, New York, New York, 269 - 366.

Amirtharajah, A. and Tambo, N. (1991). "Mixing in water treatment." *Mixing in Coagulation and Flocculation*, A. Amirtharajah, M. M. Clark, and R. R. Trussell, editors. AWWA, Denver, Colorado, 3 - 34.

Andreu - Villegas, R. and Letterman, R. D. (1976). "Optimizing flocculator power input." *Journal of the Environmental Engineering, ASCE*, 102 (EE2), 251 - 263.

Argaman, Y. A. (1971). "Pilot - plant studies of flocculation." *Journal AWWA*, 63 (12), 775 - 777.

Argaman, Y. A. and Kaufman, W. J. (1970). "Turbulence and flocculation." *Journal of the Sanitary Engineering Division, ASCE*, 96 (SA2), 223 - 241.

AWWA. (1990). *Water Treatment Plant Design*. McGraw - Hill, New York, New York.

Baines, W. D. and Peterson, E. G. (1951). "An investigation of flow through screens." *Transactions of the ASME*, 73, 467 - 480.

Batchelor, G. K. and Townsend, A. A. (1948). "Decay of isotropic turbulence in the initial period." *Proceedings of the Royal Society, A*. 193, 539 - 557.

Beard, J. D. II and Tanaka, T. S. (1977). "A comparison of particle counting and nephelometry." *Journal AWWA*, 69 (10), 533 - 538.

Bellar, T. A., Lichtenberg, J. J., and Kroner, R. C. (1974). "The Occurrence of organohalides in chlorinated water." *Journal AWWA*, 66 (12), 703 - 706.

Black, A. P. and Hannah, S. A. (1965). "Measurement of low turbidity." *Journal AWWA*, 57 (7),

Black, A. P., Birkner, F. B., and Morgan, J. J. (1965). "Destabilization of dilute clay suspensions with labeled polymers." *Journal AWWA*, 57 (12), 1547 - 1560.

Brumley, B. H. and Jirka, G. H. (1987). "Near - surface turbulence in a grid - stirred tank." *Journal of Fluid Mechanics*, 183, 235 - 263.

Bryant, E. A., Fulton, G. P., and Budd, G. C. (1992). *Disinfection Alternatives for Safe Drinking Water*, Van Nostrand Reinhold, New York, New York.

Camp, T. R. (1946). "Sedimentation and the design of settling tanks." *Proceedings of ASCE*, 72 (5), 668 - 674.

Camp, T. R. (1955). "Flocculation and flocculation basin." *Transactions of ASCE*. Paper No. 2722, 1 - 16.

Camp, T. R. (1968). "Floc volume concentration." *Journal AWWA*, 60 (6), 656 - 673.

Camp, T. R. and Stein, P. C. (1943). "Velocity gradients and internal work in fluid motion." *Journal of Boston Society of Civil Engineers*, 30 (10), 219 - 237.

Clark. M. M. and Fiessinger, F. (1991). "Mixing and scale-up." *Mixing in Coagulation and Flocculation*. A. Amirtharajah, M. M. Clark, and R. R. Trussell. editors. AWWA, Denver, Colorado, 282 - 308.

Cleasby, J. L. (1986). "Is velocity gradient a valid turbulent flocculation parameter?" *Journal of the Environmental Engineering, ASCE*, 110 (5), 875 - 897.

Comte-Bellot, G. and Corrsin, S. (1966). "The use of a contraction to improve the isotropy of grid - generated turbulence." *Journal of Fluid Mechanics*, 25, 657 - 682.

Cotruvo, J. A. and Vogt, C. D. (1990). "Rationale for water quality standards and goals." *Water Quality and Treatment, 4th Edition*, F. W. Pontius, editor. McGraw - Hill, New York, New York, 2 - 62.

Delichatsios, M. A. and Probstein, R. F. (1975). "Coagulation in turbulent flow: theory and experiment." *Journal of Colloid Interface Science*, 51 (6), 394 - 405.

Gad-El-Hak, M. and Corrsin, S. (1974). "Measurements of the nearly isotropic turbulence behind a uniform jet grid." *Journal of Fluid Mechanics*, 62, 115 - 143.

Gemmel, R. S. (1972). "Mixing and sedimentation." *Water Quality and Treatment*, McGraw - Hill, New York, New York, 123 - 159.

Gregory, J. (1978). "Effects of polymers on colloid stability." *The Scientific Basis of Flocculation*, K. J. Ives, editor. Sijthoff and Noordhoff, The Netherlands.

Hamann, C. L. Jr., McEwen, J. B., and Myers, A. G. (1990). "Guide to selection of water treatment processes." *Water Quality and Treatment, 4th Edition*, F. Pontius, editor. McGraw - Hill, New York, New York, 157 - 188.

Health Canada. (1996). *Guidelines for drinking water quality, 6th Edition*, Minister of Supply and Services Canada, Ottawa, Ontario.

Herwaldt, B. L., Craun, G. F., Stokes, S. L., and Juranek, D. D. (1992). "Outbreaks of waterborne disease in the united states: 1989 - 90." *Journal AWWA*, 84 (4), 129 - 135.

Hudson, H. E. Jr. (1962). "High quality water production and viral disease." *Journal AWWA*, 54 (10), 1265 - 1272.

Hudson, H. E. Jr. (1965). "Physical aspect of flocculation." *Journal AWWA*, 57 (7), 885 - 892.

Hudson, H. E. Jr. and Wolfner, J. P. (1967). "Design of mixing and flocculation basins." *Journal AWWA*, 59 (10), 1257 - 1267.

Hudson, H. E. Jr. and Wagner, E. G. (1981). "Conduct and use of jar tests." *Journal AWWA*, 73 (4), 218 - 224.

Hyde, C. G. and Ludwig, H. F. (1944). "Some new features in the design of vertical flocculation units." *Journal AWWA*, 36 (2), 151 - 162.

Kostazos, A. E., Apikides, P. S., Kastrinakis, E. G., and Nychas, S. G. (1994). "Oscillating grid turbulence and bulk mixing at high schmidt numbers." *Canadian Journal of Chemical Engineering*, 72, 431 - 439.

Kramer, M. H., Herwaldt, B. L., Craun, G. F., Calderon, R. L., and Juranek, D. D. (1996). "Waterborne disease in the united states: 1993 - 1994." *Journal AWWA*, 88 (3), 66 - 80.

Krasner, W. S. and Amy, G. (1995). "Jar - test evaluations of enhanced coagulation." *Journal AWWA*, 87 (10), 93 - 107.

Kresta, S. M. and Wood, P. E. (1993). "The flow field produced by a pitched blade turbine: characterization of the turbulence and estimation of the dissipation rate." *Chemical Engineering Science*, 48 (10), 1761 - 1774.

La Mer, V. K. (1964). "Coagulation symposium introduction." *Journal of Colloid Science*, 19, 291 - 293.

Liu, Hsien-Ta. (1995). "Energetics of grid turbulence in a stably stratified fluid." *Journal of Fluid Mechanics*, 296, 127 - 157.

Long, R. R. (1978). "Theory of turbulence in a homogeneous fluid induced by an oscillating grid." *Physics of Fluids*, 21 (10), 1887 - 1888.

Lykins, B. W., Koffskey, W. E., Patterson, K. S. (1994). "Alternative disinfectants for drinking water treatment." *Journal of Environmental Engineering*, 120 (4), 745 - 758.

McCooke, N. J. and West, J. R. (1978). "The coagulation of a kaolinite suspension with aluminum sulphate." *Water Research*, 12, 793 - 798.

Mohamed, S. M. and Larue, J. C. (1990). "The decay power law in grid - generated turbulence." *Journal of Fluid Mechanics*, 219, 195 - 214.

Monk, R. D. G, and Trussell, R. R. (1991). "Design of mixers for water treatment plants: rapid mixing and flocculators." *Mixing in Coagulation and Flocculation*, AWWA, Denver, Colorado, 380 - 420.

Moore, A. C. and Herwaldt, B. L., Craun, G. F, Calderon, R. L., Highsmith, A. K., and Juranek, D. D. (1994). "Waterborne disease in the united states: 1991 - 1992." *Journal of AWWA*, 86 (2), 87 - 99.

Morgan, P. G. (1960). "The stability of flow through porous screen." *Journal of the Royal Aeronautical Society*, 64, 359 - 362.

Morris, J. K. and Knocke, W. R. (1984). "Temperature effects on the use of metal ion coagulants for water treatment." *Journal AWWA*, 76 (3), 74 - 79.

Niehof, R. A. and Loeb, G. I. (1972). "The surface charge of particulate matter in sea water." *Limnology Oceanography*, 17, 7 - 16.

O'Melia, C. R. (1978). "Coagulation." *Water Treatment Plant Design*, R. L. Sanks, editor. Ann Arbor Science Inc., Ann Arbor, Michigan, 65 - 82.

Oldshue, Y. J. and Mady, O. B. (1978). Flocculation performance of mixing impellers. *Chemical Engineering Progress*, 74 (8), 103 - 108.

Parker, D. S., Kaufman, W. J., and Jenkins, D. (1972). "Floc breakup in turbulent flocculation processes." *Journal of the Sanitary Engineering Division, ASCE*. 98 (SA1), 79 - 99.

Pontius, F. W. (1996). "An update of the federal regs." *Journal AWWA*, 88 (3), 36 - 46.

Putnam, S. W. and Graham, J. D. (1993). "Chemical versus microbials in drinking water: a decision sciences perspective." *Journal AWWA*, 85 (3), 57 - 61.

Rushton, J. H. (1951). "The use of pilot plant mixing data." *Chemical Engineering Progress*, 47 (9), 485 - 488.

Saffman, P. G. and Turner, J. S. (1956). "On the collision of drops in turbulent clouds." *Journal of Fluid* Mechanics, 1, 16 - 30.

Sobsey, M. D., Dufour, A. P., Alfred, P., Gerba, C. P., LeChevallier, M. W., and Payment, P. (1993). "Using a conceptual framework for assessing risks to health from microbes in drinking water." *Journal AWWA*, 85 (3), 44 - 48.

Spielman. (1978). "Hydrodynamics Aspects on Flocculation." *The Scientific Basis of Flocculation*. K. J. Ives, editor. Sijthoff and Noordhoff, The Netherlands.

Stanley, S. J. (1995). "Measurement and analysis of mixing as it relates to flocculation." *Ph.D. Thesis*, University of Alberta, Edmonton, Alberta.

Stanley, S. J. and Smith, D. W. (1995). "Measurement of turbulent flow in standard jar test apparatus." *Journal of Environmental Engineering*, 121 (12), 902 - 910.

Stumm, W. (1977). "Chemical interaction in partial separation." *Journal of Environmental Science and Technology*, 11 (12), 1066 - 1070.

Stumm, W. and O'Melia, C. R. (1968). "Stoichiometry of coagulation." *Journal AWWA*, 69 (5), 414 - 539.

Schwartzberg, H. G. and Treybal, R. E. (1968). "Fluid and particle motion in turbulent stirred tanks." *Industrial Engineering Chemical Fundamentals*, 7 (1), 1 - 12.

Tambo, N. and Hozumi, H. (1979). "Physical characteristics of flocs-II. Strength of floc." *Water Research*, 13, 421 - 427.

Taylor, G. I. (1935a). "Statistical theory of turbulence. Part I." *Proceedings of the Royal Society, A.* 151, 421 - 443.

Taylor, G. I. (1935b). "Statistical theory of turbulence. Part II." *Proceedings of the Royal Society, A.* 151, 444 -454.

Tchobanoglous, G. and Schroeder, E. (1985). *Water Quality: Characteristics, Modeling, Modification*, Addison - Wesley, Reading, Massachusetts.

TeKippe, R. J. and Ham, R. K. (1971). "Coagulation testing: a comparison of techniques." *Journal AWWA*, 62 (9), 592 - 602.

Tennekes, H. and Lumley, J. L. (1972). *A First Course in Turbulence*, MIT Press. Cambridge, Massachusetts.

Thompson, S. M. and Turner, J. S. (1975). "Mixing across an interface due to turbulence generated by an oscillated grid." *Journal of Fluid Mechanics*, 67. 349 - 368.

Tomi, D. T. and Bagster, D. F. (1978). "The behavior of aggregates in stirred vessels. Part I. Theoretical consideration in the effects of agitation." *Transactions of the Institute of Chemical Engineers*, 56, 1 - 8.

Watanabe, Y., Fukui, M., and Miyanosita, T. (1991). Theory and performance of a jet - mixed separator. *Journal WSRT*, 39 (6), 387 - 395.

White. C. G. (1992). *The Handbook of Chlorination, 3rd Edition*. Van Nostrand Reinhold , New York, New York.

World Health Organization. (1993). *Guidelines for Drinking - Water Quality, Vol. 1: Recommendations*. World Health Organization, Geneva.

Wu, H. and Patterson, G. K. (1989). "Laser - doppler measurements of turbulent - flow parameters in stirred mixer." *Chemical Engineering Science*, 44 (10), 2207 - 2221.

Table 1.1a: Impeller Rapid Mixing Requirement

Flocculation Time (s)	20	30	40	>40
$\overline{G}$ (s^{-1})	1000	900	790	700

(adapted from Amirtharajah 1978)

Flocculation Time (s)	10 to 30	60 to 120
$\overline{G}$ (s^{-1})	700 to 1000	700 to 1000

(adapted from Gemmell 1972) (adapted from Camp 1968)

Table 1.1b: Impeller Slow Mixing Requirement

	Conventional Flocculation	Direct Flocculation
Flocculation Time (min)	17 to 25	15 to 25
$\overline{G}$ (s^{-1})	10 to 60	20 to 75

(adapted from AWWA 1990)

Table 1.1c: Temperature Correction Factor for $\overline{G}$

(adapted from Hudson and Wolfner 1967)

Water Temperature	$\overline{G}$ (s^{-1})
0	0.94
4	1.00
5	1.02
15	1.09
20	1.24
25	1.32
30	1.40

Table 1.2: Selected Contaminant Limits

(adapted Health Canada 1996)

Contaminants	MAC (mg/L)	IMAC (mg/L)	AO (mg/L)
Turbidity	1	-	5
Total trihalomethanes	-	0.1	-
Total Dissolved Solids	-	-	500
pH	-	-	6.5 to 8.5
Total Coliform	10 counts /100mL	-	-
Fecal Coliform	0 counts	-	-
Viruses and Protozoa	0 is desired	-	-

Note: MAC = maximum acceptable concentration

IMAC = interim maximum acceptable concentration

AO = aesthetic objective

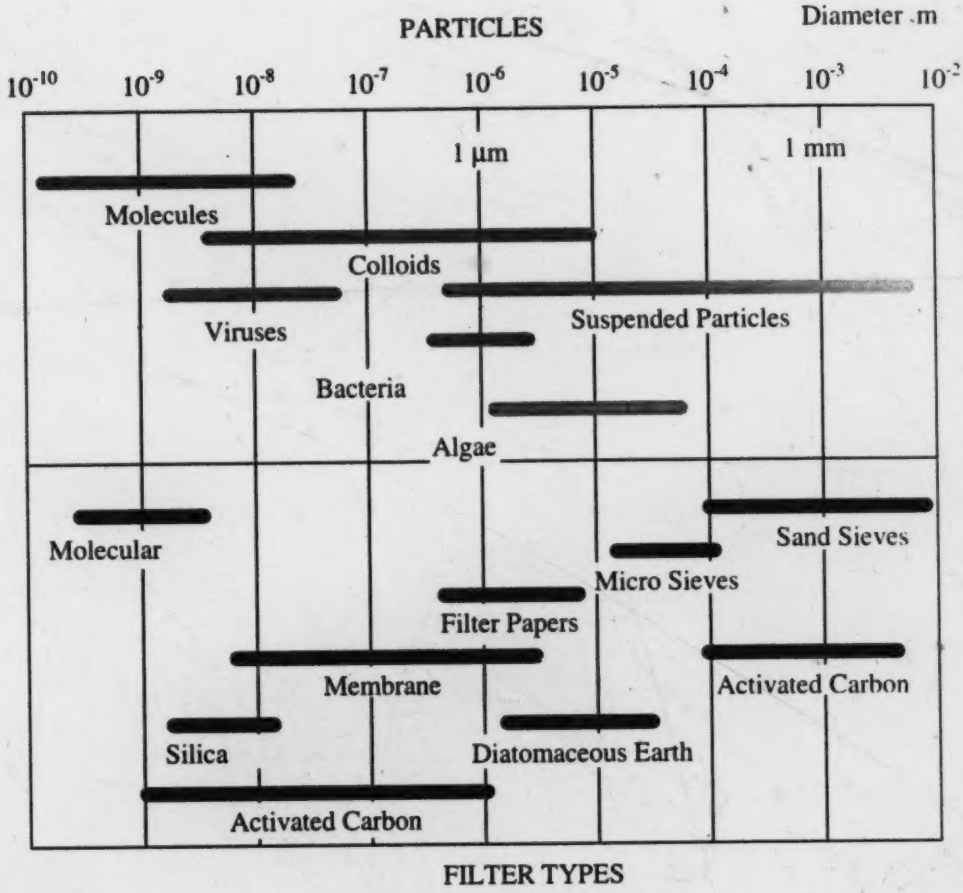

Figure 1.1: Particle Sizes
(adapted from Stumm 1977)

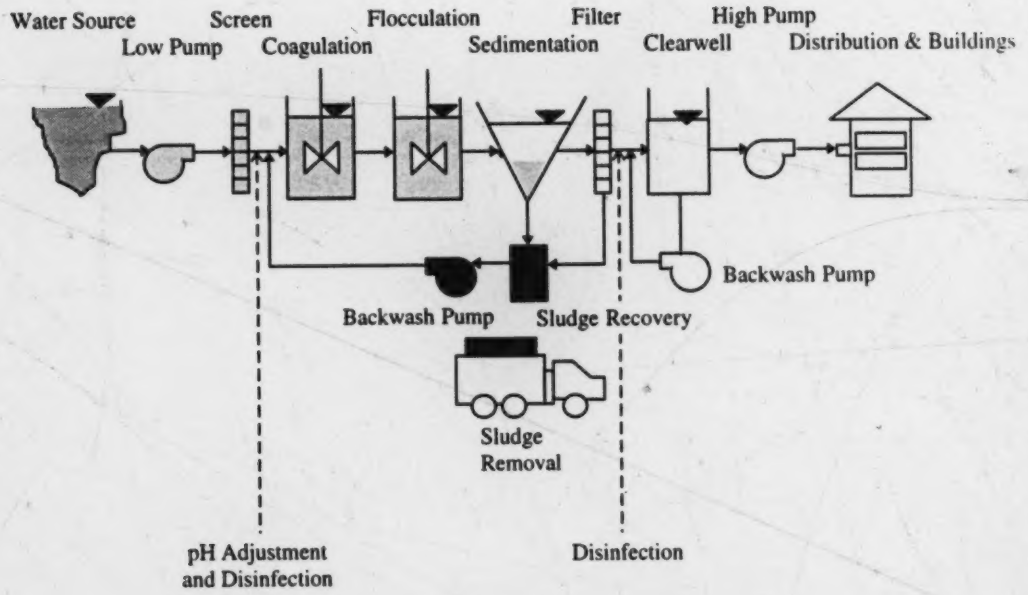

Figure1.2: Conventional Treatment Process Components

(adapted from Hamann et al. 1990)

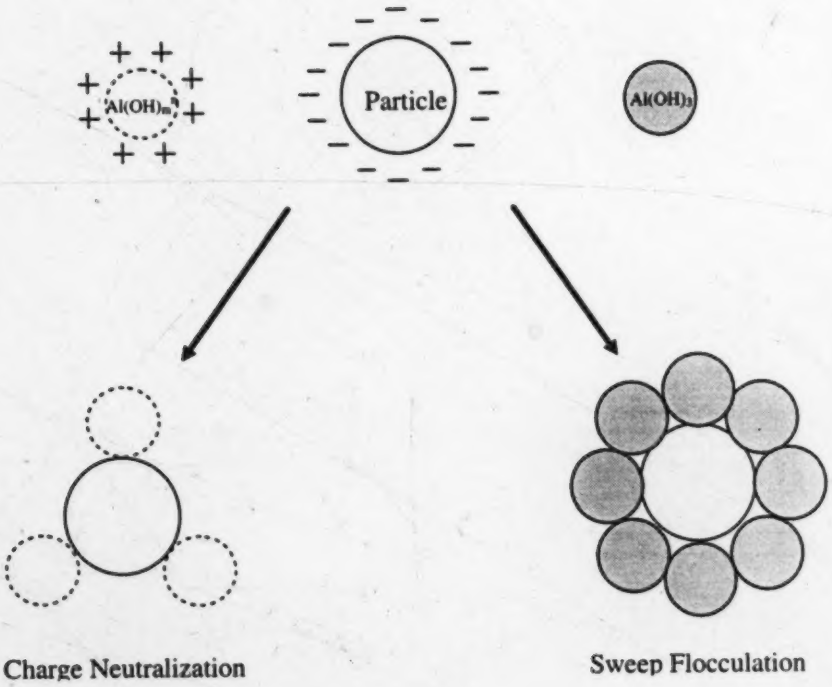

Figure 1.3: Reaction Schematics among Particles, $Al(OH)_m^{n+}$, and $Al(OH)_3$

(adapted from Amirtharajah 1978)

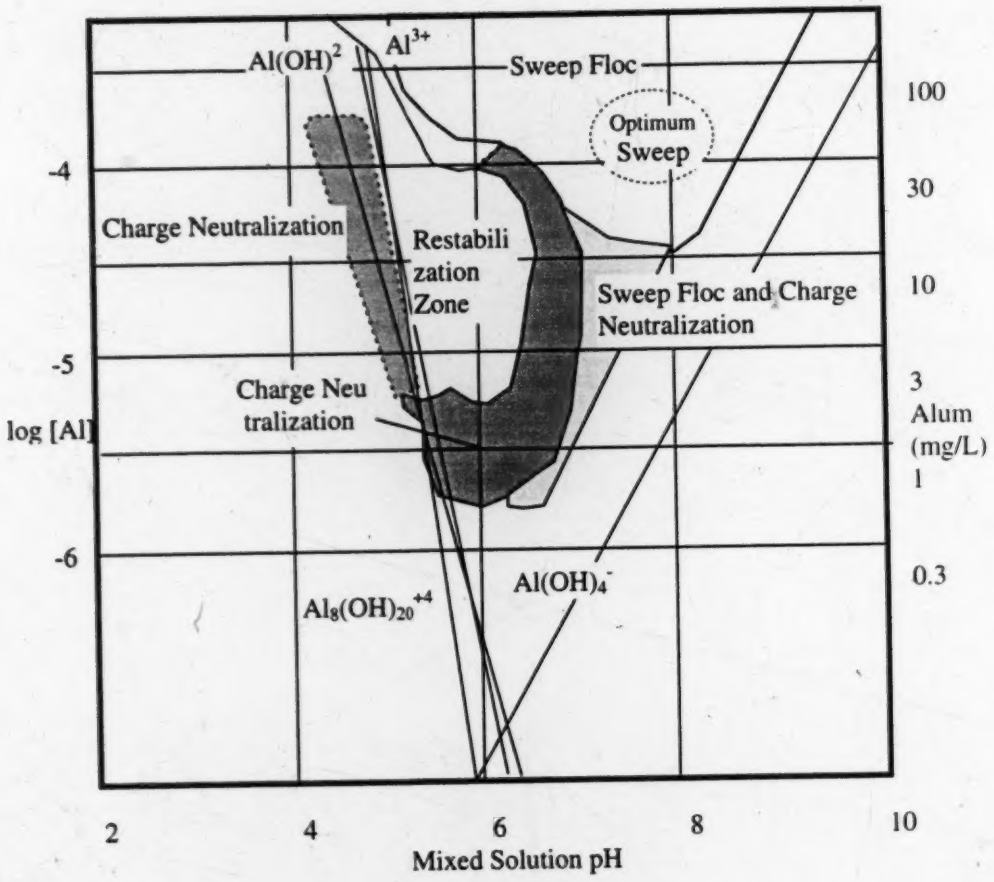

Figure 1.4: Alum Coagulation Diagram

(adapted from Amirtharajah and Mills 1982)

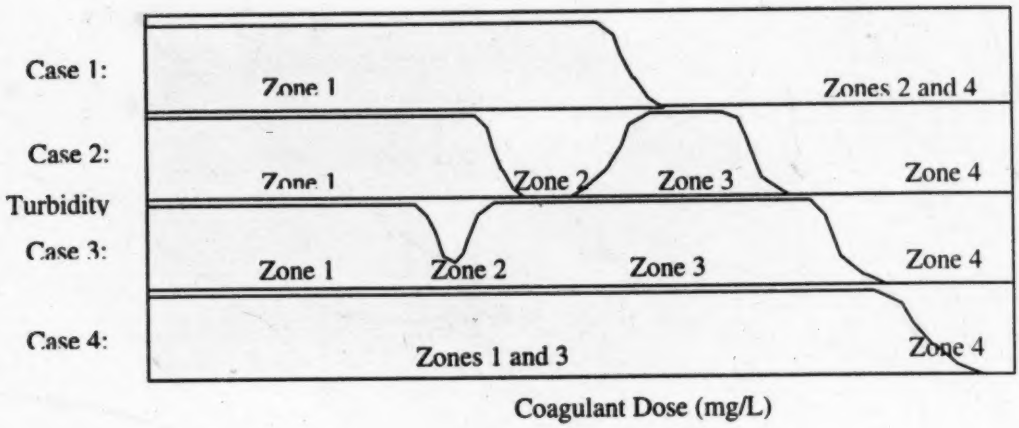

Figure 1.5a: Turbidity vs. Coagulant Dose

(adapted from Stumm and O'Melia 1968)

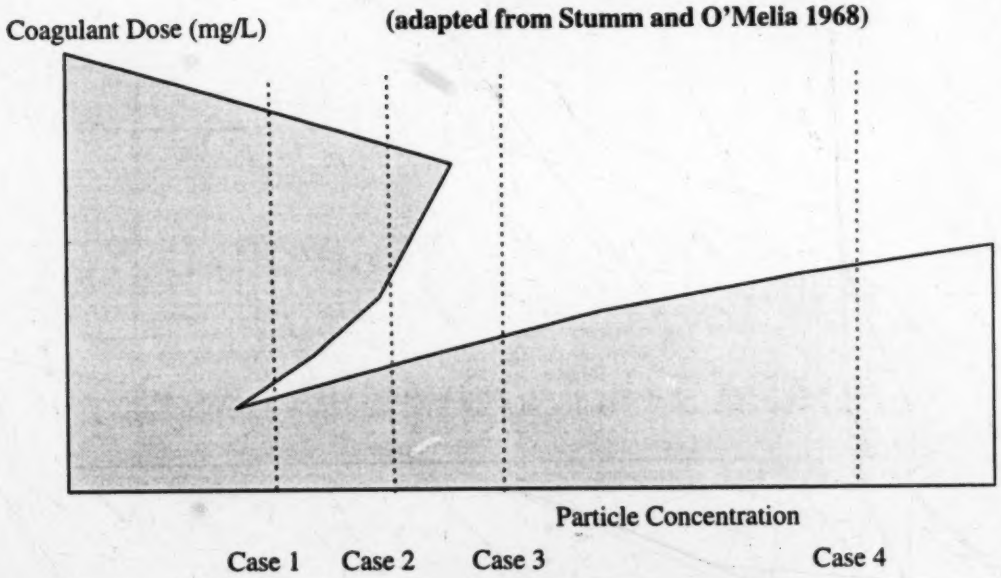

Figure 1.5b: Particle Concentration

(adapted from Stumm and O'Melia, 1968)

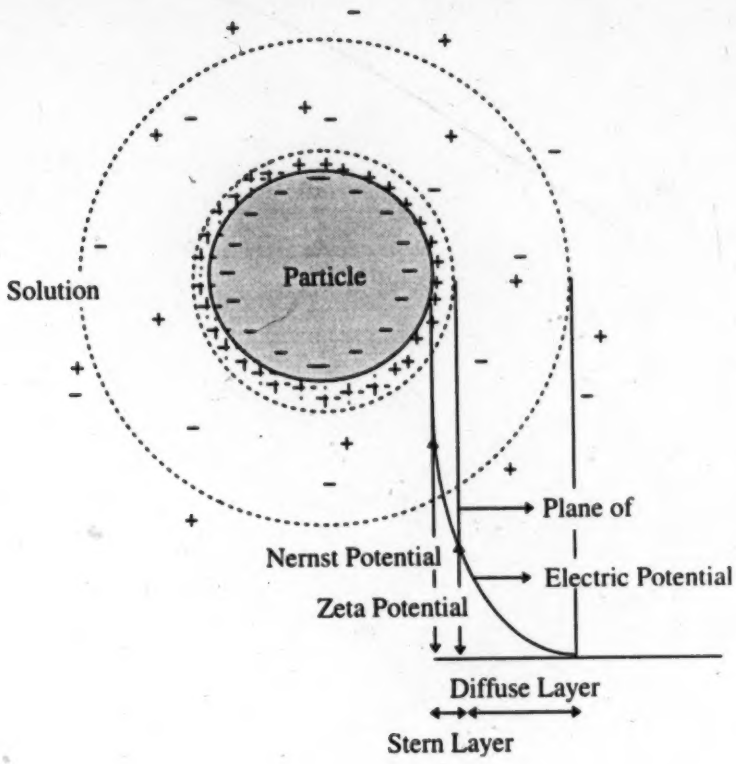

Figure 1.6a: Double Layer Compression

(adapted from Amirtharajah and O.Melia, 1990)

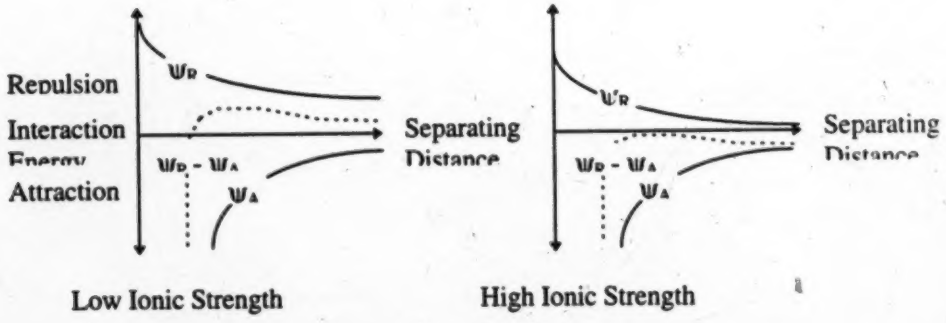

Figure 1.6b: Energies on Particles

(adapted from Amirtharajah and O'Melia 1990)

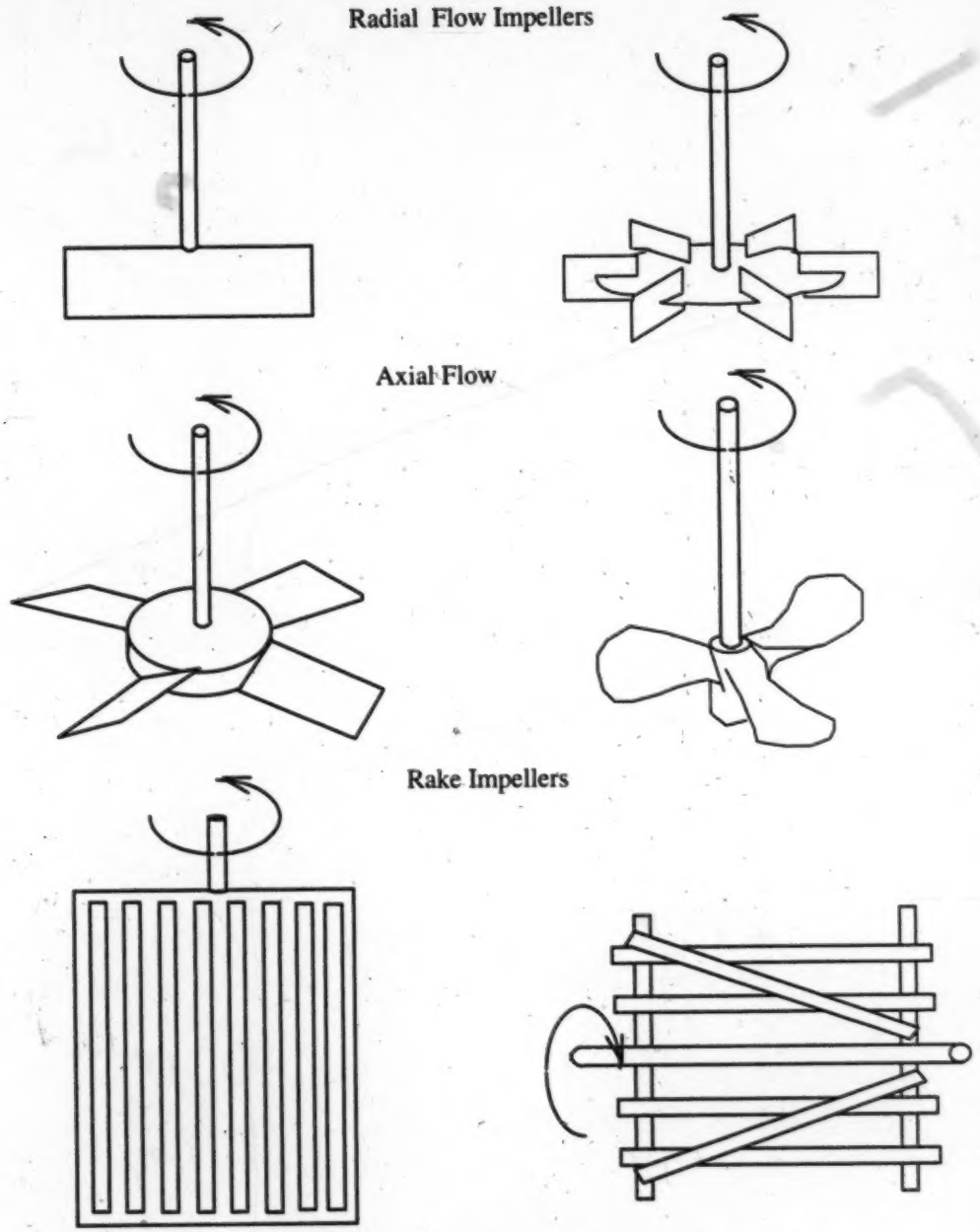

Figure 1.7: Impeller mixing Device

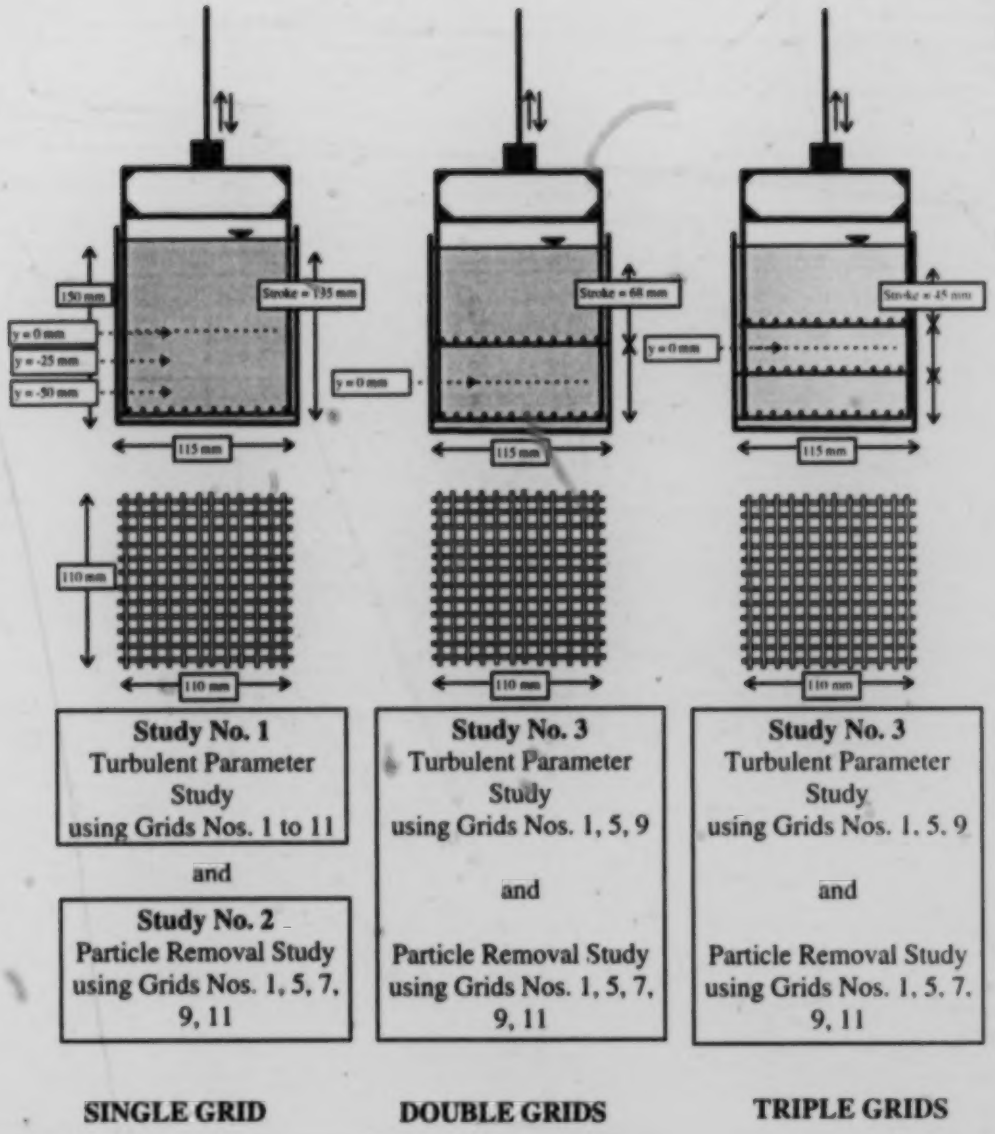

Figure 1.8: Overall Grid Mixing Study

2. TURBULENT PARAMETER STUDY*

2.1 INTRODUCTION

Mixing can be found in many drinking water treatment processes including the coagulation and flocculation process. In coagulation and flocculation, rapid mixing is necessary to disperse the chemical coagulant in water evenly and rapidly for the particle destabilization purpose. Slow mixing is then required to allow the destabilized particulates to agglomerate so that they can be removed using traditional separation processes, e. g. sedimentation and filtration (Amirtharajah and Tambo 1991). The volume average velocity gradient $\overline{G}$ has traditionally been used in the design and scale up of the mixing process components. It has traditionally been assumed that if $\overline{G}$ is held constant the mixing environment is assumed to be constant as well (Camp and Stein 1943). However, turbulent characteristic variations within a vessel were usually not taken into consideration.

Turbulent impeller mixing parameter measurements within a vessel have thoroughly been studied. Many bench scale studies have been completed using many types of vessels and impellers. A flat blade impeller and a 2L square jar as described by Hudson and Wagner (1981) were used by Stanley (1995), Stanley and Smith (1995), and Cheng et al. (1997) in some of their experiments. Stanley (1995) also applied a ten flat blade impeller. A six blade Rushton type of impeller and a fully

---

* Accepted for publication at the Journal of Environmental Engineering. ASCE.

baffled circular vessel were used by Mujumdar et al. (1970), Wu et al. (1989), and Wu and Patterson (1989), while Kresta and Wood (1993) used a four 45° pitched blade impeller. In general, they showed some significant variations of local turbulent parameters, i. e. the root mean square (rms) turbulent velocities and energy dissipation rate ε, within the vessel. These local turbulent parameters were found to be significantly different from their average volume values.

A study completed by Stanley (1995) and Stanley and Smith (1995) emphasized the importance of these variations in relation to the coagulation and flocculation process. It was found that rms turbulent velocities and ε were highly concentrated in the impeller region. The impeller was also observed to produce an impinging jet like flow in the direction of vessel wall. These caused concentrated high shear in these two regions that made the agglomerated flocs to break apart. This eventually governed the overall flocculation performance.

Due to great variation in local turbulent parameters within the vessel mixed by impellers, it is difficult to optimize the mixing condition. When higher impeller speeds are applied, more particle contacts are produced but the floc break up rate which is concentrated in certain regions also increases. For optimum flocculation mixing, a mixing device which produces homogeneous mixing will be ideal. In this case, the mixing intensity can be optimized while minimizing the floc break up rate.

Grid mixing systems have characteristics to provide this type of mixing and should be investigated as an alternative mixing device in place of traditional impeller systems. The fundamental theory of grid turbulence is based on the homogeneous

isotropic turbulence as introduced by Taylor (1935a and 1935b). Most traditional studies have been conducted using a static grid placed in a fluid tunnel. Detailed investigations were conducted for the turbulent characteristics behind the grid (Batchelor and Townsend 1948; Baines and Peterson 1951; Comte-Bellot and Corrsin 1966; and many others). Dickey and Mellor (1980) towed a single grid through an ambient fluid. Oscillating grid systems have also been studied. In this case, the grid is oscillated in a small stroke but high frequency to simulate a line source of turbulent energy (Thompson and Turner 1975; Long 1978; and Brumley and Jirka 1987). To date most research with grids tends to be more theoretical in nature with little work involving their use in engineering process. A work with grid systems was also found in a chemical engineering literature. Kostazos et al. (1994) used a vertically oscillating grid system with a long stroke and low frequency to investigate the degree of chemical mixing within the vessel. However, turbulent characteristics due to the grid movement and direct application to flocculation process were not investigated.

In this study, a grid was vertically and constantly oscillated inside a standard 2L Hudson jar. A long stroke at low frequency mode was applied such that the grid movement was able to cover the whole water depth. It was expected that the turbulent mixing intensity would be uniform within the vessel such that it provided the optimum mixing environment for floc aggregation. The main objective of this study was to identify the turbulent parameters created by many types of grids and vertical grid speeds and to relate them to characteristics of the grids and their operation. This will provide the first information in use of the vertically oscillating grid mixing system for

flocculation mixing.

2.2 METHODS AND MATERIAL

Figures 2.1a and 2.1b show the vertically oscillating grid mixing device main components used in this study. The mixing device consisted of a cam which was connected to a motor with a maximum vertical speed of 130 mm/s. This gave a constant up and down grid movement. The grid had a size of 110 x 110 mm^2 and was made of solid acrylic rods. Rod diameter d of 3.2, 4.8, and 6.4 mm were investigated. In addition, the number of rods for each grid varied from 2 x 12, 2 x 10, 2 x 8, and 2 x 6 giving 9.2, 11.0, 13.8, and 18.3 mm in mesh M (center to center distance between two rods), respectively. In total, there were 11 types of grids as the last combination of d = 6.4 mm and M = 9.2 mm was omitted due to the very high grid solidity ratio (d/M). The rods were arranged in a biplane form with the geometry described in Table 2.1 and Figures 2.2 and 2.3. Four holding rods with diameter of 4.8 mm held the grid at each of its corners to avoid any disturbance in the middle region.

The grid was oscillated inside a 2L standard Hudson jar with a size of 115 mm x 115 mm x 150 mm (Hudson and Wagner 1981). The grid was vertically oscillated with a stroke of 135 mm giving about 7 mm free space in the bottom and upper part of the water volume. Five different vertical grid speeds v_{GS} were used for each case: 10, 40, 70, 100, and 130 mm/s. In the vertical direction, 3 levels of sampling position were chosen: y = 0, -25, and -50 mm, i. e. distances from the middle part of the grid stroke (see Figure 2.2). While, 6 to 9 symmetrical sampling points were chosen in the

horizontal plane of measurement (see Figure 2.3). These points of measurement were assumed to be able to represent the turbulent characteristics in both horizontal and vertical points of measurement.

The turbulent parameter measurement was conducted using a laser doppler anemometer (LDA). The instrument consisted of several main parts, including a laser generator, transmitter, receiver, data processor, and a pair of computers with laser software for inputting, analyzing, and displaying the data. The LDA was set to obtain a minimum 1500 samples for each sampling point with a data rate up to 40 data / second. The velocity bandwidth was adjusted from 0.12 to 0.4 MHz depending on the v_{GS}. The water was seeded using TiO_2 to improve its light scattering property. The temperature was found to be constant at 20 ± 0.5 °C from one test to another. Figure 2.4 shows the LDA components used in this study. Details on the operation of the LDA can be found in Stanley (1995).

2.3 EXPERIMENT RESULT AND ANALYSIS

Considering the vertical movement of the grid, vertical direction was assumed to be the main axis (y) with the velocity component "v". Velocity component "u" was applied for horizontal direction (x). The other horizontal velocity component "w" in z direction was not measured in this experiment. Its turbulent characteristics were assumed to be equal to those of the x direction as commonly assumed in the case of grid turbulent study (Batchelor and Townsend 1948).

In the case of turbulent flow, the instantaneous velocity can statistically be

separated into mean and fluctuation (or turbulent) velocity components. From this, the root mean square (rms) turbulent velocity can be calculated as an absolute turbulent velocity fluctuation from the mean velocity. In the case of y direction, notations V, $\overline{V}$, v, and v' will be applied as the instantaneous, mean, fluctuation (turbulent), and rms turbulent velocities, respectively. U, $\overline{U}$, u, and u' are the related notations applied in the case of x direction.

In this study, the emphasis is given to the rms turbulent velocity measurement which is responsible in producing shear and mixing energy for floc aggregation and break up. However, in the case of impeller mixing the rms turbulent velocities have been observed to consist of random and periodic components. The periodic component (also known as the pseudo turbulence) is caused by the convective velocity produced by the impeller movement. This periodic component does not contribute significantly to the turbulent dissipation rate and shear in water and should therefore be eliminated (Van't Riet et al. 1976; Wu et al. 1989; Wu and Patterson 1989; Stanley 1995; and Stanley and Smith 1995). The analysis can be done as explained in detail by Wu and Patterson (1989):

$$v'^2_{total} = v'^2_{random} + v'^2_{periodic} \qquad (2.1)$$

The periodic component can be found using the time auto correlation function $R(\tau)$. The auto correlation function for the v velocity is defined as:

$$R(\tau) = \frac{\overline{v(t)v(t-\tau)}}{v'^2} \qquad (2.2)$$

where τ is the time interval, while the overbar sign indicates the time average of the turbulent velocity. In the case of impeller mixing, the $R(\tau)$ function (especially in the impeller region) forms a distinct periodic component rather than a typical asymptotic line as observed in traditional grid turbulent studies. As explained by Tennekes and Lumley (1972), positive and negative values in the $R(\tau)$ function may be caused by backmixing within the mixing region. This basically agrees with the previous finding that the periodic component is caused by convective velocity produced by the impeller movement. This periodic component can be fitted using a group of cosine functions as shown by Wu and Patterson (1989).

A similar case was also observed in this study. Figure 2.5 shows the $R(\tau)$ function for grid no. 1 at v_{GS} = 10 mm/s and y = 0 mm. The first positive peak is the time for the grid to complete 1 full stroke. The amplitude A and frequency f were found to be 0.52 and 0.037 Hz, respectively. The appropriate cosine function was found to be:

$$A\cos(2\pi f\tau) \qquad (2.3)$$

It is assumed that after a certain period of τ, the random turbulent component has

disappeared leaving only the constant periodical function (Wu and Patterson 1989). The v' random component can then be separated from the total v' using Equation 2.1 above. From now on, the term v' will be used as the random or corrected value of the rms turbulent velocity v'. In the case of u', no corrections were made since the $R(\tau)$ functions did not show any periodic components.

After the values of u' and v' have been obtained, it is possible to calculate the degree of isotropicity that can be defined as:

$$\text{isotropicity} = \frac{u'}{v'} \qquad (2.4)$$

In the case of isotropic turbulence, the value should be unity. However, a study by Comte-Bellot and Corrsin (1966) showed that even in an enhanced grid turbulence system, a 100% isotropic turbulence could not be achieved. In this study, no effort was made in improving the degree of isotropicity. The small size of the jar was also a major concern as it did not provide a "free turbulence" condition as it should be in the isotropic grid turbulence theory. It was therefore expected that the degree of isotropicity would be low. Figure 2.6 shows that the degree of isotropicity for grid no. 9 at y = 0 mm at the slowest and fastest v_{GS} (10 and 130 mm/s) varies with the horizontal points of measurement and is generally low.

Due to the turbulent anisotropicity, it was therefore necessary to use the average rms turbulent velocity q' instead of using individual u' or v'. By assuming that

w' = u', this following equation can be derived:

$$q' = \sqrt{\frac{1}{3}(v'^2 + 2u'^2)} \qquad (2.5)$$

Figure 2.7 shows the characteristics of q' vs. horizontal points of measurement for grid no. 9 at y = 0 mm and at v_{GS} of 10 to 130 mm/s. Some variations of q' are observed, however these can be considered small at least in comparison to impeller mixing studies (see the discussion below). The average q' was then calculated and assumed to be the characteristic value for each horizontal plane of measurement.

Figure 2.8 shows the profiles for $\overline{q'}$ (as the average q' value for each horizontal plane of measurement) vs. v_{GS} for grid no. 9 for three different vertical levels of measurement and five different v_{GS}. It was found for each type of grid that $\overline{q'}$ could be related to the v_{GS} in a linear equation as:

$$\overline{q'} = m\,[v_{GS}] \qquad (2.6)$$

The m value for each type of grid at different y position can be seen in Table 2.1. All of the coefficients of determination R^2 values were found to be well above 0.99. It can be noticed that m is almost constant for each type of grid regardless the vertical y position. Appendix 1 shows complete data for all types of grids.

The average m value for three different vertical levels of measurement can be obtained for each type of grid. The coefficient of variation (COV = standard deviation / average value) has been found to be small for each case (see Appendix 1). The average m value can then be assumed as the turbulent mixing characteristics for each type of grid. This finding shows that the turbulent parameters created by the grid mixing are practically constant both at horizontal and vertical points of measurement.

Subsequently, it is possible to get a relation among M, d, and m. Figure 2.9 shows the non - dimensional relation between m and solidity ratio (d/M) that can be represented as:

$$m = 0.62\,[d/M] + 0.11 \qquad (2.7)$$

with an R^2 value of 0.927.

Information about mean velocities $\overline{U}$ and $\overline{V}$ is not the interest of this study. As the grid moved up and down constantly, both average values at any horizontal planes should be zero. Some variations can be observed as a result of either flow circulation inside the jar, measurement errors, or imperfection of the equipment design. Figure 2.10 shows some variations in $\overline{V}$ for grid no. 9 at y = 0, -25, and -50 mm for five different v_{GS}. In this case, $\overline{V}$ is the average value for all points at each vertical level of measurement. v' (also the average value for the related level of measurement) is also presented. It can be seen that $\overline{V}$ values are small in comparison

to the related v' values and therefore can be assumed to be zero. A similar finding was also observed for $\overline{U}$ measurement. Appendix 3 shows complete data for $\overline{U}$ and $\overline{V}$ measurements.

2.4 VOLUME AVERAGE TURBULENT PARAMETERS

Average volume turbulent parameters, i.e. energy dissipation rate $\overline{\varepsilon}$ (mm^2/s^3) and velocity gradient $\overline{G}$ (s^{-1}), can be calculated based on drag force F_D (g mm/s^2) produced by the mixing device as follows (Camp, 1955 and Amirtharajah, 1978):

$$F_D = \frac{1}{2} \overline{V_R^2} C_D A_s \rho \qquad (2.8)$$

$$\overline{\varepsilon} = \frac{\overline{V_R} F_D}{\rho V} \qquad (2.9)$$

$$\overline{G} = \sqrt{\frac{\overline{\varepsilon}}{\nu}} \qquad (2.10)$$

where: $\overline{V_R}$ = relative mean velocity between mixing device (in this case is the grid) and fluid (mm/s), C_D = grid drag coefficient, A_s = grid solid area (mm^2), ρ = fluid density (g/mm^3), V = fluid volume (mm^3), and ν = fluid kinematic viscosity (mm^2/s).

In the case of impeller mixing studies, $\overline{V_R}$ is very difficult to be identified. $\overline{\varepsilon}$ is usually obtained from a torque meter that measures the drag force created by the impeller within the fluid. However, in the case of vertically oscillating grid mixing, $\overline{U}$ and $\overline{V}$ were found to be practically zero. $\overline{V_R}$ can then be assumed to be equal to v_{GS} ($\overline{V_R} \approx v_{GS}$). The length scale calculation below will confirm that this assumption is acceptable. This leaves only one unknown parameter C_D to be identified in Equation 2.8.

In this study, the grid drag coefficient C_D was calculated based on literature information. There have been numerous studies completed investigating the characteristics of many types of grids and screens including the porosity, pressure loss coefficient, and drag force. Porosity α and drag coefficient C_D of the biplane circular rod grid can be obtained based on these following equations (Laws and Livesey 1978 and Baines and Peterson 1951):

$$\alpha = (1 - \frac{d}{M})^2 \qquad (2.11)$$

$$C_D = \frac{\lambda}{(1-\alpha)} \qquad (2.12)$$

where: d = rod diameter (mm), M = mesh (mm), and λ = pressure loss coefficient. As

compiled by Pinker and Herbert (1967), the pressure loss coefficient λ can be obtained as a combination between grid geometric factor C and rod Reynolds number (Re_d):

$$\lambda = C\, f(Re_d) \tag{2.13}$$

$$Re_d = \frac{\overline{V_R}\, d}{\nu} \tag{2.14}$$

where: $\overline{V_R}$ is the fluid relative velocity or in this case is equal to v_{GS}. The identification of C and $f(Re_d)$ is slightly complicated. There have been studies conducted to obtain the values of C and $f(Re_d)$ (Annand 1953 and Pinker and Herbert 1967). Laws and Livesey (1978) and Roach (1987) summarized the findings to provide these following equations:

$$C = \frac{(1-\alpha^2)}{\alpha^2} \tag{2.15}$$

$$f(Re_d) = 0.52 + \frac{66}{Re_d^{4/3}} \tag{2.16}$$

Figure 2.11 shows some variations of $\overline{G}$ with respect to the types of grids and v_{GS}. Subsequently, $\overline{G}$ vs. Re_d profiles can also be developed as shown in Figure

2.12. Referring to Schubauer as cited by Baines and Peterson (1951) and Roach (1987), circular biplane grid mixing reaches turbulent regime when $Re_d > 100$ (see Equations 2.13 to 2.16 for the effect of low Re_d to the pressure loss coefficient). Based on Figure 2.12, this value roughly corresponds to $\overline{G} > 20\ s^{-1}$. Referring to Camp (1955), $\overline{G}$ values in the range of 20 to 74 s^{-1} are the optimum mixing intensity for floc aggregation. This indicates that grids will produce turbulent mixing at their most common practical $\overline{G}$ values.

The average macro length scale L (mm), representing the average size of eddy produced by the turbulent mixing or the characteristic length of the mixing device, can be calculated based on this simple dimensional analysis (Tennekes and Lumley, 1972):

$$L \sim \frac{q'^3}{\overline{\varepsilon}} \qquad (2.17)$$

The sign "~" indicates proportionality in the order of unity. For the sake of simplicity, this sign can be changed into equality sign ("=") giving an approximation value of L. Equation 2.17 basically involves two parameters: q' which was experimentally obtained using the LDA and $\overline{\varepsilon}$ which was calculated from the drag force.

Figure 2.13 shows that L is constant at high v_{GS} or when turbulent mixing regime has been achieved. This corresponds to $v_{GS} > 40$ mm/s for low solidity ratio types of grids or $Re_d > 200$. Smaller v_{GS} were monitored for high solidity ratio types

of grids. This finding agrees with the previous argument that turbulent regime is achieved when $Re_d > 100$. This finding is also in accordance with impeller mixing studies that the macro length scale in turbulent mixing regime should be constant (Stanley 1995 and Cheng et al. 1997). The average L value at high v_{GS} can then be assumed as the characteristic length of the related type of grid. This figure also shows that L is proportional to either grid diameter d or mesh M. This can clearly be seen in Figure 2.14 (L/M vs. d/M profiles). The dimensionless L (L/M) values are small at both low and high d/M values, and reach a maximum value at medium d/M values. This can physically be explained as follows. When a low d/M type of grid is applied, the size of eddy will be proportional to the rod diameter d (which is small). However, when a high d/M type of grid is used, the size of eddy will be proportional to the grid mesh or spacing (which is also small). In short, Figures 2.13 and 2.14 indicate that L is proportional to the physical characteristics of the mixing grid as it should be in reality. This basically verifies the validity of the assumption $\overline{V_R} \approx v_{GS}$ taken above. This also confirms that $\overline{\varepsilon}$ (and also $\overline{G}$) values obtained from the drag force calculation are correct.

The Kolmogoroff microscale η (defined as the smallest sustainable size of eddy) can then be calculated using a simple dimensional analysis (Tennekes and Lumley 1972):

$$\eta = [\frac{\nu^3}{\varepsilon}]^{1/4} \qquad (2.18)$$

This equation calculates the average size of η based on the average volume energy dissipation rate $\overline{\varepsilon}$. Figure 2.15 shows η vs. v_{GS} for grids nos. 1, 5, and 9 representing low, medium, and high solidity ratio types of grids. This information can be used to compare the turbulent mixing intensity created by different types of grids. This is also useful when analyzing floc break up mechanisms. Most models have been developed based on two conditions: when η is larger or smaller than the particle size or known as the viscous and inertial turbulent regimes (Parker et al. 1972 and others). In the viscous turbulent regime, laminar shear is dominant causing little shear stress on flocs, while turbulent shear becomes dominant in the inertial turbulent regime causing significant shear stresses on flocs.

2.5 DISCUSSION

One of the most important parts of this study is to show that the turbulent mixing intensity, represented by the average rms turbulent velocity q', is relatively constant at all points of measurement. It is therefore necessary to present this part of study in a separate section. As can be seen in Figure 2.7 above, the q' values at 9 horizontal points of measurement for grid no. 9 at y = 0 mm are relatively constant. For v_{GS} = 10 mm/s, the average of q' value is 3.65 mm/s with the standard deviation

(SD) of 0.72 mm/s. The coefficient of variation (COV = SD / average q') can then be calculated as 0.20 and the ratio between the maximum and minimum values of q' (range) is equal to 1.70. The complete results for all of the eleven types of grids and five v_{GS} can be seen in Figures 2.16 and 2.17. These figures show the COV and range for each type of grid at five different v_{GS} at y = 0 mm. Results for y = -25 and -50 mm show the same trend as that of y = 0 mm (see Appendix 1). Both figures show that in the case of medium to high v_{GS} (40 to 130 mm/s), the COV and range values are small. Most of the COV and range values are less than 0.25 and 2, respectively. Higher variations are observed for v_{GS} = 10 mm/s. Based on this finding, the average q' value for each horizontal plane of measurement can therefore be assumed as the characteristic turbulent intensity for the related plane of measurement. Variation of q' values among three different vertical planes of measurement represented by the linear line slope m (= q' / v_{GS}) can be seen in Table 2.1. It is evident that m values are quite constant. An average value can then be calculated for each type of grid. Table 1 shows that the COV for m values are small indicating that q' variation in the vertical direction is small.

As a comparison, impeller mixing studies have shown more significant variations in the turbulent mixing intensity within a vessel. Detailed variations in the root mean square (rms) of radial velocities can be seen in Mujumdar et al. (1970), Wu and Patterson (1989), Wu et al. (1989), Stanley (1995), and Stanley and Smith (1995). They applied different types of impellers and water vessels, however the results basically agreed with each other. The radial and vertical (r, y) coordinate systems were

used to identify the measurement points. The impeller center line served as the initial point (0, 0). The tangential coordinate was not considered since the mixing behavior was assumed to be symmetrical in this direction. In general, the closer the point to the impeller the higher its rms radial turbulent velocity. The maximum velocity was observed at the impeller tip (r = impeller radius, y = 0). In order to simplify the comparison, the velocity in this point is assumed to be unity, then velocities at (r = impeller radius, y = 0.5 impeller width), (r = impeller radius, y = impeller width), and (r = 2.3 impeller radius, y = impeller width) are: 0.5, 0.2, and 0.3. This means that the ratio between the maximum and minimum values of the rms turbulent radial velocity in the vessel can be as high as 5. The same behavior can also be seen in the case of the rms turbulent tangential velocity. A slightly different measurement was conducted by Cheng et al. (1997) by dividing the vessel into several rectangular areas. The turbulent mixing measurement was conducted within each of the area in which some turbulent variations were monitored. At a certain area, the difference between the highest and lowest rms of horizontal velocity was about 6.

Another comparison that can be made is the intensity of turbulent mixing created by both mixing devices. This can be made by comparing η vs. $\overline{G}$ profiles from grid mixing with standard impeller mixing as can be seen in Figure 2.18. Note: different types of grids will produce the same η at a given $\overline{G}$ but at a different v_{GS}. The impeller mixing results were taken from Stanley and Smith (1995) and Stanley (1995). This figure shows that grid mixing in the $\overline{G}$ range of 20 to 74 s^{-1} (which is

the optimum mixing intensity according to Camp 1955) produces basically the same turbulent mixing intensity as that of jar mean values created by the impeller. Their values are less than those of impeller region values indicated by larger η values. This indicates that grid mixing produces roughly the same intensity of turbulent mixing as that of standard impeller mixing but with less turbulent variation.

2.6 CONCLUSIONS

This study has shown that the oscillating grid mixing device produces relatively constant average root mean square (rms) turbulent velocity q' values at any points of measurement. This indicates that characteristic of the turbulent mixing is spatially uniform in comparison to that of impeller mixing even though the intensity of turbulent mixing has been found to be roughly the same.

Average volume velocity gradient $\overline{G}$ vs. vertical grid speed v_{GS} profiles have been obtained for each type of grid. Since the turbulent mixing intensity is uniform within the vessel, $\overline{G}$ may be used as the surrogate mixing intensity parameter. q' and $\overline{G}$ can also easily be controlled from the vertical grid speed and grid physical characteristics (solidity ratio) that basically gives a major practical advantage of using grids as a mixing device.

Results obtained from this study provide the first information needed to investigate the overall performance of the vertically oscillating grid mixing device to promote floc aggregation. A direct flocculation study by means of the vertically

oscillating grid mixing device will be conducted as the follow up of this study. This can be found in Chapter 3. It is expected that the grid mixing will give an optimum mixing environment for floc aggregation.

2.7 REFERENCES

Amirtharajah, A. (1978). "Design of rapid mixing units." *Water Treatment Plant Design*, R. L. Sanks, editor. Ann Arbor Science Inc., Ann Arbor, Michigan. 131 - 148.

Amirtharajah, A. and Tambo, N. (1991). "Mixing in water treatment." *Mixing in Coagulation and Flocculation*, A. Amirtharajah, M. M. Clark, and R. R. Trussell, editors. AWWA, Denver, Colorado, 3 - 34.

Annand, W. J. D. (1953). "The resistance to air flow of wire gauzes." *Journal of the Royal Aeronautical Society*, 57, 141 - 146.

Baines, W. D. and Peterson, E. G. (1951). "An investigation of flow through screens." *Transactions of the ASME*, 73, 467 - 480.

Batchelor, G. K. and Townsend, A. A. (1948). "Decay of isotropic turbulence in the initial period." *Proceedings of the Royal Society, A.* 193, 539 - 557.

Brumley, B. H. and Jirka, G. H. (1987). "Near - surface turbulence in a grid - stirred tank." *Journal of Fluid Mechanics*, 183, 235 - 263.

Camp, T. R. (1955). "Flocculation and flocculation basin". *Transactions of ASCE*. Paper No. 2722, 1 - 16.

Camp, T. R. and Stein, P. C. (1943). "Velocity gradients and internal work in fluid

motion." *Journal of Boston Society of Civil Engineers*, 30 (10), 219 - 237.

Cheng, Chen-Yu, Atkinson, J. F., and Bursik, M. I. (1997). "Direct measurement of turbulence structures in mixing jar using PIV." *Journal of Environmental Engineering*, 123 (2), 115 - 125.

Comte-Bellot, G. and Corrsin, S. (1966). "The use of a contraction to improve the isotropy of grid - generated turbulence." *Journal of Fluid Mechanics*, 25, 657 - 682.

Dickey. T. D and Mellor, G. L. (1980). "Decaying turbulence in stratified and normal fluids." *Journal of Fluid Mechanics*, 99, 13 - 31.

Hudson, H. E. Jr. and Wagner, E. G. (1981). "Conduct and use of jar tests." *Journal AWWA*, 73 (4), 218 - 224.

Kostazos, A. E., Apikides, P. S., Kastrinakis, E. G., and Nychas, S. G. (1994). "Oscillating grid turbulence and bulk mixing at high schmidt numbers." *Canadian Journal of Chemical Engineering*, 72, 431 - 439.

Kresta, S. M. and Wood, P. E. (1993). "The flow field produced by a pitched blade turbine: characterization of the turbulence and estimation of the dissipation rate." *Chemical Engineering Science*, 48 (10), 1761 - 1774.

Laws, E. M. and Livesey, J. L. (1978). Flow through screens. *Annual Review of Fluid Mechanics*, 10, 247 - 266.

Long, R. R. (1978). "Theory of turbulence in a homogeneous fluid induced by an oscillating grid." *Physics of Fluids*, 21 (10), 1887 - 1888.

Mujumdar, A. S., Huang, B., Wolf, D., Weber, M. E., Douglas, W. J. M. (1970).

"Turbulence parameters in a stirred tank." *Canadian Journal of Chemical Engineering*, 48, 475 - 483.

Parker, D. S., Kaufman, W. J., and Jenkins, D. (1972). "Floc breakup in turbulent flocculation processes." *Journal of the Sanitary Engineering Division, ASCE.* 98, (SA1), 79 - 99.

Pinker, R. A. and Herbert, M. V. (1967). "Pressure loss associated with compressible flow through square - mesh wire gauzes." *Journal of Mechanical Engineering and Science*, 9 (1), 11 - 23.

Roach, P. E. (1987). "The generation of nearly isotropic turbulence by means of grids." *Journal of Heat and Flow*, 8 (2), 82 - 92.

Stanley, S. J. (1995). "Measurement and analysis of mixing as it relates to flocculation." *Ph.D. Thesis*, University of Alberta, Edmonton, Alberta.

Stanley, S. J. and Smith, D. W. (1995). "Measurement of turbulent flow in standard jar test apparatus." *Journal of Environmental Engineering*, 121 (12), 902 - 910.

Taylor, G. I. (1935a). "Statistical theory of turbulence. Part I." *Proceedings of the Royal Society, A.* 151, 421 - 443.

Taylor, G. I. (1935b). "Statistical theory of turbulence. Part II." *Proceedings of the Royal Society, A.* 151, 444 -454.

Tennekes, H. and Lumley, J. L. (1972). *A First Course in Turbulence*, MIT Press. Cambridge, Massachusetts.

Thompson, S. M. and Turner, J. S. (1975). "Mixing across an interface due to turbulence generated by an oscillated grid." *Journal of Fluid Mechanics*, 67,

349 - 368.

Van't Riet, K., Bruijn, W., and Smith, J. M. (1976). "Real and pseudo - turbulence in the discharge stream from a rushton turbine." *Chemical Engineering Science*. 31, 407 - 412.

Wu, H. and Patterson, G. K. (1989). "Laser - doppler measurements of turbulent - flow parameters in stirred mixer." *Chemical Engineering Science*, 44 (10), 2207 - 2221.

Wu, H., Patterson, G. K., and Van Doorn, M. (1989). "Distribution of turbulence energy dissipation rate in a rushton turbine stirred mixer." *Experiments in Fluids*, 8, 153 - 160.

Table 2.1: Grid Geometry and m (q` / VGS)

TYPE OF GRID	GRID CHARACTERISTICS				m = q` / VGS				
	Rod d (mm)	# of Rods	Mesh M (mm)	d/M	y	Slope m	R^2	Average of m	COV of m
1	3.2	2x6	18.3	0.17	0 -25 -50	0.201 0.201 0.206	0.998 0.996 0.996	0.203	0.009
2	4.8	2x6	18.3	0.26	0 -25 -50	0.283 0.296 0.280	0.998 0.999 0.999	0.286	0.025
3	6.4	2x6	18.3	0.35	0 -25 -50	0.377 0.379 0.373	0.999 0.999 0.997	0.376	0.009
4	3.2	2x8	13.8	0.23	0 -25 -50	0.242 0.245 0.236	0.998 0.999 0.997	0.241	0.013
5	4.8	2x8	13.8	0.35	0 -25 -50	0.332 0.334 0.340	0.998 0.995 0.998	0.335	0.011
6	6.4	2x8	13.8	0.46	0 -25 -50	0.410 0.416 0.403	0.999 0.998 0.995	0.410	0.017
7	3.2	2x10	11.0	0.29	0 -25 -50	0.269 0.275 0.278	0.998 0.998 0.997	0.274	0.013
8	4.8	2x10	11.0	0.43	0 -25 -50	0.362 0.385 0.358	0.999 0.999 0.999	0.368	0.038
9	6.4	2x10	11.0	0.58	0 -25 -50	0.452 0.463 0.475	0.998 0.995 0.996	0.463	0.029
10	3.2	2x12	9.2	0.35	0 -25 -50	0.313 0.299 0.303	0.998 0.995 0.994	0.305	0.020
11	4.8	2x12	9.2	0.52	0 -25 -50	0.413 0.408 0.414	0.994 0.999 0.999	0.412	0.008

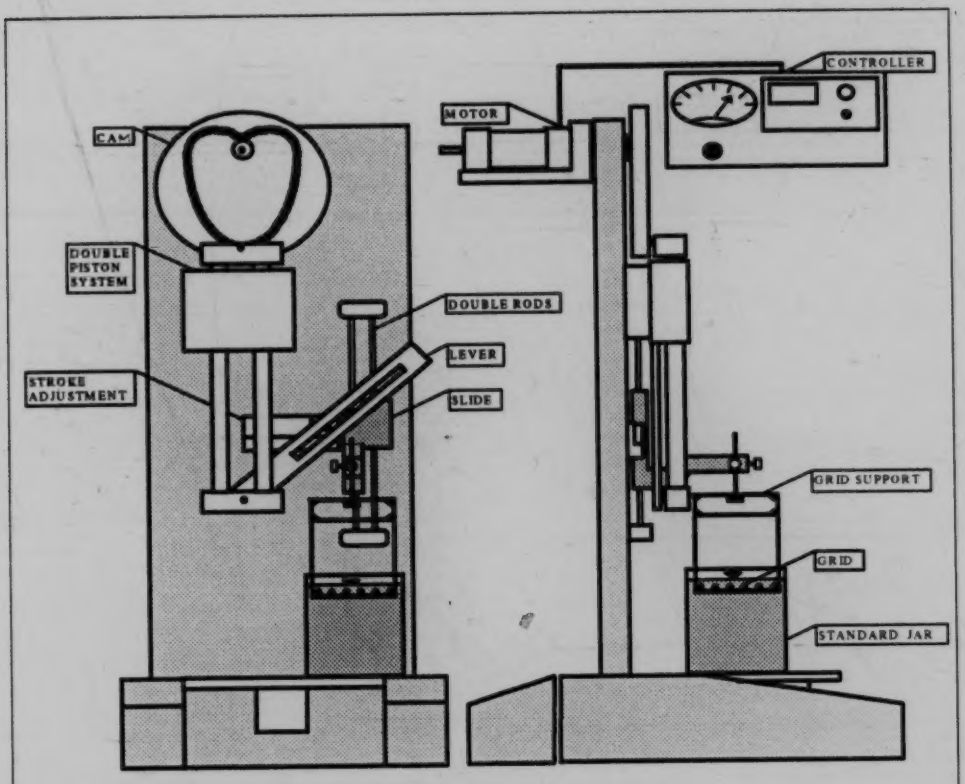

Figure 2.1a: Vertically Oscillating Grid Mixing Device

Figure 2.1b: Vertically Oscillating Grid Mixing Device

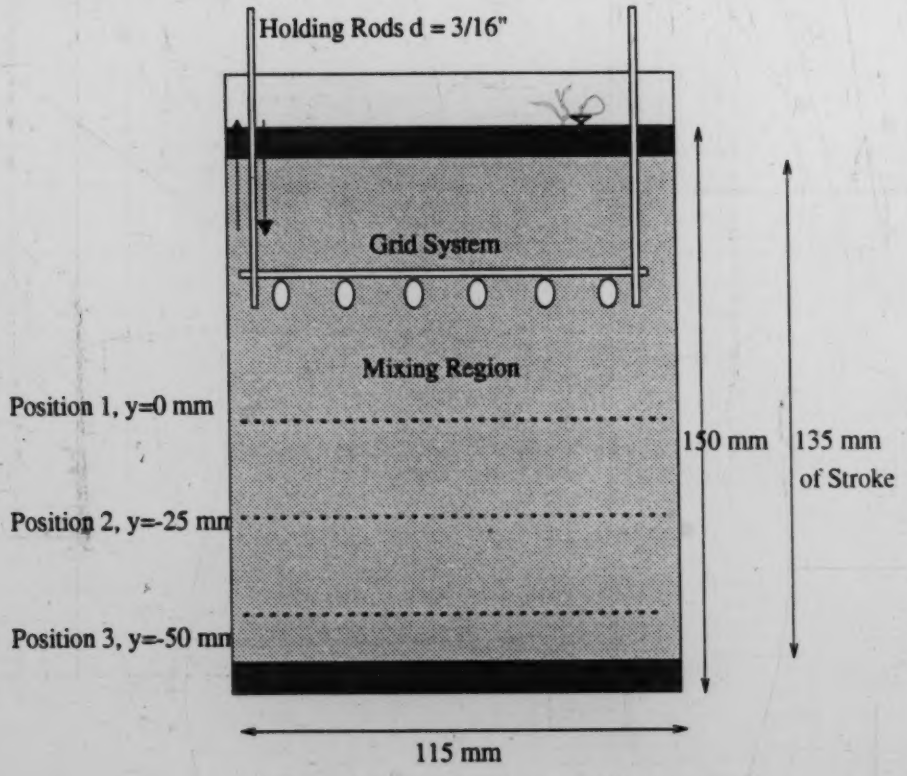

Figure 2.2: Vertical Levels of Measurement

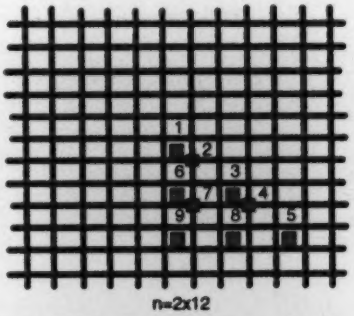

n=2x12

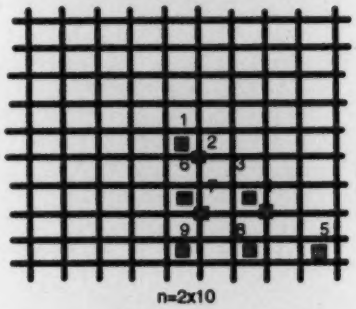

n=2x10

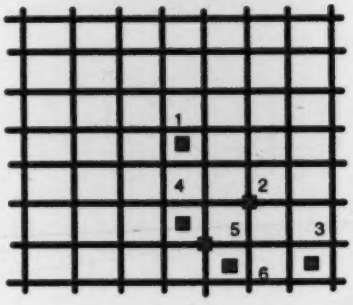

n=2x8

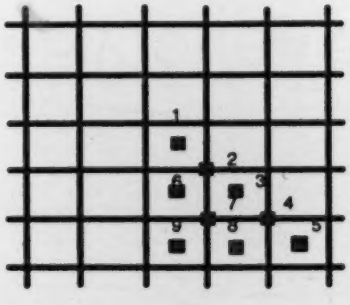

n=2X6

Figure 2.3: Horizontal Points of Measurement

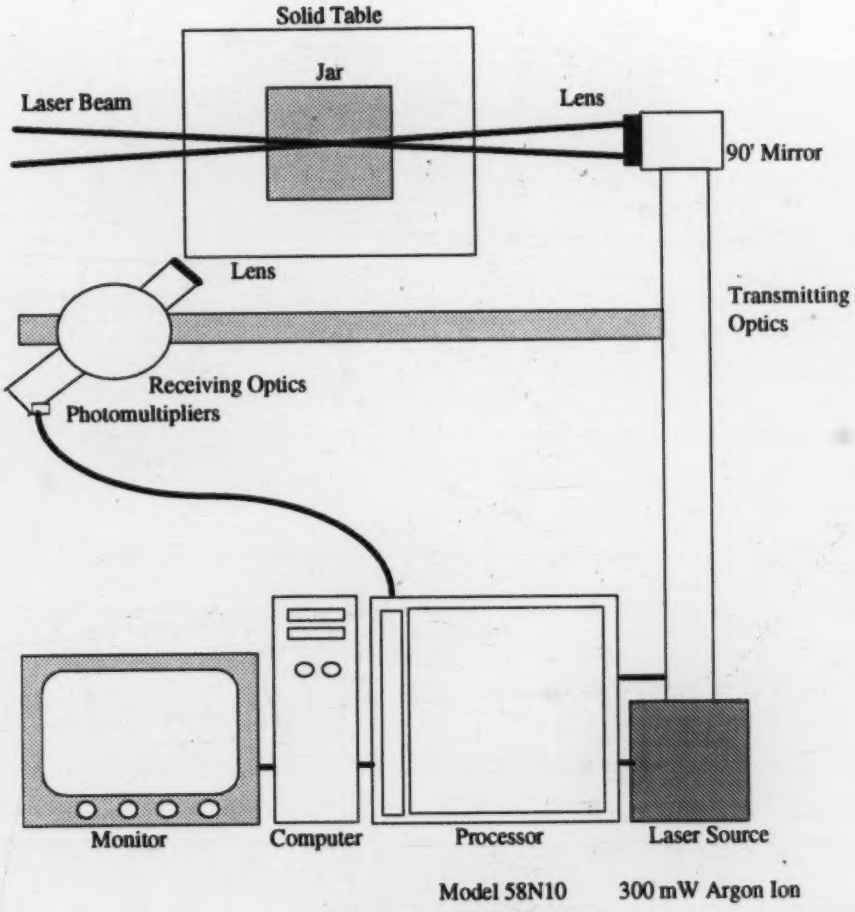

Figure 2.4: LDA System

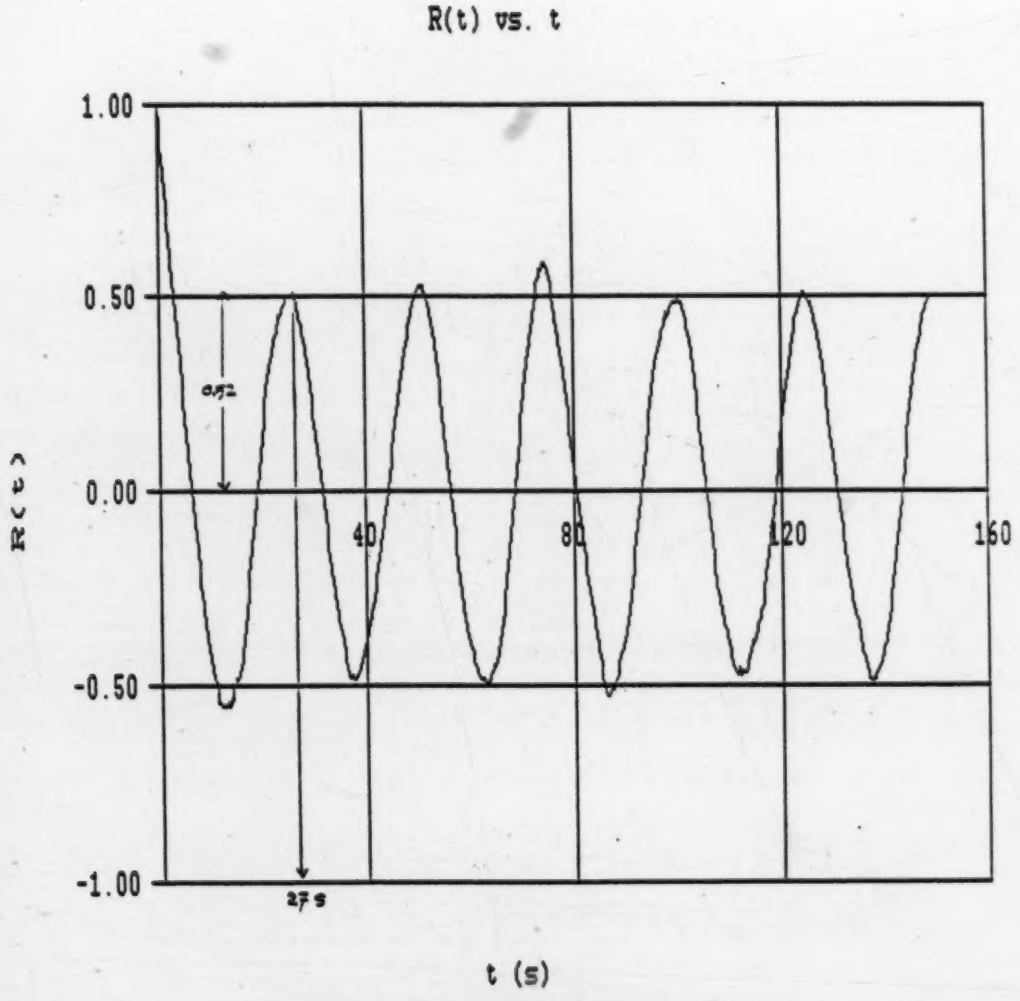

Figure 2.5 : Autocorrelation Correction for Grid No. 1 for Vertical Grid Speed = 10 mm/s and y = 0 mm

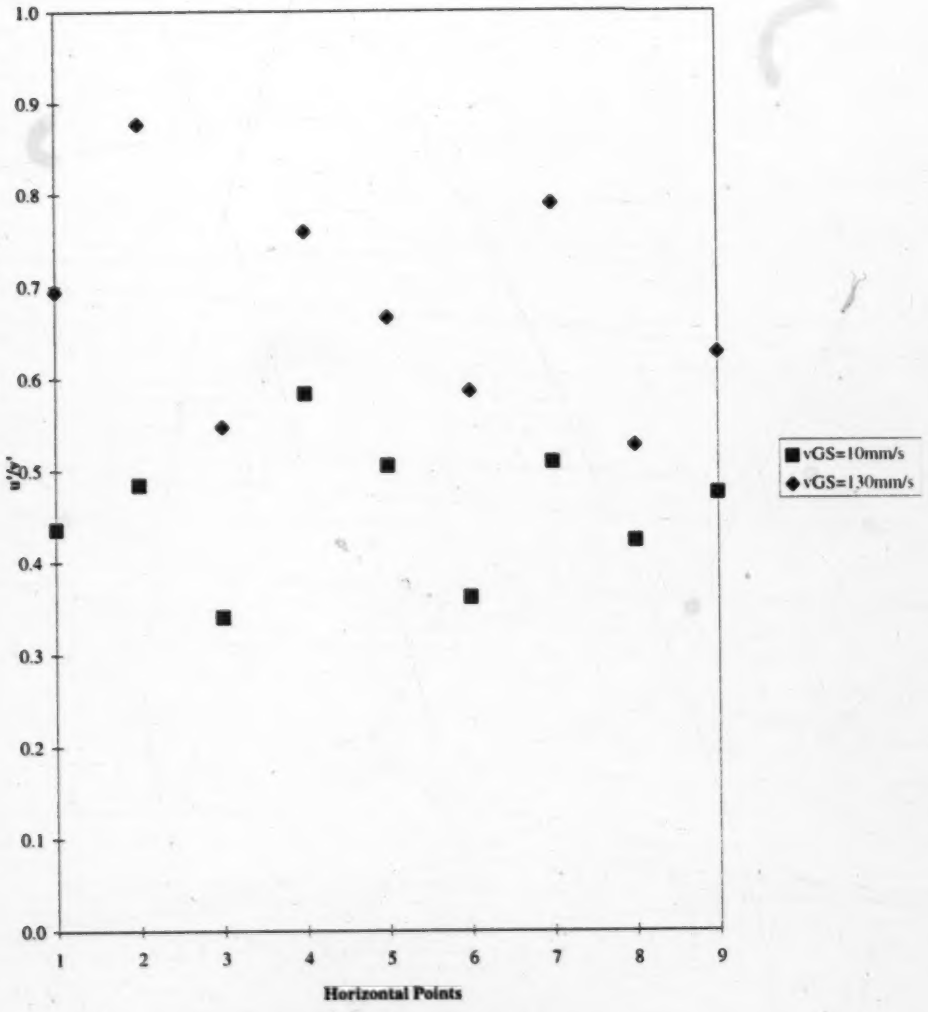

Figure 2.6: Isotropicity vs. Horizontal Points for Grid No.9 at y=0mm

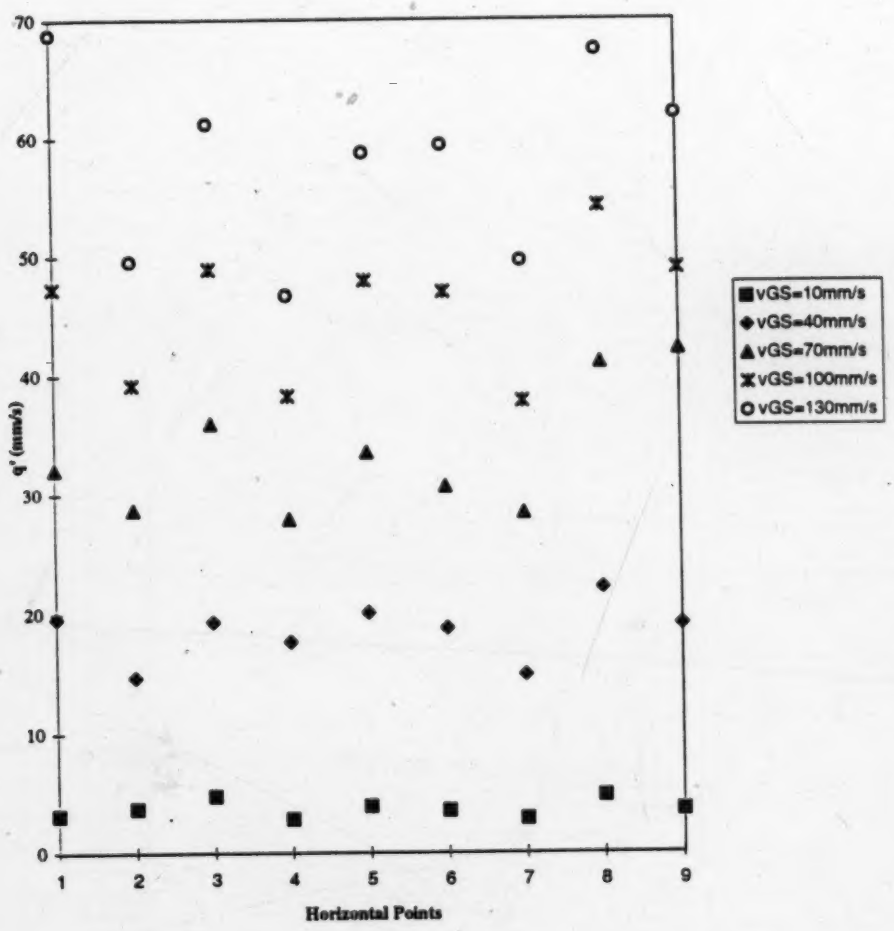

Figure 2.7: Average rms Turbulent Velocity vs. Horizontal Points for Grid No.9 at y=0mm

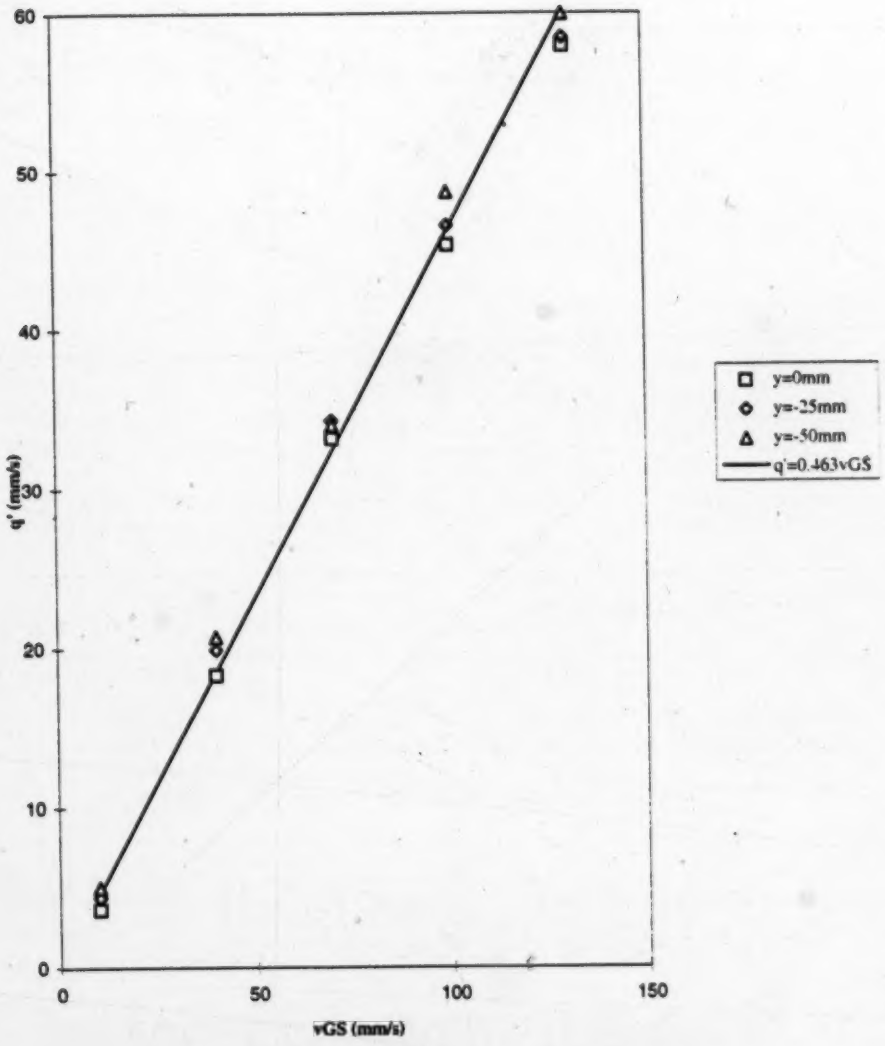

Figure 2.8: Average rms Turbulent Velocity vs. Vertical Grid Speed

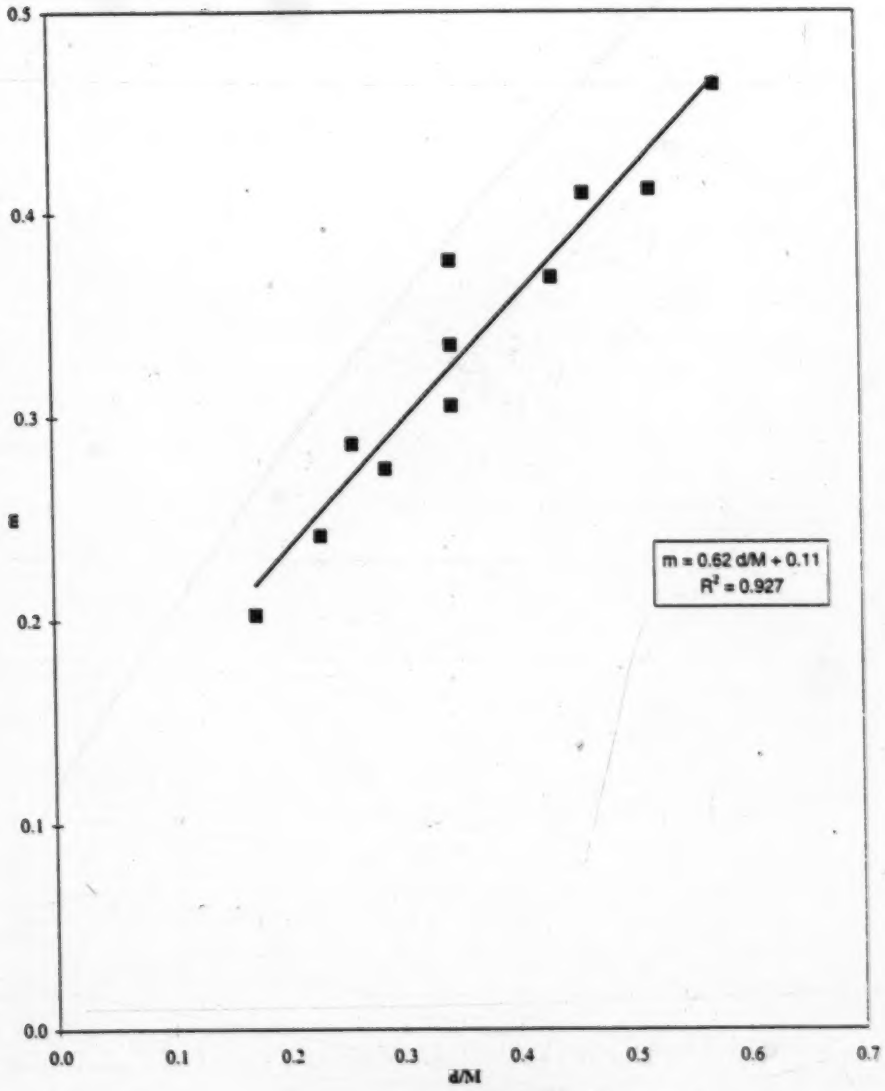

Figure 2.9: Slope vs. Solidity Ratio

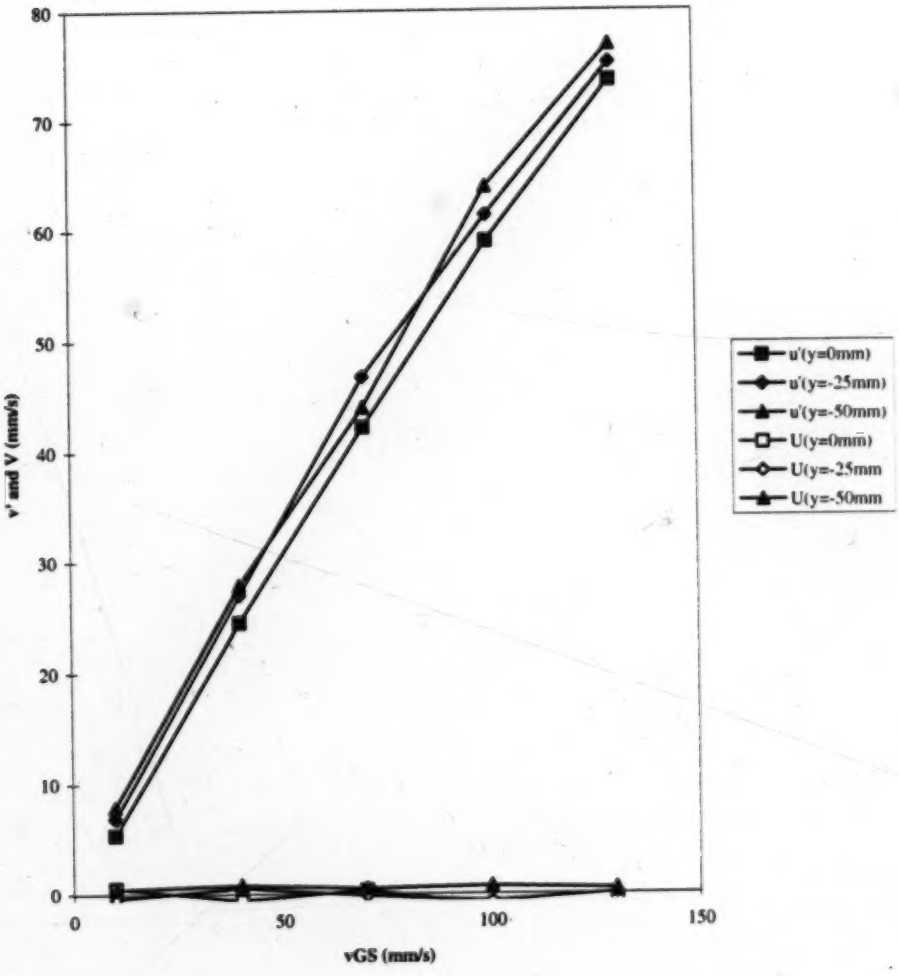

Figure 2.10: Vertical Velocities vs. Vertical Grid Speed for Grid No. 9

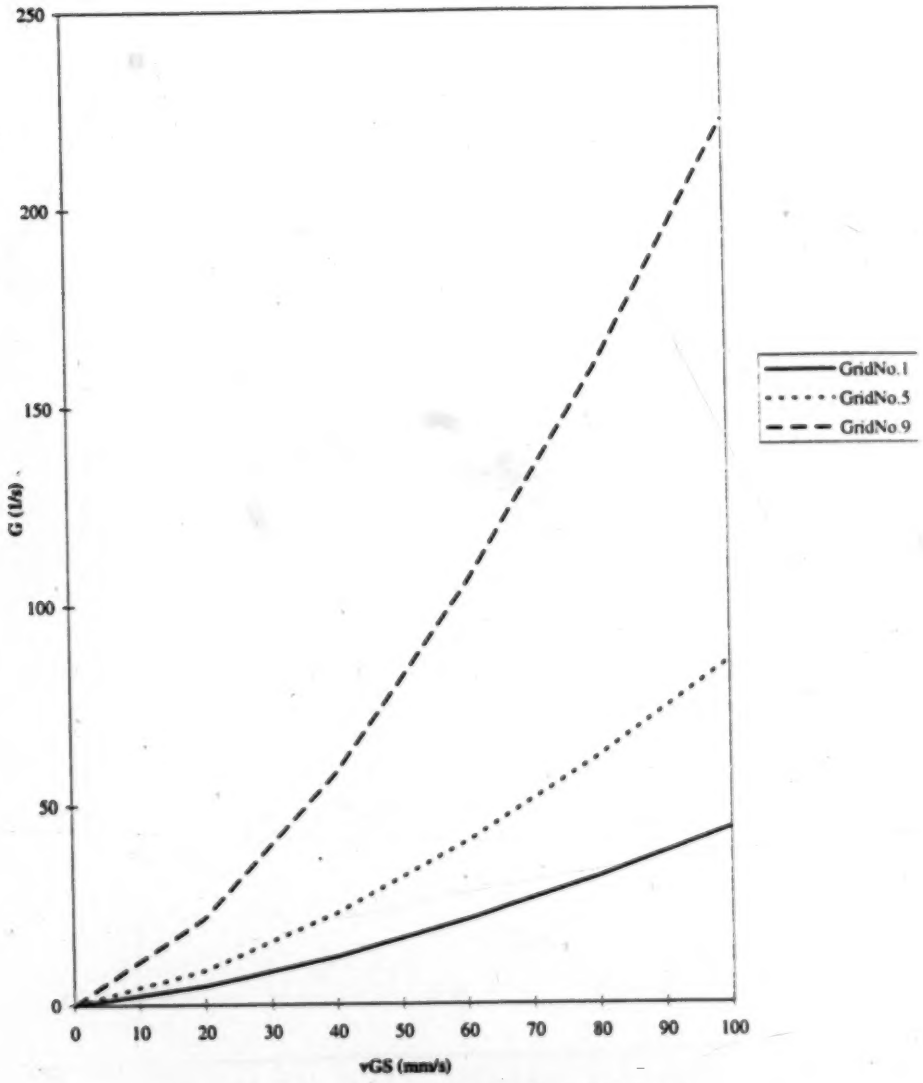

Figure 2.11: Velocity Gradient vs. Vertical Grid Speed

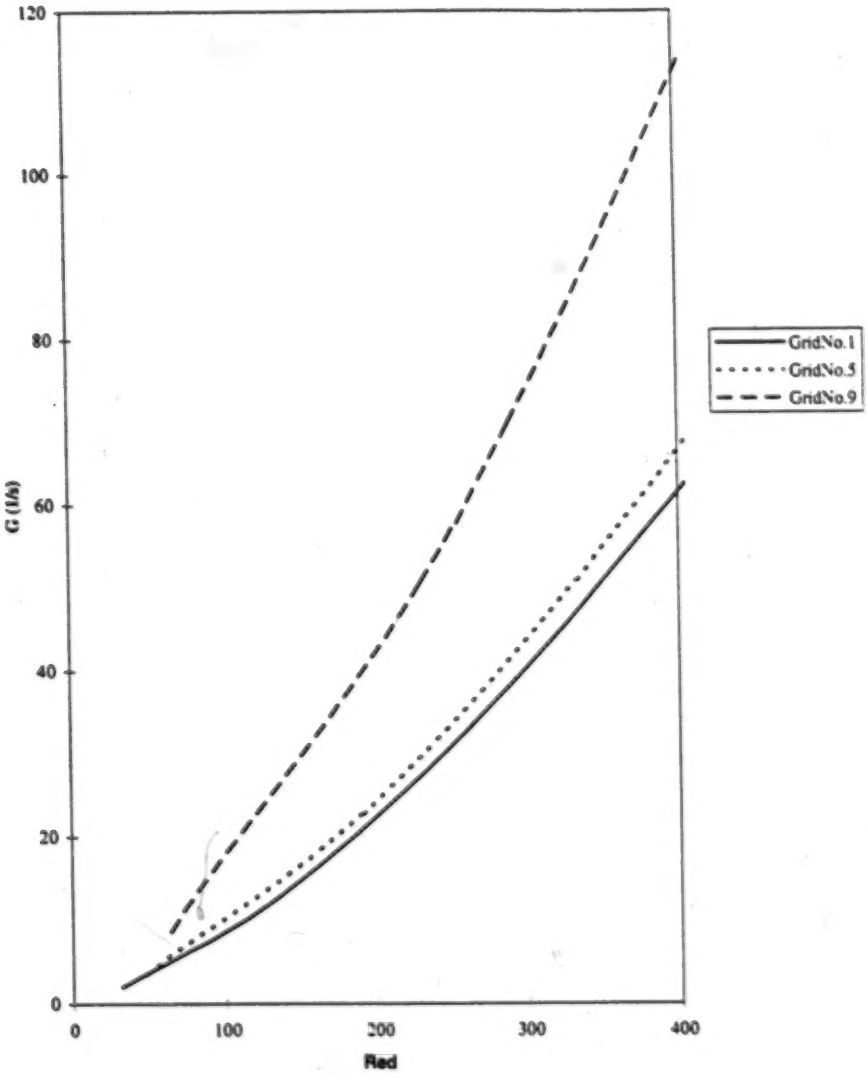

Figure 2.12: Velocity Gradient vs. Reynolds Number

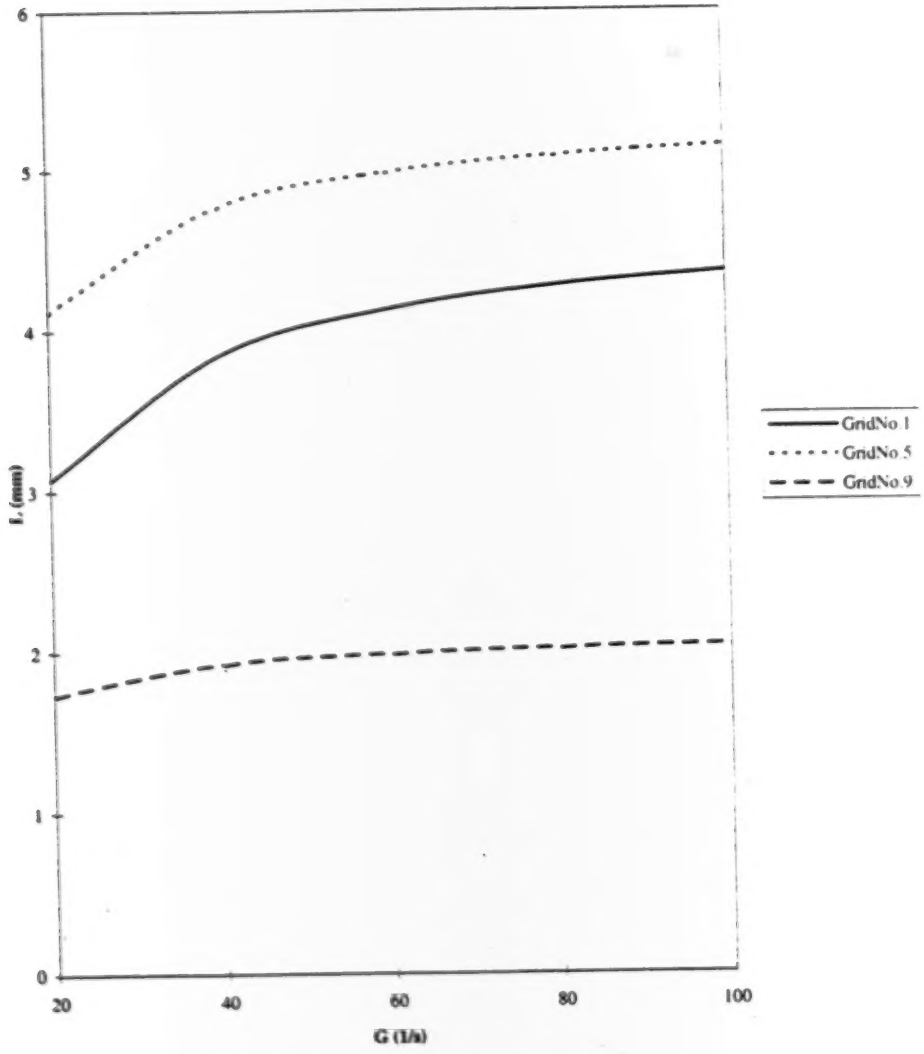

Figure 2.13: Macro Length Scale vs. Velocity Gradient

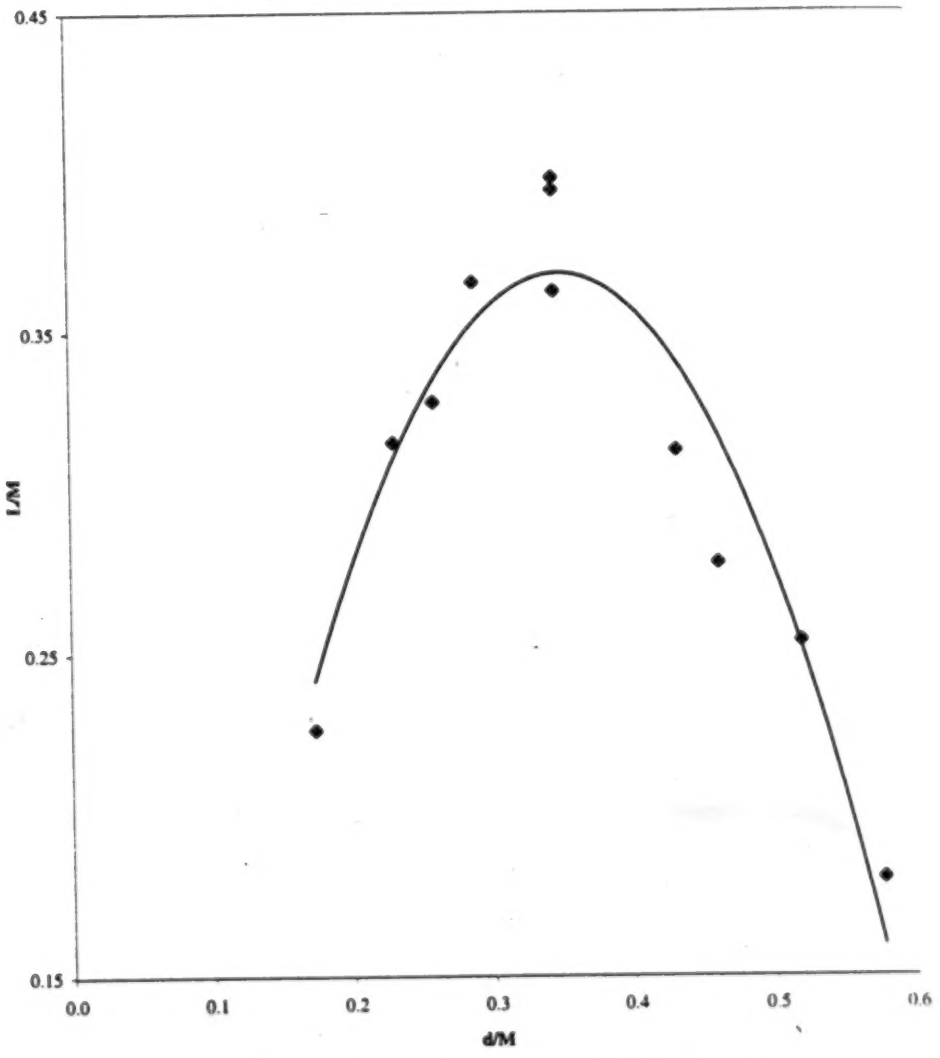

Figure 2.14: Dimensionless Length Scale vs. Solidity Ratio

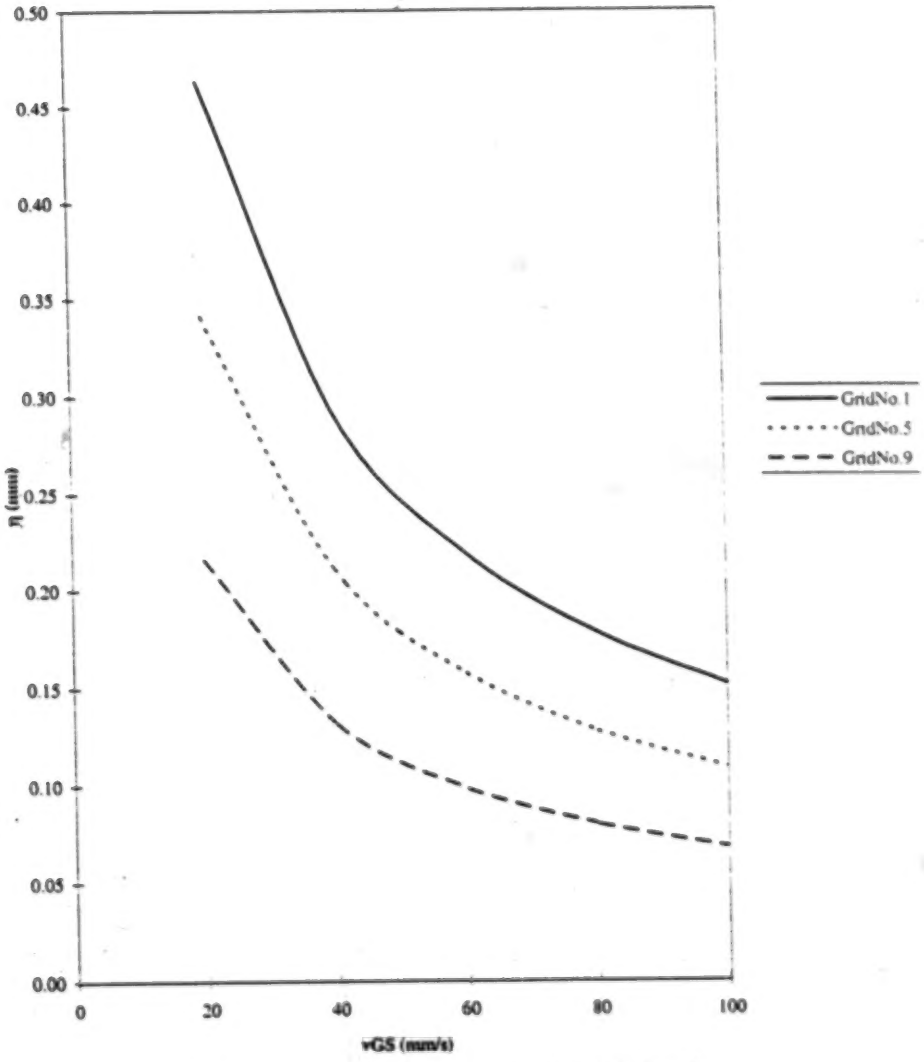

Figure 2.15: Kolmogoroff Microscale vs. Vertical Grid Speed

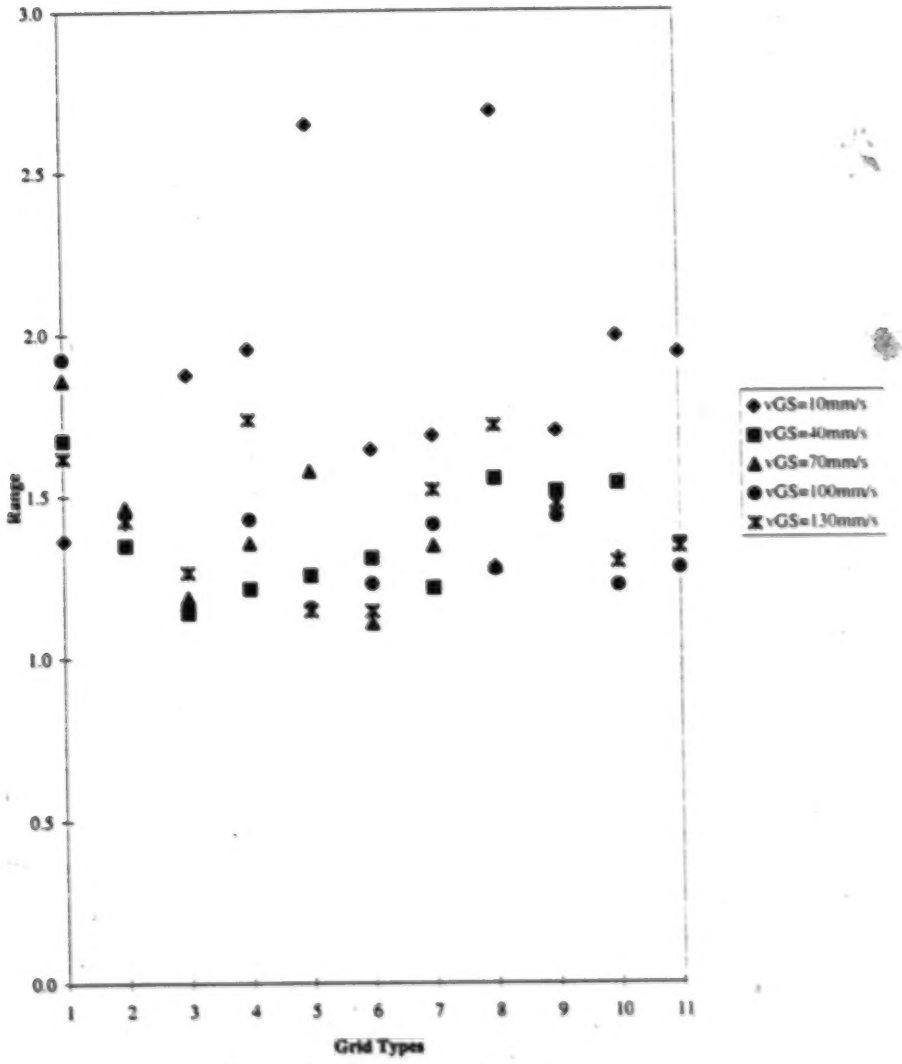

Figure 2.16: Range vs. Grid Types
y = 0 mm

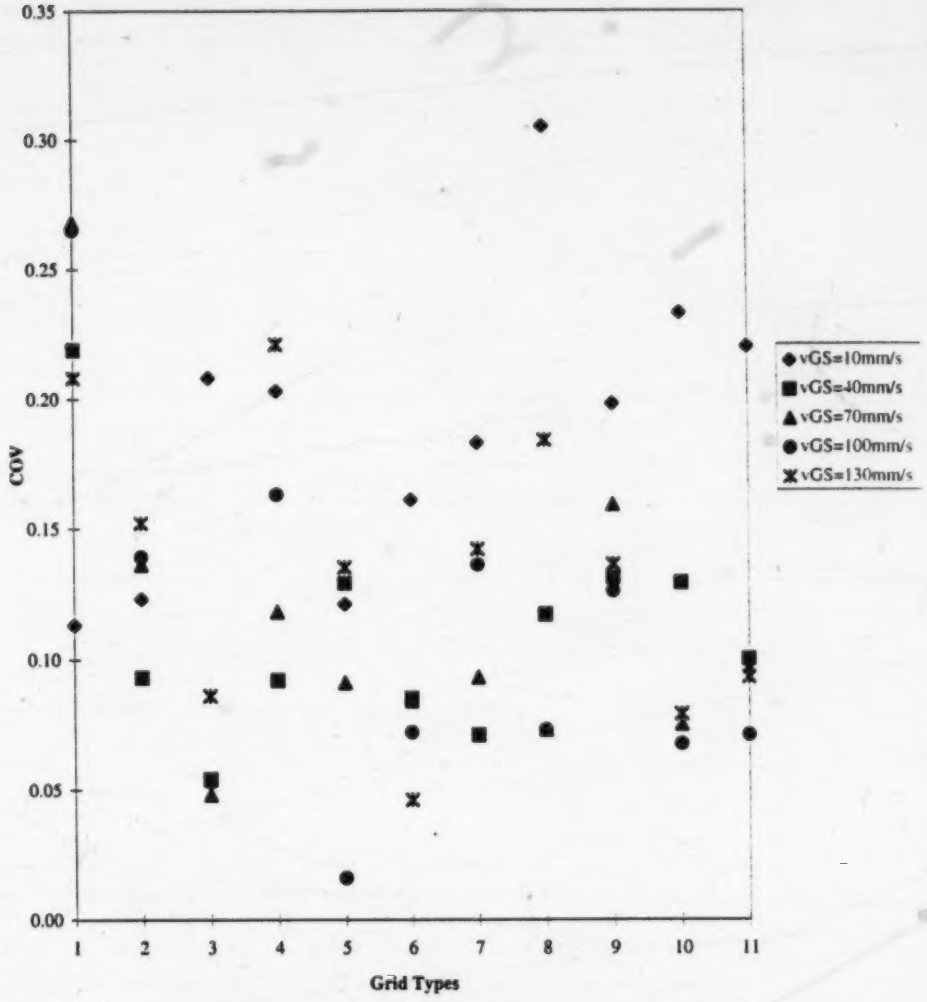

Figure 17: Coefficient of Variation vs. Grid Types
y = 0 mm

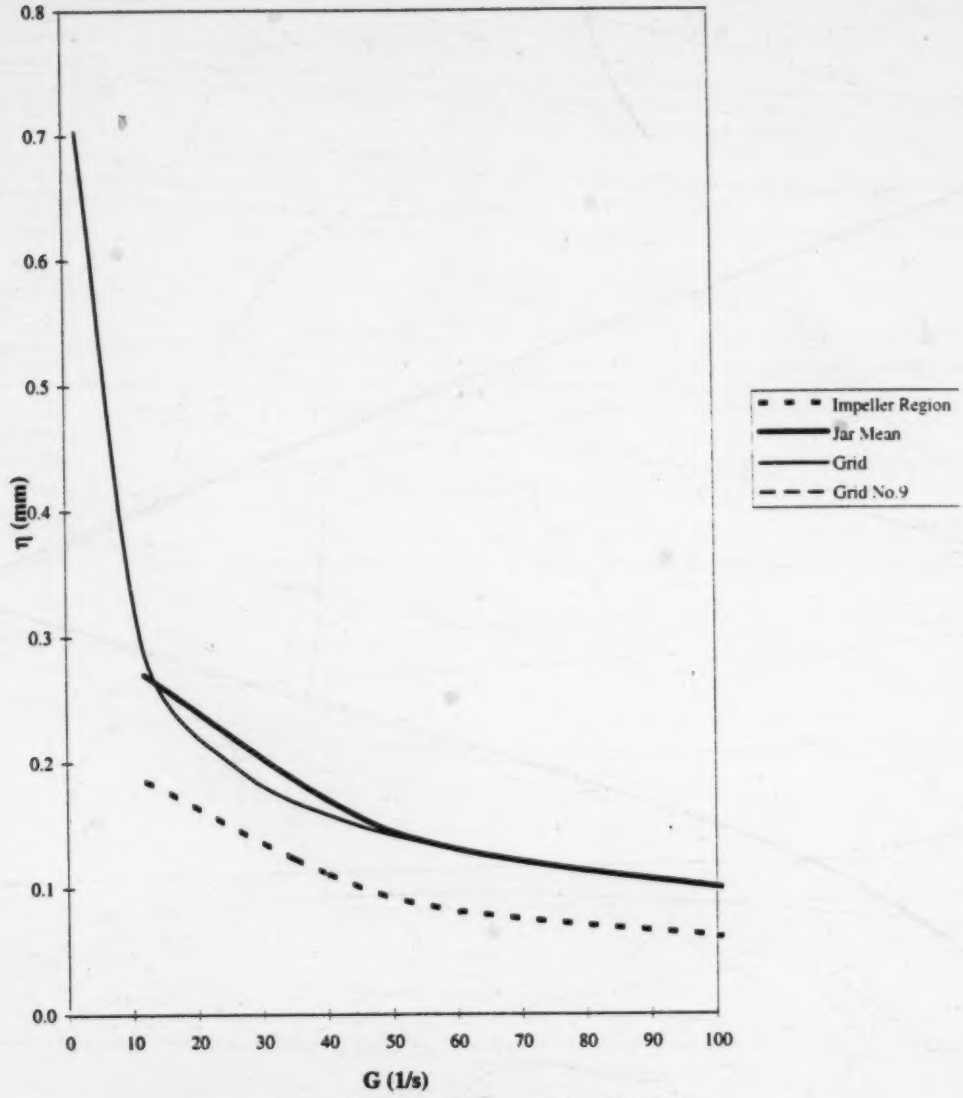

Figure 2.18: Kolmogoroff Microscale vs. Velocity Gradient

3. PARTICLE REMOVAL STUDY**

3.1 INTRODUCTION

The coagulation and flocculation process is one of the most important process components used in drinking water production. First, a chemical coagulant is added to stabilize small particles in water, or known as the coagulation process. This requires rapid mixing characterized by high intensity mixing for a short time period to disperse the chemical creating uniform chemical reactions. This is followed by slow mixing for a relatively long period of time to allow maximum contacts among the particles, which is known as the flocculation process. This process allows small particles to agglomerate so that they can be separated from the water using sedimentation and filtration processes (Amirtharajah and O'Melia 1990).

Properly designed rapid and slow mixing steps provide an optimum mixing sequence to create the best floc aggregation environment. When sedimentation is used as the separation process, sweep flocculation mechanism is commonly applied in water treatment practices. In this case, water is supersaturated by the chemical coagulant so that the hydroxide component is quickly formed. Rapid mixing is not critical since the rapid hydroxide precipitation followed by colloid flocculation is more important than the transport interaction between the hydrolysis components and the colloids (Amirtharajah and Tambo 1991).

** Accepted for publication at the Canadian Journal of Civil Engineering.

Most flocculation mixing studies have been focused on the slow mixing aspect. These investigations were traditionally conducted through bench scale studies using various impellers and jars. Hudson (1965) used a square jar and a single flat blade impeller in his experiments. Circular jars and a single flat blade impeller were employed by Camp (1968 and 1969). Rake impellers were used by Argaman and Kaufman (1970) and Argaman (1971). Packham (1962), Letterman et al. (1973), and Andreu - Villegas and Letterman (1976) used multiple flat blade impellers and circular jars. McConnachie (1990) compared the performance of single and multiple flat blade impellers as well as a rake impeller. Mixing in these studies have been characterized by the average volume velocity gradient $\overline{G}$ (s^{-1}). The value of $\overline{G}$ can directly be obtained from the impeller speed. Cornwell and Bishop (1983) presented $\overline{G}$ vs. impeller speed profiles for many types of impellers and jar shapes.

However, the use of impellers as a flocculation mixing device has been criticized due to high turbulent mixing intensity in the impeller region and the occurrence of a jet like flow in the direction of vessel wall. High floc break up rates were observed in these regions that tend to govern the size of the formed flocs (Tomi and Bagster 1978; Stanley 1995; and Stanley and Smith 1995).

It is generally acknowledged that more uniform mixing should give the best environment for floc aggregation. Many investigators have used different types of mixing devices that would create more uniform mixing environment. Casson and Lawler (1990) used a series of porous plates which were vertically oscillated in a small

stroke and high frequency mode. Watanabe et al. (1991) and Sobrinho et al. (1996) used multiple and single porous plates to create a gentle jet mixing system.

In this study, a vertically oscillating grid mixing device was used as a newly designed flocculation mixing device. The grid was moved constantly in a low frequency and long stroke mode to produce uniform mixing throughout the mixing region. The turbulent parameter measurement of the grid mixing has thoroughly been investigated in Chapter 2. It was found that the turbulent mixing intensity represented by the root mean square (rms) turbulent velocity q' was relatively uniform both in vertical and horizontal points of measurement; a condition that could not be achieved in the case of impeller mixing. This finding shows that the grid mixing device has a potential to produce an optimum mixing condition for floc aggregation. q' was also found to be proportional to rod diameter d and grid mesh M. Subsequently, the average volume velocity gradient $\overline{G}$ was developed for each case based on the drag force created from the vertical grid movement. These indicate that grid mixing intensity within the vessel can easily be controlled from its physical characteristics and grid movement.

In this study, the emphasis was on the use of the grid mixing device for particle removal represented by the settled water turbidity. Low turbidity readings were expected to be achieved at reasonably low $\overline{G}$ values. It was also expected that the mixing would create particle contacts with low break up rate. Relations among the flocculation performance parameters, $\overline{G}$, and grid physical characteristics should be

obtained. Since the focus was on the mixing behavior, it was necessary to set chemical and physical (temperature) properties constant for all tests.

3.2 METHODS AND MATERIAL

The same mixing device as described in Chapter 2 was also used in this study. Four important characteristics of the mixing device can be described as follows. By applying a cam, the mixing device produced a constant vertical up and down movement. A controllable motor was used to create up to 100 mm/s of vertical grid speed v_{GS}. Vertical strokes could be adjusted to achieve the desired mixing environment. The mixing grid could easily be placed and changed to provide various mixing environments. Detailed components of this device can be seen in Chapter 2.

A standard 2L jar with the size of 115 x 115 x 150 mm^3 as described by Hudson and Wagner (1981) was used as the water container. Circular rods with diameter d and mesh (center to center distance between two rods) M were arranged to form a biplane grid matrix with the size of 110 x 110 mm^2 giving about 2 mm of free spacing at the wall side. A total of five types of grids were employed. These represented grids with low, medium, and high solidity ratio. These were grids numbers 1, 5, 7, 9, and 11 with their physical characteristics described in Table 3.1. The grid numbers refer to the previous work described in Chapter 2. Four holding rods held the grid on each of its corners to avoid any disturbance in the middle part of the mixing region. The vertical stroke was fixed at 135 mm leaving about 7 mm of free spacing at the bottom and upper parts of the water height.

Since the investigation was focused on the mixing characteristics within the vessel, all of the chemical properties were set constant. Table 3.2 shows types of chemicals and their doses used in this study. Distilled water was used for dilution in all cases to avoid any interference from other impurities in water. The chemical choices and doses were made merely based on practical considerations. As shown by Packham (1962), kaolin performed similarly to that of turbid river waters. It was also mentioned that particle concentrations found in the river waters were about 50 mg/L. Alkalinity was kept constant at 2 meq/L by applying 168 mg/L of sodium bicarbonate ($NaHCO_3$). The kaolin and sodium bicarbonate concentration combination would create a "high turbidity and high alkalinity" type of water. As mentioned by O'Melia (1978), this was the easiest type of water to treat. In this case, alum could effectively be applied without coagulant aids as long as it was operated at the optimum pH. Alum dose of 25 mg/L was used as the chemical coagulant. Concentrated sodium hydroxide NaOH and hydrochlorous acid HCl solutions were used to adjust the initial water pH to 8.1. The pH decreased to 6.9 after alum addition. As shown by pH vs. alum dose profiles developed by Amirtharajah and Mills (1982), this combination of alum dose and pH will lead to the optimum sweep flocculation mechanism. Other flocculation studies, such as Letterman et al. (1973); Andreu - Villegas and Letterman (1976); and McConnachie (1990), also conducted studies using this flocculation mechanism region.

The stock solutions were made by weighing 2.50, 1.00, and 6.72 g of kaolin, alum, and sodium bicarbonate, respectively. They were then put in a 100 °C oven for 2

hours and cooled in a desiccator for 1 hour. Stock solutions of 250, 100, and 100 mL of kaolin, alum, and sodium bicarbonate were then made. A high concentration stock solution of alum was made to minimize the alum hydrolysis before its use (Packham 1962). The stock solutions were rigorously mixed at $\overline{G}$ about 700 s^{-1} for 2 hours before being used and continuously mixed from one test to another. All of the stock solutions were used up and renewed every other day.

A 2L solution was then made of distilled water, 5 mL of sodium bicarbonate stock solution, and 10 mL of kaolin stock solution. The pH was adjusted and the solution was vigorously mixed at 700 s^{-1} for about 30 minutes. The average initial turbidity reading T_o was found to be 60 NTU (nephelometric turbidity unit). Alum was quickly added and the solution was continuously mixed for another minute. A standard flat blade impeller (76 x 25 mm^2) was used as the rapid mixing device. Temperature of the water was found to be constant at 20 ± 0.5 °C from one test to another. A direct relation between the standard impeller mixing speed in a standard Hudson jar and the average volume velocity gradient $\overline{G}$ at 20 °C was found based on Cornwell and Bishop (1983). This gave $\overline{G}$ and $\overline{G}\,t_R$ ($\overline{G}$ multiplied by rapid mixing time t_R) values of about 700 s^{-1} and 40,000, respectively which was commonly used in water treatment practices (Amirtharajah 1978). This was also supported by Amirtharajah and Mills (1982). They found that in the case of sweep flocculation mechanism, rapid mixing with $\overline{G}$ values in the range of 300 to 16,000 s^{-1} did not make any significant differences in the settled water turbidity. It was then assumed that

the particle destabilization process was completely achieved during this rapid mixing process.

The jar was then moved to the vertically oscillating grid mixing device where the slow mixing was conducted. Six flocculation times t_F (2, 5, 10, 20, 40, and 60 minutes) were applied for each case. Seven types vertical grid speeds v_{GS} were used for each case until a minimum turbidity reading was monitored.

Referring to Hudson (1965) and Argaman and Kaufman (1970), the sample solution was pipetted from the middle of the water depth at sedimentation time of 30 minutes. The amount of solution was 40 mL which was sufficient for the turbidity measurement. Two drops of concentrated hydrochlorous acid were added followed by a manual mixing to break up the agglomerated flocs. As mentioned by Andreu - Villegas and Letterman (1976), this was necessary in order to negate any effects of the particle size and distribution to turbidity measurement.

The turbidity measurement was conducted using a Hach turbidity meter in nephelometric turbidity unit (NTU) according to APHA - AWWA - WEF (1992). The accuracy of the readings varied with the range of turbidity: 0.1, 1, and 5 NTU for turbidity readings in the range of 1 to 10, 10 to 40, and 40 to 100 NTU, respectively.

3.3 TURBIDITY ANALYSIS

The settled water turbidity represented by the relative turbidity (turbidity T divided by initial turbidity $T_o = T/T_o$) was measured for each combination of vertical grid speed v_{GS} (mm/s), grid type, and flocculation mixing time t_F (minute). This was

conducted to follow the most traditional procedure of flocculation process performance control in real water treatment works, i.e. to obtain the minimum T/T_o as well as to identify the optimum mixing intensity and mixing time. Further analysis incorporated the floc aggregation and erosion rate coefficients will be discussed in a separate section. As has been shown in Chapter 2, the mixing intensity created by the oscillating grid mixing device within the vessel is relatively uniform. The traditional $\overline{G}$ value (defined as the volume average velocity gradient in s^{-1}) may then be used as the surrogate mixing intensity parameter. This value can be obtained based on the drag force created by the mixing grid movement. In general this relationship can be expressed as:

$$\overline{G} \sim (v_{GS}, d/M) \tag{3.1}$$

Based on Chapter 2, v_{GS} vs. $\overline{G}$ profiles for five types of grids can be developed as shown in Figure 3.1.

T/T_o vs. t_F profiles at various v_{GS} for grid no. 9 are shown in Figure 3.2. Two types of curve trends can be observed from this figure. The first type of trend is the one with a definite minimum T/T_o value (known as T/T_o^{**}) at a given v_{GS}. This occurs only for grid no. 9 at high v_{GS}. The second one is the exponential type of curve with an asymptotic value at large t_F. In this case, the minimum T/T_o^{**} value is equal to the asymptotic value of T/T_o for the related v_{GS}. This type of relationship is observed in all

cases (grids nos. 1 to 11) with the exception mentioned above. This shows that the longer the t_F the better the particle removal. The turbidity will finally increase at large t_F when large solidity ratio types of grids and $\overline{G}$ values are applied. This figure also indicates that t_F longer than 20 minutes will not significantly reduce the turbidity. T/T_o vs. $\overline{G}$ profiles at various t_F for grid no. 9 can be seen in Figure 3.3. This figure shows that there is an optimum $\overline{G}$ (known as $\overline{G}$*) that gives the minimum T/T_o for the related t_F (called as T/T_o*). The longer the t_F, the lower the T/T_o*, and the less $\overline{G}$* required. Appendix 4 provides the complete data for all different cases.

For each type of grid, it is possible to find the relation between $\overline{G}$* and t_F (Letterman et al. 1973 and Andreu - Villegas and Letterman 1976). Since there are five types of grids with different solidity ratio, a factor is used to develop a general relation among them. This will be useful when designing different solidity ratio types of grids. This also shows that the grid mixing is easily controlled by the grid physical characteristics. In this case, solidity ratio (d/M) has successfully been used as the generalizing factor. Figure 3.4 shows $\overline{G}$*/$[d/M]^{0.85}$ vs. t_F profiles for the five types of grids. The factor coefficient 0.85 was found through a trial and error method to give the highest coefficient of determination ($R^2 = 0.949$). As can be seen in the figure, data from the five types of grids collapse quite well forming a linear line with slope -0.22 and constant 2.17. This following relation can then be obtained:

$$\left[\left(\frac{\overline{G}^{*}}{[d/M]^{0.85}}\right)^{4.5}\right] t_F = 10^{9.9} \qquad (3.2)$$

This equation is very useful to determine the optimum $\overline{G}^{*}$ based on the desired t_F to give the T/T_o^{*} at sedimentation time = 30 minutes. This equation shows that high solidity ratio types of grids require more $\overline{G}^{*}$ to achieve the related T/T_o^{*} than that of low solidity ratio types of grids.

However, T/T_o vs. $\overline{G}$ profiles show that high solidity ratio types of grids have a major advantage. Figure 3.3 above (for grid no. 9) shows that constant low T/T_o values (which are close to T/T_o^{*}) in the case of t_F = 20 minutes can be obtained from $\overline{G}$ values in the range of 22 to 60 s^{-1}. This can be compared to grids nos. 11, 5, 7, and 1 (with high to low solidity ratio values) with $\overline{G}$ values in the range of 30 to 48, 30 to 42, 20 to 27, and 16 to 22 s^{-1} (see Table 3.3). The same trend can also be seen in the case of t_F = 40 and 60 minutes, while some of the pattern still can be seen for t_F = 10 minutes. No clear patterns can be seen for t_F = 2 and 5 minutes in which no significant particle removals are observed. This indicates that high solidity ratio types of grids have a more stable performance by having a wider range of $\overline{G}$ values. Camp (1955) mentioned that $\overline{G}$ values in the range of 20 to 74 s^{-1} with $\overline{G}$ multiplied by t_F ($\overline{G}\,t_F$) values of 10^4 to 10^5 would provide the best mixing environment for floc aggregation. Based on this assumption, all of the five types of grids especially high solidity ratio

types of grids (grids nos. 9 and 11) will likely fit the above criteria.

Figure 3.5 shows T/T_o^* vs. t_F profiles for five types of grids with $[d/M]^{0.00}$ as the generalizing factor. It can be seen that all data collapse very well. This figure shows that the types of grids do not make any differences to the T/T_o^* as long as the appropriate combination of $\overline{G}^*$ and t_F (using Equation 3.2 above) is chosen.

Figure 3.6 shows the relation between T/T_o^* and $\overline{G}^*$ multiplied by t_F ($\overline{G}^* t_F$) with $[d/M]^{-0.08}$ as the generalizing factor. Similar to the previous calculation, exponents 0.00 and -0.08 were found through a trial and error method to give the highest R^2 values. Figures 3.4 to 3.6 are very useful to determine the optimum mixing condition to achieve the desired flocculation performance.

3.4 PARTICLE ANALYSIS

Turbidity should directly be related to the number of particles. This assumption is acceptable as long as there are no variations in the particle size and distribution. It is therefore necessary to negate any of these effects by breaking up the formed flocs (Andreu - Villegas and Letterman 1976). Concentrated acid and manual mixing were applied to break up the agglomerated flocs before the turbidity measurement was conducted. The particle characteristics are expected to be the same as those of the original unflocculated particles. It is therefore acceptable to assume that the relative turbidity (T/T_o) will be proportional to the relative number of particles (N/N_o):

$$T/T_o \approx N/N_o \qquad (3.3)$$

where N is the number of particles and N_o is the initial number of particles.

Several tests were conducted using a Hyac Royco particle count analyzer and Hach turbidity meter to verify the validity of this assumption. Twelve kaolin suspensions from 0.25 to 50 mg/L were made. The particle count analyzer with a maximum measurement opening of 150 μm was set to have 8 threshold channels, i.e. 2, 5, 8, 11, 14, 17, 20, and 23 μm. These channels were chosen so that very small number of particles were left at the largest channel (in this case threshold channel 23 μm). Figure 3.7 shows the particle distribution characteristics of the 12 different unflocculated kaolin concentration suspensions. It can be seen that almost 99% of the particles have the size of less than 8 μm. This figure indicates that the particle distribution for low to high kaolin concentration suspensions is quite constant. The particle size of each kaolin concentration suspension was also calculated. It was found that the particle size was quite constant with its concentration. The mean particle size of 3.9 μm with the standard deviation SD of 0.05 μm was obtained from the 12 kaolin suspensions. In this case, the arithmetic mean diameter D(1,0) as defined by Alderliesten (1984) was used since this gave the closest approximation of the particle characteristics:

$$D(1,0) = \frac{\Sigma ND}{\Sigma N} \qquad (3.4)$$

where N was the number of particles and D was the particle diameter for each channel. In this case D was assumed to be the average of two adjacent threshold channels (Hargesheimer et al. 1992).

As mentioned by Hudson (1965), most natural particles causing turbidity in water are smaller than 10 μm with the majority smaller than 1.5 μm. This indicates that kaolin with the mean size of about 4 μm is an appropriate representation of turbidity causing natural particles.

It was then found that the number of particles was linearly related with its concentration as it should be in reality. Furthermore, it was found that the kaolin concentration was also linearly related with the turbidity reading (see Figure 3.8). These findings confirm the validity of Equation 3.3 above.

3.5 FLOC AGGREGATION AND EROSION COEFFICIENTS

Floc aggregation and erosion are two opposing mechanisms that finally govern the size of the agglomerated flocs. Turbulent mixing intensity within the vessel causes particles to collide but also generates forces on the agglomerated flocs. The analysis has traditionally been conducted in two turbulent regimes. When flocs are larger than the Kolmogoroff microscale η (defined as the smallest eddy that can be sustained) turbulent shear is dominant causing particle shear, pressure forces, and surface drag. When η is larger than the flocs, laminar shear is dominant causing little shear stress on the flocs. The first case is called inertial turbulent regime, while the latter is identified

as the viscous turbulent regime. Floc break up mechanism as well as floc characteristics and strength have been studied by many investigators such as Argaman and Kaufman (1970), Parker et al. (1972), Tambo and Hozumi (1979), and Clark (1988). In this study, the only parameter measured was the settled water turbidity. The following analyses will therefore be made based on this available information.

Slow mixing with high floc aggregation and low floc erosion rate coefficients is expected to produce larger and stronger flocs. The flocculated particles will settle rapidly during the sedimentation process that can be represented by a low turbidity reading. Assuming that the turbidity reading is directly related to the number of particles (see Equation 3.3 above), it is possible to obtain the floc aggregation and erosion rate coefficients as defined by Argaman and Kaufman (1970) and Argaman (1971):

$$\frac{dN}{dt} = -k_1 N + k_2 \qquad (3.5)$$

where $\frac{dN}{dt}$ is the rate of disappearance of the initial particle (min^{-1}), t is equal to the flocculation time t_F (min), k_1 is the floc aggregation rate (min^{-1}), and k_2 is the floc erosion rate (min^{-1}). In this case, the relative turbidity T/T_o ($\approx N/N_o$) is substituted as the number of particles N (no unit). This is done to account for any variations in the initial turbidity reading T_o for one test to another. These following relationships were then obtained:

$$k_1 \sim \overline{G}^{b1} \qquad (3.6)$$

$$k_2 \sim \overline{G}^{b2} \qquad (3.7)$$

Coefficient b_1 in Equation 3.6 can be found based on the Smoluchowski equation assuming that the particles are monosized and that each effective collision results in the loss of one initial particle. Subsequently, coefficient b_1 can be found to be unity (Amirtharajah and O'Melia, 1990). Coefficient b_2 in Equation 3.7 can be obtained from the floc break up model. Argaman and Kaufman (1970) and Parker et al. (1972) developed a floc break up model by incorporating the surface erosion of flocs by turbulent drag. Flocs were assumed to have a random motion that could be characterized as the energy spectrum of the turbulence field. Based on their derivation, coefficient b_2 was found to be 4 and 2 for inertial and viscous turbulent regimes, respectively.

In the case of a batch reactor, the exact solution for Equation 3.5 can be obtained by integrating the equation from t = 0 (for $N = N_o/N_o = 1$) to $t = t_F$ (for $N = N/N_o$):

$$\ln\left[\frac{\left(\frac{N}{N_o} - \frac{k_2}{k_1}\right)}{\left(1 - \frac{k_2}{k_1}\right)}\right] = -k_1 t_F \qquad \text{or}$$

$$\frac{N}{N_o} = [(1 - \frac{k_2}{k_1}) \exp(-k_1 t_F)] + \frac{k_2}{k_1} \qquad (3.8)$$

where $\frac{k_2}{k_1}$ is the asymptotic value of T/T_o at large t_F.

Using Equation 3.8, k_1 and k_2 can be obtained based on T/T_o ($\approx N/N_o$) vs. t_F profiles for various v_{GS} (see Figure 3.2 for grid no. 9 for example). As has been mentioned above, almost all of the curve patterns have an asymptotic profile that follow Equation 3.8 well. The asymptotic value ($=T/T_o^{**}$) can directly be substituted as k_2/k_1. In the case of curve with a definite T/T_o^{**} value (only occurs for grid no. 9 at high v_{GS}), this value is assumed as k_2/k_1. This phenomenon may be caused by any k_1 and k_2 variations with time that can be observed in a certain condition (Andreu - Villegas and Letterman 1976). A non - linear regression method was used to obtain coefficient k_1 for each case. The lowest coefficient of determination R^2 for all cases was found to be 0.962. k_2 could then be calculated based on the related k_1 value.

To obtain a general form for all types of grids, the solidity ratio (d/M) was applied as the generalizing factor. Figure 3.9 shows that $k_1/[d/M]^{-0.45}$ can be related according to Equation 3.6. The curve slope was found to be equal to 0.05, while the exponent was found to be 0.55. Equation 3.6 above can be rewritten as:

$$\frac{k_1}{[d/M]^{-0.45}} = 0.05\ \overline{G}^{0.55} \qquad (3.9)$$

Subsequently, the erosion rate coefficient k_2 can also be obtained based on $\overline{G}$. Figure 3.10 shows $k_2/[d/M]^{-2.01}$ vs. $\overline{G}$ profiles. Equation 3.7 above can be expressed as:

$$\frac{k_2}{[d/M]^{-2.01}} = 3.9E\text{-}7\ \overline{G}^{\,2.42} + 0.0015 \qquad (3.10)$$

Similar to the previous procedure, generalizing factor coefficients -0.45 and -2.01 were obtained through a trial and error method to give the largest R^2 values (0.968 and 0.978, respectively). Equation 3.10 contains constant 0.0015 that can be considered as an experimental error since k_2 should be zero when $\overline{G}$ is zero.

Equations 3.9 and 3.10 can be combined to obtain the rate of disappearance of the initial particle as shown by Equation 3.5. The best floc aggregation should occur when k_2/k_1 is minimum. Figure 3.11 shows k_2/k_1 vs. $\overline{G}$ profiles for the five types of grids. This figure shows that practically the same minimum k_2/k_1 values are observed for all types of grids but at different $\overline{G}$*. Grid no. 1 has the smallest $\overline{G}$* (18 s^{-1}) while the largest $\overline{G}$* (47 s^{-1}) is observed for grid no. 9 (Table 3.3 shows values for all types of grids). The $\overline{G}$* values can be found at the same locations where k_2/k_1 are minimum as shown in Figure 3.11.

Equations 3.9 and 3.10 indicate that when high v_{GS} is applied, floc break up

becomes more dominant than floc aggregation. This has been shown in Figures 3.2 and 3.3 above, high turbidity readings are observed at high v_{GS} or $\overline{G}$ values. Equations 3.9 and 3.10 also indicate that low solidity ratio types of grids have higher k_1 and k_2 values than those of high solidity ratio types of grids for the same $\overline{G}$ values. This is possible since grids with low solidity ratio require higher v_{GS} to achieve the same $\overline{G}$. This also agrees with the previous finding that low solidity ratio types of grids have smaller $\overline{G}^*$ but in a narrower range of $\overline{G}$ values. High solidity ratio types of grids are then favorable due to their more stable performance. Appendix 5 provides complete data for k_2 and k_1 values.

It is important to note that the agglomeration and erosion rate coefficients were developed based on the relative turbidity T/T_o ($\approx N/N_o$) vs. t_F profiles. T ($\approx$ N) can also be used instead of T/T_o ($\approx N/N_o$). The value of k_1 will remain the same since k_1 is the slope of the T/T_o vs. t_F curve which has an identical shape to that of the T vs. t_F curve. While the value of k_2 should be multiplied by 60 (i.e. the average T_o reading for all tests). However, all of the trends and analyses will remain the same.

b_1 and b_2 can be compared with the theoretical values as mentioned above. There is a slight difference in the case of b_1 (0.55 compared to 1). This may be caused by any imperfection of the mixing process that cannot produce high particle contact as it should be in theory. Particle contacts may be improved by applying more number of grids. This requires a more specific study about the use of multiple mixing grids as the mixing device as will be covered in Chapter 4.

However, a good agreement can be seen for b_2 with the value of 2.42 compared to the theoretical values in the range of 2 to 4 for viscous and inertial turbulent regimes, respectively. It can then be suggested that the flocculation process in this study may occur in the viscous regime which is desirable due to little stress on flocs.

The identification of turbulent regimes can also be made by comparing the size of particles with the Kolmogoroff microscale η as shown above. When the particle collision process is the main interest (such as Saffman and Turner 1956), the initial particle diameter is compared with η to define the turbulent regime. The size of η produced by grid mixing has been identified in Chapter 2. Figure 3.12 shows that in the range of optimum $\overline{G}$ ($\overline{G}$*) values of about 20 to 60 s^{-1}, the size of η is in the range of 0.15 to 0.20 mm. The collision process that occurs in this study is then found in the viscous turbulent regime since the initial diameter of the unflocculated kaolin (about 0.004 mm) is less than η. However, from the agglomerated floc point of view (especially when the break up mechanism is of interest), the floc diameter or even maximum floc diameter will be compared with η to define its turbulent regime (Parker et al. 1972; Clark 1988; and Tambo and Hozumi 1979). Since the agglomerated floc diameter was not measured, the same procedure cannot be made for this study.

3.6 CONCLUSIONS

The grid mixing has been found to be able to produce low relative turbidity T/T_o values at reasonable volume velocity gradient $\overline{G}$ values. It has been found that

flocculation time t_F greater than 20 minutes does not significantly improve the turbidity reduction. It has been found that high solidity ratio types of grids performed the best. Even though their optimum $\overline{G}$ ($\overline{G}$*) values are higher than those of low solidity ratio types of grids, these optimum values are located in a wider range of $\overline{G}$ values. Also, in the case of t_F = 20 minutes, $\overline{G}$* values for all types of grids lie in the optimum range of $\overline{G}$ ($20 < \overline{G} < 74\ s^{-1}$).

The agglomeration and erosion rate coefficient analysis also shows that high solidity ratio types of grids are able to produce particle contacts with low floc break up. This indicates that grid mixing has its best performance when high solidity ratio types of grids are applied.

General relations among the flocculation performance parameters, $\overline{G}$, and grid physical characteristics have also been obtained. This indicates that flocculation mixing produced by the mixing grid can easily be controlled. This becomes important when determining the optimum mixing condition for a desired flocculation performance. This is also useful when designing mixing grids with different physical characteristics.

This study has shown that vertically oscillating grid mixing provides an excellent flocculation mixing environment. A more detailed investigation into the use of multiple mixing grids is necessary as will be considered in Chapter 4. This arrangement is expected to improve the overall grid mixing performance. Lower

vertical grid speed v_{GS} will be required to produce the same $\overline{G}$. Particle contacts will be increased while the floc erosion rate lowered.

3.7 REFERENCES

Alderliesten, M. (1984). "A nomenclature for mean particle diameters." *Analytical Proceedings*, 21 (5), 167 - 172.

Amirtharajah, A. (1978). "Design of rapid mixing units." *Water Treatment Plant Design*, R. L. Sanks, editor. Ann Arbor Science Inc., Ann Arbor, Michigan. 131 - 148.

Amirtharajah, A. and Mills, K. M. (1982). "Rapid - mix design for mechanisms of alum coagulation." *Journal AWWA*, 74 (4), 210 - 216.

Amirtharajah, A. and O'Melia, C. R. (1990). "Coagulation processes: Destabilization, mixing, and flocculation." *Water Quality and Treatment*, F. W. Pontius, editor. McGraw - Hill, New York, New York, 269 - 366.

Amirtharajah, A. and Tambo, N. (1991). "Mixing in water treatment." *Mixing in Coagulation and Flocculation*, A. Amirtharajah, M. M. Clark, and R. R. Trussell, editors. AWWA, Denver, Colorado, 3 - 34.

Andreu - Villegas, R. and Letterman, R. D. (1976). "Optimizing flocculator power input." *Journal of the Environmental Engineering, ASCE*, 102 (EE2), 251 - 263.

APHA - AWWA - WEF. (1992). *Standard Methods for the Examination of Water and*

Wastewater, A. E. Greenberg, L. S. Clesceri, and A. D. Eaton, editors. APHA. Washington, District of Columbia, 2-8 - 2-11.

Argaman, Y. A. (1971). "Pilot - plant studies of flocculation." *Journal AWWA*. 63 (12), 775 - 777.

Argaman, Y. A. and Kaufman, W. J. (1970). "Turbulence and flocculation." *Journal of the Sanitary Engineering Division, ASCE*, 96 (SA2), 223 - 241.

Camp, T. R. (1955). "Flocculation and flocculation basin." *Transactions of ASCE*. Paper No. 2722, 1 - 16.

Camp, T. R. (1968). "Floc volume concentration." *Journal AWWA*, 60 (6), 656 - 673.

Camp, T. R. (1969). "Hydraulics of mixing tanks." *Journal of the Boston Society of Civil Engineers*, 56 (1), 1 - 28.

Casson, L. W. and Lawler, D. F. (1990). "Flocculation in turbulent flow: Measurement and modeling of particle size distributions." *Journal AWWA*, 82 (8), 54 - 68.

Cornwell, D. A and Bishop, M. M. (1983). "Determining velocity gradients in laboratory and full - scale system." *Journal AWWA*, 75 (9), 470 - 475.

Clark, M. M. (1988). Drop breakup in a turbulent flow - I. Conceptual and modeling considerations." *Chemical Engineering Science*, 43 (3), 671 - 679.

Hargesheimer, E. E., Lewis, C. M., and Yentsch, C. M. (1992). *Evaluation of Particle Counting as a Measure of Treatment Plant Performance*, AWWARF, Denver, Colorado, 1 - 319.

Hudson, H. E. Jr. (1965). "Physical aspect of flocculation." *Journal AWWA*, 57 (7), 885 - 892.

Hudson, H. E. Jr. and Wagner, E. G. (1981). "Conduct and use of jar tests." *Journal AWWA*, 73 (4), 218 - 224.

Letterman, R. D., Quon, J. E., and Gemmel, R. S. (1973). "Influence of rapid - mix parameters on flocculation." *Journal AWWA*, 65 (11), 716 - 722.

McConnachie, G. L. (1991). "Turbulence intensity of mixing in relation to flocculation." *Journal of Environmental Engineering*, 177 (6), 731 - 750.

O'Melia, C. R. (1978). "Coagulation." *Water Treatment Plant Design*, R. L. Sanks, editor. Ann Arbor Science Inc., Ann Arbor, Michigan, 65 - 82.

Packham, R. F. (1962). "The coagulation process. I. Effect of pH and the nature of the turbidity." *Journal of Applied Chemistry*, 12, 556 - 564.

Parker, D. S., Kaufman, W. J., and Jenkins, D. (1972). "Floc breakup in turbulent flocculation processes." *Journal of the Sanitary Engineering Division, ASCE*, 98 (SA1), 79 - 99.

Saffman, P. G. and Turner, J. S. (1956). "On the collision of drops in turbulent clouds." *Journal of Fluid* Mechanics, 1, 16 - 30.

Sobrinho, J. A. H., Thiem, L. T., and Alkhatib, E. A. (1996) . "Optimizing submerged jet flocculator performance." *Journal AWWA*, 88 (8), 81 - 92.

Stanley, S. J. (1995). "Measurement and analysis of mixing as it relates to flocculation." *Ph.D. Thesis*, University of Alberta, Edmonton, Alberta.

Stanley, S. J. and Smith, D. W. (1995). "Measurement of turbulent flow in standard jar test apparatus." *Journal of Environmental Engineering*, 121 (12), 902 - 910.

Tambo, N. and Hozumi, H. (1979). "Physical characteristics of flocs-II. Strength of

floc." *Water Research*, 13, 421 - 427.

Tomi, D. T. and Bagster, D. F. (1978). "The behavior of aggregates in stirred vessels. Part I. Theoretical consideration in the effects of agitation." *Transactions of the Institute of Chemical Engineers*, 56, 1 - 8.

Watanabe, Y., Fukui, M., and Miyanosita, T. (1991). Theory and performance of a jet - mixed separator. *Journal WSRT*, 39 (6), 387 - 395.

Table 3.1: Grid Physical Characteristics

Type of Grid	Grid Physical Characteristics			
	Rod Diameter d (mm)	# of Rods	Mesh M (mm)	Solidity Ratio (d/M)
1	3.2	2x6=12	18	0.17
5	4.8	2x8=16	14	0.35
7	3.2	2x10=20	11	0.29
9	6.4	2x10=20	11	0.58
11	4.8	2x12=24	9	0.52

Table 3.2: Chemical Setup

Parameter	Chemical	Concentration (mg/L)
Simulated Particle	Kaolin	50 *)
Coagulant	Alum	25
pH Buffer	Sodium Bicarbonate	168
Solution	Distilled Water	-
pH Adjustment	NaOH and HCl	pH = 8.1 **)

*) Turbidity = 60 NTU

**) pH decreased to 6.9 after alum addition

Table 3.3: Range of G and G* Values

Type of Grid	Solidity Ratio (d/M)		G Value Ranges at tF = 20 minutes (1/s)	G*(1/s)
1	low	0.17	16 to 22	18
7		0.29	20 to 27	26
5	medium	0.35	30 to 42	32
11		0.52	30 to 48	43
9	high	0.58	22 to 60	47

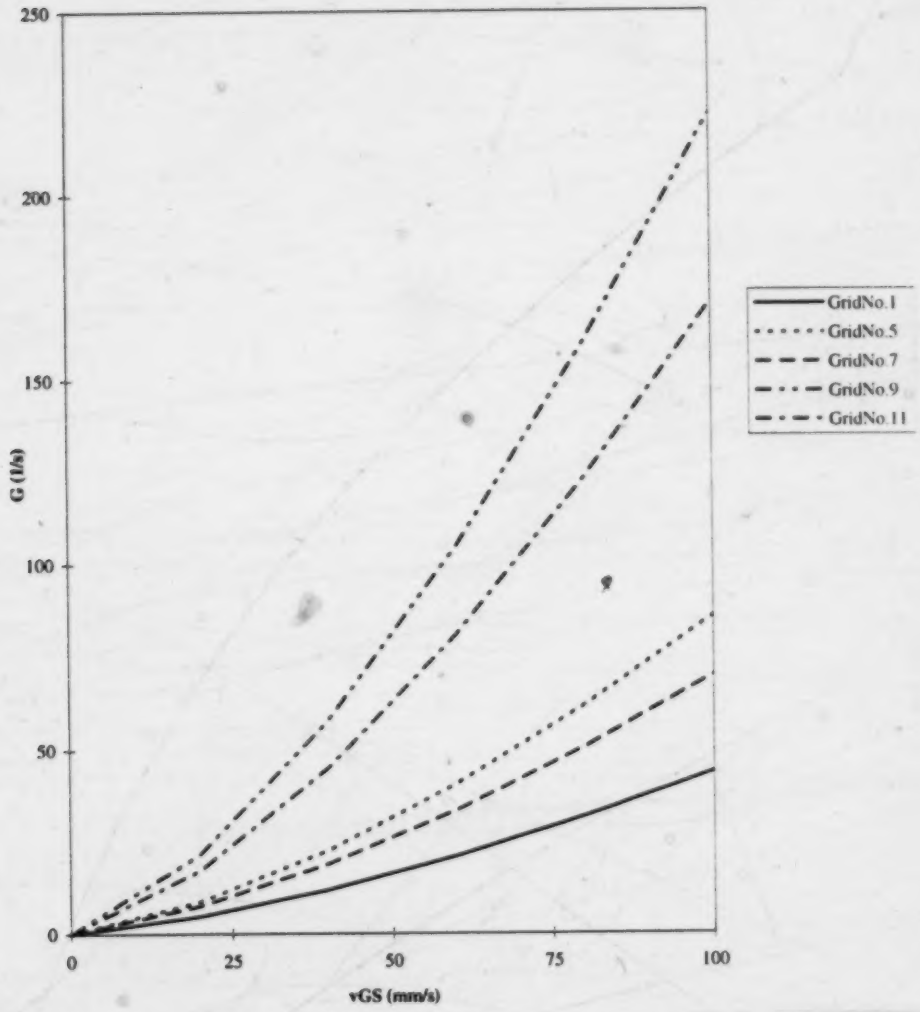

Figure 3.1: Velocity Gradient vs. Vertical Grid Speed

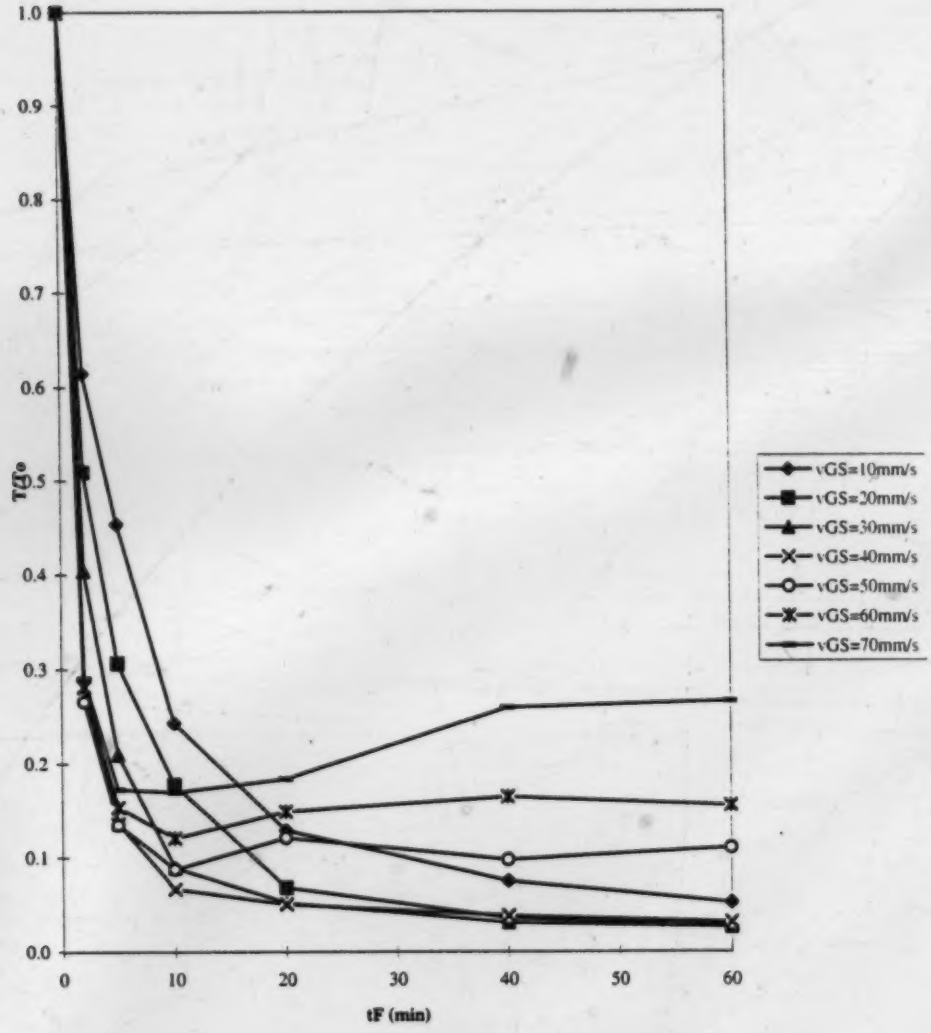

Figure 3.2: Relative Turbidity vs. Flocculation Time for Grid No. 9

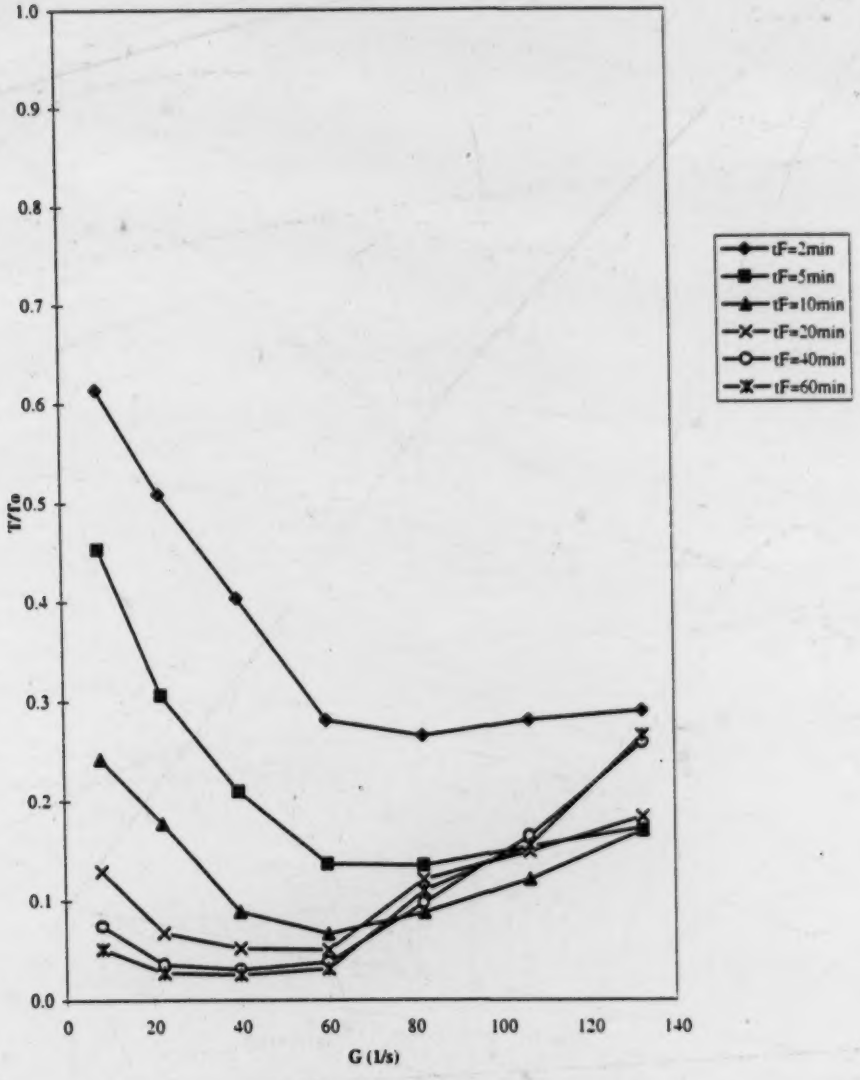

Figure 3.3: Relative Turbidity vs. Velocity Gradient for Grid No. 9

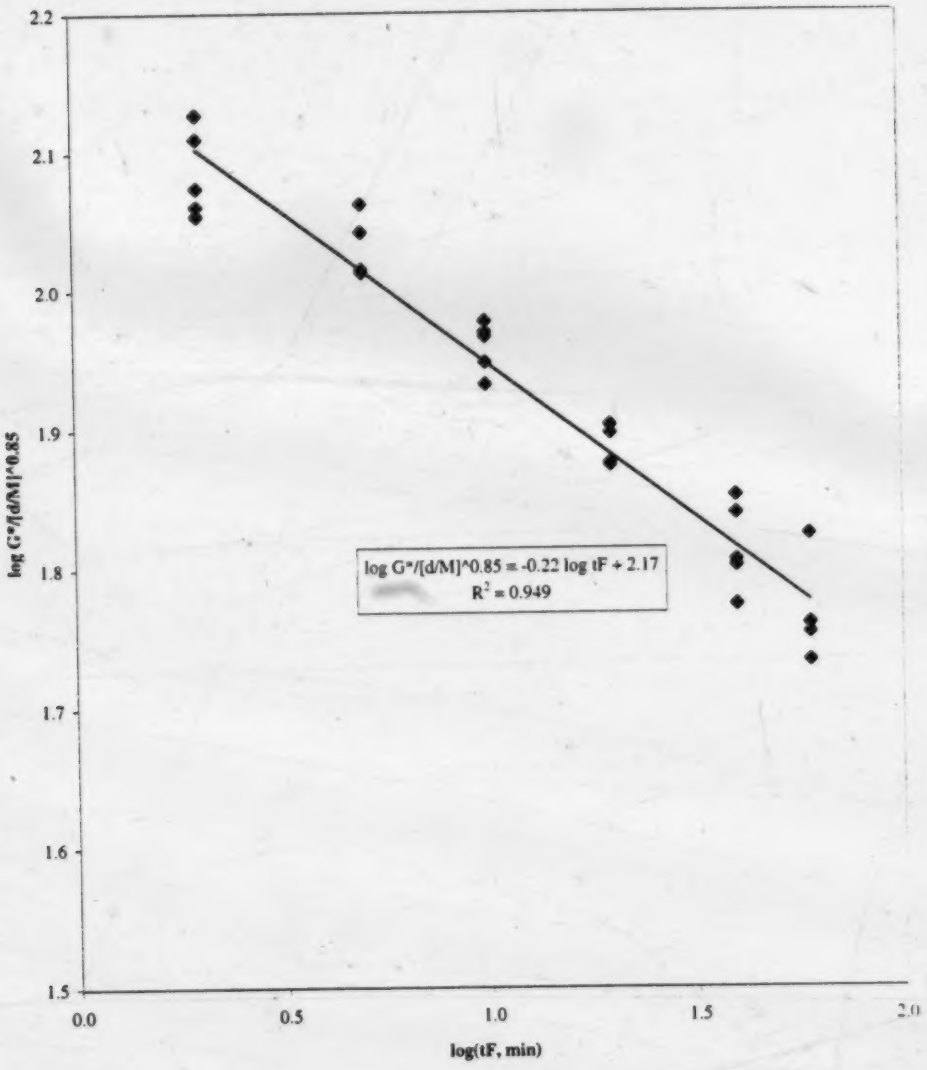

Figure 3.4: Optimum Velocity Gradient vs. Flocculation Time

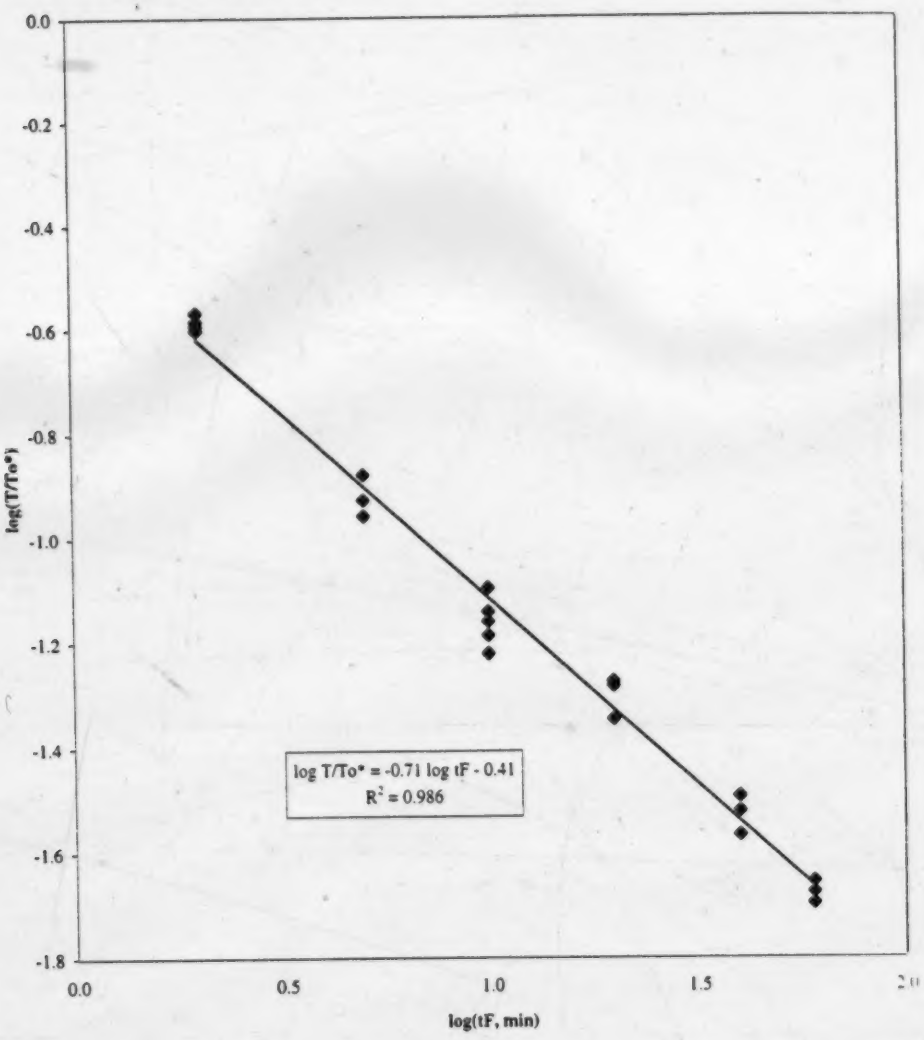

Figure 3.5: Minimum Relative Turbidity vs. Flocculation Time

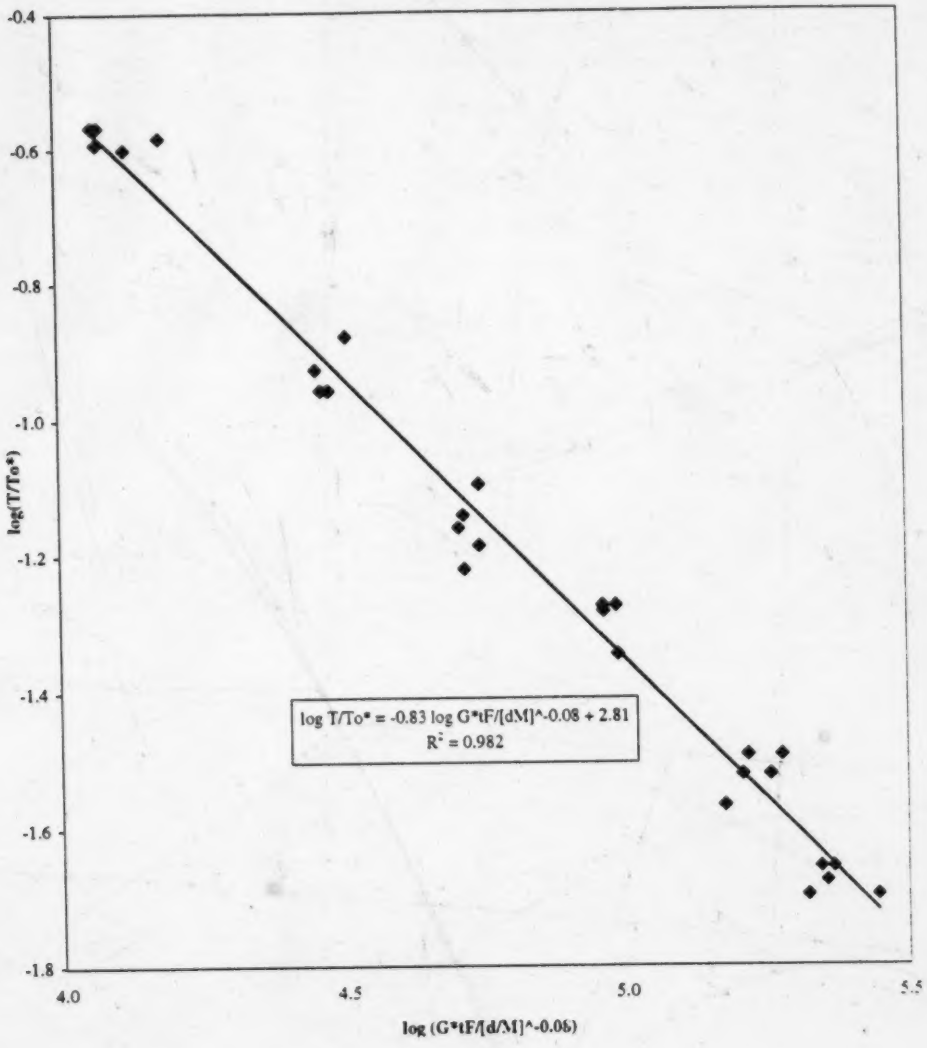

Figure 3.6: Minimum Relative Turbidity vs. Velocity Gradient * Flocculation Time

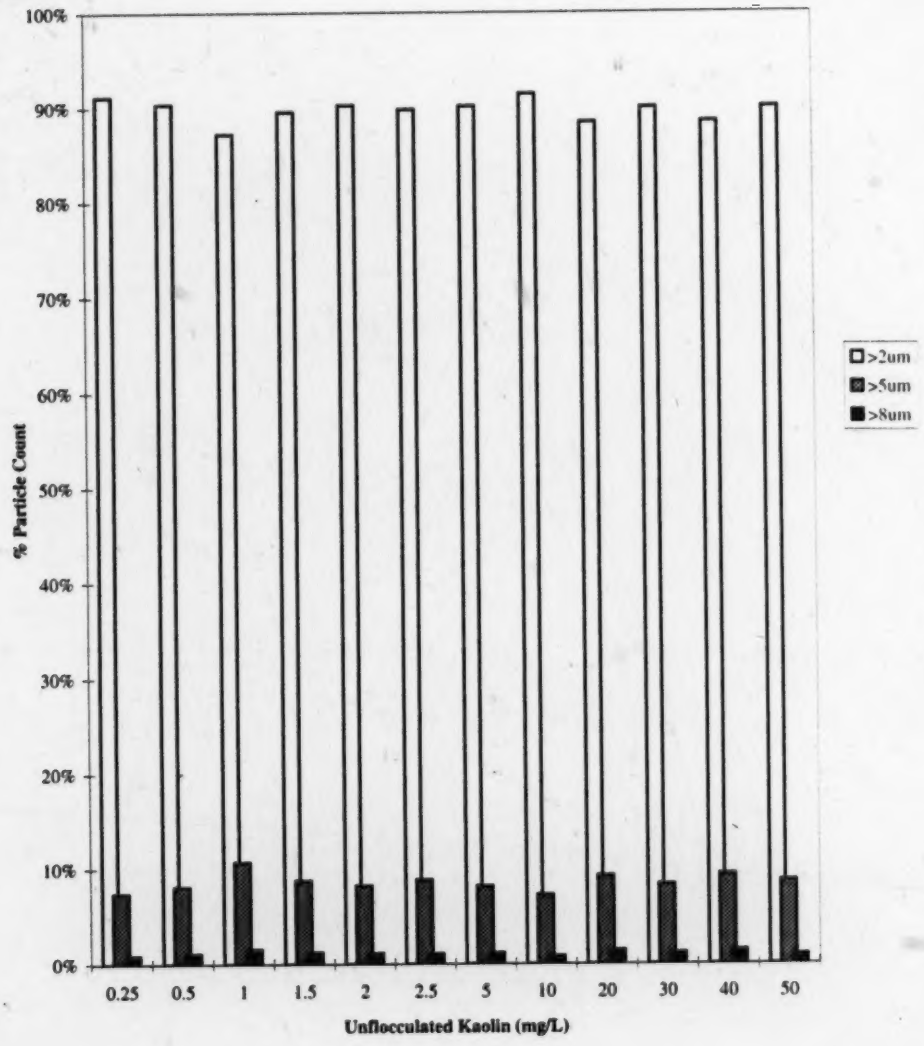

Figure 3.7: % Particle Count vs. Unflocculated Kaolin

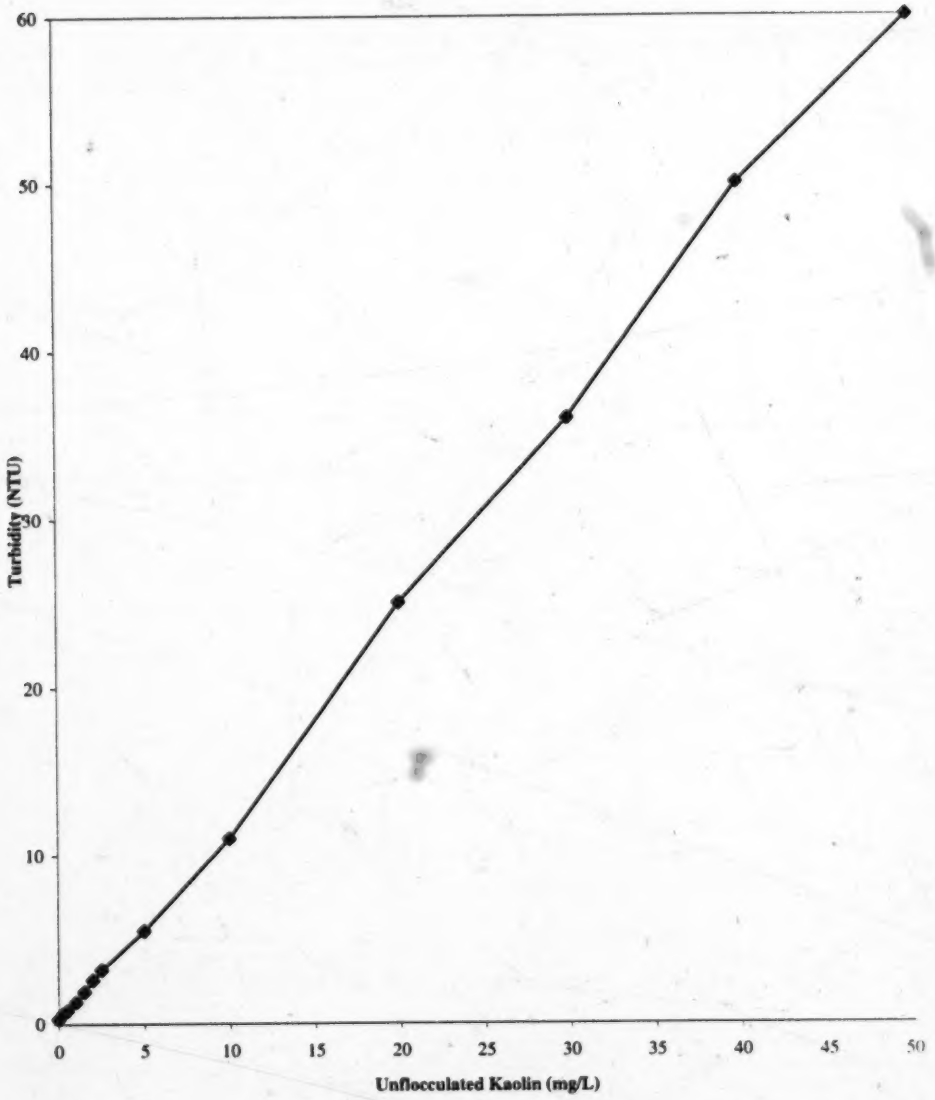

Figure 3.8: Turbidity vs. Unflocculated Kaolin

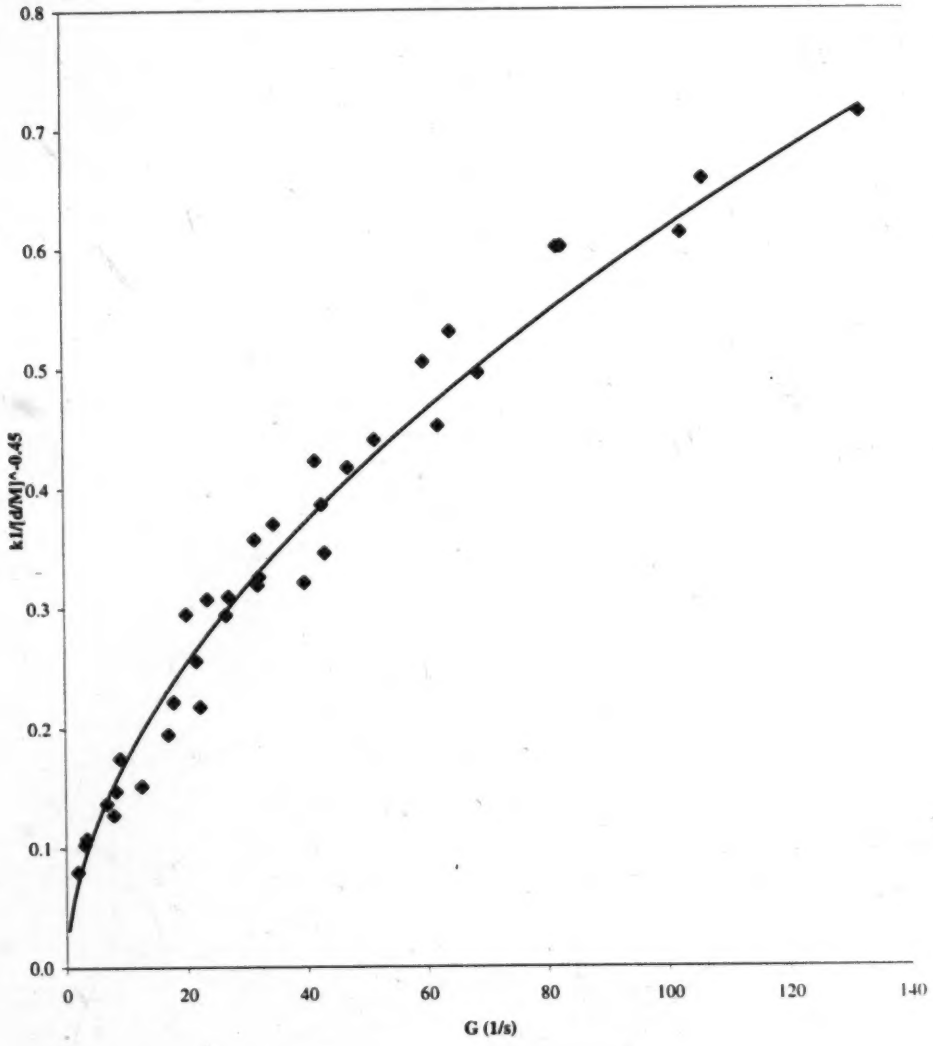

Figure 3.9: Agglomeration Rate vs. Velocity Gradient

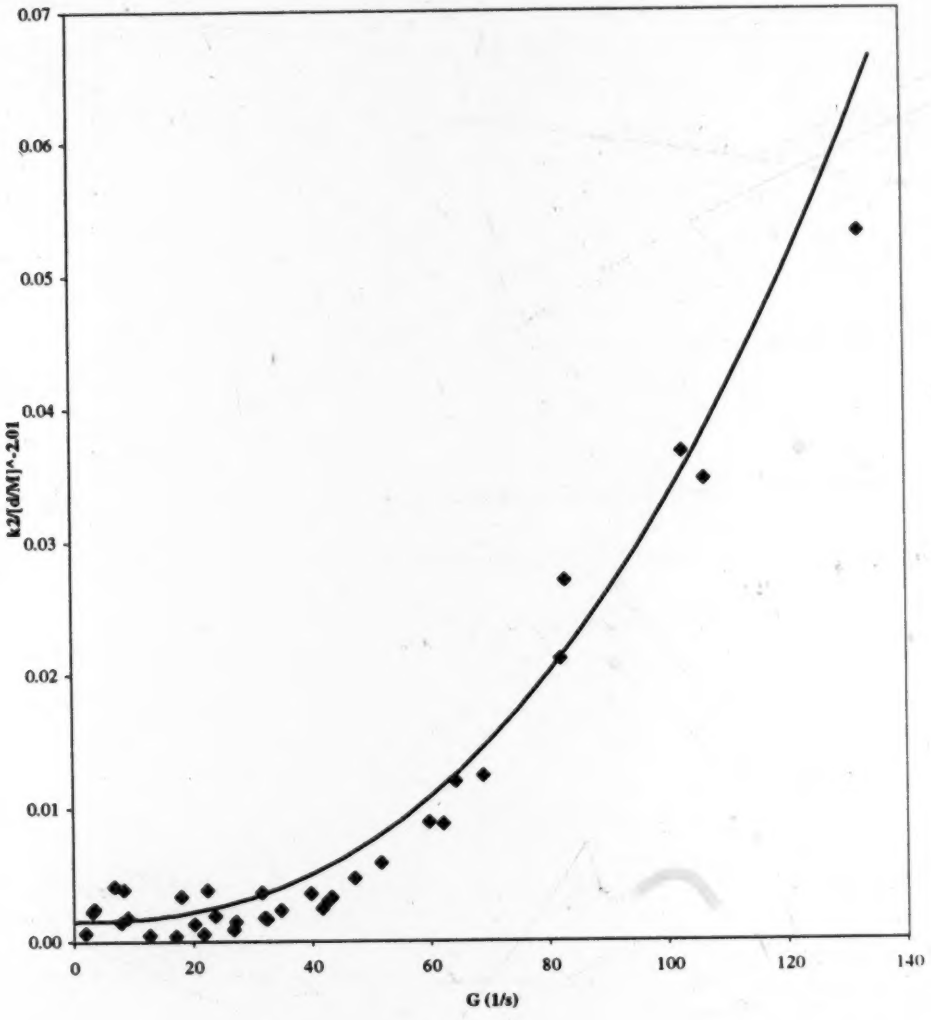

Figure 3.10: Erosion Rate vs. Velocity Gradient

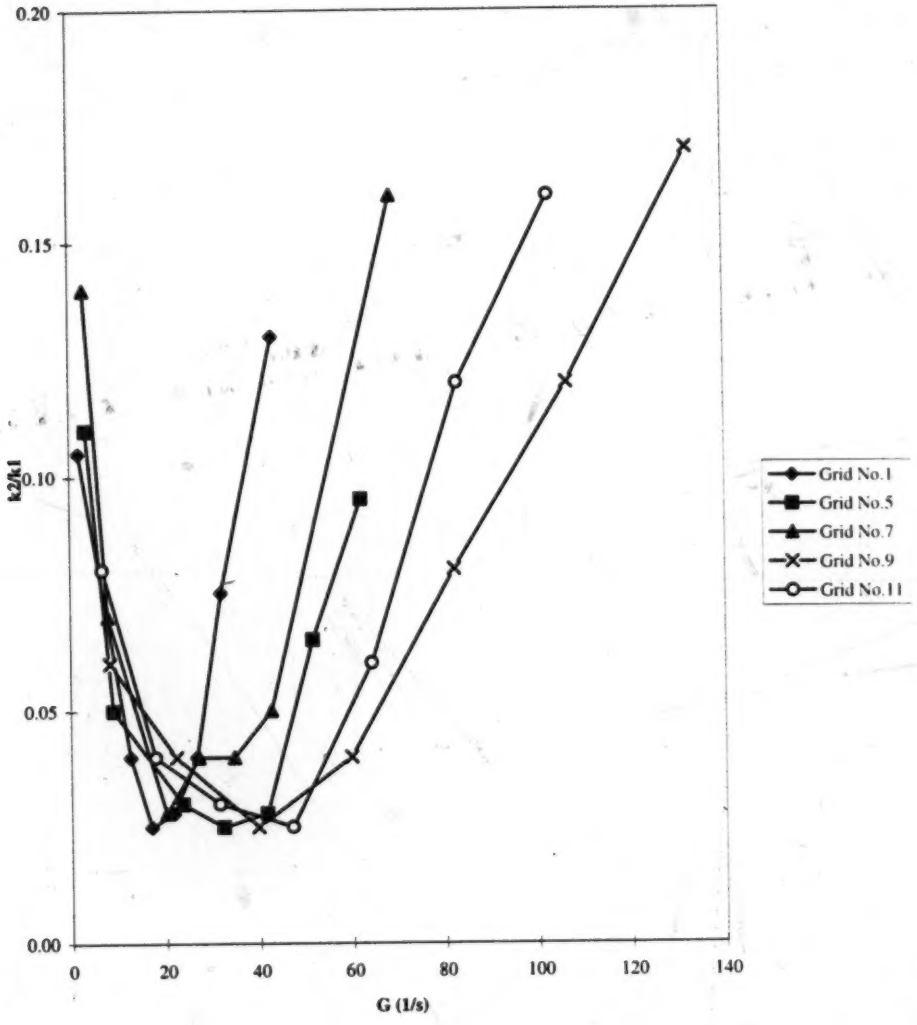

Figure 3.11: k2/k1 vs. Velocity Gradient

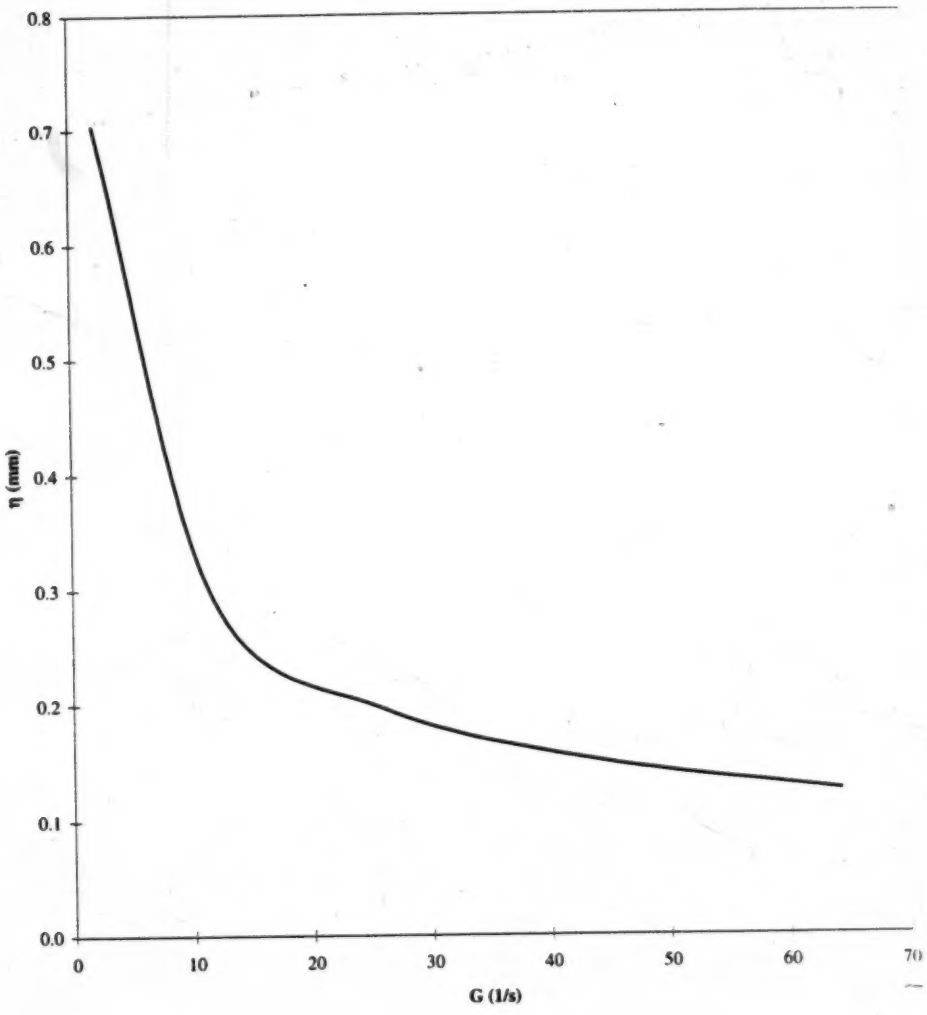

Figure 3.12: Komogoroff Microscale vs. Velocity Gradient

4. COMPARATIVE STUDY***

4.1 INTRODUCTION

Mixing is a required component of the flocculation process to produce particle contacts that cause floc growth. However, excessive mixing can cause floc break up. The goal of flocculation mixing is therefore to select a mixing intensity that will maximize particle contacts while maintaining minimal floc break up. In this case, a uniform mixing environment within a vessel is desired to allow easy optimization of mixing intensity. In most cases, impellers have been used as the flocculation mixing device. However, the use of impellers have been criticized due to the non uniform turbulent mixing characteristics within the vessel. Tomi and Bagster (1978), Stanley (1995), and Stanley and Smith (1995) found that the turbulent mixing intensity was much greater in the impeller region. It was also found that the impeller produced a jet like flow in the direction of vessel wall causing high shear forces on flocs. These regions of high shear tend to cause the agglomerated flocs to break up. As a result, mixing intensities in the remainder of the vessel are far from optimum for particle contacts. These studies have indicated that mixing intensity and forces on flocs within the vessel varied significantly from average volume values. Mixing intensities in impeller and vessel wall regions must then be lowered for an acceptable mixing

*** Submitted to the Journal of Environmental Engineering ASCE, April 1998.

performance.

Grid mixing can be used as an alternative mixing device in place of impellers. As has been found in traditional grid turbulence studies, turbulent intensities behind grids are close to uniform. In this study, a vertically oscillating grid mixing device was applied to promote floc aggregation. A slow frequency and long stroke was used to create a uniform mixing throughout the mixing region. The turbulent mixing characteristics could be modified from the vertical grid speed and grid physical characteristics. It was expected that this mixing device would create a better mixing environment for floc aggregation than that of impellers.

This study was conducted as a continuation of the two previous studies as described in Chapters 2 and 3. The first study (Chapter 2) applied eleven types of single grids (size of 110 x 110 mm^2) with different solidity ratio (d/M, where d = rod diameter and M = mesh or center to center distance between two rods). A standard 2L Hudson jar with a size of 115 x 115 x 150 mm^2 (Hudson and Wagner 1981) was used as the water vessel. A vertical stroke of 135 mm was applied for all cases. Five different vertical grid speeds v_{GS} from 10 to 130 mm/s were applied for each case. The emphasis of this study was to identify the mixing intensity created by the grid mixing. The measurement was completed using a 2D laser doppler anemometer (LDA). It was found that the root mean square (rms) turbulent velocity q' was uniform both in vertical and horizontal points of measurement; a condition that could not be achieved using traditional impellers. The average volume velocity gradient $\overline{G}$ vs. v_{GS} profiles

for all types of grids were developed. Since the mixing intensity was relatively constant, $\overline{G}$ could be used as the surrogate mixing parameter. The turbulent intensity was also found to easily be controlled from the v_{GS} and grid physical characteristics. The performance of impellers was also investigated. This study has shown that grid mixing is able to produce a more uniform mixing intensity than that of traditional impellers.

The second study (Chapter 3) applied five from the same types of grids used in the first study. These were grids nos. 1, 5, 7, 9, and 11 according to the notation used in the first study. Similar to the first study, a single grid with a vertical stroke of 135 mm was used for all cases. A standard 2L Hudson jar (Hudson and Wagner 1981) was used as the water vessel. The emphasis of the second study was to investigate the particle removal represented by the settled water turbidity. Five different v_{GS} (from 10 to 100 mm/s), six different flocculation times t_F (from 2 to 60 minutes), and a 30 minute sedimentation time were used for all cases. Kaolin and alum were used as the simulated turbid particles and chemical coagulant, respectively. High solidity ratio types of grids were found to have the best performance. Low turbidity readings were monitored over a wide range of $\overline{G}$ indicating a more stable performance for any mixing variations in the vessel. Floc agglomeration and erosion rate coefficients (k_1 and k_2) were obtained and showed that the grid mixing provided particle contacts with low floc break - up. General relations among $\overline{G}$, flocculation performance parameters, and grid physical characteristics were obtained. This showed that the overall

flocculation performance could directly be controlled. This study has shown an excellent performance of grid mixing for particle removal process.

The study presented here was completed as a continuation of these two studies. Multiple (double and triple) grids were applied as the mixing grids to observe any improvement over the single mixing grid case. Mixing intensity and settled water turbidity measurements similar to the two previous studies were conducted. General relations among flocculation performance parameters, $\overline{G}$, types of grids, and numbers of grids were expected. As a comparison, flocculation performance of a flat blade impeller was also investigated. It was expected that grid mixing would have a better flocculation performance than would the standard impeller.

4.2 METHODS AND MATERIAL

The same vertically oscillating grid mixing device used in the two previous studies was applied. The mixing device consisted of a variable speed controllable motor which was connected to a cam creating a constant vertical movement. The cam was connected to two vertical pistons to ensure a near perfect vertical movement. The pistons were connected by a lever to two small rods where the mixing grid moved vertically through them. The center of the lever could be slid horizontally to adjust the vertical stroke. Double and triple grids (each formed by the same type of grid) were used as the mixing grids. Vertical distances between two adjacent grids were set at 68 and 45 mm for double and triple grids, respectively. The vertical strokes were also

adjusted to 68 and 45 mm for the related condition. These settings would cover the same vertical mixing region of 135 mm as that in the case of single grid mixing. A standard 2L Hudson jar (115 mm x 115 mm x 150 mm) according to Hudson and Wagner (1981) was used as the water vessel.

The first part of this study measured the turbulent mixing intensity within the jar. Only grids nos. 1, 5, and 9 (according to the notation used in the previous studies) were used, representing low, medium, and high solidity ratio types of grids (see Table 4.1). Nine horizontal points of measurement were chosen for grid nos. 1 and 9, while six points were chosen for grid no. 5. These were the same horizontal points of measurement used in the first study (Chapter 2). Only one vertical sampling position was taken, i.e. in the middle of the vertical stroke. This can be compared to y = 0 mm in the case of single grid mixing. Figures 4.1a and 4.1b show the sampling point locations. Five different vertical grid speeds v_{GS} were used: 10, 20, 40, 40, and 50 mm/s for double grids, and 7, 10, 20, 27, and 33 mm/s for triple grids. TiO_2 was mixed in water to improve its light scattering property. The equipment was set to obtain a minimum of 1500 samples for each point of measurement. The velocity bandwidth was adjusted from 0.12 to 0.4 MHz depending on the v_{GS}.

The second part of this study was to measure the particle removal performance represented by the settled water turbidity. The same experimental setup as that of the second study was used. Distilled water was used as the main solution. The temperature was set held constant at 20 ± 0.5 °C from one test to another. Kaolin (50 mg/L), alum (25 mg/L), and sodium bicarbonate (168 mg/L) were used to simulate turbid

particles, chemical coagulant, and pH buffer, respectively. The solution pH before alum addition was set to 8.1 using hydrochlorous acid and sodium hydroxide solutions, which was found to be the optimum pH condition. In this case, sweep floc mechanism was dominant for the coagulation and flocculation process.

A standard flat blade impeller (76 mm x 25 mm) was used for rapid mixing. The mixing was conducted at 300 rpm for 1 minute. This was equal to $\overline{G}$ of about 700 s^{-1} (based on the impeller speed and $\overline{G}$ profiles as shown by Cornwell and Bishop 1983). This was the recommended $\overline{G}$ value for rapid mixing according to Amirtharajah (1978). Slow or flocculation mixing was completed using five types of grids (grids nos. 1, 5, 7, 9, and 11) which were set for double and triple grid arrangements. Five different v_{GS} were used, i.e. 5 to 50 mm/s and 10 to 40 mm/s for double and triple grid mixing, respectively. Flocculation times t_F of 2, 5, 10, 20, 40, and 60 minutes were used in this study.

In order to make a direct comparison to the impeller mixing study, similar bench scale tests were completed using a standard flat blade impeller (76 x 25 mm^2) as the slow mixing device. Seven different impeller speeds N were tried (i.e. 5, 20, 25, 30, 40, 50, and 75 rpm). Other experimental setups were made the same as those of the grid mixing study.

The particle removal was measured based on the settled water turbidity. Sedimentation time of 30 minutes was used for all cases. A large diameter pipette was used to withdraw 40 mL of sample from a point of 75 mm below the water surface.

Two drops of concentrated hydrochlorous acid and manual shaking were used to break the agglomerated flocs. This was conducted to negate any particle size and distribution effects (Andreu - Villegas and Letterman 1976). The turbidity was measured using a Hach turbidity meter in nephelometric turbidity unit (NTU) according to APHA - AWWA - WEF (1992). The accuracy of the reading varied with its turbidity reading: 0.1, 1, and 5 for turbidity readings in the range of 1 to 10, 10 to 40, and 40 to 100 NTU, respectively.

4.3 RESULTS AND ANALYSIS

Discussion of results and analysis is separated into three parts, the results and analysis for the turbulent mixing parameter measurement, particle removal, and standard impeller mixing studies. In order to make a comparison for single, double, and triple mixing grid performances, related results obtained from two earlier studies for the single grid mixing will also be presented. Chapters 2 and 3 are used as the references for the turbulent parameter measurement and particle removal studies, respectively.

4.3.1 Turbulent Parameter Results and Analysis

By applying a larger number of grids, it is expected that mixing intensity within the vessel can be improved. When a larger number of grids is applied, the same mixing intensity should be achieved at lower v_{GS} . A general relationship between the numbers of grids and types of grids should be obtained. This shows that grid mixing is

easily controlled that can be useful when designing mixing grids at different sizes and numbers of grids.

Turbulent mixing intensity can be represented using the root mean square (rms) turbulent velocity. This parameter basically measures the absolute fluctuation velocity component relative of the mean velocity (Tennekes and Lumley, 1972). Due to the vertical grid movement, vertical direction y is assumed as the main direction with rms turbulent velocity v' and mean velocity $\overline{V}$. In the horizontal direction x, u' and $\overline{U}$ are the rms turbulent and mean velocities. w' and $\overline{W}$ are the other horizontal velocity components in the z direction. These values were not measured in this study, and were assumed to be the same as those in the x direction.

The LDA measures directly both rms turbulent velocities u' and v' and mean velocities $\overline{U}$ and $\overline{V}$. However, in the case of grid mixing as shown in Chapter 2, the rms turbulent velocity consists of random and periodic components. The periodic component must be eliminated in further turbulent parameter calculations (Van't Riet et al. 1976; Wu et al. 1989; Wu and Patterson 1989; Stanley and Smith 1995; and Stanley 1995). A cosine function can be fit to the periodic component in the time auto correlation function $R(\tau)$. It is assumed that at large time τ, the random component disappears leaving only the periodic component. The random component can then be calculated from the difference between the total and periodic components. Subsequently, the terms u' and v' are now used as the random rms turbulent velocity components.

Similar to the first study (Chapter 2), the average rms turbulent velocity q' is used as the surrogate turbulent mixing intensity:

$$q' = \sqrt{\frac{1}{3}(v'^2 + 2u'^2)} \qquad (4.1)$$

q' vs. horizontal points of measurement profiles for grids nos. 1, 5, and 9 for double and triple grids were then developed. Figure 4.2 shows q' vs. horizontal points of measurement for triple grids no. 9 (n = number of grids = 3). A comparison among all types of grids and numbers of grids can be seen in Figures 4.3a and 4.3b. These figures show the coefficient of variation (COV = standard deviation / average value) and range (= maximum / minimum value) for all cases. In most cases, COV is found to be less than 0.25, while the range is less than 2. More variation can be seen in the case of low v_{GS}. Mixing intensity created by all grid mixing can then be considered as uniform since in the case of impeller mixing, the range can be found as high as 5 or even 6 (Wu et al. 1989; Wu and Patterson 1989; Stanley 1995; Stanley and Smith 1995; and Cheng et al. 1997). However, no specific patterns can be observed for three different numbers of grids. This indicates that a larger number of grids does not seem to improve its turbulent mixing uniformity. Appendices 2 and 3 provide complete data for double and triple grids.

In the case of single grid, three vertical planes of measurement were taken. It was found that q' values were very uniform with depth. In this current study, only one vertical position was taken, i.e. in the middle of the vertical stroke that could be

compared to y = 0 mm in the case of single grid (see Figure 4.1a). It was assumed that in the case of double and triple grids, the turbulent mixing intensity would also be uniform in the vertical direction.

Based on the above analysis, the average $\overline{q'}$ value taken from horizontal points of measurement can be assumed as the characteristic q' value for the specific type of grid. Similar to single grid mixing study, $\overline{q'}$ and v_{GS} for double and triple grids can also be correlated in a simple linear equation $\overline{q'} = m\, v_{GS}$ with coefficients of determination $R^2 > 0.97$ (see Table 4.1). It is then necessary to identify a general pattern of mixing created by different types of grids and numbers of grids. This provides information for further studies such as designing grids with different solidity ratio and different numbers of grids. As shown in the first study, m ($= \overline{q'} / v_{GS}$) can directly be correlated with the solidity ratio d/M. In this current study, $n^{0.29}$ (where n is the number of grids) was found to be the appropriate generalizing factor. The power coefficient 0.29 was chosen as the one to give the highest R^2 value (= 0.940). As can be seen in Figure 4.4, $m/n^{0.29}$ is linearly related to the grid solidity ratio d/M:

$$\frac{m}{n^{0.29}} = 0.61\, d/M + 0.11 \qquad (4.2)$$

This indicates that mixing intensity created by the grid mixing is easily controlled by the grid physical characteristics. Equation 4.2 indicates that higher mixing intensity is

achieved when applying 1) a larger number of grids and 2) higher solidity ratio types of grids as it should be in reality.

Average mean velocities $\overline{U}$ and $\overline{V}$ at any horizontal planes were found to be practically zero. Small values were observed that could be caused by back mixing flows in the vessel or other imperfection of the mixing design.

Since the turbulent mixing intensity is quite constant throughout the mixing region, the average volume turbulent velocity gradient $\overline{G}$ (s^{-1}) may be applied as the surrogate mixing parameter. $\overline{G}$ can be calculated based on drag force created by the mixing device movement that can be expressed as (Amirtharajah 1978):

$$\overline{G} = \sqrt{\frac{0.5\,\overline{V_R}^3\,C_D\,A_s}{V\,\nu}} \qquad (4.3)$$

where: $\overline{V_R}$ = relative mean velocity between mixing device (in this case is the grid) and fluid (mm/s), C_D = grid drag coefficient, A_s = grid solid area (mm^2), V = fluid volume (mm^3), and ν = fluid kinematic viscosity (mm^2/s).

In this study, $\overline{V_R}$ can be assumed to be the v_{GS} as the average mean velocities $\overline{U}$ and $\overline{V}$ ≈ 0 (see Chapter 2). The grid drag coefficient C_D was calculated based on literature that can be summarized as follows (Baines and Peterson 1951; Annand 1953; Pinker and Herbert 1967; and Roach 1987):

$$C_D = \frac{(d/M)^2 - 2(d/M) + 2}{[(d/M)-1]^4} \left[0.52 + \frac{66}{Re_d^{4/3}}\right] \quad (4.4)$$

$$Re_d = \frac{\overline{V_R}\, d}{\nu} \quad (4.5)$$

The first part of Equation 4.4 involves grid physical characteristics represented by its solidity ratio, while the second part shows the effect of Reynolds number. This equation is valid when $0 < (d/M) < 1$. Equation 4.5 expresses Reynolds number based on the rod diameter.

Based on Equations 4.3 to 4.5, $\overline{G}$ vs. v_{GS} profiles for all types of grids and numbers of grids can be found. In the case of double and triple grids, one half and one third of the original 2L volume values were substituted in Equation 4.3. Figure 4.5 shows $\overline{G}$ vs. v_{GS} for grid no. 9 (with the highest d/M) at three different numbers of grids. This figure shows that the same $\overline{G}$ can be achieved at lower v_{GS} when a larger number of grids is applied. Another comparison can also be made from $\overline{G}$ vs. Re_d profiles as shown in Figure 4.6. When a larger number of grids is applied, the same Re_d produces larger $\overline{G}$. As mentioned by Roach (1987), turbulent condition in the case of grid mixing is achieved when $Re_d > 100$. Referring to Camp (1955), the optimum $\overline{G}$ values for flocculation are in the range of 20 to 74 s^{-1}. Based on

Figure 4.6, it can be concluded that the optimum $\overline{G}$ values roughly lie in the turbulent region. Other types of grids with lower solidity ratio will have higher Re_d for the same $\overline{G}$ values.

A verification can be made by calculating the macro length scale L that is actually the characteristic length of the mixing device. This can be obtained using a dimensional analysis (Tennekes and Lumley 1972):

$$L = \frac{q'^3}{\overline{\varepsilon}} \qquad (4.6)$$

where $\overline{\varepsilon}$ is the average volume energy dissipation rate which is a direct function of $\overline{G}$ and ν (Amirtharajah 1978):

$$\overline{G} = \sqrt{\frac{\overline{\varepsilon}}{\nu}} \qquad (4.7)$$

Figure 4.7 shows L vs. v_{GS} profiles for grids nos. 1, 5, and 9 for all cases. It is evident that L is constant at high v_{GS} and does not change with the number of grids applied. This can be related with the previous findings. When turbulent mixing condition has been reached ($Re_d > 100$), macro length scale L will be constant. This finding also agrees with impeller mixing studies that the macro length scale in turbulent mixing

regime is constant (Stanley 1995 and Cheng et al. 1997). This basically shows that the above assumption ($\overline{V_R} \approx v_{GS}$) as well as the obtained $\overline{G}$ values are acceptable.

Kolmogoroff microscale η (defined as the smallest sustainable eddy) can then be calculated based on a dimensional analysis (Tennekes and Lumley 1972):

$$\eta = [\frac{\nu^3}{\varepsilon}]^{1/4} \tag{4.8}$$

Figure 4.8 shows η vs. v_{GS} for grids nos. 1, 5, and 9 for single, double, and triple grids, respectively. This figure shows the largest, medium, and smallest sizes of η. This relationship can be used to compare the intensity of turbulent mixing created by different types of grids. This microscale is also useful when analyzing forces acting on flocs. Many models have been developed based on the relationship between size of flocs and η (such as Parker et al. 1972). At the viscous turbulent regime (η > floc size), laminar shear is dominant that provides little stress on flocs. When η < floc size or known as the turbulent regime, turbulent shear is dominant causing significant drag, shear, and pressure forces.

4.3.2 Particle Removal Analysis and Result

The relative turbidity T/T_o (where T is the settled water turbidity and T_o is the initial water turbidity) and its related mixing intensity $\overline{G}$ were observed for different

flocculation mixing times t_F. Information obtained from this study is useful to define the optimum mixing intensity and mixing time that provides the best turbidity reduction. Since the same $\overline{G}$ can be achieved at less v_{GS}, it is expected that a larger number of grids will produce high particle contacts while maintaining a low floc break up rate. A general relationship that includes types of grids and numbers of grids is also expected that can be used for further designing purposes.

T/T_o vs. $\overline{G}$ profiles were developed for all cases. Each profile (at a given t_F) formed a curve from which a minimum point of T/T_o (T/T_o*) and its related optimum $\overline{G}$ ($\overline{G}$ *) were identified. T/T_o vs. t_F profiles were also developed. In this case, each profile (for a specific v_{GS}) formed an asymptotic line with T/T_o** as the asymptotic value. Similar to the single grid mixing study, t_F greater than 20 minutes did not improve the turbidity reduction significantly. t_F = 20 minutes was then assumed as the optimum t_F.

High solidity ratio types of grids were found to have higher $\overline{G}$ * values than those of low solidity ratio. However, these optimum values were monitored at a wider range of $\overline{G}$ values. This indicates that high solidity ratio types of grids have a more stable performance that is not greatly affected by any mixing variations in the vessel. Subsequently, the effect of number of grids was observed. It was found that a larger number of grids would decrease $\overline{G}$ * values and widened the range of $\overline{G}$ values from which low T/T_o were observed. Figures 4.9a and 4.9b show T/T_o vs. $\overline{G}$

and T/T_o vs. t_F profiles for grid no. 9 at t_F = 20 minutes and $\overline{G}$ of about 40 s^{-1}, respectively for three different numbers of grids (n = 1, 2, and 3, where n is the number of grids). Table 4.2 shows all results for different types of grids and numbers of grids. This table shows that almost all $\overline{G}^*$ values are in the range of 20 to 74 s^{-1} which is the optimum mixing intensity range for floc aggregation (Camp 1955).

Subsequently, a general relationship for different types of grids can be obtained. This information can be useful when designing mixing grids with different solidity ratio. As shown in the single grid mixing study, solidity ratio d/M has been found to be the appropriate generalizing factor. A general relationship between $\overline{G}^*$ and t_F can be obtained by applying $[d/M]^a$ as the generalizing factor. The values for a were found to be relatively constant at about 0.9 (i.e. 0.85 for single grid and 0.89 for double and triple grids). These values were obtained as the ones that gave the highest R^2 values (see Table 4.3). By applying 0.9 as the a value, an average value of $G^*/[d/M]^{0.9}$ was then taken for each t_F leaving only six data points in the curve for each number of grid applied. Table 4.4 shows the COV values for n = 1, 2, and 3. Figure 4.10 shows $\overline{G}^*/[d/M]^{0.9}$ vs. t_F profiles for all numbers of grids. This figure shows that lower $\overline{G}^*$ values are required when a larger number of grids is applied. The same procedure was also made for T/T_o^* vs. $\overline{G}^* t_F$ ($\overline{G}^*$ multiplied by t_F) and T/T_o^* vs. t_F profiles. In these cases, $[d/M]^{-0.08}$ and $[d/M]^0$ were found to be the appropriate generalizing factors, respectively (see Tables 4.3 and 4.4). Figures 4.11

then developed for T/T_o^* vs. $\overline{G}^* t_F / [d/M]^{-0.08}$ and T/T_o^* vs. t_F relationships.

Figures 4.10 to 4.12 are very useful to determine optimum conditions for grid mixing performance. Mixing intensity, flocculation time, types of grids, and numbers of grids can be set to achieve a desired particle removal. Figure 4.10 shows that $\overline{G}^*$ decreases with t_F and numbers of grids. However, t_F greater than 20 minutes do not seem to have any significant effect especially for n = 1. This agrees with the first study that t_F = 20 minutes can be assumed as the optimum flocculation mixing time. Figure 4.11 shows that T/T_o^* decreases with $\overline{G}^* t_F$. $\overline{G}^* t_F / [d/M]^{-0.08}$ equals to 100,000 produces T/T_o^* below 5% that can be considered as the optimum value. Figures 4.10 and 11 indicate that applying a larger number of grids will improve the performance. However, increasing the numbers of grids from 2 to 3 does not seem to make a significant difference. Figure 4.12 shows that T/T_o^* decreases with t_F without any significant effect from the types of grids (indicating by $[d/M]^0$ as the generalizing factor) and numbers of grids. This indicates that the same T/T_o^* will be achieved no matter what the grid arrangement as long as the appropriate combination of $\overline{G}^*$ and t_F has been chosen based on Figures 4.10 and 4.11. Figure 4.12 also indicates that t_F = 20 minutes produces $T/T_o^* < 5\%$ that can be considered as the optimum flocculation mixing time.

It is then possible to obtain general forms of $\overline{G}^*$ vs. t_F and $\overline{G}^* t_F$ vs. T/T_o^* relationships for different numbers of grids as follows:

$$\log\left[\frac{\overline{G}^{*}}{[d/M]^{0.9}\, n^{0.05}}\right] = -0.15 \log t_F + 2.09 \qquad R^2 = 0.902 \qquad (4.9)$$

$$\log T/T_o^{*} = -1.27 \log\left[\frac{\overline{G}^{*}\, t_F}{[d/M]^{-0.08}\, n^{-0.02}}\right] + 3.29 \qquad R^2 = 0.993 \qquad (4.10)$$

where n is the number of grids (valid for n = 1 to 3). $n^{0.05}$ and $n^{-0.02}$ were identified as values that gave the highest R^2 values.

Particle agglomeration and break up can then be analyzed for any specific combinations of mixing intensity, mixing time, and types of grids. Agglomeration and erosion rate coefficients (k_1 and k_2 in min^{-1}) can be obtained based on an ordinary differential equation developed by Argaman and Kaufman (1970) and Parker et al.(1972). They derived the particle disappearance rate as a function of the number of particles, t_F, k_1, and k_2. As mentioned by Andreu - Villegas and Letterman and also shown in Chapter 3, the number of particles can be represented by turbidity reading as long as the effect of particle size and distribution has been eliminated. As mentioned in the above experimental procedure, concentrated hydrochlorous acid and manual mixing was used to negate the effects of particle size and distribution. The solution of the ordinary differential equation can be expressed as:

$$\frac{T}{T_o} = [(1 - \frac{k_2}{k_1}) \exp(-k_1 tF)] + \frac{k_2}{k_1} \qquad (4.11)$$

where k_2/k_1 is the asymptotic value of T/T_o for each given v_{GS}. Different from its original equation, relative turbidity T/T_o is applied instead of turbidity T in order to avoid any variations in the initial turbidity reading T_o. The k_1 result will be unchanged, while k_2 will be smaller but still has the same trend compared to those of the original equation. Equation 4.11 basically produces T/T_o vs. t_F profiles at various $\overline{G}$ values. For each t_F, k_1 values were obtained using a non - linear regression method. k_2 could then be calculated based on k_1. A general relation for different types of grids was found by applying d/M as the generalizing factor. Table 4.3 shows that generalizing factors for three different numbers of grids are roughly constant at $[d/M]^{-0.5}$ and $[d/M]^{-2.0}$ for k_1 and k_2, respectively. Generalizing factors $[d/M]^{-0.5}$ and $[d/M]^{-2.0}$ show that higher solidity ratio types of grids produce lower k_1 and k_2 due to slower v_{GS} to achieve the same $\overline{G}$. This agrees with the previous finding that higher solidity ratio types of grids have larger optimum $\overline{G}$ ($\overline{G}$*) than those of low solidity ratio types of grids but have a wider range of $\overline{G}$ producing low T/T_o* values.

Subsequently, k_1 and k_2 were correlated with $\overline{G}$ using a non - linear regression method according to Argaman and Kaufman (1970) and Parker et al. (1972):

$$\frac{k_1}{[d/M]^{-0.5}} \sim \overline{G}^{\,b1} \qquad (4.12)$$

$$\frac{k_2}{[d/M]^{-2.0}} \sim \overline{G}^{\,b2} \qquad (4.13)$$

Tables 4.5a and 5b shows R^2 values for k_1 and final results for k_1 and k_2 for three different numbers of grids. b_1 and b_2 vary from 0.51 to 0.53 and 1.69 to 2.42. respectively based on the number of grids. Equations 4.12 and 4.13 can be presented in graphical forms as shown in Figures 4.13a and 4.13b. This figure shows that both k_1 and k_2 increase with $\overline{G}$. k_1 also increases with the number of grids, while k_2 decreases when more grids are applied. This indicates that a larger number of grids will improve particle contacts while maintaining a low floc break up rate.

The number of grids can be incorporated by applying a generalizing factor n (number of grids) as expressed in the following equations:

$$\log\left[\frac{k_1}{[d/M]^{-0.5}\, n^{0.20}}\right] = 0.53 \log[\overline{G}] - 1.29 \qquad R^2 = 0.935 \qquad (4.14)$$

$$\log\left[\frac{k_2}{[d/M]^{-2.0}\, n^{0.08}}\right] = 1.45 \log[\overline{G}] - 3.57 \qquad R^2 = 0.998 \qquad (4.15)$$

in this case, $n^{0.20}$ and $n^{0.08}$ were identified as the values that gave the highest R^2

values.

Exponents for $\overline{G}$ (about 0.5 and 2 for k_1 and k_2, respectively) can be compared with the theoretical values, i.e. 1 for k_1 and 2 to 4 for k_2 (Argaman and Kaufman 1970; Parker et al. 1972; and Amirtharajah and O'Melia 1990). For floc break up model, $\overline{G}^2$ has been derived in the case of viscous turbulent regime (diameter of flocs < Kolmogoroff microscale η), while $\overline{G}^4$ is the expression for the inertial turbulent regime (diameter of flocs > η). The difference in the floc aggregation rate may be caused by imperfection of the mixing device. Applying a larger number of grids improves the overall aggregation rate as shown in Figure 4.13a. but does not change the power coefficient which stays at about 0.5. Based on the exponent developed for k_2, mixing created by grids can be suggested to occur in the viscous turbulent regime. In this region, laminar shear is dominant that does not produce high shear on flocs. A more detailed study can be completed by measuring the size of flocs that will be compared with the Kolmogoroff microscale η as mentioned above.

4.3.3 Standard Impeller Analysis and Result

Detailed turbulent mixing parameter measurement studies have been completed by other investigators (Wu and Patterson 1989; Wu et al. 1989; Stanley 1995; Stanley and Smith 1995; and Cheng et al. 1997). In general, they showed some significant variations in the local turbulent intensity represented by the rms

radial and tangential turbulent velocities. As summarized in Chapter 2, the variation can be as high as five to six times. As a comparison, in the case of grid mixing the variation is small (see Figures 4.3a and 4.3b).

The same particle removal analyses as those of the grid mixing studies were completed. The relation between impeller speed N and $\overline{G}$ can be found based on Cornwell and Bishop (1983). A direct performance comparison between the standard impeller and grid mixing device can be completed. In general, the standard impeller performs similarly to low solidity ratio types of grids at a smaller number of grids. Low $\overline{G}$* in a narrower range of $\overline{G}$ values were found, which was caused by high agglomeration but also high erosion rate coefficients. This shows that grid mixing in its best performance (triple high solidity ratio types of grids) will provide better flocculation performance than will standard impeller mixing. Figures 4.14, 4.15a, and 4.15b show the performance differences between triple grids no. 9 (with the highest solidity ratio) and standard impeller.

4.4 CONCLUSIONS

This study has shown that the same turbulent mixing intensity $\overline{G}$ can be achieved at less vertical grid speed v_{GS} when a larger number of grids are applied. This will create more particle contacts while maintaining a low floc break up rate.

This study has also shown that triple high solidity ratio types of grids produce the best flocculation performance. Low turbidity readings (T/T_o) can be achieved

at a wide range of $\overline{G}$. Optimum $\overline{G}$ ($\overline{G}$*) values were observed in the range of optimum mixing intensity for floc aggregation (20 to 74 s^{-1}). Agglomeration and erosion rate coefficient analyses have also shown that higher particle contacts and lower floc break up are produced when applying a larger number of grids.

Excellent general relations among turbulent mixing intensity, grid physical characteristics, numbers of grids, and flocculation performance parameters have been found. This indicates that the mixing environment created by the vertically oscillating grid mixing device can easily be controlled which becomes important to determine the optimum condition for a desired flocculation performance. This is also useful when designing grids with different types of grids and numbers of grids.

The standard flat blade impeller has been found to have a lower optimum $\overline{G}$ located in a narrower range of $\overline{G}$ values caused by high floc agglomeration but also high erosion rate coefficients. This indicates that grid mixing in its best arrangement provides a better flocculation mixing performance than that of impeller.

4.5 REFERENCES

Amirtharajah, A. (1978). "Design of rapid mixing units." *Water Treatment Plant Design*, R. L. Sanks, editor. Ann Arbor Science Inc, Ann Arbor, Michigan, 131 - 148.

Amirtharajah, A. and O,Melia, C. R. (1990). "Coagulation processes: Destabilization, mixing, and flocculation." *Water Quality and Treatment*, F. W. Pontius,

editor. McGraw - Hill, New York, New York, 269 - 366.

Andreu - Villegas, R. and Letterman, R. D. (1976). "Optimizing flocculator power input." *Journal of the Environmental Engineering, ASCE*, 102 (EE2), 251 - 263.

Annand, W. J. D. (1953). "The resistance to air flow of wire gauzes." *Journal of the Royal Aeronautical Society*, 57, 141 - 146.

APHA - AWWA - WEF. (1992). *Standard methods for the examination of water and wastewater*, A. E. Greenberg, L. S. Clesceri, and A. D. Eaton, editors. APHA. Washington, District of Columbia, 2-8 - 2-11.

Argaman, Y. A. and Kaufman, W. J. (1970). "Turbulence and flocculation." *Journal of the Sanitary Engineering Division, ASCE*, 96 (SA2), 223 - 241.

Baines, W. D. and Peterson, E. G. (1951). "An investigation of flow through screens." *Transactions of the ASME*, 73, 467 - 480.

Camp, T. R. (1955). "Flocculation and flocculation basin". *Transactions of ASCE*, Paper No. 2722, 1 - 16.

Cheng, Chen-Yu, Atkinson, J. F., and Bursik, M. I. (1997). "Direct measurement of turbulence structures in mixing jar using PIV." *Journal of Environmental Engineering*, 123 (2), 115 - 125.

Cornwell, D. A and Bishop, M. M. (1983). "Determining velocity gradients in laboratory and full - scale system." *Journal AWWA*, 75 (9), 470 - 475.

Hudson, H. E. Jr. and Wolfner, J. P. (1967). "Design of mixing and flocculation basins." *Journal AWWA*, 59 (10), 1257 - 1267.

Hudson, H. E. Jr. and Wagner, E. G. (1981). "Conduct and use of jar tests." *Journal AWWA*, 73 (4), 218 - 224.

Parker, D. S., Kaufman, W. J., and Jenkins, D. (1972). "Floc breakup in turbulent flocculation processes." *Journal of the Sanitary Engineering Division, ASCE*, 98 (SA1), 79 - 99.

Pinker, R. A. and Herbert, M. V. (1967). "Pressure loss associated with compressible flow through square - mesh wire gauzes." *Journal of Mechanical Engineering and Science*, 9 (1), 11 - 23.

Roach, P. E. (1987). "The generation of nearly isotropic turbulence by means of grids." *Journal of Heat and Flow*, 8 (2), 82 - 92.

Stanley, S. J. (1995). "Measurement and analysis of mixing as it relates to flocculation." *Ph.D. Thesis*, University of Alberta, Edmonton, Alberta.

Stanley, S. J. and Smith, D. W. (1995). "Measurement of turbulent flow in standard jar test apparatus." *Journal of Environmental Engineering*, 121 (12), 902 - 910.

Tennekes, H. and Lumley, J. L. (1972). *A first course in turbulence*, MIT Press. Cambridge, Massachusetts.

Tomi, D. T. and Bagster, D. F. (1978). "The behavior of aggregates in stirred vessels. Part I. Theoretical consideration in the effects of agitation." *Transactions of the Institute of Chemical Engineers*, 56, 1 - 8.

Van't Riet, K., Bruijn, W., and Smith, J. M. (1976). "Real and pseudo - turbulence in the discharge stream from a rushton turbine." *Chemical Engineering*

Science, 31, 407 - 412.

Wu, H. and Patterson, G. K. (1989). "Laser - doppler measurements of turbulent - flow parameters in stirred mixer." *Chemical Engineering Science*, 44 (10), 2207 - 2221.

Wu, H., Patterson, G. K., and Van Doorn, M. (1989). "Distribution of turbulence energy dissipation rate in a rushton turbine stirred mixer." *Experiments in Fluids*, 8, 153 - 160.

Table 4.1: m vs. d/M

Type of Grid	Grid Geometry				$q' = m \cdot vGS$					
					n = 1		n = 2		n = 3	
	Rod d (mm)	# of Rods	Mesh M (mm)	d/M	Slope m*)	R^2	Slope m	R^2	Slope m	R^2
1	3.2	2x6	18.3	0.17	0.203	> 0.99	0.259	0.981	0.300	0.990
5	4.8	2x8	13.8	0.35	0.335	> 0.99	0.430	0.973	0.489	0.972
9	6.4	2x10	11.0	0.58	0.463	> 0.99	0.555	0.996	0.649	0.997

Note: *) = average value for three vertical levels of measurement

Table 4.2: Range for G values and G*

Type of Grid	Sodility Ratio (d/M)		G Values Giving Low T/To for tF = 20 minutes			G*(1/s)		
			n = 1	n = 2	n = 3	n = 1	n = 2	n = 3
1	0.17	low	16 to 22	13 to 24	13 to 22	18	15	14
7	0.29		20 to 27	18 to 28	16 to 27	26	22	21
5	0.35	medium	30 to 42	20 to 33	20 to 41	32	27	25
11	0.52		30 to 48	30 to 60	29 to 62	43	38	37
9	0.58	high	22 to 60	23 to 69	20 to 76	47	43	42

Table 4.3:Generalizing Factors

Analysis	n = 1		n = 2		n = 3	
	Factor	R^2	Factor	R^2	Factor	R^2
G* vs. tF	[d/M]^0.85	0.949	[d/M]^0.89	0.934	[d/M]^0.89	0.932
T/To* vs. tF	[d/M]^0	0.986	[d/M]^0	0.987	[d/M]^0	0.986
T/To* vs. G*tF	[d/M]^-0.08	0.982	[d/M]^-0.08	0.988	[d/M]^-0.08	0.986
k1 vs. G	[d/M]^-0.45	0.968	[d/M]^-0.46	0.963	[d/M]^-0.46	0.979
k2 vs. G	[d/M]^-2.01	0.978	[d/M]^-2.00	0.835	[d/M]^-1.99	0.828

Table 4.4: Coefficient of Variation for Average Values

tF (min)	n = 1			n = 2			n = 3		
	T/To*	G*(ω/MI)^0.9	G*(ω/MI)^-0.1	T/To*	G*(ω/MI)^0.9	G*(ω/MI)^-0.1	T/To*	G*(ω/MI)^0.9	G*(ω/MI)^-0.1
2	0.034	0.074	0.120	0.028	0.049	0.162	0.063	0.041	0.137
5	0.083	0.051	0.049	0.185	0.023	0.094	0.109	0.030	0.099
10	0.109	0.042	0.040	0.098	0.028	0.074	0.069	0.023	0.076
20	0.066	0.032	0.030	0.067	0.027	0.035	0.088	0.030	0.054
40	0.068	0.069	0.091	0.098	0.040	0.037	0.100	0.019	0.018
60	0.048	0.078	0.116	0.079	0.047	0.051	0.063	0.026	0.026

Table 4.5a: R^2 Values for k1

Grid No.	vGS (low to high)	R^2 for k1		
		n = 1	n = 2	n = 3
1	1	0.983	0.974	0.903
	2	0.986	0.959	0.926
	3	0.993	0.962	0.953
	4	0.995	0.977	0.984
	5	1.000	0.980	0.987
	6	0.999	0.980	0.984
	7	0.974	0.986	0.988
5	1	0.983	0.946	0.958
	2	0.988	0.960	0.984
	3	0.982	0.972	0.992
	4	0.990	0.967	0.996
	5	0.994	0.982	0.994
	6	0.997	0.982	0.998
	7	0.999	0.985	0.998
7	1	0.993	0.970	0.952
	2	0.983	0.974	0.961
	3	0.985	0.961	0.980
	4	0.986	0.969	0.976
	5	0.990	0.985	0.986
	6	0.991	0.988	0.991
	7	0.999	0.993	0.995
9	1	0.982	0.993	0.978
	2	0.980	0.965	0.977
	3	0.987	0.989	0.992
	4	0.993	0.992	0.997
	5	0.994	0.996	0.996
	6	0.994	0.995	0.994
	7	0.962	0.995	0.998
11	1	0.974	0.988	0.925
	2	0.976	0.967	0.952
	3	0.994	0.985	0.970
	4	0.989	0.993	0.986
	5	0.992	0.994	0.991
	6	0.999	0.995	0.996
	7	0.998	0.998	0.998

Table 4.5b: k1 and k2 vs. G

Parameter	n = 1	n = 2	n = 3
k1=	0.048 G^0.55	0.065 G^0.51	0.062 G^0.53
R^2=	0.968	0.963	0.979
k2=	3.91E-7 G^2.42+0.015	5.02E-7 G^2.28 + 0.015	5.72E-7 G^1.69 + 0.015
R^2=	0.978	0.835	0.828

Figure 4.1a: Vertical Levels of Sampling Points

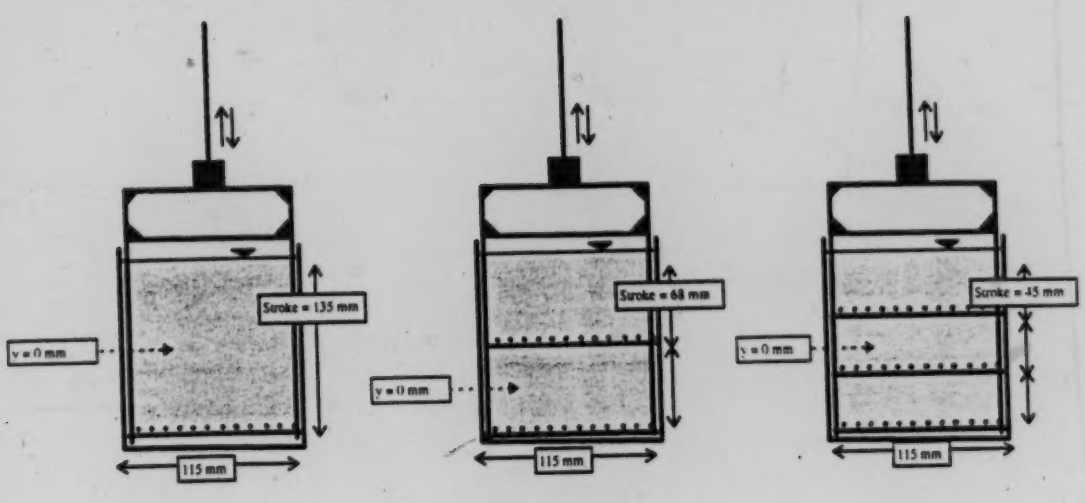

Single Grid Double Grids Triple Grids

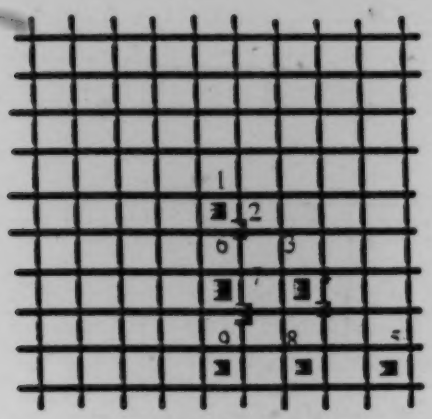

n=2x10 (Grid No. 9)

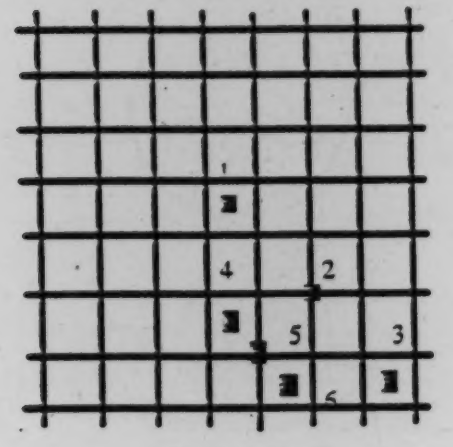

n=2x8 (Grid No. 5)

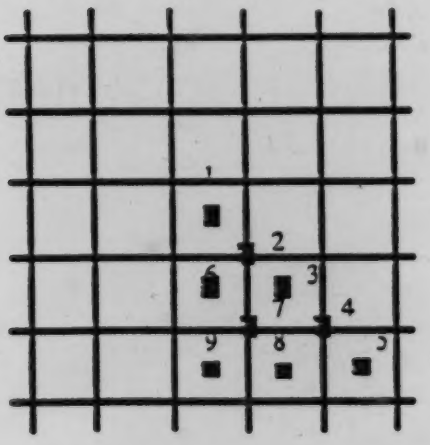

n=2X6 (Grid No. 1)

Figure 4.1b : Horizontal Points of Measurement

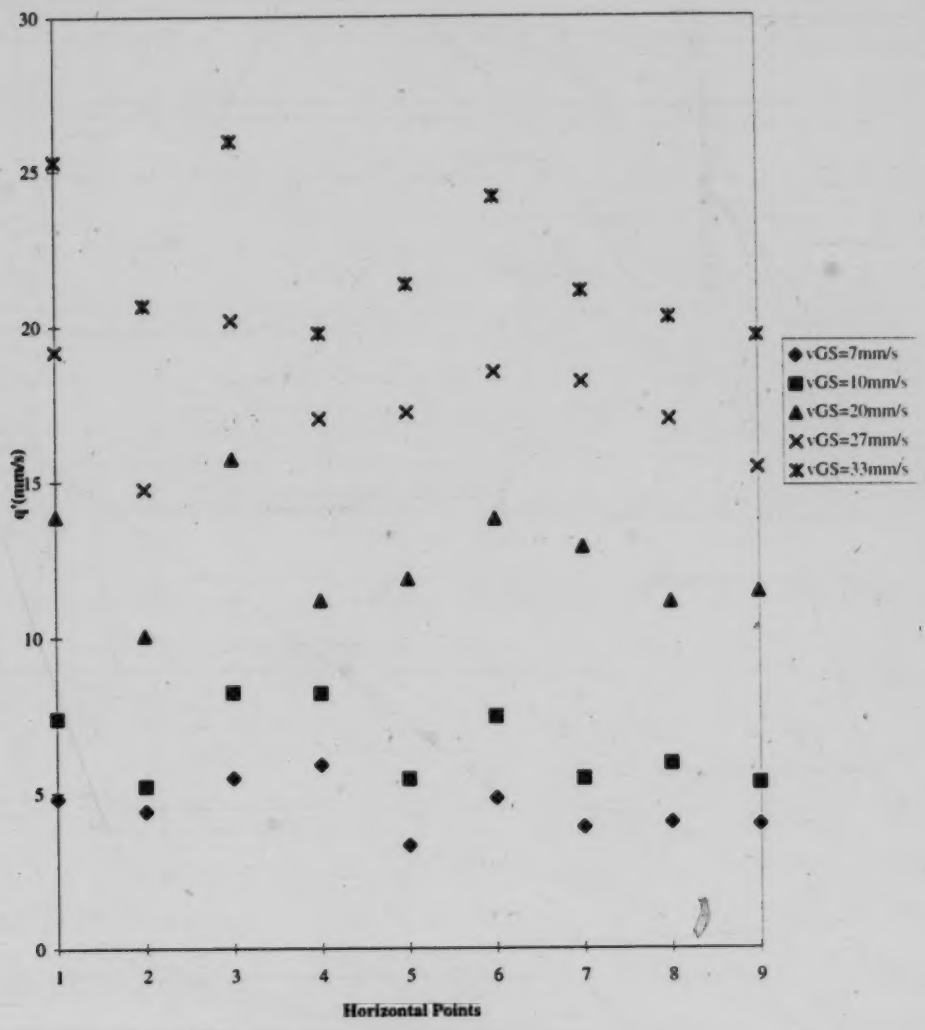

Figure 4.2: Average rms Turbulent Velocity vs. Horizontal Points forGrid No. 9, n=3

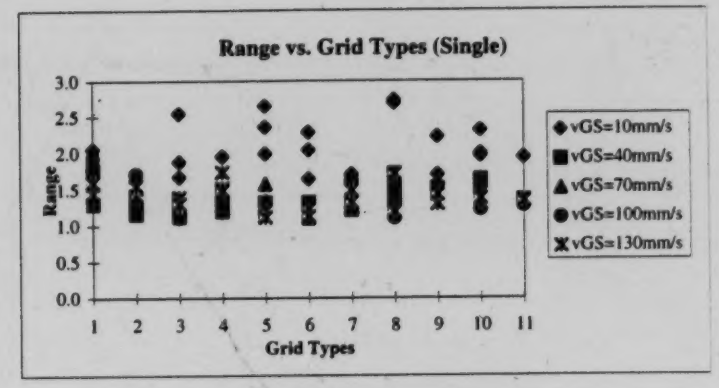

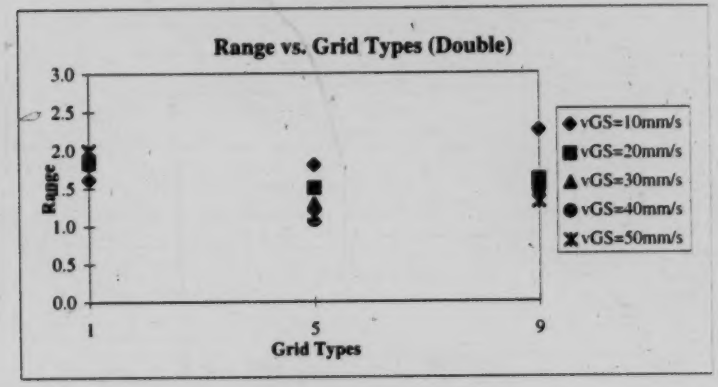

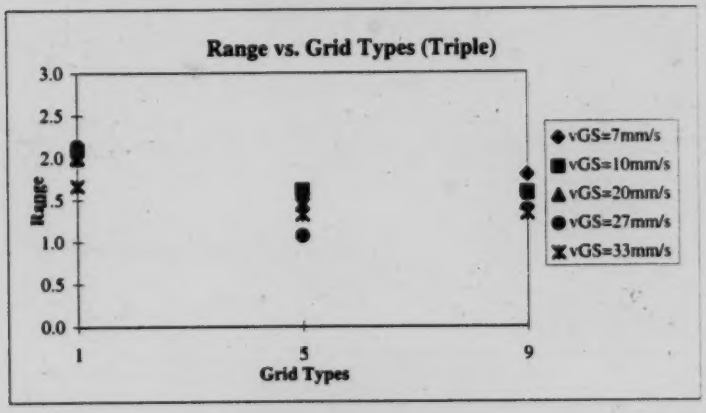

Figure 4.3a: Range Values

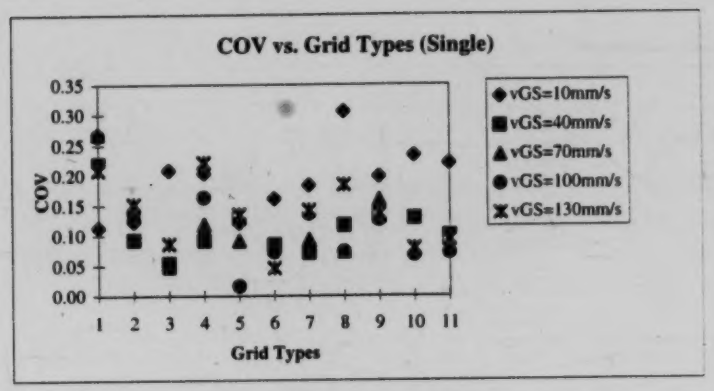

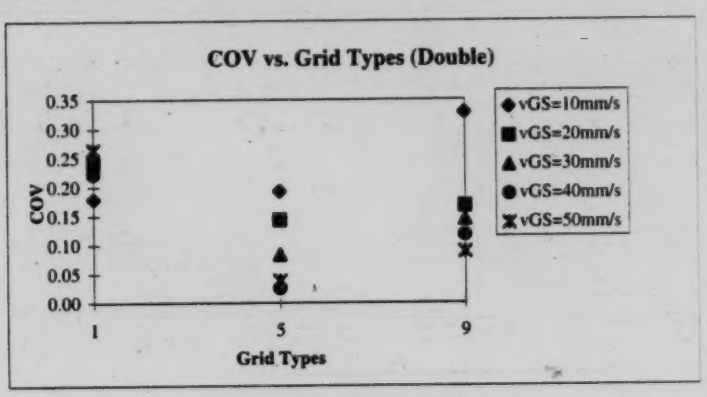

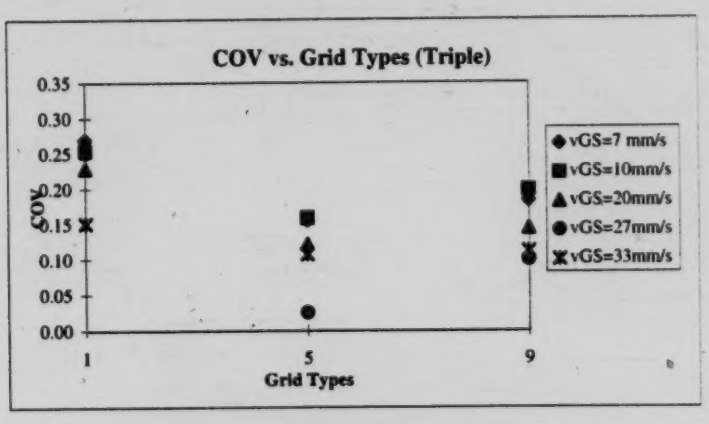

Figure 4.3b: Coefficient of Variation Values

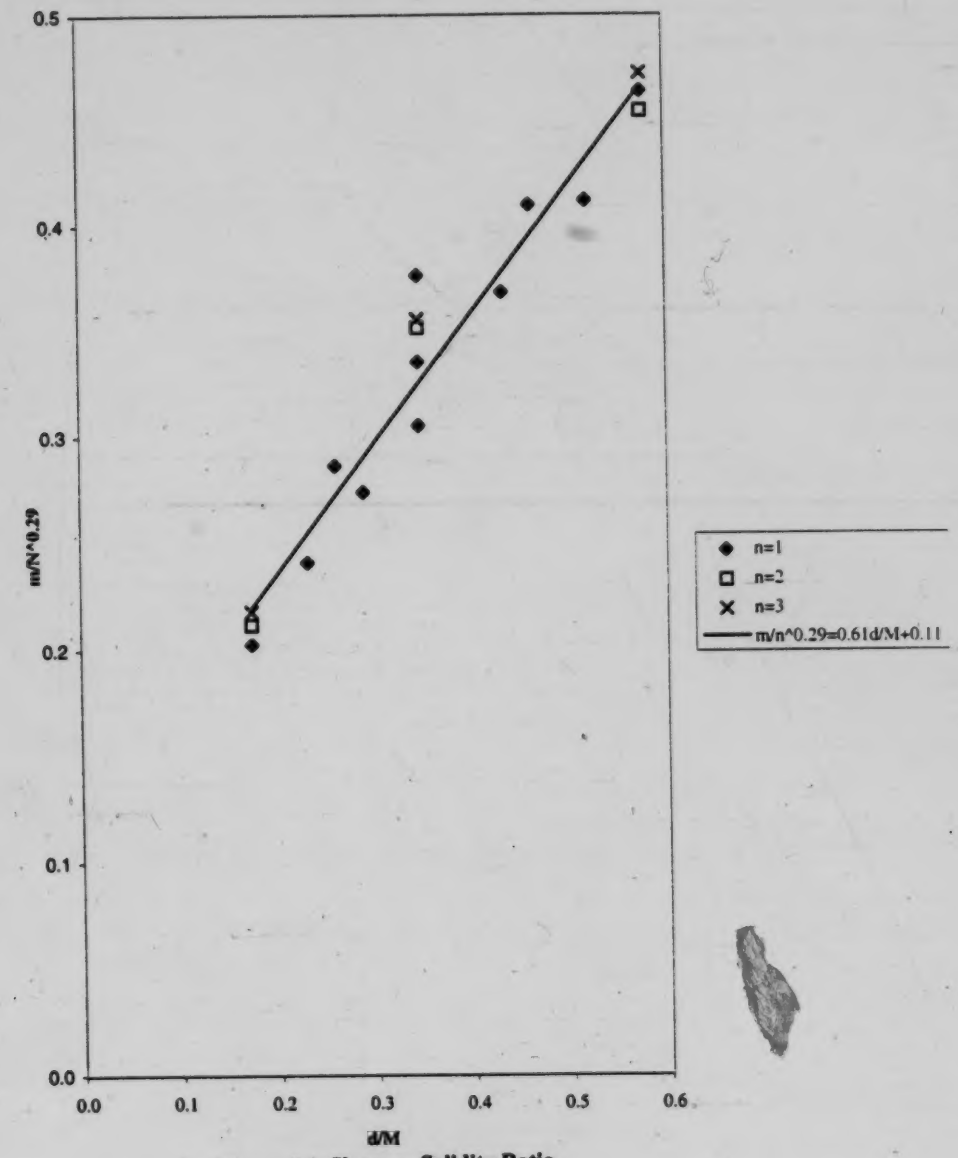

Figure 4.4: Slope vs. Solidity Ratio

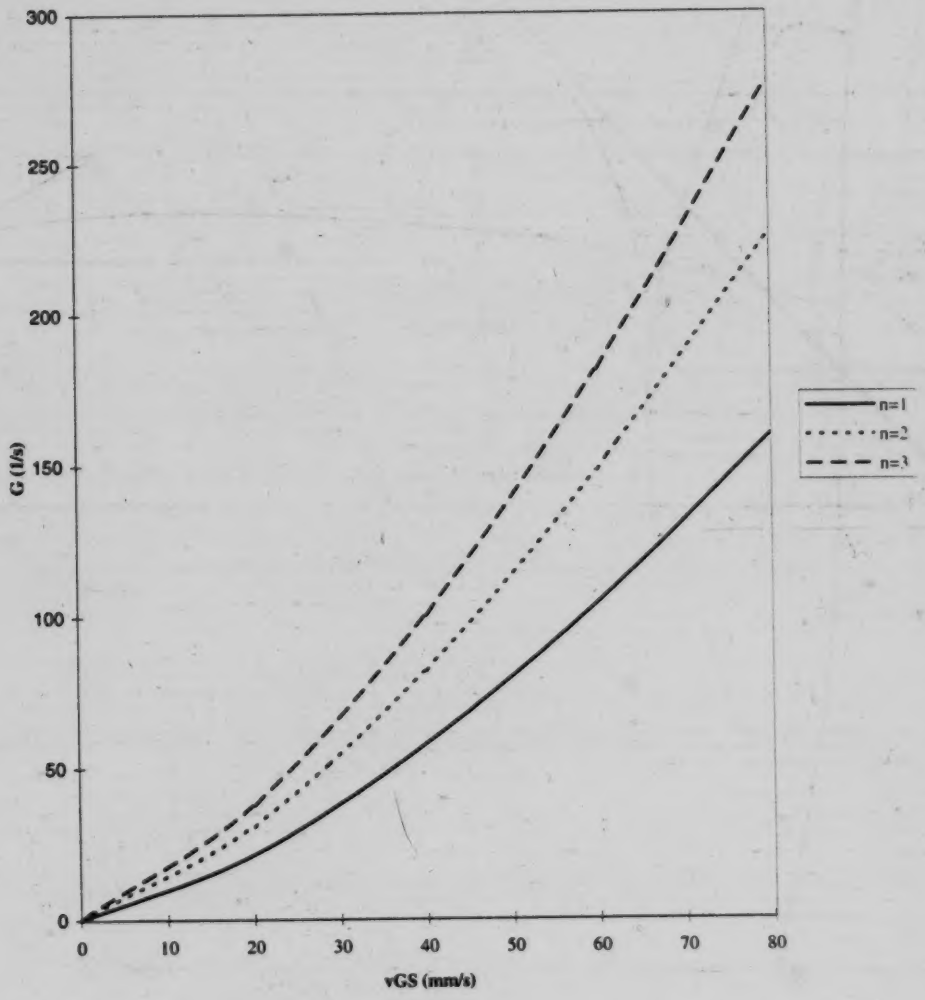

Figure 4.5: Velocity Gradient vs. Vertical Grid Speed for Grid No. 9

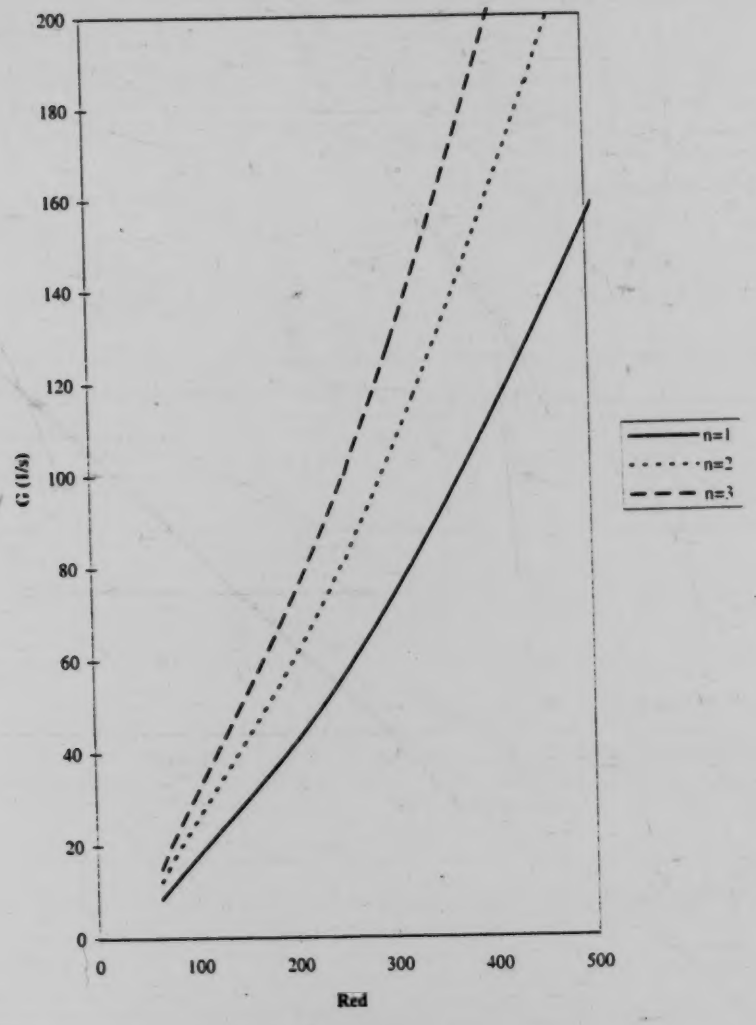

Figure 4.6: Velocity Gradient vs. Reynolds Number for Grid No. 9

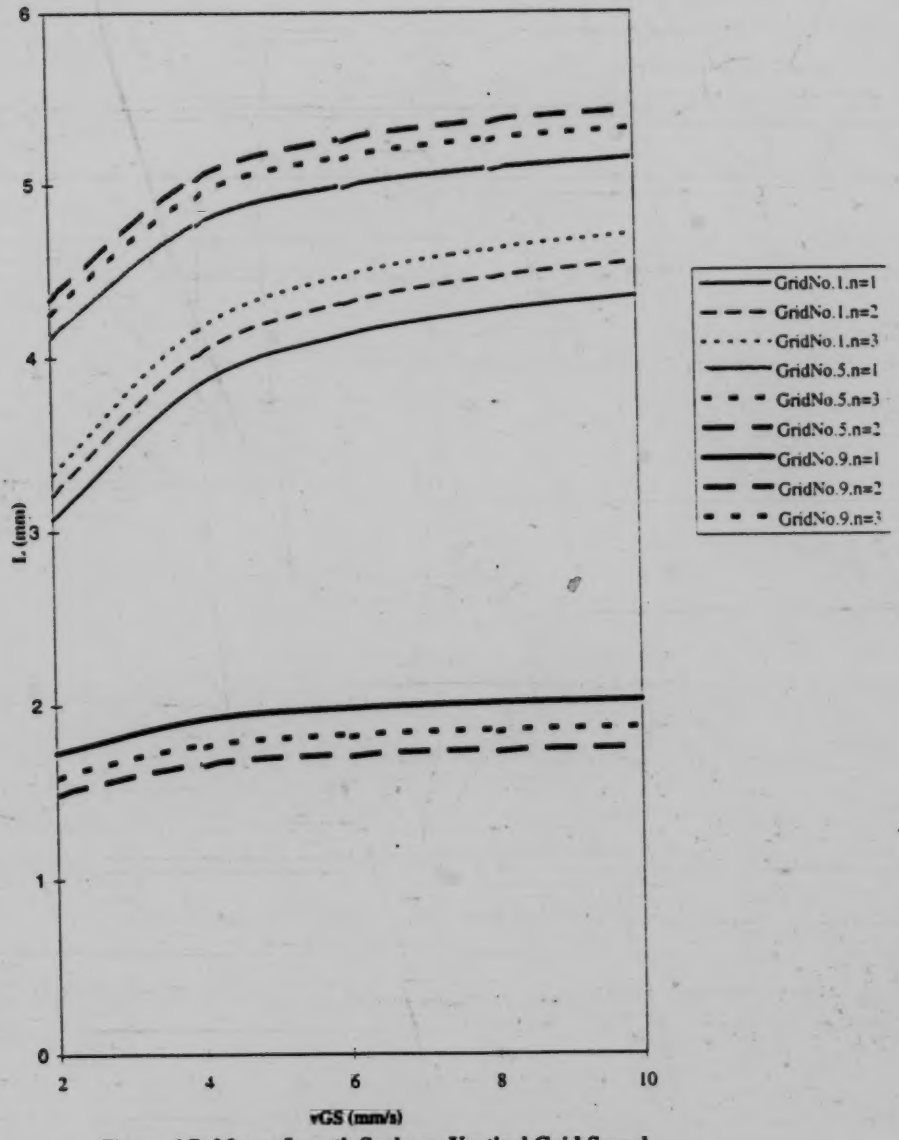

Figure 4.7: Macro Length Scale vs. Vertical Grid Spped

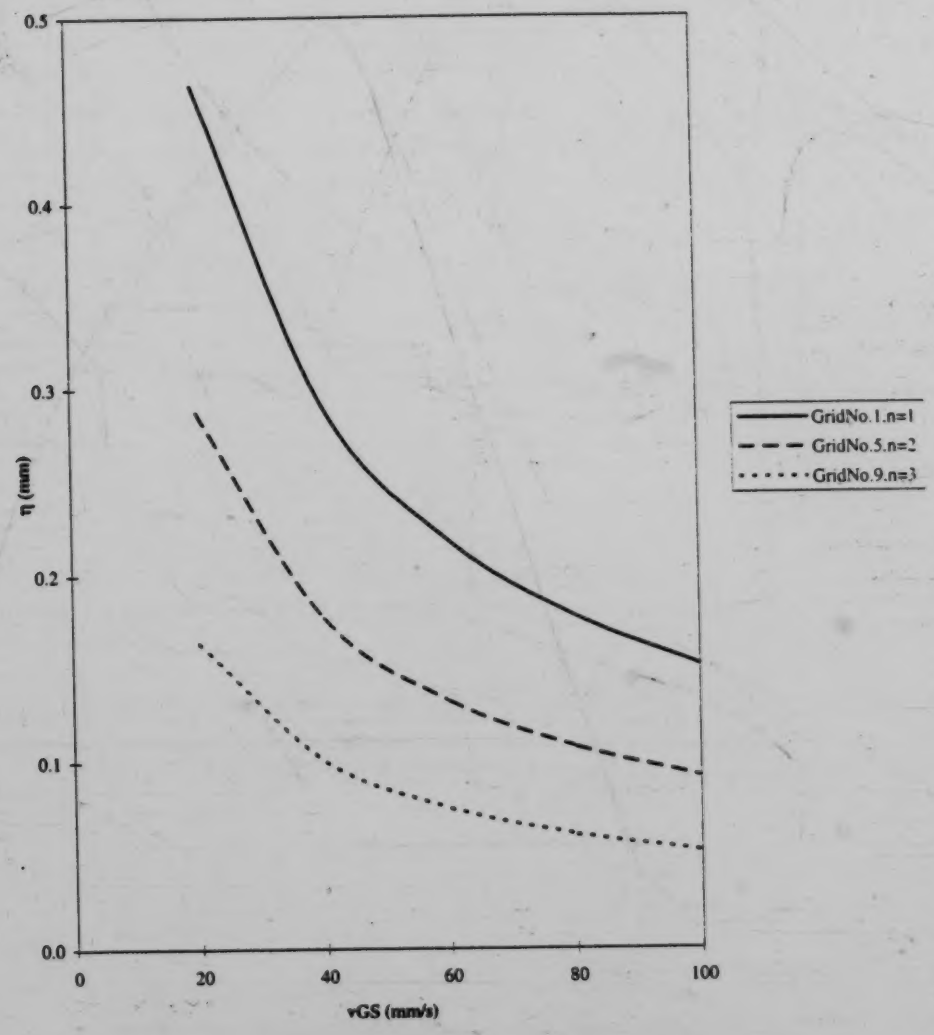

Figure 4.8: Kolmogoroff Microscale vs. Vertical Grid Speed

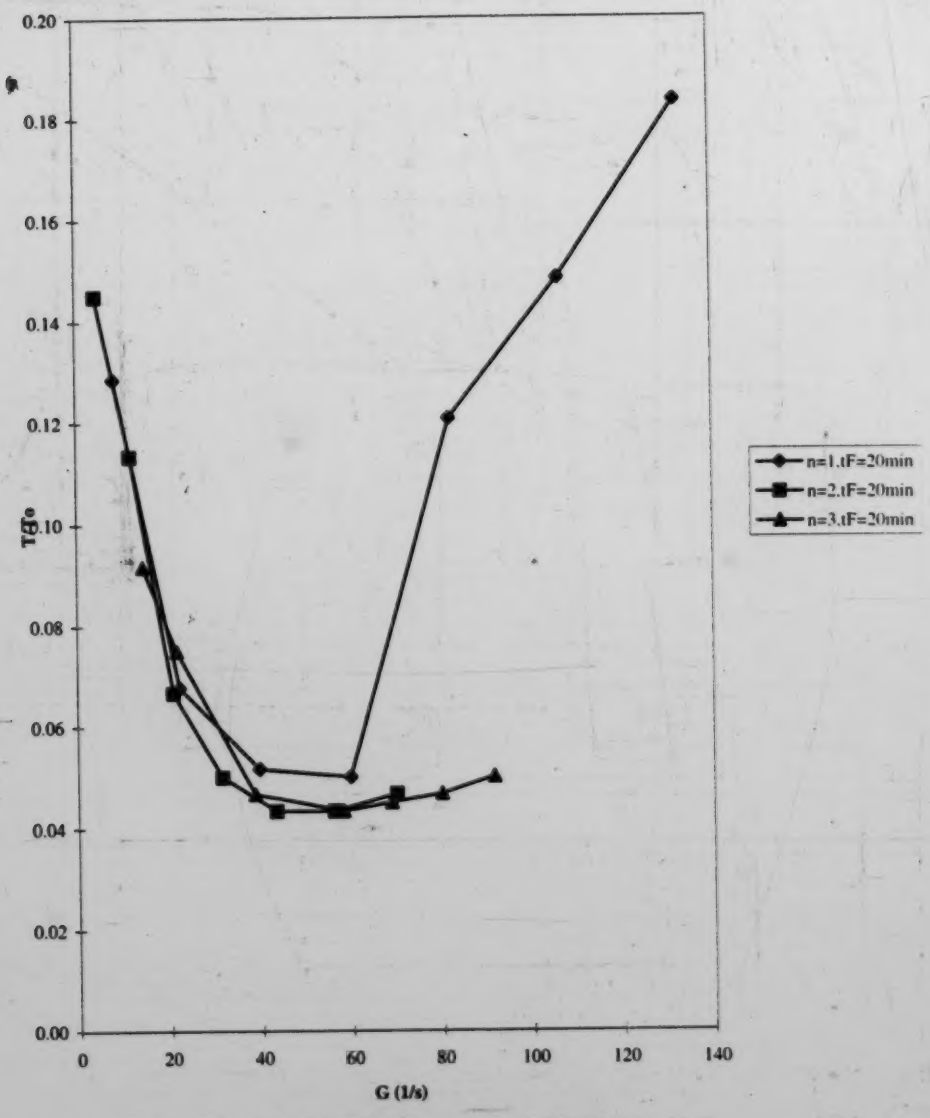

Figure 4.9a: Relative Turbidity vs. Velocity Gradient for Grid No. 9

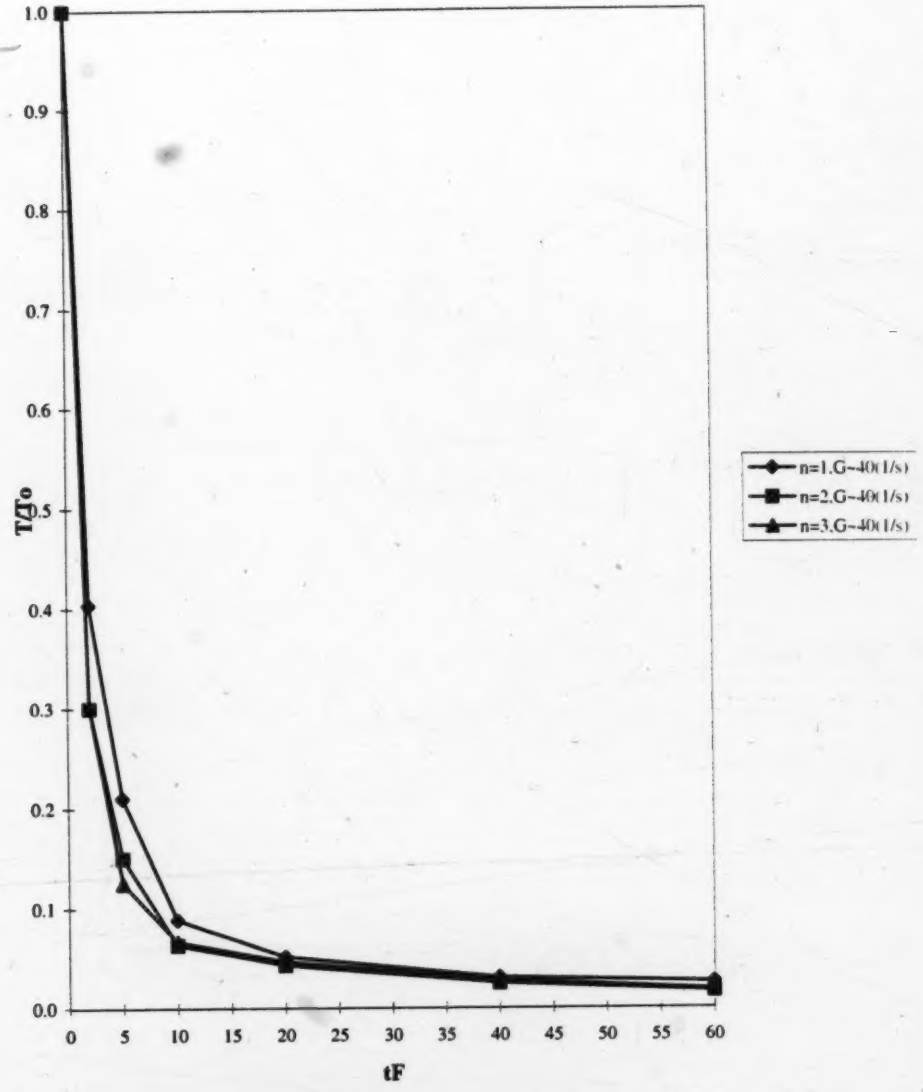

Figure 4.9b: Relative Turbidity vs. Flocculation Time for Grid No. 9

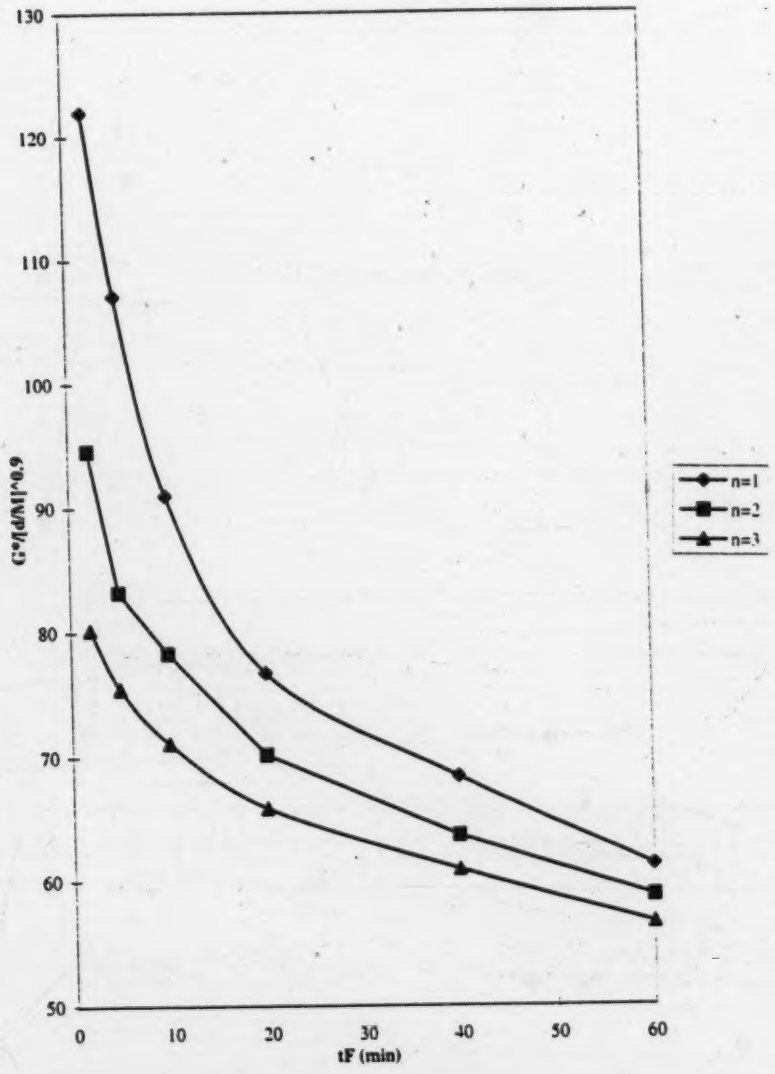

Figure 4.10: Optimum Velocity Gradient vs. Flocculation Time

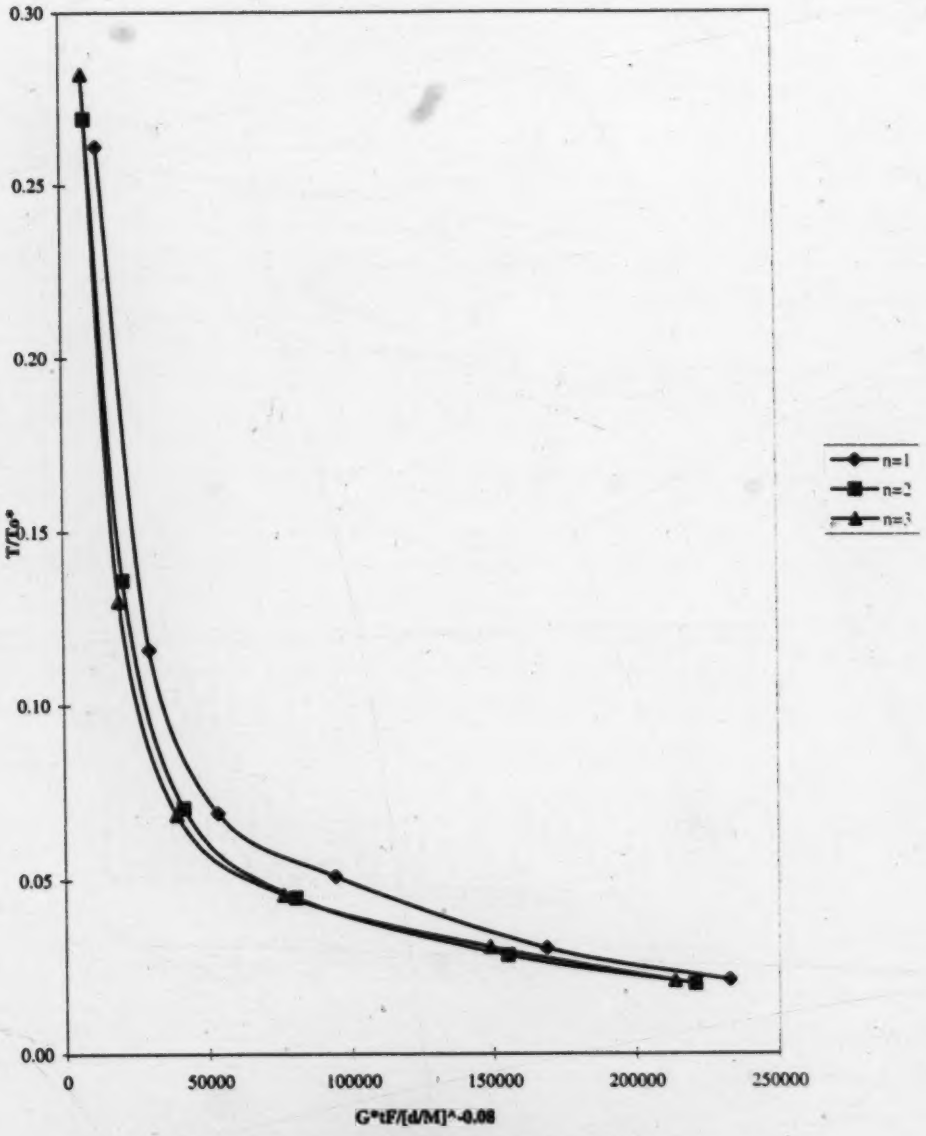

Figure 4.11: Minimum Relative Turbidity vs. Optimum Velocity Gradient * Flocculation Time

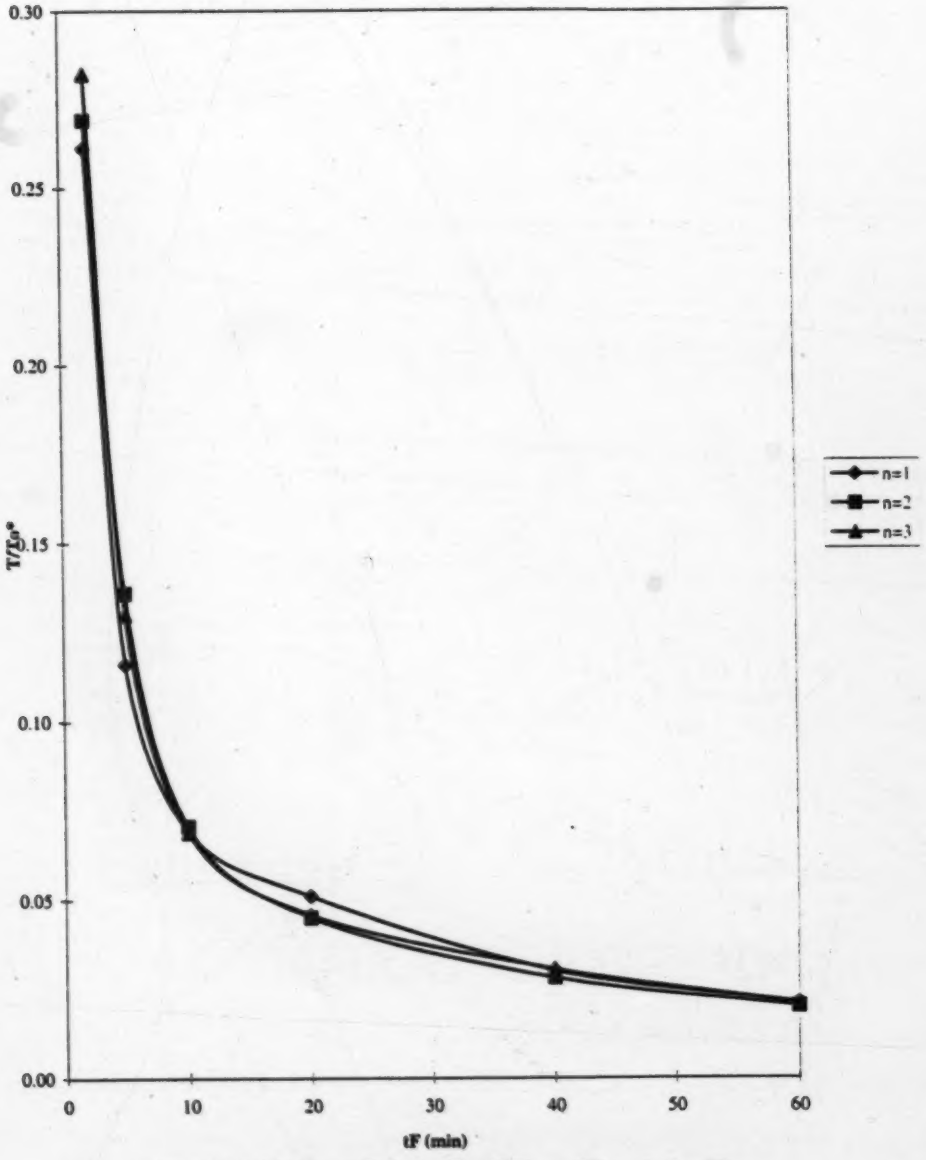

Figure 4.12: Minimum Relative Turbidity vs. Flocculation Time

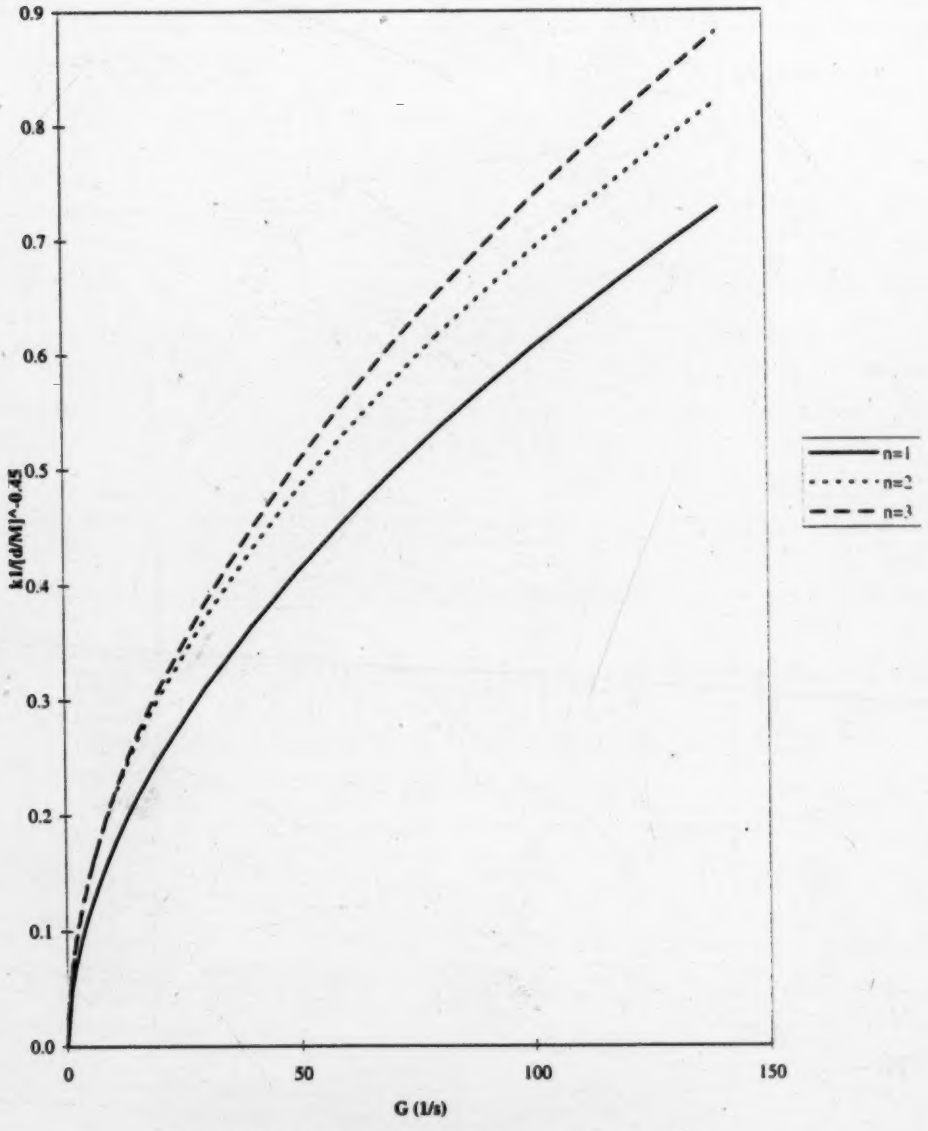

Figure 4.13a: Agglomeration Rate vs. Velocity Gradient

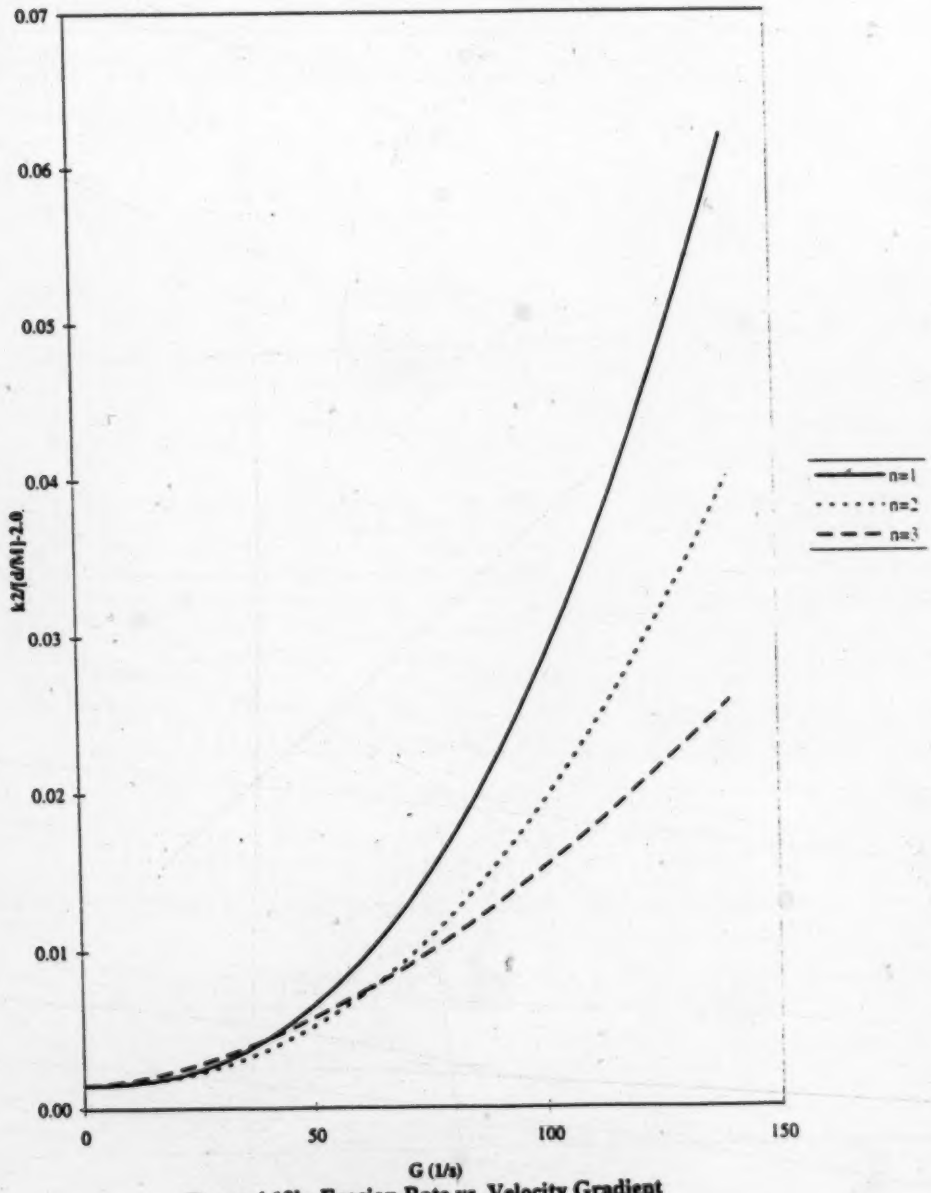

Figure 4.13b: Erosion Rate vs. Velocity Gradient

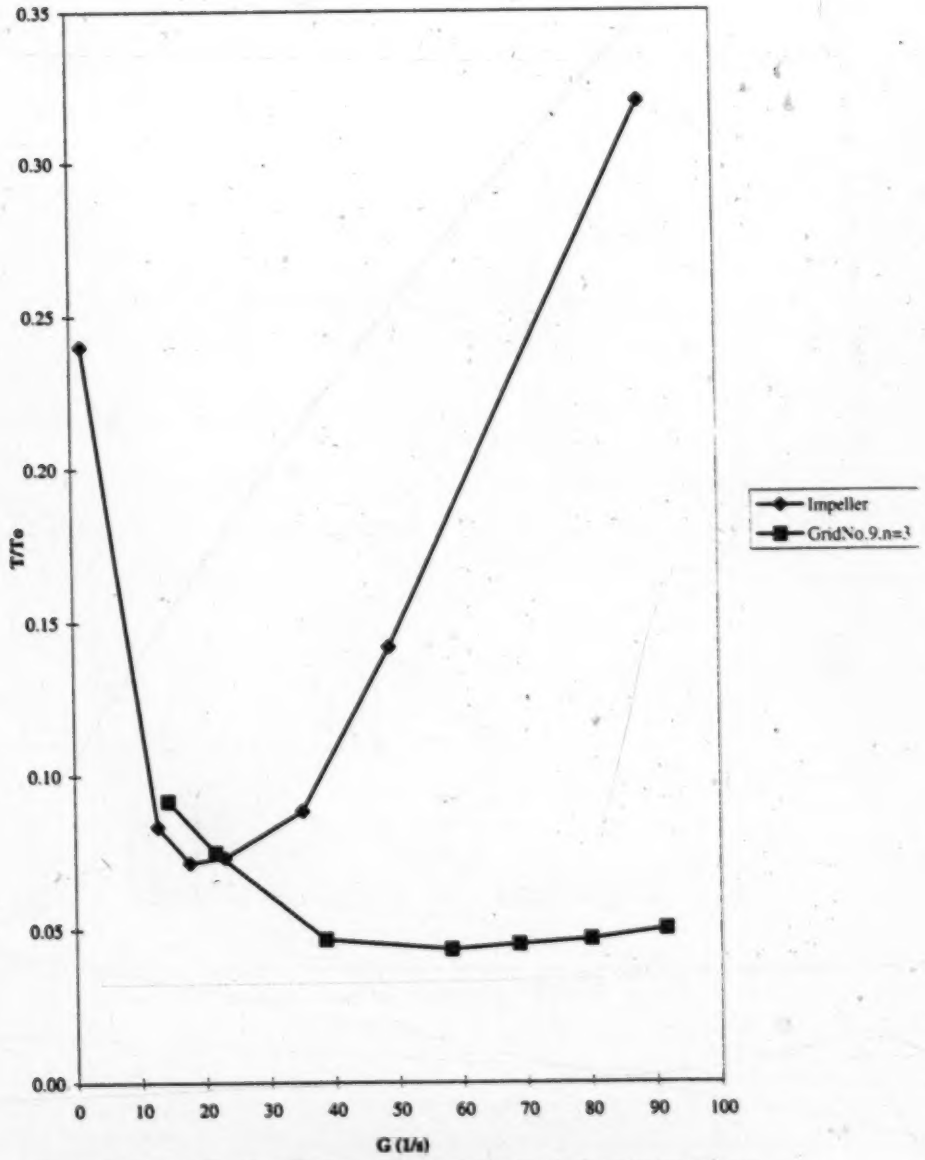

Figure 4.14: Relative Turbidity vs. Velocity Gradient (Flocculation Time = 20 min)

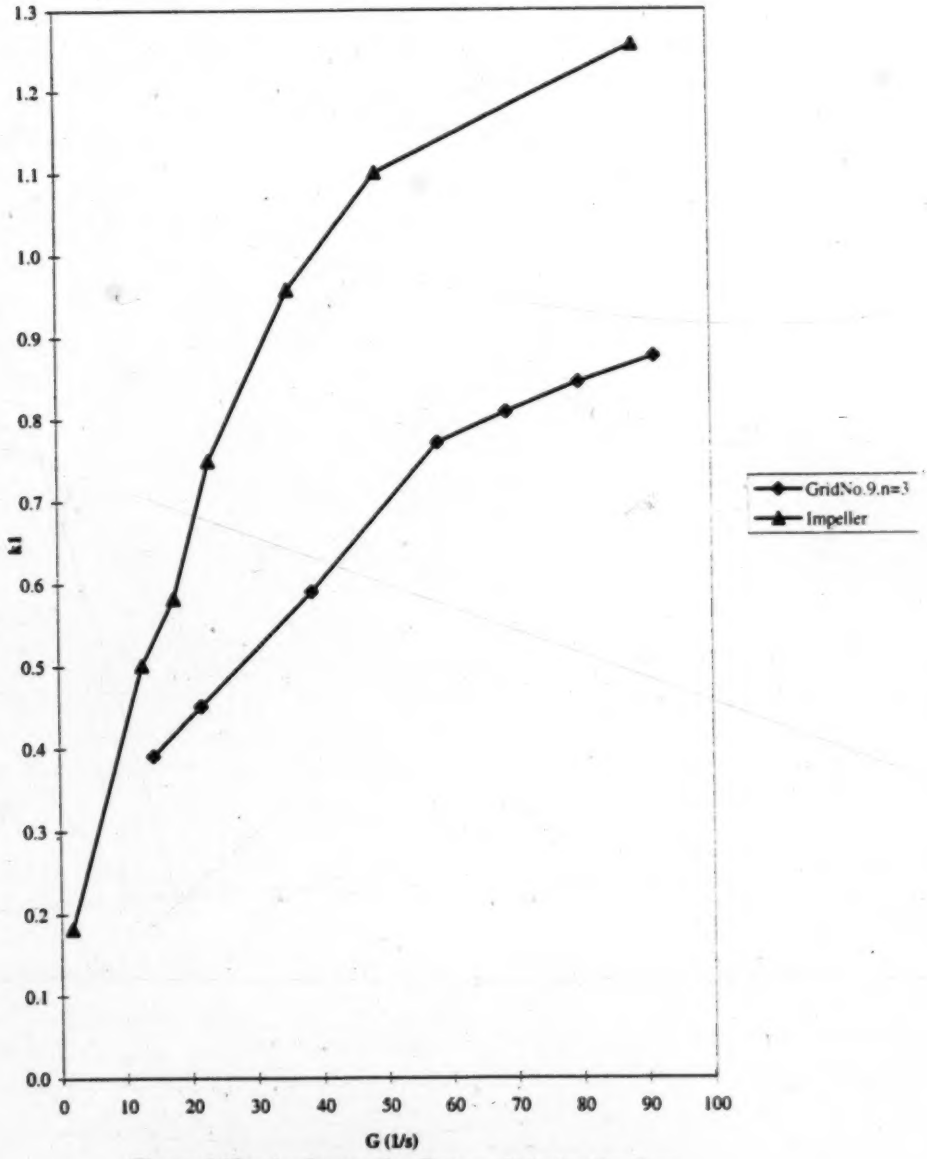

Figure 4.15a: Agglomeration Rate vs. Velocity Gradient

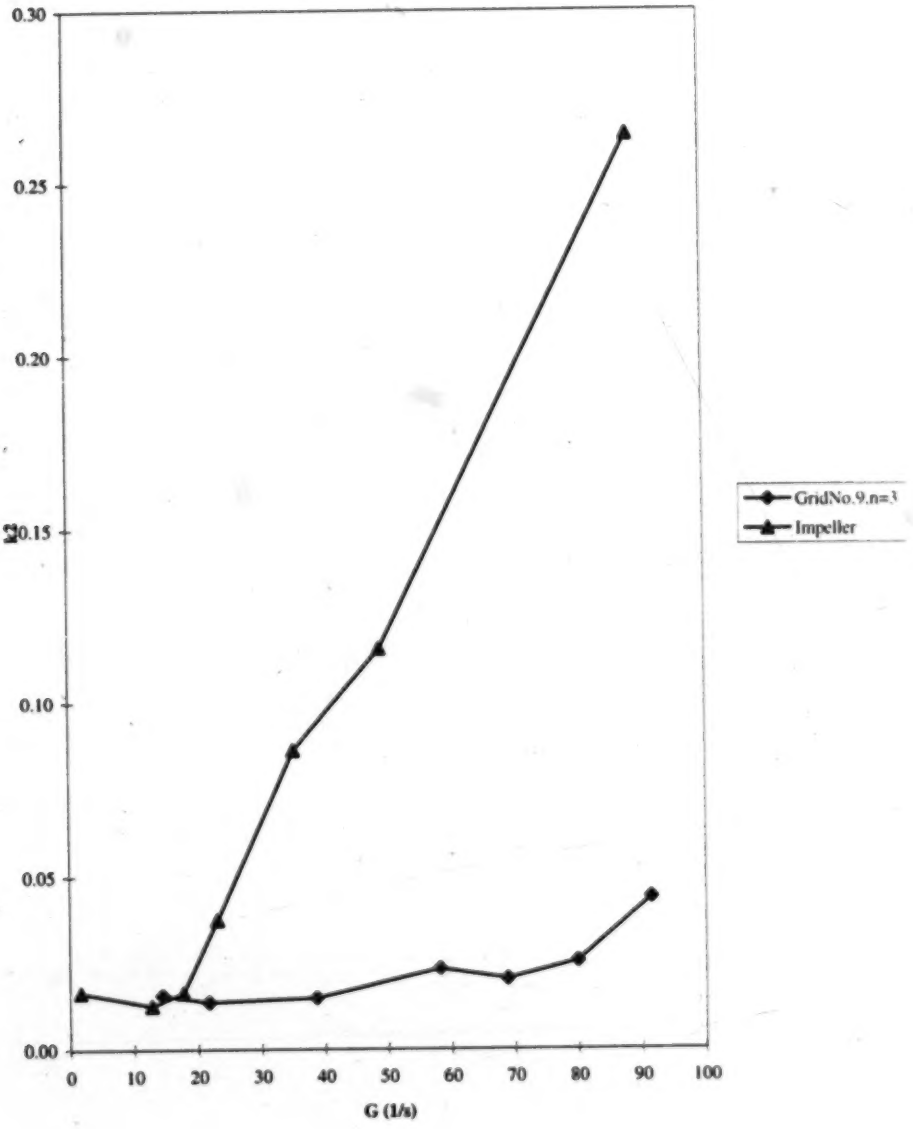

Figure 4.15b: Erosion Rate vs. Velocity Gradient

5. GENERAL DISCUSSION AND CONCLUSIONS

5.1 INTRODUCTION

This study was focused on the practical application of grids to create an ideal flocculation mixing. A vertically oscillating grid mixing device was especially designed to create constant movement at various controllable vertical speeds. A low frequency in long stroke mixing was applied to cover the whole vertical mixing region. The grid mixing was expected to provide uniform mixing intensity within the vessel; a condition that could not be achieved by means of traditional impellers. This kind of mixing would provide an ideal mixing environment for floc aggregation, i. e. high particle contacts with low floc break up, represented by low turbidity readings. Single, double, and triple biplane circular rod grids with different solidity ratio were applied from which the optimum condition could be identified. A general relationship among mixing parameters, flocculation parameters, types of grids (in terms of different solidity ratio), and number of grids was expected indicating that the overall grid mixing performance was easily controlled. In general, it was expected that grid mixing would perform better than would traditional impellers.

Three individual but closely related experimental studies were completed. All studies were completed on bench scales using a standard 2L jar from which all

parameters could easily be controlled and monitored. The first study (Chapter 2) was focused on the turbulent parameter measurement created by single grids with different solidity ratio (= d/M, where d is the rod diameter and M is the mesh or center to center distance between two grids). The measurement was completed using a 2D LDA. The average root mean square (rms) turbulent velocity q' and mean velocities in the vertical and horizontal directions ($\overline{U}$ and $\overline{V}$) for numerous points of measurement within the jar were identified. Average volume energy dissipation rate $\overline{\varepsilon}$ and velocity gradient $\overline{G}$ for each type of grid were then calculated based on the drag force created by the vertical grid speed v_{GS}. Subsequently, macro length scale L and Kolmogoroff microscale η were then calculated. Mixing intensity characteristics of impellers were also discussed.

The second study (Chapter 3) was focused on the particle removal performance of grid mixing represented by the settled water turbidity. Kaolin and alum were used as the simulated turbid particle and chemical coagulant, respectively. While, sodium bicarbonate was used as the pH buffer. These chemical settings would create an ideal sweep floc mechanism commonly applied in water treatment works. Chemical doses and temperature were held constant for all tests. Therefore the observation could be focused on the effect of mixing only. Rapid mixing was created by applying a standard flat blade impeller followed by slow or flocculation mixing produced by grid mixing. The settled water turbidity (T/T_o where T is turbidity and T_o is initial turbidity) was monitored for many different mixing intensities $\overline{G}$,

flocculation time t_F, and types of grids from which its optimum condition could be identified. Based on the turbidity reading, particle agglomeration and erosion rate coefficients were developed. These parameters provided additional information about mixing characteristics created by grids.

The third study (Chapter 4) was completed as the continuation of the two previous studies. In this study, multiple (double and triple) of the same type of grids were applied to observe any improvement to the single grid mixing. The vertical stroke was adjusted to one half and one third of the original setting to provide the same vertical mixing region within the jar. Similar investigation and analyses as those of single grid mixing studies were made. A direct flocculation performance comparison with a standard flat blade impeller was also made.

5.2 HIGHLIGHTS OF STUDY

There are three important findings that have to be highlighted. These are related to the turbulent mixing parameter characteristics created by grid mixing, flocculation performance represented by the settled water turbidity, and general relationships among various controlling parameters.

5.2.1 Turbulent Mixing Parameters

Turbulent mixing intensity has been found to be related directly to v_{GS}, types of grids (with different solidity ratio d/M), and number of grids. The best performance

can be achieved by applying a larger number of high solidity ratio types of girds as they produce the same mixing intensity at lower v_{GS}. Grid mixing has also been observed to produce uniform q' values at both vertical and horizontal points of measurement within the jar. This can be shown by the low coefficient of variation (COV = standard deviation divided by average values) and range (ratio between maximum and minimum values) of q'. Most COV and range values are less than 0.25 and 2, respectively. Slightly higher values can be observed at low v_{GS} which are not in the range of flocculation mixing practices. However, solidity ratio d/M and number of grids do not seem to improve the mixing uniformity. As a comparison, in the case of impeller mixing studies, range values for turbulent velocity components can be as high as 5 or even 6. The highest values can be found in the impeller tip region (Mujumdar et al. 1970; Wu and Patterson 1989; Wu et al. 1989; Stanley 1995; Stanley and Smith 1995; and Cheng et al. 1997).

Due to its turbulent intensity uniformity within the jar, $\overline{\varepsilon}$ and $\overline{G}$ can then be applied as the surrogate mixing intensity parameters. Both values can directly be calculated based on drag force created by the grid movement. The use of $\overline{G}$ as a surrogate mixing intensity gives a practical advantage due to its simplicity.

Subsequently, Reynolds number based on rod diameter Re_d can be found as a function of $\overline{G}$ and types of grids. As mentioned by Baines and Peterson (1951) and Roach (1987), turbulent mixing regime can be produced by grids when $Re_d > 100$. In this study, this value is equal roughly to $\overline{G} > 20\ s^{-1}$ for any types of grids and number

of grids. As mentioned by Camp (1955), the optimum range of $\overline{G}$ values for floc aggregation is 20 to 74 s^{-1}. This indicates that turbulent mixing is achieved by grid mixing under the optimum flocculation mixing intensity.

Macro length scale L has been calculated based on $\overline{\varepsilon}$ or $\overline{G}$ (obtained from the drag force calculation) and q' (obtained from the experiment). As it should be in theory, L has been found to be 1) constant at high v_{GS} when the turbulent regime has been reached, 2) constant with the number of grids, and 3) proportional to the physical characteristics of the mixing device i. e. grid d or M. This can be compared to impeller turbulent mixing studies that L is constant and proportional to the impeller width (Stanley 1995; Stanley and Smith 1995; and Cheng et al. 1997). These findings basically verify the validity of results obtained from the turbulent mixing parameter studies.

5.2.2 Particle Removal Study

From T/T_o vs. $\overline{G}$, T/T_o vs. t_F, and T/T_o vs. $\overline{G}\,t_F$ profiles, optimum values for $\overline{G}$ ($\overline{G}^*$) were identified with their related minimum T/T_o (T/T_o^*). High solidity ratio types of grids have larger $\overline{G}^*$ values than those of low solidity ratio types of grids. However, these values are located at a wider range of low $\overline{G}$ values producing low T/T_o. Less $\overline{G}^*$ have also been observed when applying a larger number of grids. In

general, t_F = 20 minutes can be assumed as the optimum t_F as no significant particle removal can be achieved beyond this t_F value.

From the settled water turbidity result, agglomeration and erosion rate coefficients (k_1 and k_2) can also be calculated. It has been found that high solidity ratio types of grids have lower k_1 but also less k_2 values than those of low solidity ratio types of grids. This is possible since high solidity ratio types of grids require less v_{GS} to obtain the same $\overline{G}$. The same $\overline{G}$ can also be achieved at less v_{GS} by applying a larger number of grids indicated by higher k_1 and lower k_2 values.

Based on these finding, triple high solidity ratio types of grids will perform the best. It has also been observed that the $\overline{G}^*$ values are located at the optimum range for floc aggregation, i. e. 20 to 74 s^{-1}. Grid mixing at its best arrangement has also been found to perform better than that of the standard flat blade impeller indicated by its wider range of $\overline{G}$ at low T/T_o. This shows that grid mixing has a more stable flocculation performance from any hydraulic mixing variations within the vessel.

5.2.3 General Relationships among Parameters

General relationships among several controlling parameters are important indicating that the overall flocculation performance is easily controlled. These parameters can then be adjusted to achieve the desired flocculation performance. This

is also useful when designing mixing grids with different types of grids (different solidity ratio), numbers of grids, and even different scales.

Solidity ratio d/M and number of grids n have successfully been used as the generalizing factors. Table 5.1 shows generalizing factors for both turbulent mixing and flocculation parameters. Power coefficients have been found as the ones that give the highest coefficient of determination R^2 values (see Chapters 2 to 4 for detailed results).

5.3 LIMITATIONS AND SUGGESTIONS

Due to a limited scope of this study, there are some limitations that should be taken into consideration when using results obtained from this experimental work. The limitations and their suggestions are presented as follows.

The scaling effect from bench to pilot or full scale studies is the first important concern. In this study, rods with diameter in the range of 3.2 to 6.4 mm and mesh in the range of 9 and 18 mm have been used. It has been found that the turbulent mixing parameter can linearly be correlated with solidity ratio d/M. However, this results may be questioned when much larger rod diameter and mesh are applied. It is therefore important to conduct laboratory experiments in a larger scale to observe some variations in both small and large scales. The traditional dimensional analyses incorporating Reynolds number as shown by Rushton (1951) and Clark and Fiessinger (1991) could be considered.

Another scaling effect may appear from the water vessel size. A wider vessel will unlikely to change the turbulent mixing characteristics. This has been shown by relatively uniform turbulent mixing intensity values across a horizontal plane of measurement. However, increasing the water depth significantly will affect the mixing characteristics. This study has shown that reducing the vertical stroke by adding a larger number of grids will increase the mixing intensity in proportion to $n^{0.29}$. Again, this relation has to be reconsidered when much deeper water depth (that requires a much longer vertical stroke) is applied.

Another practical concern is that this study has been completed in a batch type of reactor. While, a continuous flow type of reactor is always encountered in real water work practices. Leprise as cited by Clark and Fiessinger (1991) suggested that a 1L jar test should behave similarly to a 1L continuous flow reactor. However, Argaman and Kaufman (1970) and Argaman (1971) investigated the performance of a series of complete mixed reactor types of vessels. They found that the overall floc agglomeration from primary particles was improved compared to that of a single vessel with the same detention time. This leads to a detailed investigation of the residence time distribution analysis. Residence time t_D is defined as the time needed for a segment of fluid to pass through a system. The residence time distribution of a water vessel can be obtained through tracer tests. Subsequently, the vessel can be assumed to behave as a combination of complete mixed and plug flow reactors with some dead volume (Wolf and Resnick 1963 and Rebhun and Argaman 1965). Figure 5.1 shows a possible set up for the vertically oscillating grid mixing device in a

continuous flow. The flocculation basin is separated into three zones. The rapid mixing zone applies a conventional impeller to disperse the chemical coagulant in water as fast as possible. The vertically oscillating grids can be applied in the flocculation zone. When an appropriate combination of $\overline{G}$ and t_F is applied, large flocs are expected to be formed and settle in the sedimentation zone.

The particle size and distribution of the formed flocs with time should also be investigated. The measurement can be made at different t_F and $\overline{G}$ values. In general, there are two measurement methods that can be conducted, i.e. using a particle count analyzer and a photographic camera. It is then possible to obtain the floc density and floc strength that should be related to the mixing intensity (say $\overline{G}$). Previous impeller mixing studies have shown that maximum floc diameter d_{max} is proportional to $\overline{G}^{-n}$. The values of n depend on the turbulent regime as well as the types of particles used in the experiment (Tambo and Hozumi 1979; Tomi and Bagster 1978; and Parker et al. 1972). Also in this study, kaolin (a monosized type of particle) has been used as the simulated turbid particle. This may not fully represent the actual incoming particles in a water treatment plant. Some performance differences from the bench scale study may be expected.

Another important parameter that should be observed is the recirculation time. Circulation or turnover time t_C is defined as the time needed for a segment of water to fully circulate the vessel. Even though both vertical and horizontal mean velocities are practically zero, it does not mean that a particle within the vessel stays at the same

place all the time. t_C may change when a larger number of grids is applied influencing the particle interaction behavior within the vessel. In the case of impeller mixing studies, t_C can be found from tracer studies (Godfrey and Amirtharajah 1991) or be calculated based on the vessel volume and pumping rate (Uhl and Gray 1966). When applied for grid mixing environment, these methods may need some modifications due to the absence of mean velocities.

Turbulent mixing intensity decay with time behind the moving grid is very complicated to be investigated. When a grid passes through a certain point, its mixing intensity will reach a maximum value. This decreases to a minimum value until the grid passes through the same point from the opposite direction. Different vertical points of measurement experience different mixing conditions as well as when different number of mixing grids are applied. This can be investigated by combining information obtained from this study (turbulent mixing intensity measurement at a certain point within the vessel) with an additional study investigating the turbulent mixing intensity at fixed distances behind the moving grid. The LDA has to be mounted on a moving table which has the same vertical speed as the grid movement creating a similar case towing tank study with reciprocal grid movement (Gad-el-Hak 1987).

Power required for the mixing process can be found based on the drag force calculation. However, the best way is through a direct measurement using a transducer that can be mounted on the holding rod. The transducer records the drag force created by the grid movement and converts it into power unit. However, disturbances due to a

vertical up and down movement of grid may become a major concern using this measurement device.

The use of coagulant aids and polymers should also be investigated. As mentioned by Leu and Ghosh (1988), polymer formed flocs tend to have a stronger bond that resists to higher $\overline{G}$. This becomes an important additional experimental work that can be combined with the flocculation mixing study to improve the overall performance of the vertically oscillating grid mixing device. The use of polymers is expected to produce lower T/T_o* at a wider range of $\overline{G}$.

5.4 CONCLUSIONS

In general, it is possible to conclude that the vertically oscillating grid mixing device is able to create a uniform mixing environment within the vessel; a condition that cannot be achieved in the case of impeller mixing. Due to the mixing uniformity, average volume velocity gradient $\overline{G}$ may be applied as the surrogate mixing parameter. At the optimum mixing arrangement (triple high solidity ratio types of grids), the grid mixing device is able to provide a very stable flocculation performance in terms of low settled water turbidity at a wide range of $\overline{G}$.

It has also been proven that the mixing intensity and flocculation performance can directly be controlled by the grid vertical speed, number of grids, and grid solidity ratio which is very important from a practical point of view.

5.5 REFERENCES

Argaman, Y. A. (1971). "Pilot - plant studies of flocculation." *Journal AWWA*, 63 (12), 775 - 777.

Argaman, Y. A. and Kaufman, W. J. (1970). "Turbulence and flocculation." *Journal of the Sanitary Engineering Division, ASCE*, 96 (SA2), 223 - 241.

Clark. M. M. and Fiessinger, F. (1991). "Mixing and scale-up." *Mixing in Coagulation and Flocculation*. A. Amirtharajah, M. M. Clark, and R. R. Trussell. editors. AWWA, Denver, Colorado, 282 - 308.

Gad-el-Hak, M. (1987). "The water towing tank as an experimental facility." *Experiments in Fluids*, 5, 289 - 297.

Godfrey, J. C. and Amirtharajah, A. (1991). "Mixing in Liquids." *Mixing in Coagulation and Flocculation*, AWWA, Denver, Colorado, 35 - 79.

Hudson, H. E. Jr. and Wagner, E. G. (1981). "Conduct and use of jar tests." *Journal AWWA*, 73 (4), 218 - 224.

Leu, R. J. and Ghosh, M. M. (1988). "Polyelectrolite characteristics and flocculation". *Journal AWWA*, 80 (4), 159 - 167.

Parker, D. S., Kaufman, W. J., and Jenkins, D. (1972). "Floc breakup in turbulent flocculation processes." *Journal of the Sanitary Engineering Division, ASCE*. 98 (SA1), 79 - 99.

Rebhun, M. and Argaman, Y. (1965). "Evaluation of hydraulic efficiency of sedimentation basins." *Journal of the Sanitary Engineering Division*, 91 (5). 37 - 45.

Rushton, J. H. (1951). "The use of pilot plant mixing data." *Chemical Engineering Progress*, 47 (9), 485 - 488.

Stanley, S. J. (1995). "Measurement and analysis of mixing as it relates to flocculation." *Ph.D. Thesis*, University of Alberta, Edmonton, Alberta.

Tambo, N. and Hozumi, H. (1979). "Physical characteristics of flocs-II. Strength of floc." *Water Research*, 13, 421 - 427.

Tomi, D. T. and Bagster, D. F. (1978). "The behavior of aggregates in stirred vessels. Part I. Theoretical consideration in the effects of agitation." *Transactions of the Institute of Chemical Engineers*, 56, 1 - 8.

Uhl, V. W. and Gray, J. B. (1966). *Mixing: Theory and Practices. Vol. 1*, Academic Press, New York, New York.

Wolf, D. and Resnick, W. (1963). "Residence time distribution in real system." *Journal of Industrial and Engineering Chemical Fundamentals*, 2 (4), 287 - 293.

Wu, H. and Patterson, G. K. (1989). "Laser - doppler measurements of turbulent - flow parameters in stirred mixer." *Chemical Engineering Science*, 44 (10), 2207 - 2221.

Wu, H., Patterson, G. K., and Van Doorn, M. (1989). "Distribution of turbulence energy dissipation rate in a rushton turbine stirred mixer." *Experiments in Fluids*, 8, 153 - 160.

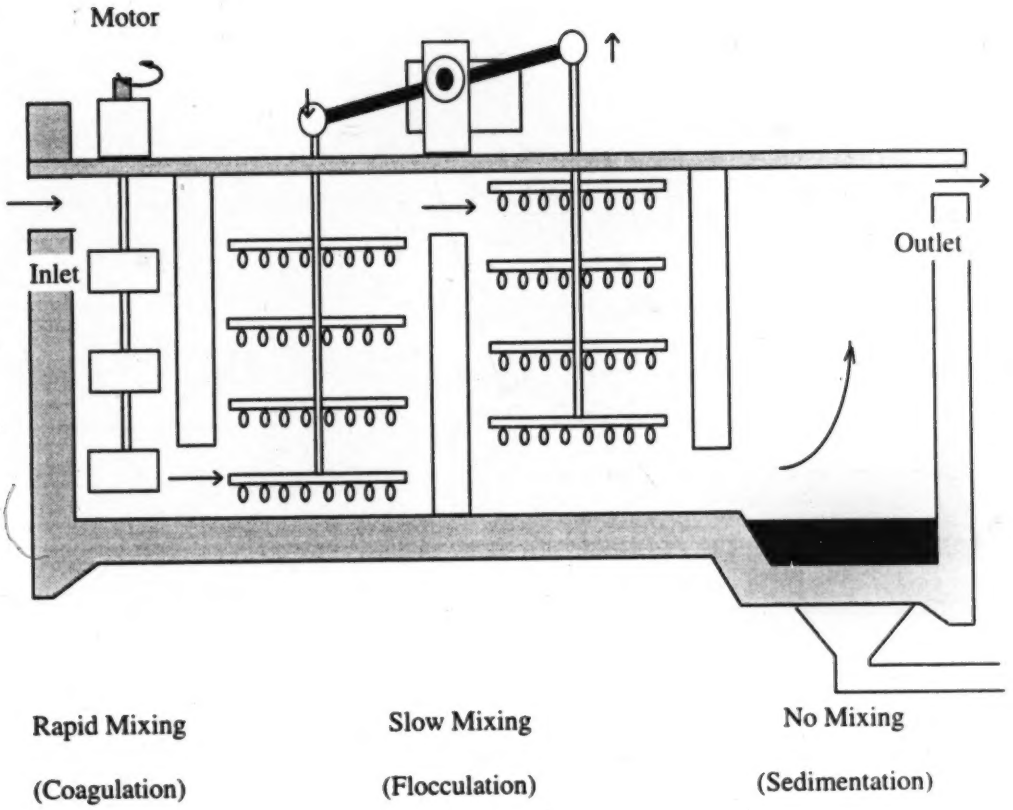

Figure 5.1: Oscillating Grid Mixing in a Continuous System

Table 5.1: Generalizing Factors

Turbulent Parameters	Factors	
m vs. d/M	$[d/M]^{1}$	$n^{0.28}$

Flocculation Parameters		
$\overline{G}$ * vs. t_F	$[d/M]^{0.85 \text{ to } 0.89}$	$n^{0.05}$
T/T_o* vs. t_F	$[d/M]^{0.00}$	n^{0}
T/T_o* vs. $\overline{G}$ * t_F	$[d/M]^{-0.08}$	$n^{-0.02}$
k_1 vs. $\overline{G}$	$[d/M]^{-0.45- \text{ to } -0.46}$	$n^{0.20}$
k_2 vs. $\overline{G}$	$[d/M]^{-1.99 \text{ to } -2.01}$	$n^{0.08}$

Note: small variations may be found for [d/M] factors due to different numbers of grids.

APPENDICES

APPENDIX 1:

Turbulent Parameters for Single Grid (n = 1)

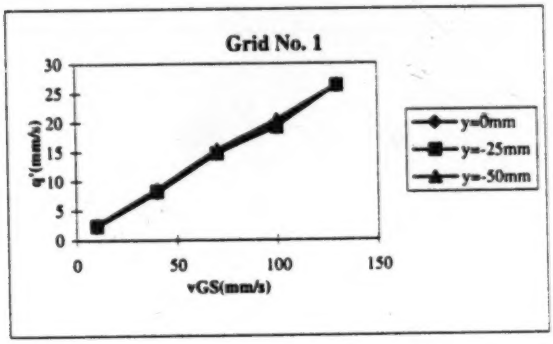
Grid No. 1
q'(mm/s)
vGS(mm/s)
y=0mm
y=-25mm
y=-50mm

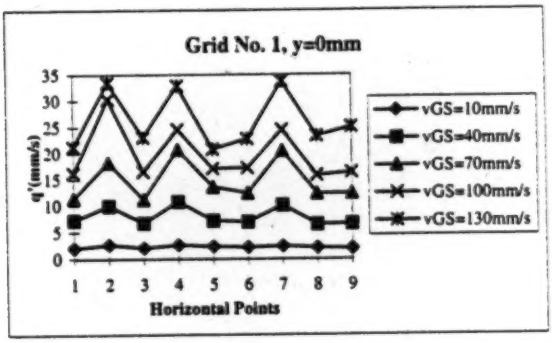
Grid No. 1, y=0mm
q'(mm/s)
Horizontal Points
vGS=10mm/s
vGS=40mm/s
vGS=70mm/s
vGS=100mm/s
vGS=130mm/s

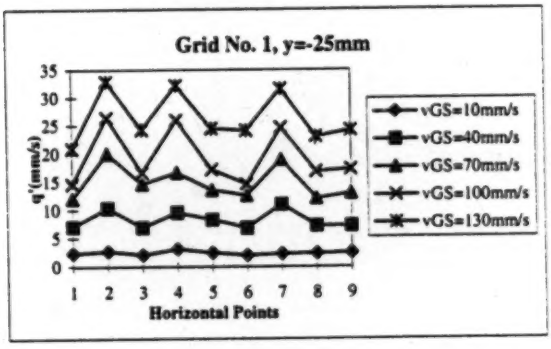
Grid No. 1, y=-25mm
q'(mm/s)
Horizontal Points
vGS=10mm/s
vGS=40mm/s
vGS=70mm/s
vGS=100mm/s
vGS=130mm/s

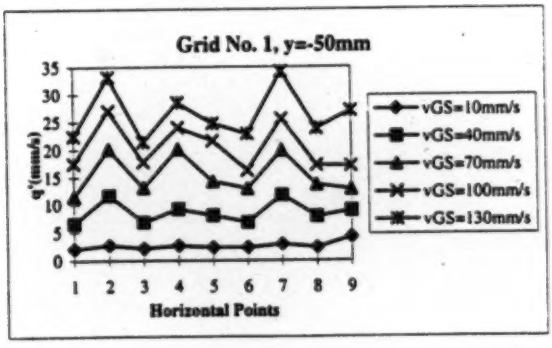
Grid No. 1, y=-50mm
q'(mm/s)
Horizontal Points
vGS=10mm/s
vGS=40mm/s
vGS=70mm/s
vGS=100mm/s
vGS=130mm/s

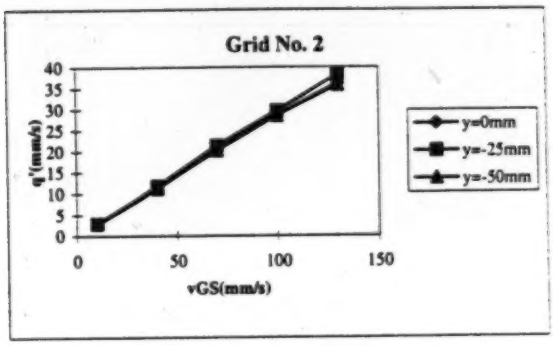
Grid No. 2
q'(mm/s)
vGS(mm/s)
y=0mm
y=-25mm
y=-50mm

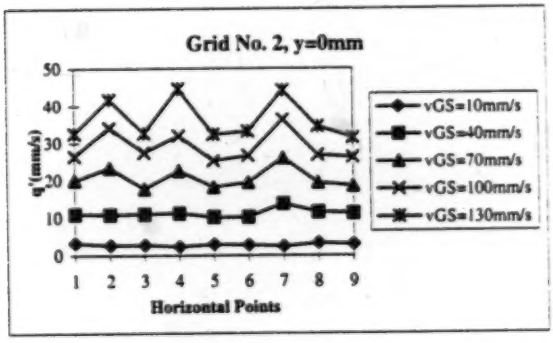
Grid No. 2, y=0mm
q'(mm/s)
Horizontal Points
vGS=10mm/s
vGS=40mm/s
vGS=70mm/s
vGS=100mm/s
vGS=130mm/s

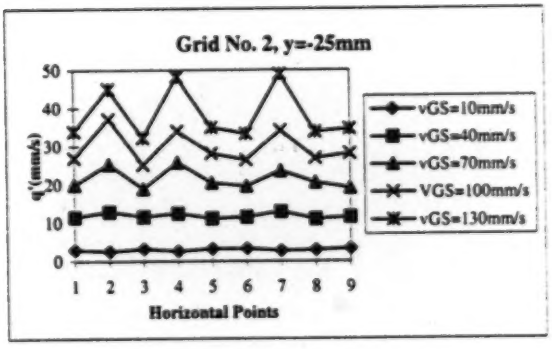
Grid No. 2, y=-25mm
q'(mm/s)
Horizontal Points
vGS=10mm/s
vGS=40mm/s
vGS=70mm/s
VGS=100mm/s
vGS=130mm/s

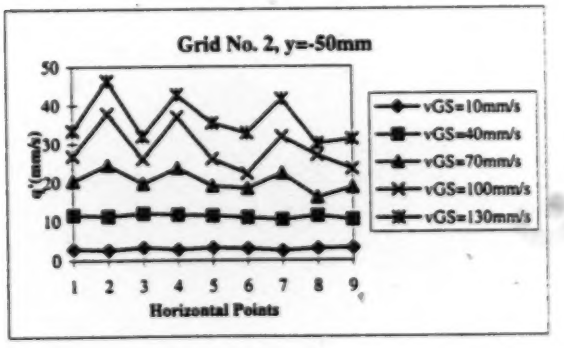
Grid No. 2, y=-50mm
q'(mm/s)
Horizontal Points
vGS=10mm/s
vGS=40mm/s
vGS=70mm/s
vGS=100mm/s
vGS=130mm/s

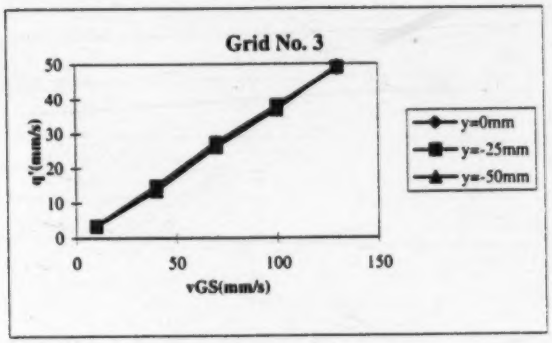
Grid No. 3
q'(mm/s)
vGS(mm/s)
y=0mm
y=-25mm
y=-50mm

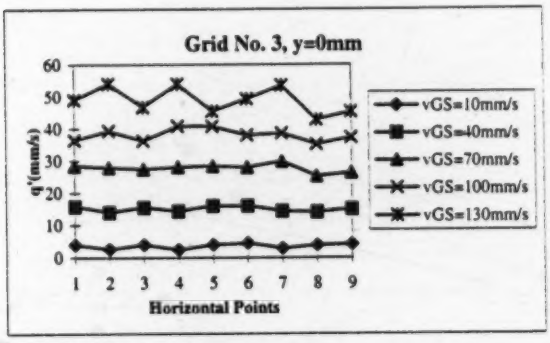
Grid No. 3, y=0mm
q'(mm/s)
Horizontal Points
vGS=10mm/s
vGS=40mm/s
vGS=70mm/s
vGS=100mm/s
vGS=130mm/s

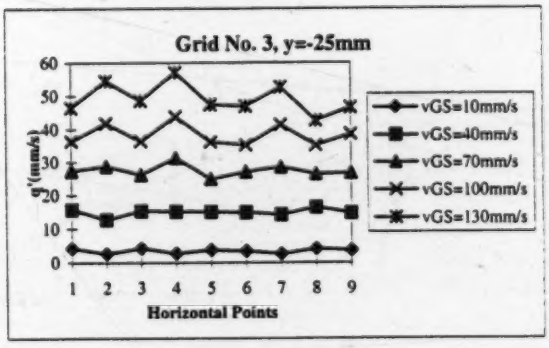
Grid No. 3, y=-25mm
q'(mm/s)
Horizontal Points
vGS=10mm/s
vGS=40mm/s
vGS=70mm/s
vGS=100mm/s
vGS=130mm/s

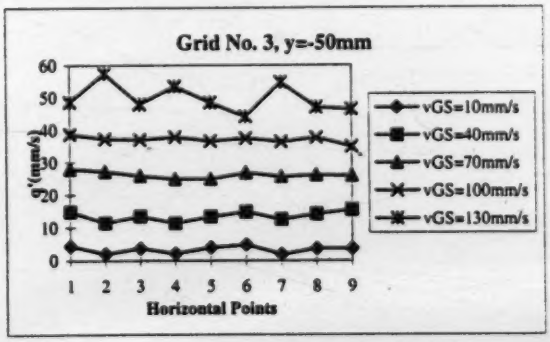
Grid No. 3, y=-50mm
q'(mm/s)
Horizontal Points
vGS=10mm/s
vGS=40mm/s
vGS=70mm/s
vGS=100mm/s
vGS=130mm/s

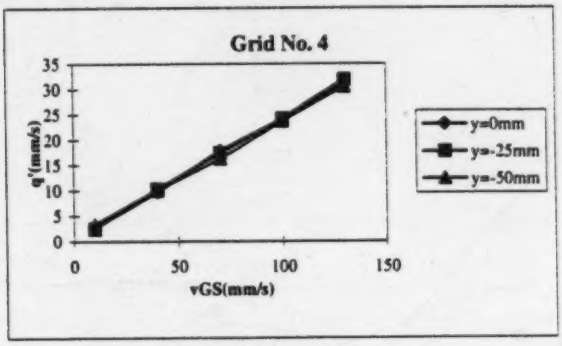
Grid No. 4
q'(mm/s)
vGS(mm/s)
y=0mm
y=-25mm
y=-50mm

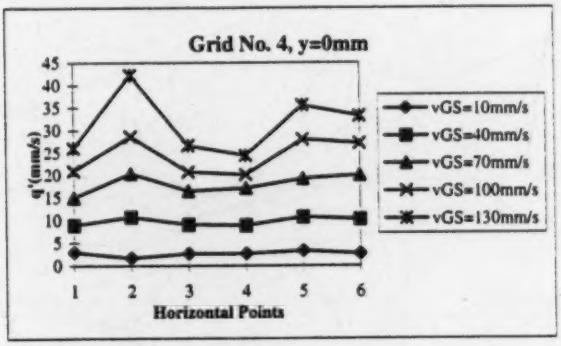
Grid No. 4, y=0mm
q'(mm/s)
Horizontal Points
vGS=10mm/s
vGS=40mm/s
vGS=70mm/s
vGS=100mm/s
vGS=130mm/s

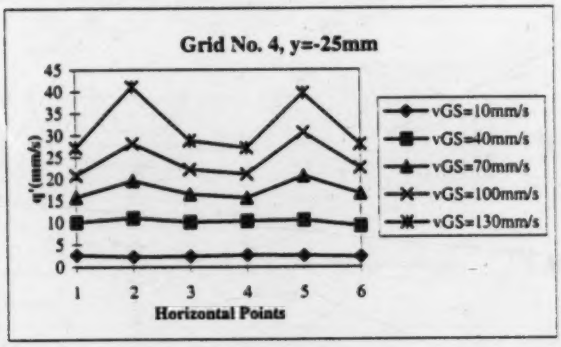
Grid No. 4, y=-25mm
q'(mm/s)
Horizontal Points
vGS=10mm/s
vGS=40mm/s
vGS=70mm/s
vGS=100mm/s
vGS=130mm/s

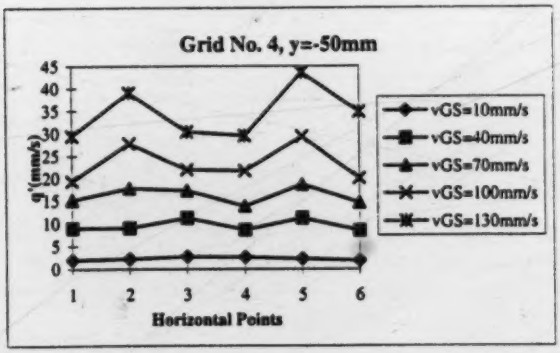
Grid No. 4, y=-50mm
q'(mm/s)
Horizontal Points
vGS=10mm/s
vGS=40mm/s
vGS=70mm/s
vGS=100mm/s
vGS=130mm/s

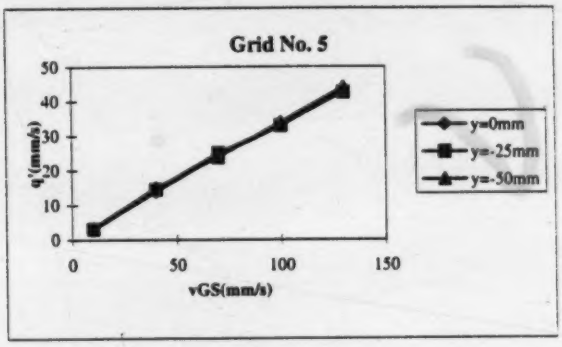
Grid No. 5
q'(mm/s)
vGS(mm/s)
y=0mm
y=-25mm
y=-50mm

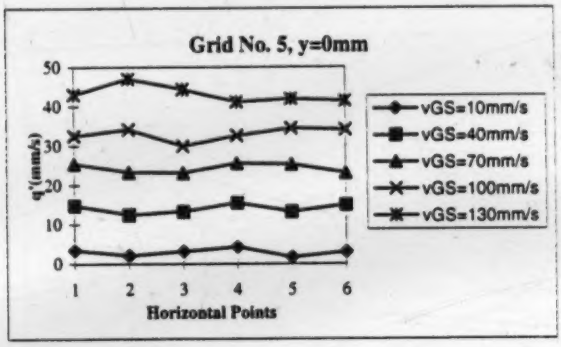
Grid No. 5, y=0mm
q'(mm/s)
Horizontal Points
vGS=10mm/s
vGS=40mm/s
vGS=70mm/s
vGS=100mm/s
vGS=130mm/s

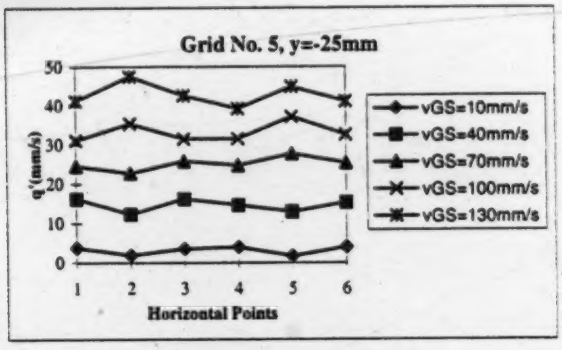
Grid No. 5, y=-25mm
q'(mm/s)
Horizontal Points
vGS=10mm/s
vGS=40mm/s
vGS=70mm/s
vGS=100mm/s
vGS=130mm/s

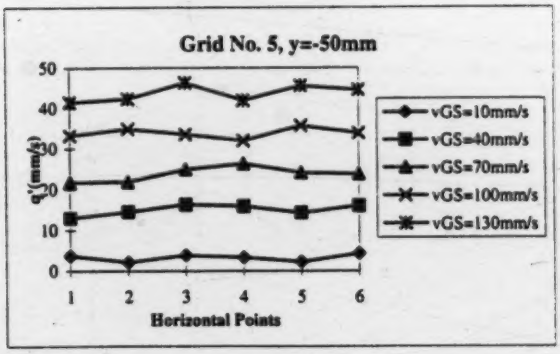
Grid No. 5, y=-50mm
q'(mm/s)
Horizontal Points
vGS=10mm/s
vGS=40mm/s
vGS=70mm/s
vGS=100mm/s
vGS=130mm/s

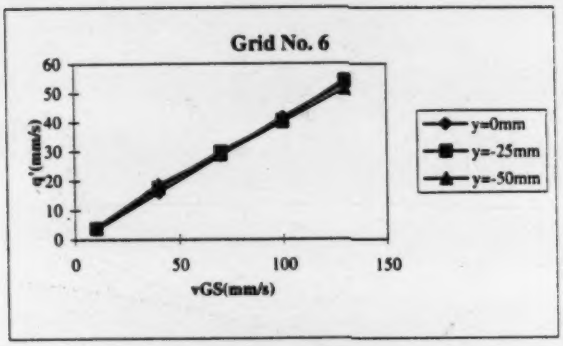
Grid No. 6
q'(mm/s)
vGS(mm/s)
y=0mm
y=-25mm
y=-50mm

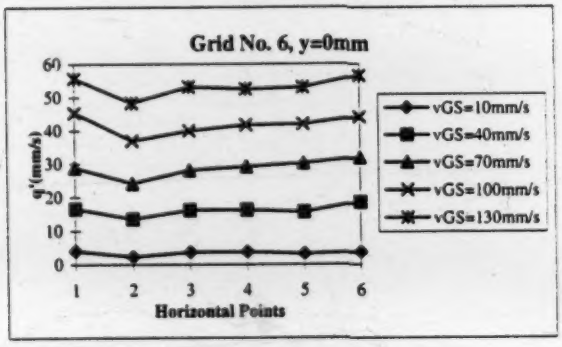
Grid No. 6, y=0mm
q'(mm/s)
Horizontal Points
vGS=10mm/s
vGS=40mm/s
vGS=70mm/s
vGS=100mm/s
vGS=130mm/s

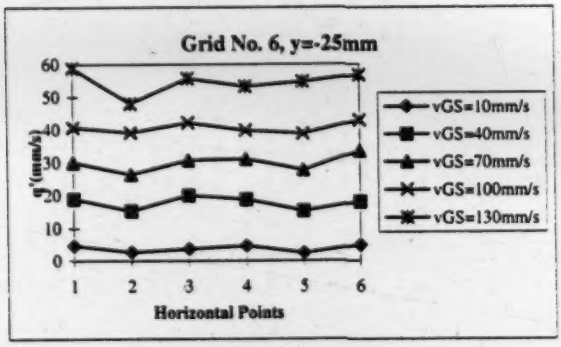
Grid No. 6, y=-25mm
q'(mm/s)
Horizontal Points
vGS=10mm/s
vGS=40mm/s
vGS=70mm/s
vGS=100mm/s
vGS=130mm/s

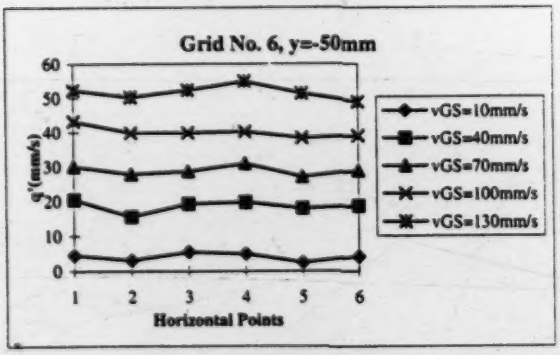
Grid No. 6, y=-50mm
q'(mm/s)
Horizontal Points
vGS=10mm/s
vGS=40mm/s
vGS=70mm/s
vGS=100mm/s
vGS=130mm/s

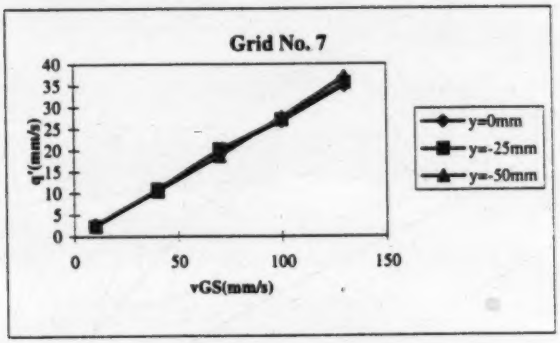
Grid No. 7
q'(mm/s)
vGS(mm/s)
y=0mm
y=-25mm
y=-50mm

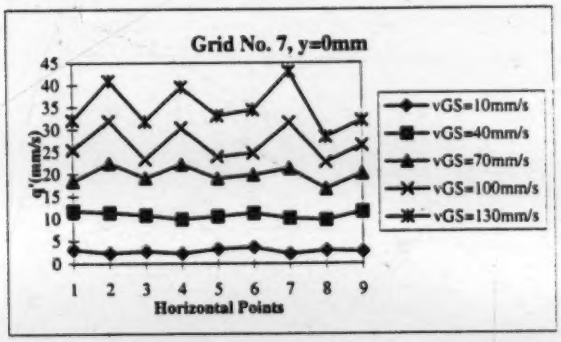
Grid No. 7, y=0mm
q'(mm/s)
Horizontal Points
vGS=10mm/s
vGS=40mm/s
vGS=70mm/s
vGS=100mm/s
vGS=130mm/s

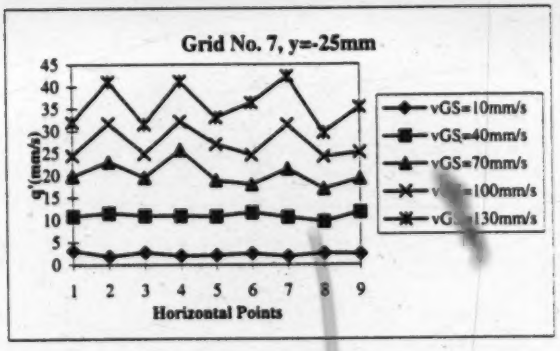
Grid No. 7, y=-25mm
q'(mm/s)
Horizontal Points
vGS=10mm/s
vGS=40mm/s
vGS=70mm/s

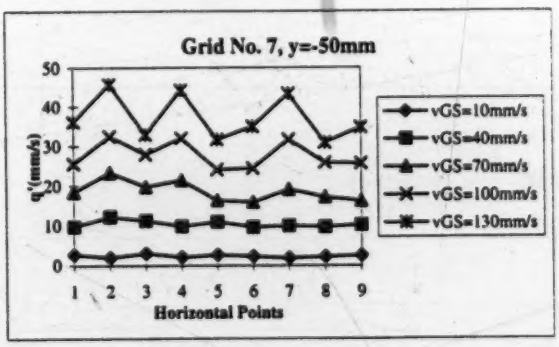
Grid No. 7, y=-50mm
q'(mm/s)
Horizontal Points
vGS=10mm/s
vGS=40mm/s
vGS=70mm/s
vGS=100mm/s
vGS=130mm/s

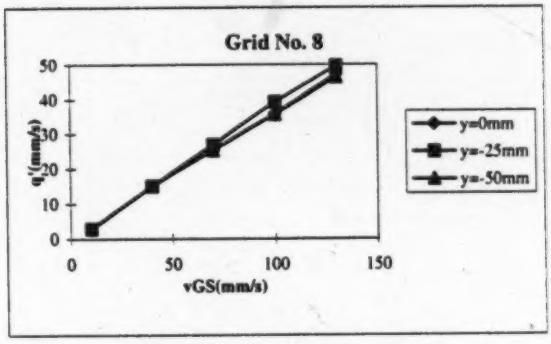
Grid No. 8
q'(mm/s)
vGS(mm/s)
y=0mm
y=-25mm
y=-50mm

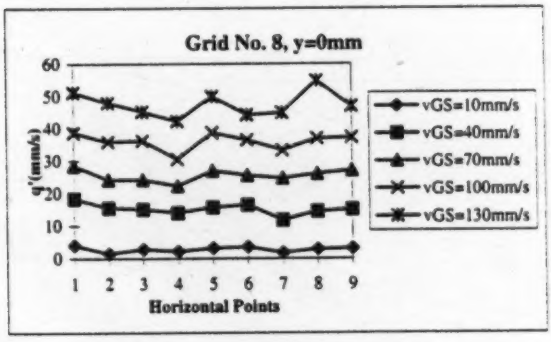
Grid No. 8, y=0mm
q'(mm/s)
Horizontal Points
vGS=10mm/s
vGS=40mm/s
vGS=70mm/s
vGS=100mm/s
vGS=130mm/s

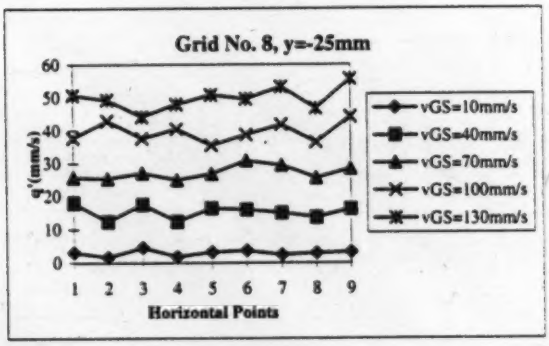
Grid No. 8, y=-25mm
q'(mm/s)
Horizontal Points
vGS=10mm/s
vGS=40mm/s
vGS=70mm/s
vGS=100mm/s
vGS=130mm/s

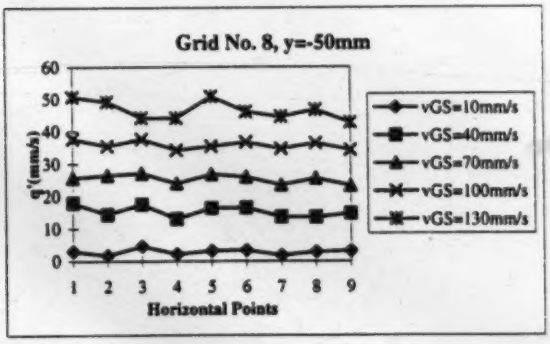
Grid No. 8, y=-50mm
q'(mm/s)
Horizontal Points
vGS=10mm/s
vGS=40mm/s
vGS=70mm/s
vGS=100mm/s
vGS=130mm/s

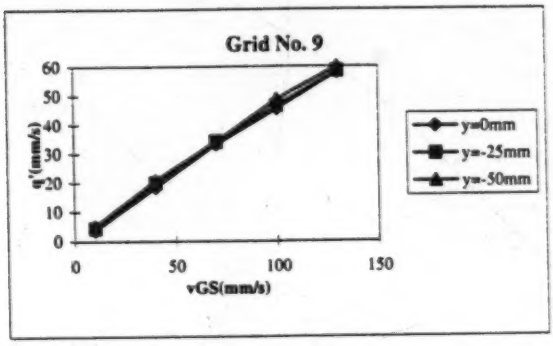
Grid No. 9
q'(mm/s)
vGS(mm/s)
y=0mm
y=-25mm
y=-50mm

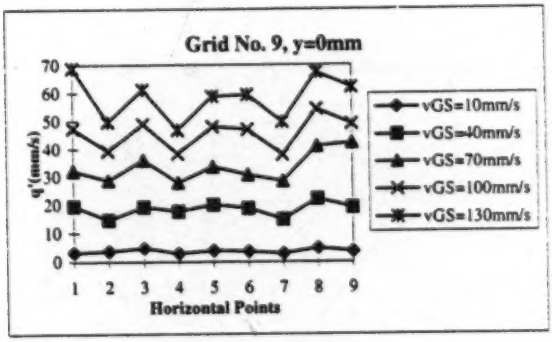
Grid No. 9, y=0mm
q'(mm/s)
Horizontal Points
vGS=10mm/s
vGS=40mm/s
vGS=70mm/s
vGS=100mm/s
vGS=130mm/s

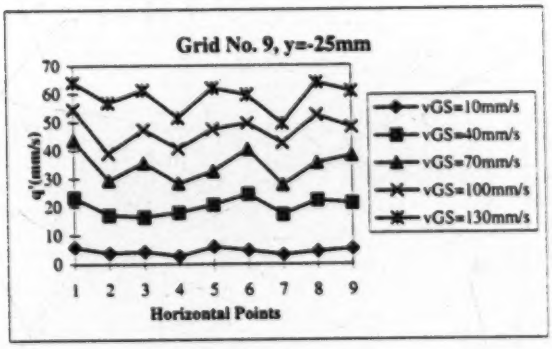
Grid No. 9, y=-25mm
q'(mm/s)
Horizontal Points
vGS=10mm/s
vGS=40mm/s
vGS=70mm/s
vGS=100mm/s
vGS=130mm/s

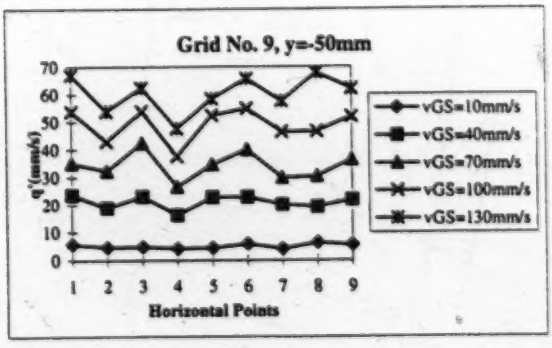
Grid No. 9, y=-50mm
q'(mm/s)
Horizontal Points
vGS=10mm/s
vGS=40mm/s
vGS=70mm/s
vGS=100mm/s
vGS=130mm/s

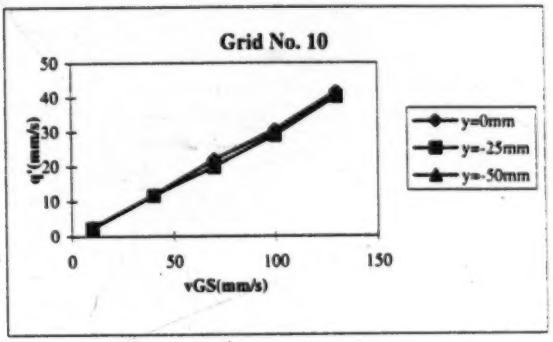
Grid No. 10
50
40
30
20
10
0
0
50
100
150
vGS(mm/s)
y=0mm
y=-25mm
y=-50mm

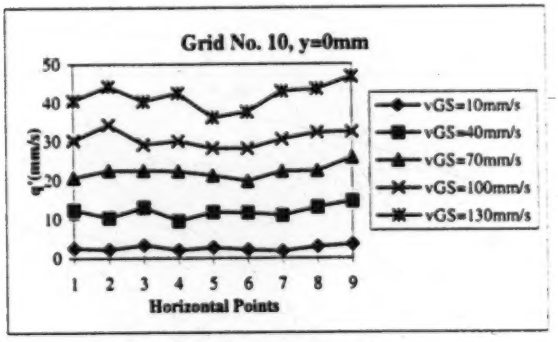
Grid No. 10, y=0mm
50
40
30
20
10
0
1 2 3 4 5 6 7 8 9
Horizontal Points
vGS=10mm/s
vGS=40mm/s
vGS=70mm/s
vGS=100mm/s
vGS=130mm/s

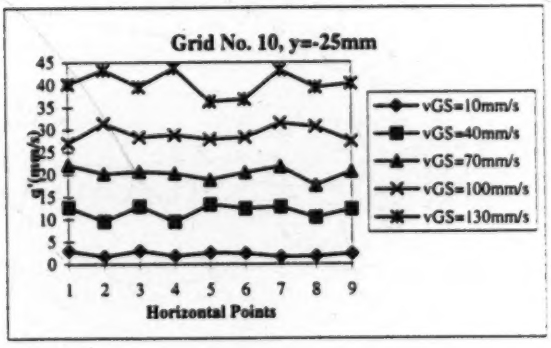
Grid No. 10, y=-25mm
45
40
35
30
25
20
15
10
5
0
1 2 3 4 5 6 7 8 9
Horizontal Points
vGS=10mm/s
vGS=40mm/s
vGS=70mm/s
vGS=100mm/s
vGS=130mm/s

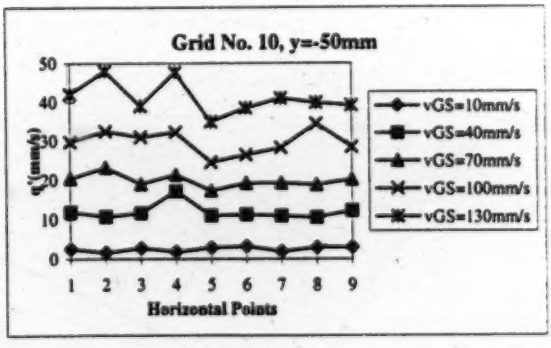
Grid No. 10, y=-50mm
50
40
30
20
10
0
1 2 3 4 5 6 7 8 9
Horizontal Points
vGS=10mm/s
vGS=40mm/s
vGS=70mm/s
vGS=100mm/s
vGS=130mm/s

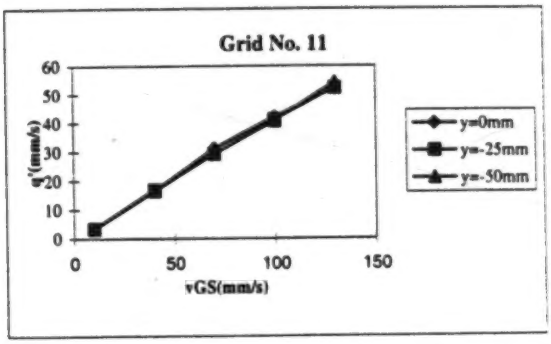
Grid No. 11
q'(mm/s)
vGS(mm/s)
y=0mm
y=-25mm
y=-50mm

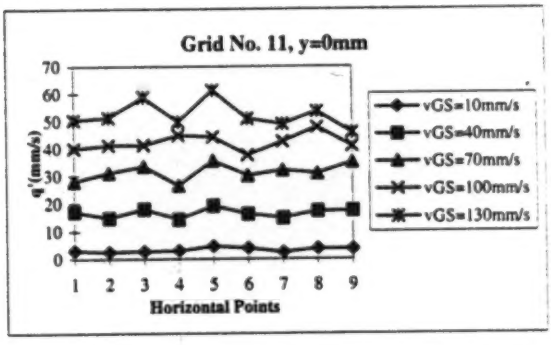
Grid No. 11, y=0mm
q'(mm/s)
Horizontal Points
vGS=10mm/s
vGS=40mm/s
vGS=70mm/s
vGS=100mm/s
vGS=130mm/s

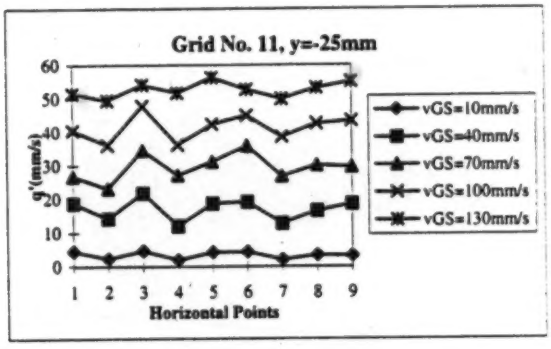
Grid No. 11, y=-25mm
q'(mm/s)
Horizontal Points
vGS=10mm/s
vGS=40mm/s
vGS=70mm/s
vGS=100mm/s
vGS=130mm/s

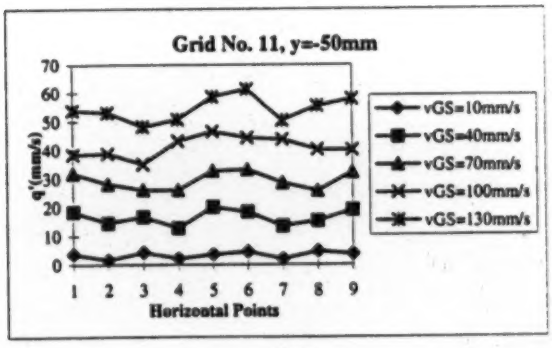
Grid No. 11, y=-50mm
q'(mm/s)
Horizontal Points
vGS=10mm/s
vGS=40mm/s
vGS=70mm/s
vGS=100mm/s
vGS=130mm/s

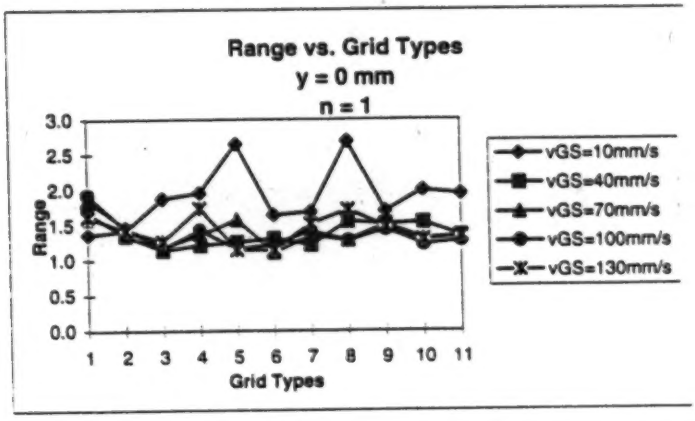
Range vs. Grid Types
y = 0 mm
n = 1
Range
Grid Types
vGS=10mm/s
vGS=40mm/s
vGS=70mm/s
vGS=100mm/s
vGS=130mm/s

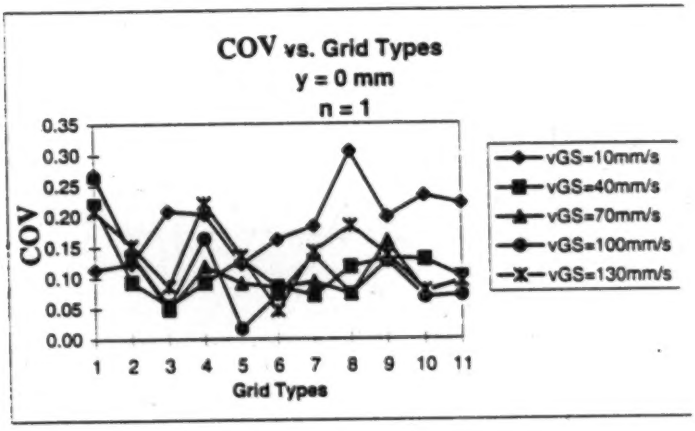
COV vs. Grid Types
y = 0 mm
n = 1
COV
Grid Types
vGS=10mm/s
vGS=40mm/s
vGS=70mm/s
vGS=100mm/s
vGS=130mm/s

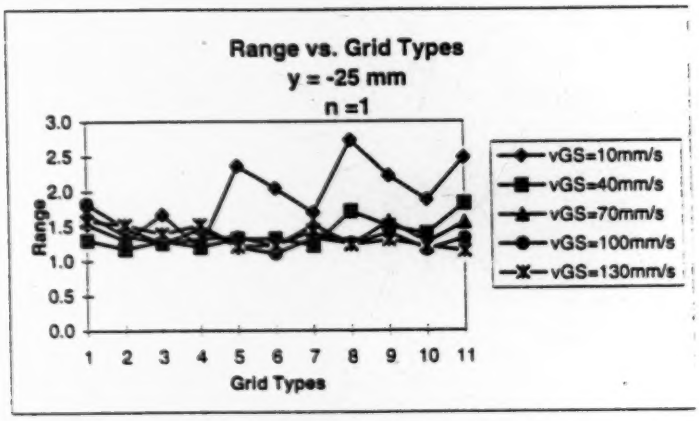
Range vs. Grid Types
y = -25 mm
n =1
Range
3.0
2.5
2.0
1.5
1.0
0.5
0.0
1 2 3 4 5 6 7 8 9 10 11
Grid Types
vGS=10mm/s
vGS=40mm/s
vGS=70mm/s
vGS=100mm/s
vGS=130mm/s

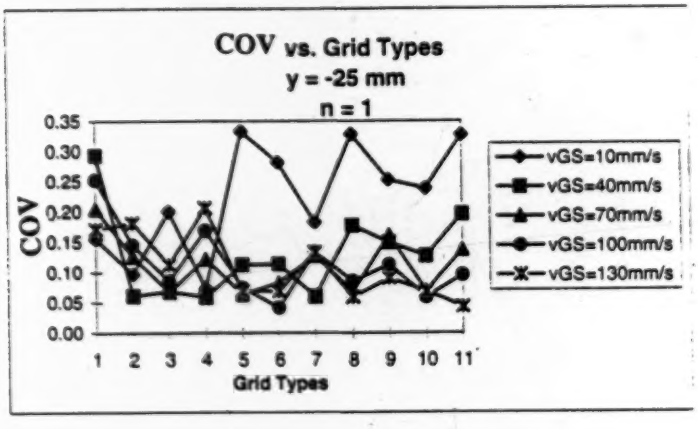
COV vs. Grid Types
y = -25 mm
n = 1
COV
0.35
0.30
0.25
0.20
0.15
0.10
0.05
0.00
1 2 3 4 5 6 7 8 9 10 11
Grid Types
vGS=10mm/s
vGS=40mm/s
vGS=70mm/s
vGS=100mm/s
vGS=130mm/s

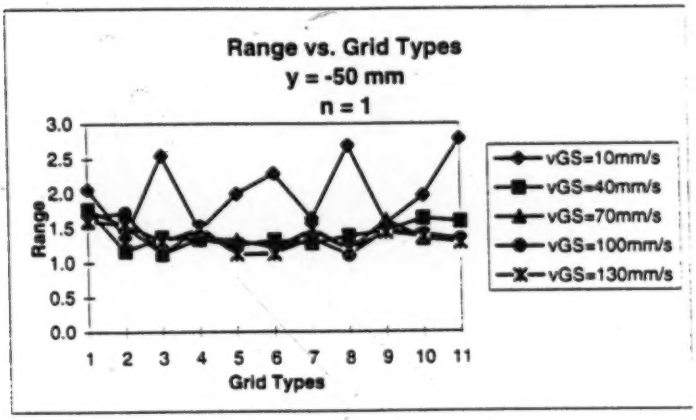
Range vs. Grid Types
y = -50 mm
n = 1
Range
3.0
2.5
2.0
1.5
1.0
0.5
0.0
1 2 3 4 5 6 7 8 9 10 11
Grid Types
vGS=10mm/s
vGS=40mm/s
vGS=70mm/s
vGS=100mm/s
vGS=130mm/s

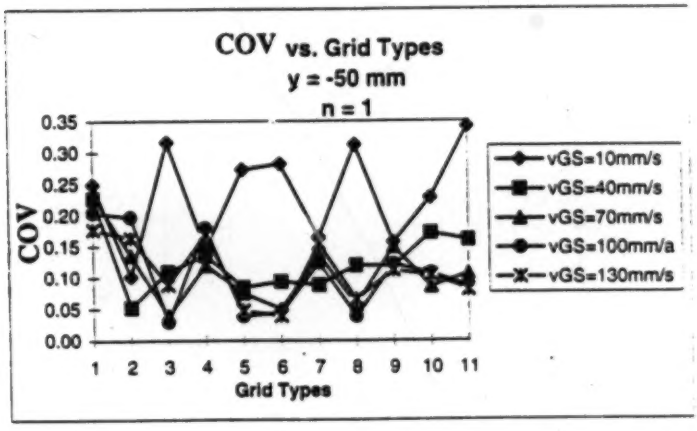
COV vs. Grid Types
y = -50 mm
n = 1
COV
0.35
0.30
0.25
0.20
0.15
0.10
0.05
0.00
1 2 3 4 5 6 7 8 9 10 11
Grid Types
vGS=10mm/s
vGS=40mm/s
vGS=70mm/s
vGS=100mm/a
vGS=130mm/s

APPENDIX 2:

Turbulent Parameters for Double and Triple Grids

(n = 2 and 3)

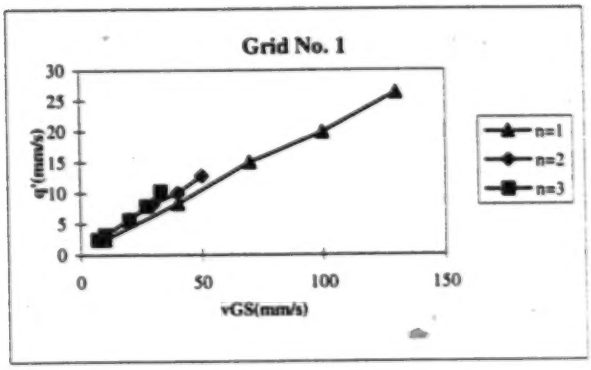
Grid No. 1
q'(mm/s)
vGS(mm/s)
n=1
n=2
n=3

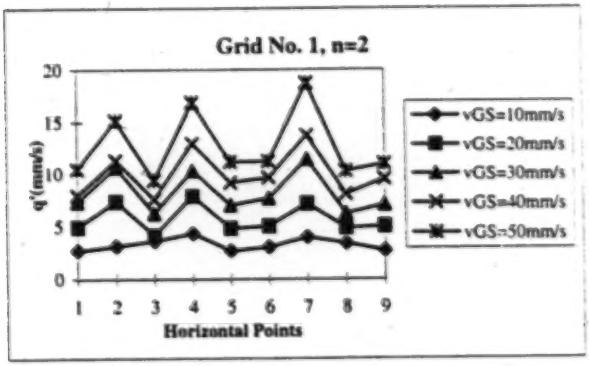
Grid No. 1, n=2
q'(mm/s)
Horizontal Points
vGS=10mm/s
vGS=20mm/s
vGS=30mm/s
vGS=40mm/s
vGS=50mm/s

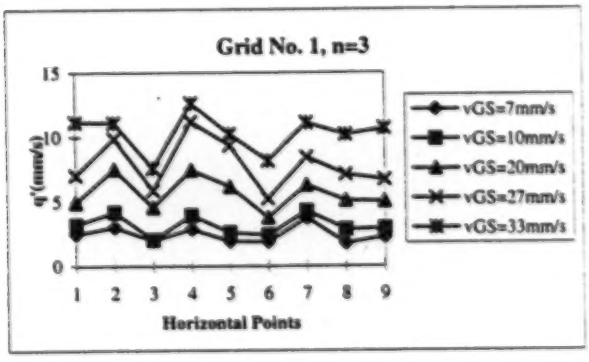
Grid No. 1, n=3
q'(mm/s)
Horizontal Points
vGS=7mm/s
vGS=10mm/s
vGS=20mm/s
vGS=27mm/s
vGS=33mm/s

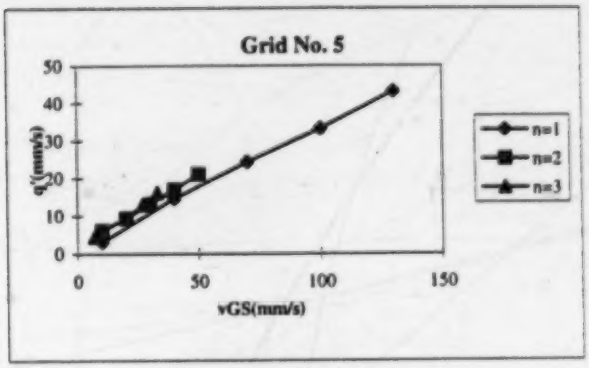
Grid No. 5
50
40
30
20
10
0
0
50
100
150
q''(mm/s)
vGS(mm/s)
n=1
n=2
n=3

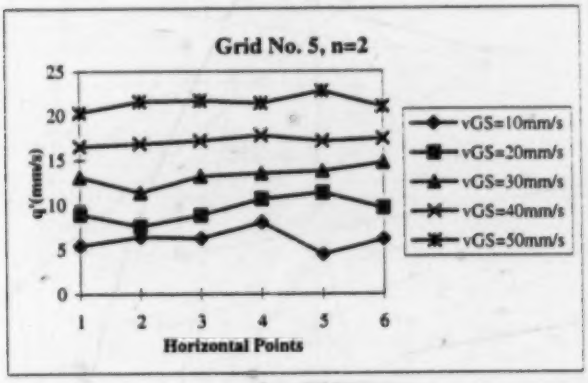
Grid No. 5, n=2
25
20
15
10
5
0
1
2
3
4
5
6
q''(mm/s)
Horizontal Points
vGS=10mm/s
vGS=20mm/s
vGS=30mm/s
vGS=40mm/s
vGS=50mm/s

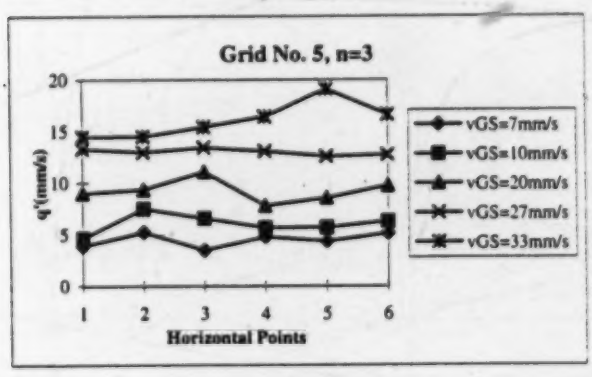
Grid No. 5, n=3
20
15
10
5
0
1
2
3
4
5
6
q''(mm/s)
Horizontal Points
vGS=7mm/s
vGS=10mm/s
vGS=20mm/s
vGS=27mm/s
vGS=33mm/s

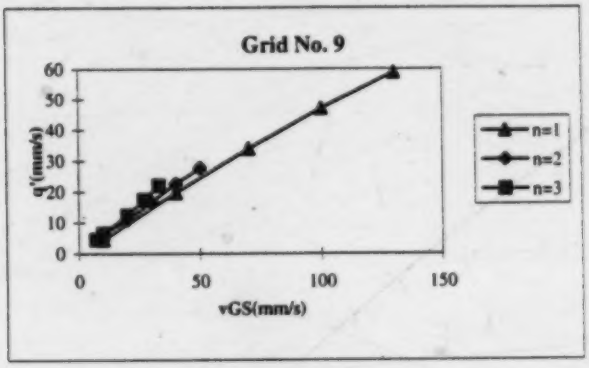
Grid No. 9
q'(mm/s)
vGS(mm/s)
n=1
n=2
n=3

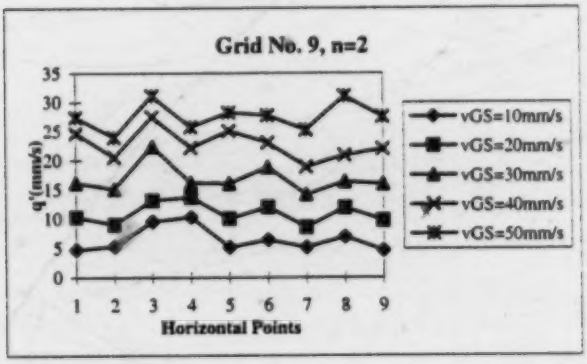
Grid No. 9, n=2
q'(mm/s)
Horizontal Points
vGS=10mm/s
vGS=20mm/s
vGS=30mm/s
vGS=40mm/s
vGS=50mm/s

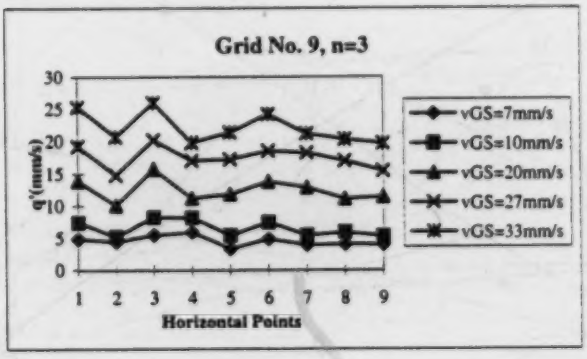
Grid No. 9, n=3
q'(mm/s)
Horizontal Points
vGS=7mm/s
vGS=10mm/s
vGS=20mm/s
vGS=27mm/s
vGS=33mm/s

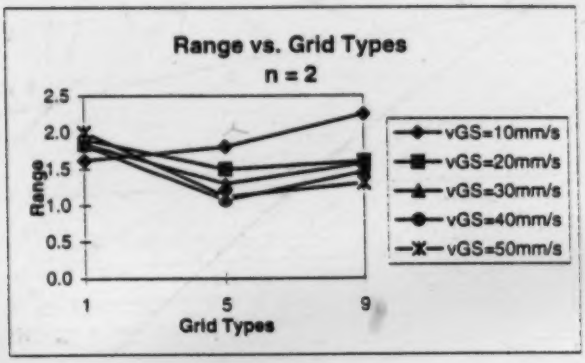
Range vs. Grid Types
n = 2
Range
2.5
2.0
1.5
1.0
0.5
0.0
1
5
9
Grid Types
vGS=10mm/s
vGS=20mm/s
vGS=30mm/s
vGS=40mm/s
vGS=50mm/s

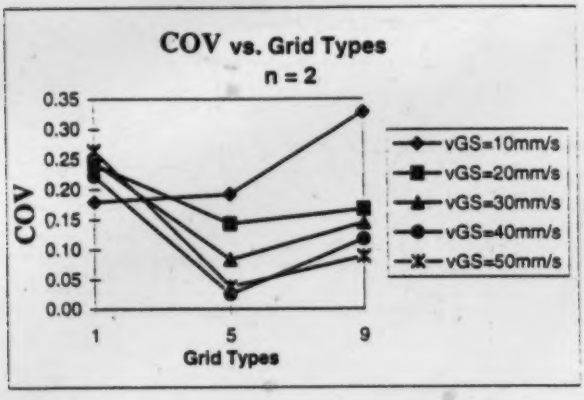
COV vs. Grid Types
n = 2
COV
0.35
0.30
0.25
0.20
0.15
0.10
0.05
0.00
1
5
9
Grid Types
vGS=10mm/s
vGS=20mm/s
vGS=30mm/s
vGS=40mm/s
vGS=50mm/s

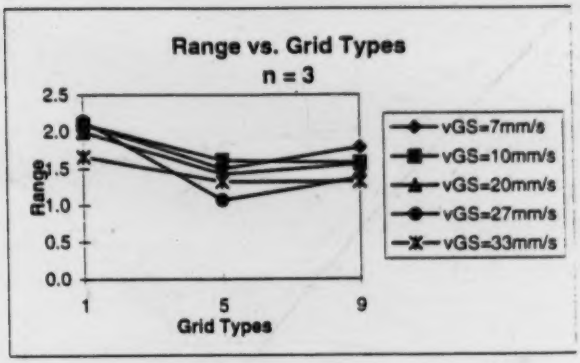
Range vs. Grid Types
n = 3
Range
2.5
2.0
1.5
1.0
0.5
0.0
1
5
9
Grid Types
vGS=7mm/s
vGS=10mm/s
vGS=20mm/s
vGS=27mm/s
vGS=33mm/s

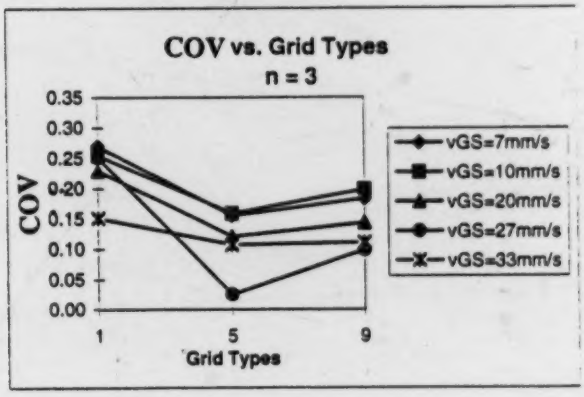
COV vs. Grid Types
n = 3
COV
0.35
0.30
0.25
0.20
0.15
0.10
0.05
0.00
1
5
9
Grid Types
vGS=7mm/s
vGS=10mm/s
vGS=20mm/s
vGS=27mm/s
vGS=33mm/s

APPENDIX 3:

Mean Velocities for All Grids

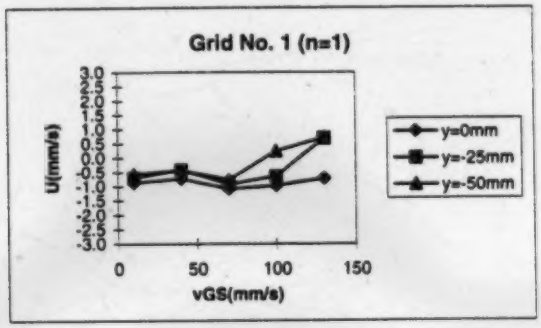
Grid No. 1 (n=1)
U(mm/s)
vGS(mm/s)
y=0mm
y=-25mm
y=-50mm

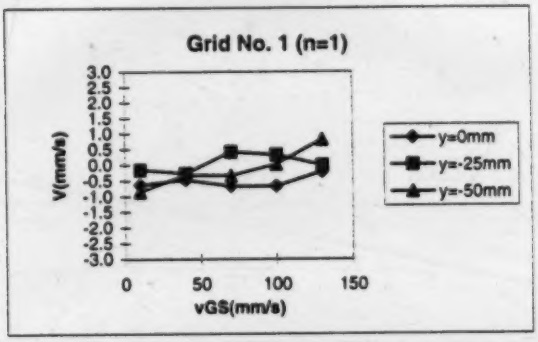
Grid No. 1 (n=1)
V(mm/s)
vGS(mm/s)
y=0mm
y=-25mm
y=-50mm

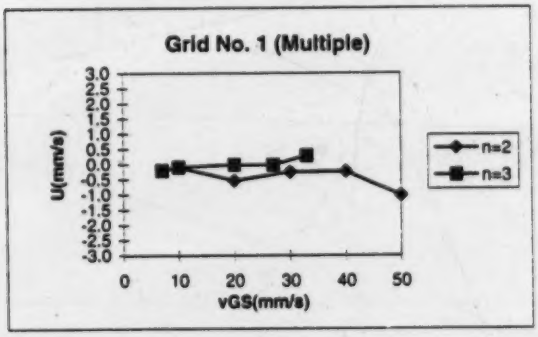
Grid No. 1 (Multiple)
U(mm/s)
vGS(mm/s)
n=2
n=3

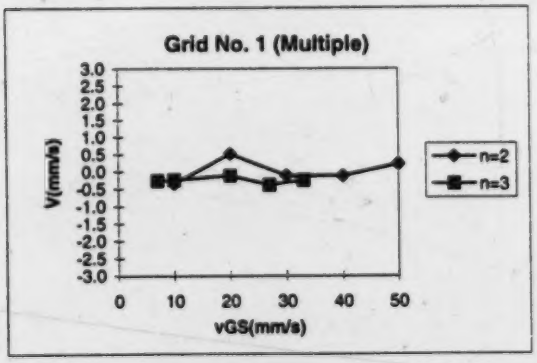
Grid No. 1 (Multiple)
V(mm/s)
vGS(mm/s)
n=2
n=3

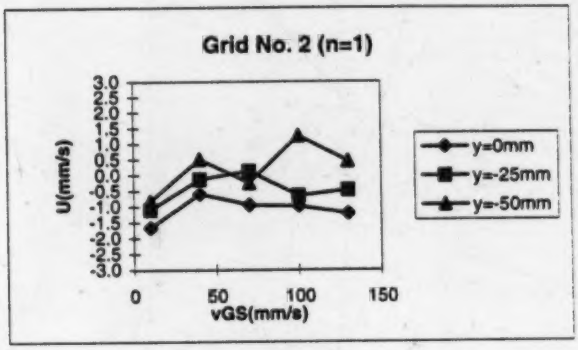
Grid No. 2 (n=1)
U(mm/s)
3.0
2.5
2.0
1.5
1.0
0.5
0.0
-0.5
-1.0
-1.5
-2.0
-2.5
-3.0
0
50
100
150
vGS(mm/s)
y=0mm
y=-25mm
y=-50mm

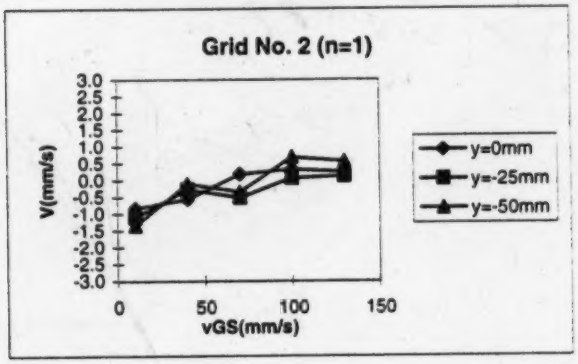
Grid No. 2 (n=1)
V(mm/s)
3.0
2.5
2.0
1.5
1.0
0.5
0.0
-0.5
-1.0
-1.5
-2.0
-2.5
-3.0
0
50
100
150
vGS(mm/s)
y=0mm
y=-25mm
y=-50mm

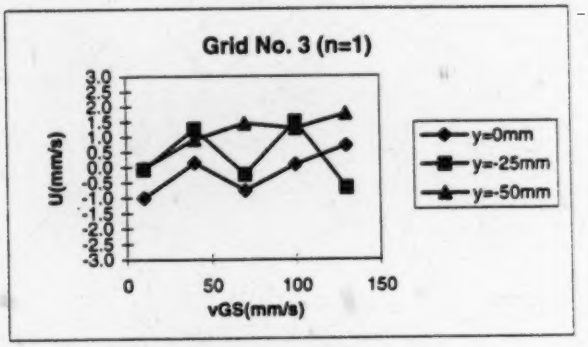
Grid No. 3 (n=1)
U(mm/s)
3.0
2.5
2.0
1.5
1.0
0.5
0.0
-0.5
-1.0
-1.5
-2.0
-2.5
-3.0
0
50
100
150
vGS(mm/s)
y=0mm
y=-25mm
y=-50mm

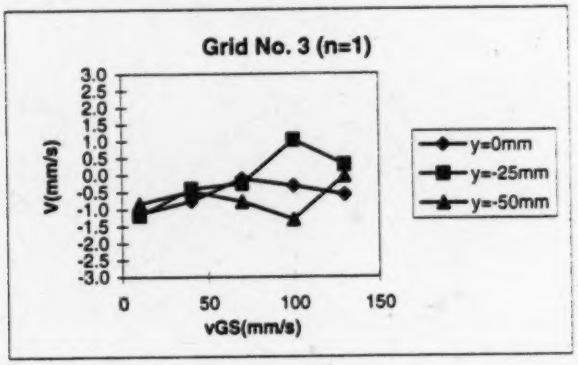
Grid No. 3 (n=1)
V(mm/s)
3.0
2.5
2.0
1.5
1.0
0.5
0.0
-0.5
-1.0
-1.5
-2.0
-2.5
-3.0
0
50
100
150
vGS(mm/s)
y=0mm
y=-25mm
y=-50mm

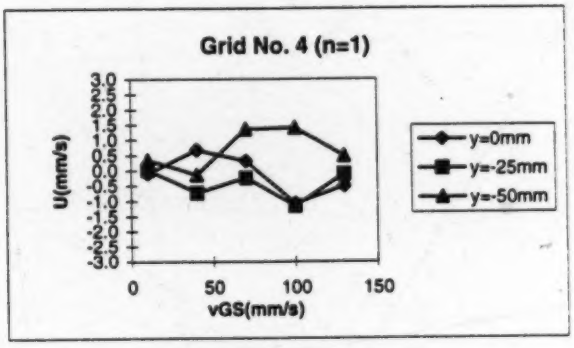
Grid No. 4 (n=1)
U(mm/s)
3.0
2.5
2.0
1.5
1.0
0.5
0.0
-0.5
-1.0
-1.5
-2.0
-2.5
-3.0
0
50
100
150
vGS(mm/s)
y=0mm
y=-25mm
y=-50mm

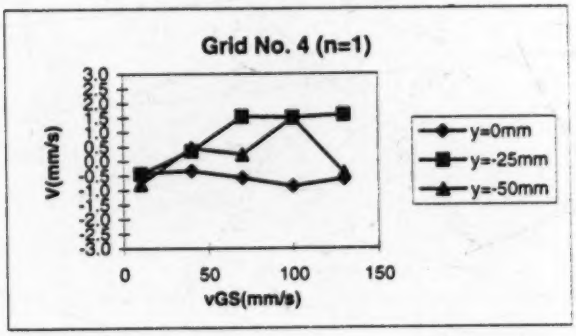
Grid No. 4 (n=1)
V(mm/s)
3.0
2.5
2.0
1.5
1.0
0.5
0.0
-0.5
-1.0
-1.5
-2.0
-2.5
-3.0
0
50
100
150
vGS(mm/s)
y=0mm
y=-25mm
y=-50mm

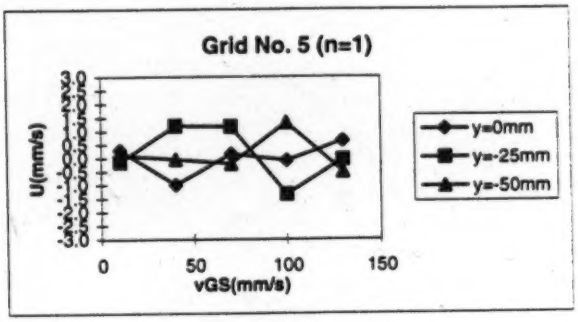
Grid No. 5 (n=1)
U(mm/s)
vGS(mm/s)
y=0mm
y=-25mm
y=-50mm

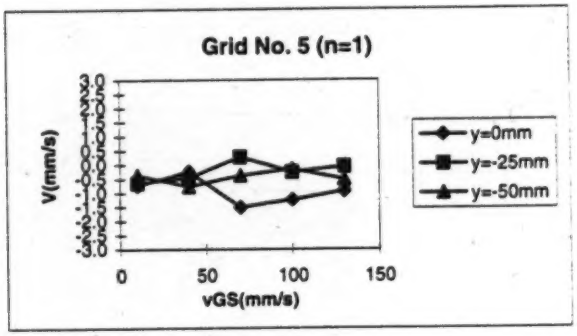
Grid No. 5 (n=1)
V(mm/s)
vGS(mm/s)
y=0mm
y=-25mm
y=-50mm

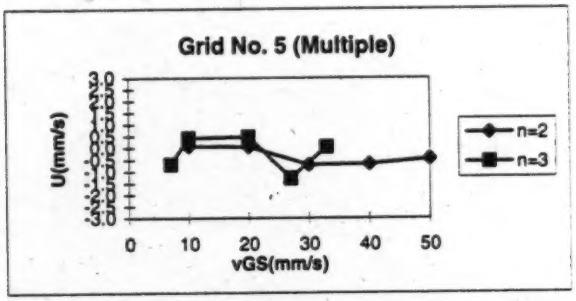
Grid No. 5 (Multiple)
U(mm/s)
vGS(mm/s)
n=2
n=3

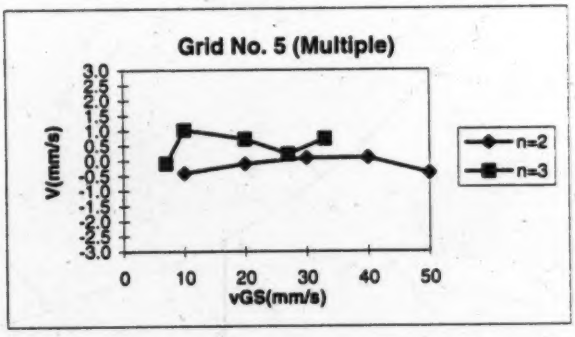
Grid No. 5 (Multiple)
V(mm/s)
vGS(mm/s)
n=2
n=3

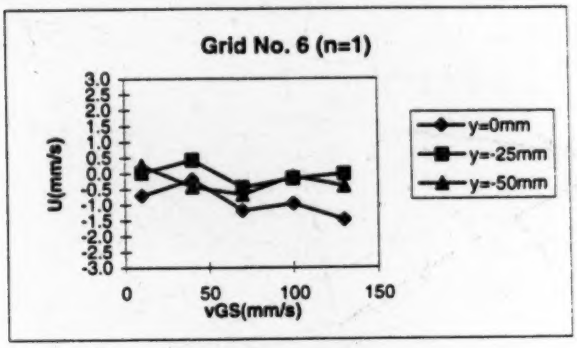
Grid No. 6 (n=1)
U(mm/s)
3.0
2.5
2.0
1.5
1.0
0.5
0.0
-0.5
-1.0
-1.5
-2.0
-2.5
-3.0
0
50
100
150
vGS(mm/s)
y=0mm
y=-25mm
y=-50mm

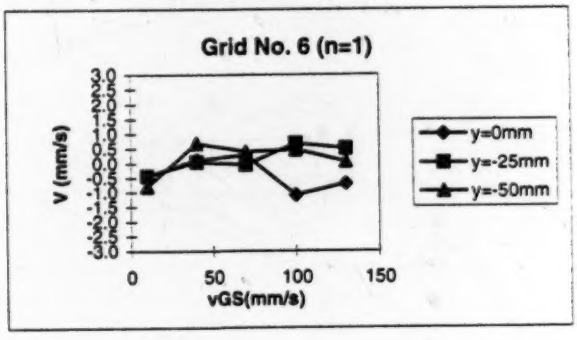
Grid No. 6 (n=1)
V (mm/s)
3.0
2.5
2.0
1.5
1.0
0.5
0.0
-0.5
-1.0
-1.5
-2.0
-2.5
-3.0
0
50
100
150
vGS(mm/s)
y=0mm
y=-25mm
y=-50mm

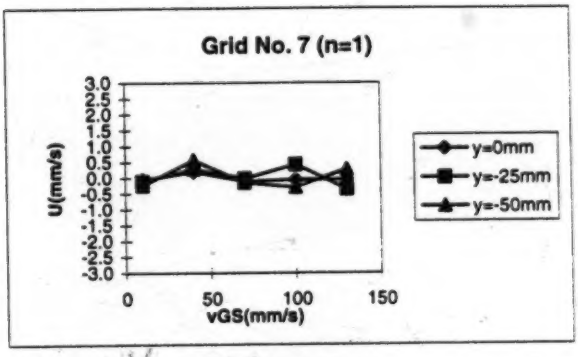
Grid No. 7 (n=1)
U(mm/s)
3.0
2.5
2.0
1.5
1.0
0.5
0.0
-0.5
-1.0
-1.5
-2.0
-2.5
-3.0
0
50
100
150
vGS(mm/s)
y=0mm
y=-25mm
y=-50mm

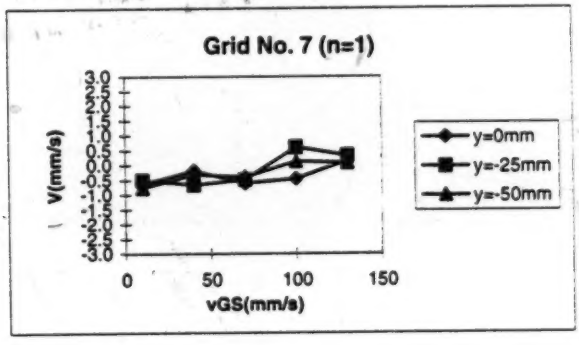
Grid No. 7 (n=1)
V(mm/s)
3.0
2.5
2.0
1.5
1.0
0.5
0.0
-0.5
-1.0
-1.5
-2.0
-2.5
-3.0
0
50
100
150
vGS(mm/s)
y=0mm
y=-25mm
y=-50mm

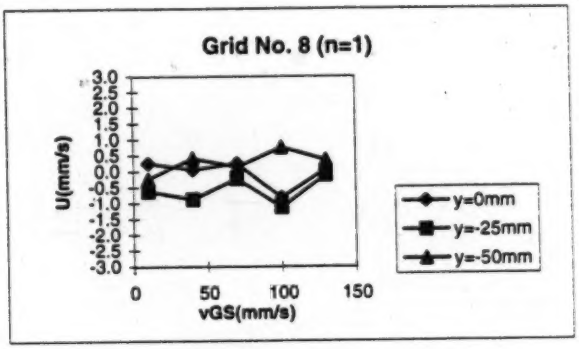
Grid No. 8 (n=1)
U(mm/s)
3.0
2.5
2.0
1.5
1.0
0.5
0.0
-0.5
-1.0
-1.5
-2.0
-2.5
-3.0
0
50
100
150
vGS(mm/s)
y=0mm
y=-25mm
y=-50mm

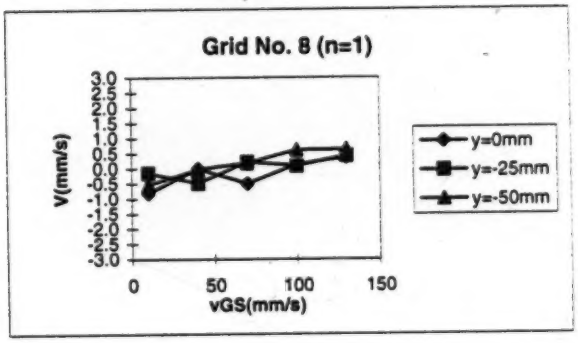
Grid No. 8 (n=1)
V(mm/s)
3.0
2.5
2.0
1.5
1.0
0.5
0.0
-0.5
-1.0
-1.5
-2.0
-2.5
-3.0
0
50
100
150
vGS(mm/s)
y=0mm
y=-25mm
y=-50mm

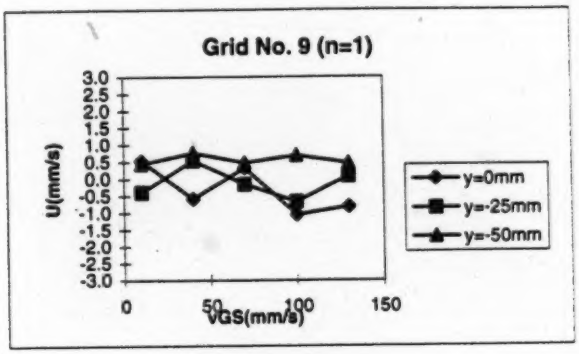
Grid No. 9 (n=1)
U(mm/s)
3.0
2.5
2.0
1.5
1.0
0.5
0.0
-0.5
-1.0
-1.5
-2.0
-2.5
-3.0
0
50
100
150
vGS(mm/s)
y=0mm
y=-25mm
y=-50mm

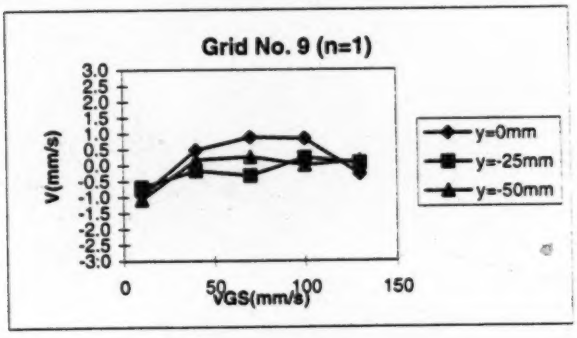
Grid No. 9 (n=1)
V(mm/s)
3.0
2.5
2.0
1.5
1.0
0.5
0.0
-0.5
-1.0
-1.5
-2.0
-2.5
-3.0
0
50
100
150
vGS(mm/s)
y=0mm
y=-25mm
y=-50mm

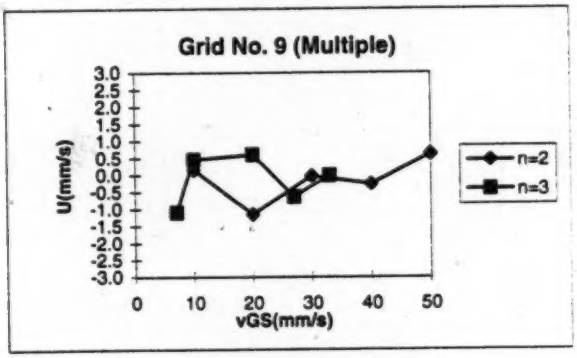
Grid No. 9 (Multiple)
U(mm/s)
3.0
2.5
2.0
1.5
1.0
0.5
0.0
-0.5
-1.0
-1.5
-2.0
-2.5
-3.0
0
10
20
30
40
50
vGS(mm/s)
n=2
n=3

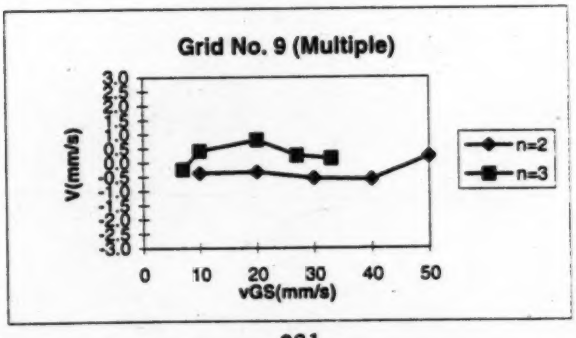
Grid No. 9 (Multiple)
V(mm/s)
0
10
20
30
40
50
vGS(mm/s)
n=2
n=3

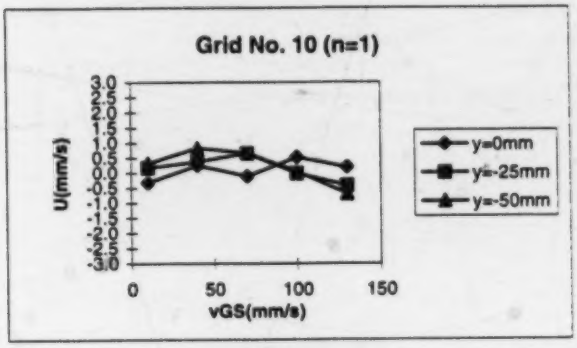
Grid No. 10 (n=1)
U(mm/s)
vGS(mm/s)
0
50
100
150
y=0mm
y=-25mm
y=-50mm

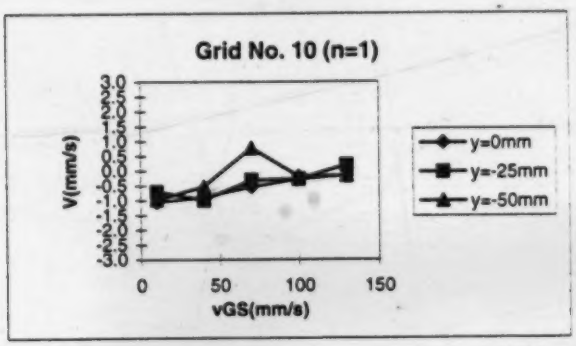
Grid No. 10 (n=1)
V(mm/s)
vGS(mm/s)
0
50
100
150
y=0mm
y=-25mm
y=-50mm

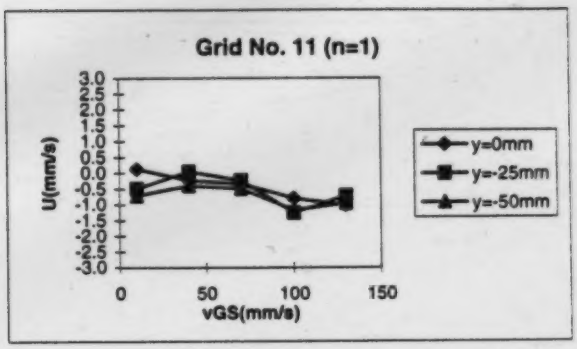
Grid No. 11 (n=1)
U(mm/s)
3.0
2.5
2.0
1.5
1.0
0.5
0.0
-0.5
-1.0
-1.5
-2.0
-2.5
-3.0
0
50
100
150
vGS(mm/s)
y=0mm
y=-25mm
y=-50mm

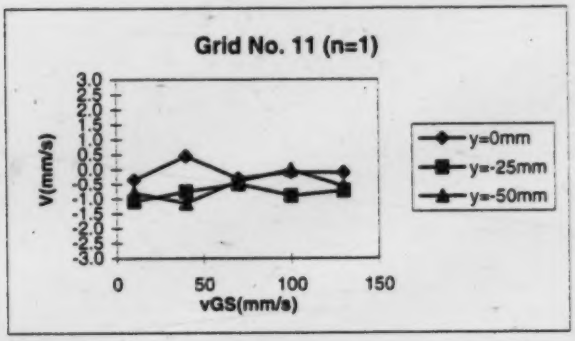
Grid No. 11 (n=1)
V(mm/s)
3.0
2.5
2.0
1.5
1.0
0.5
0.0
-0.5
-1.0
-1.5
-2.0
-2.5
-3.0
0
50
100
150
vGS(mm/s)
y=0mm
y=-25mm
y=-50mm

APPENDIX 4:

Turbidity Results for All Grids and Impeller

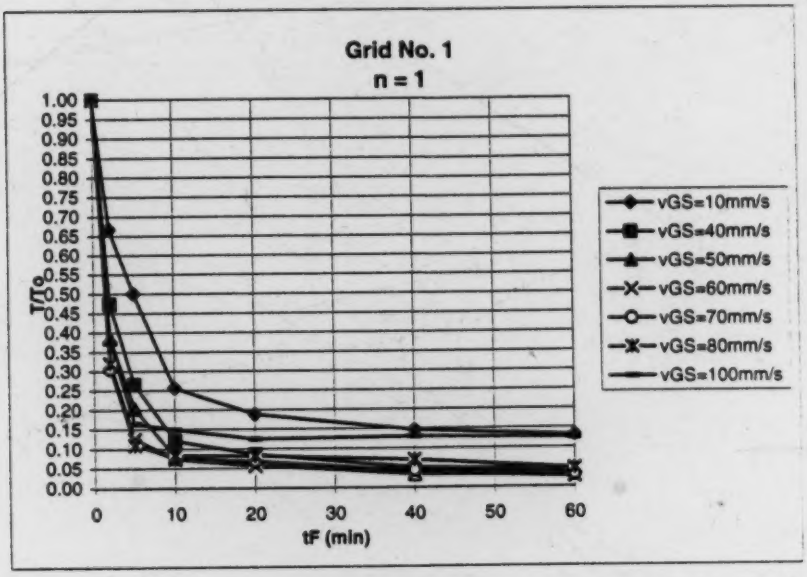
Grid No. 1
n = 1
T/To
tF (min)
vGS=10mm/s
vGS=40mm/s
vGS=50mm/s
vGS=60mm/s
vGS=70mm/s
vGS=80mm/s
vGS=100mm/s

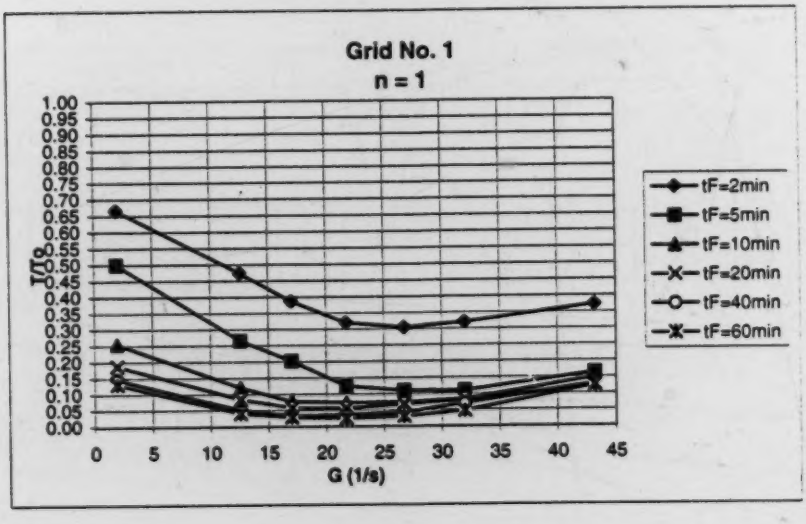
Grid No. 1
n = 1
T/To
G (1/s)
tF=2min
tF=5min
tF=10min
tF=20min
tF=40min
tF=60min

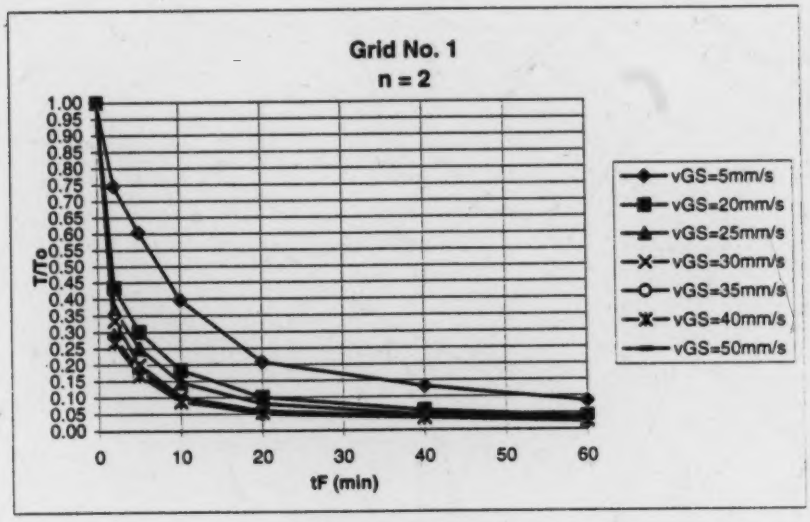
Grid No. 1
n = 2
T/To
tF (min)
vGS=5mm/s
vGS=20mm/s
vGS=25mm/s
vGS=30mm/s
vGS=35mm/s
vGS=40mm/s
vGS=50mm/s

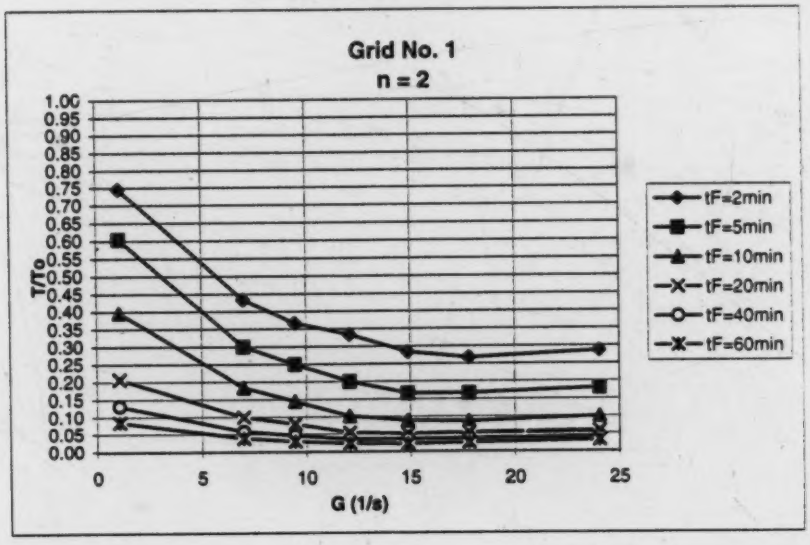
Grid No. 1
n = 2
T/To
G (1/s)
tF=2min
tF=5min
tF=10min
tF=20min
tF=40min
tF=60min

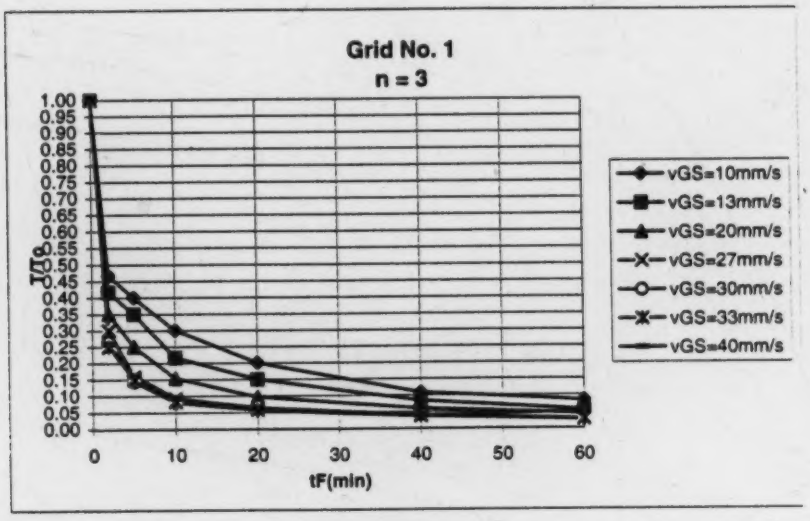
Grid No. 1
n = 3
T/To
tF(min)
vGS=10mm/s
vGS=13mm/s
vGS=20mm/s
vGS=27mm/s
vGS=30mm/s
vGS=33mm/s
vGS=40mm/s

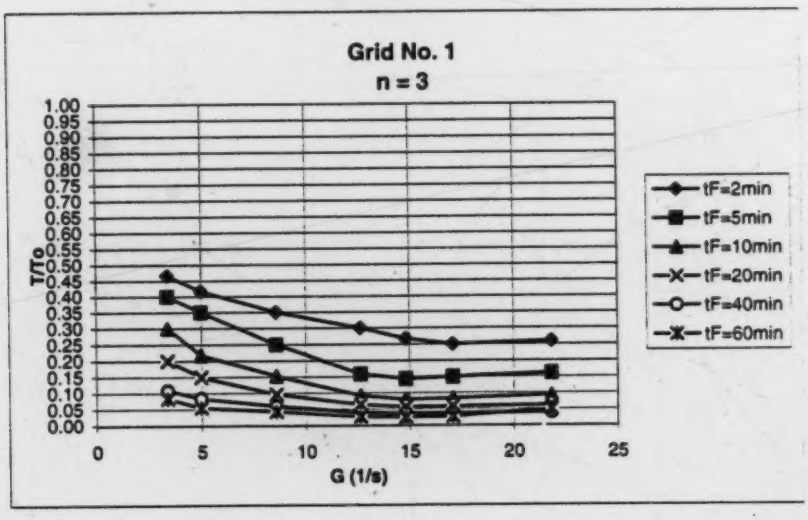
Grid No. 1
n = 3
T/To
G (1/s)
tF=2min
tF=5min
tF=10min
tF=20min
tF=40min
tF=60min

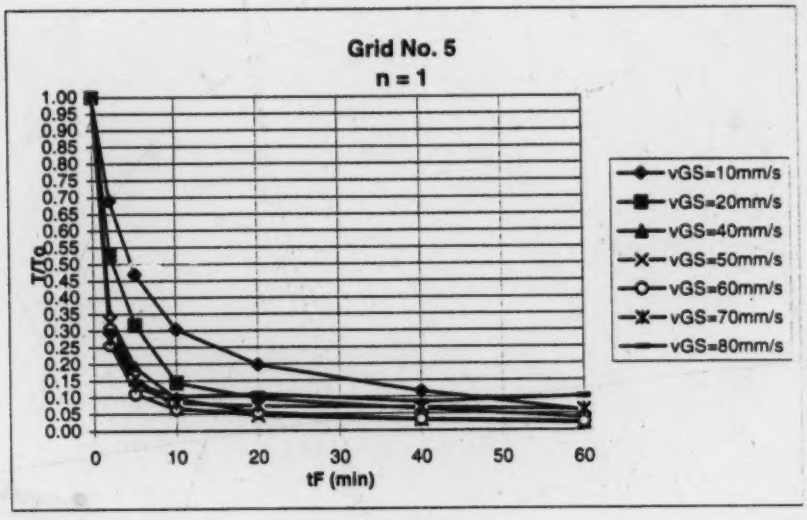
Grid No. 5
n = 1
1.00
0.95
0.90
0.85
0.80
0.75
0.70
0.65
0.60
0.55
0.50
0.45
0.40
0.35
0.30
0.25
0.20
0.15
0.10
0.05
0.00
0
10
20
30
40
50
60
tF (min)
vGS=10mm/s
vGS=20mm/s
vGS=40mm/s
vGS=50mm/s
vGS=60mm/s
vGS=70mm/s
vGS=80mm/s

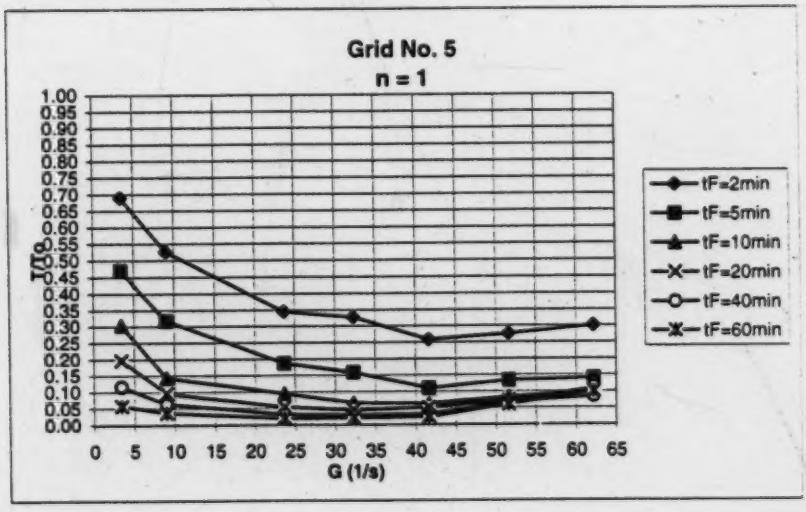
Grid No. 5
n = 1
1.00
0.95
0.90
0.85
0.80
0.75
0.70
0.65
0.60
0.55
0.50
0.45
0.40
0.35
0.30
0.25
0.20
0.15
0.10
0.05
0.00
0
5
10
15
20
25
30
35
40
45
50
55
60
65
G (1/s)
tF=2min
tF=5min
tF=10min
tF=20min
tF=40min
tF=60min

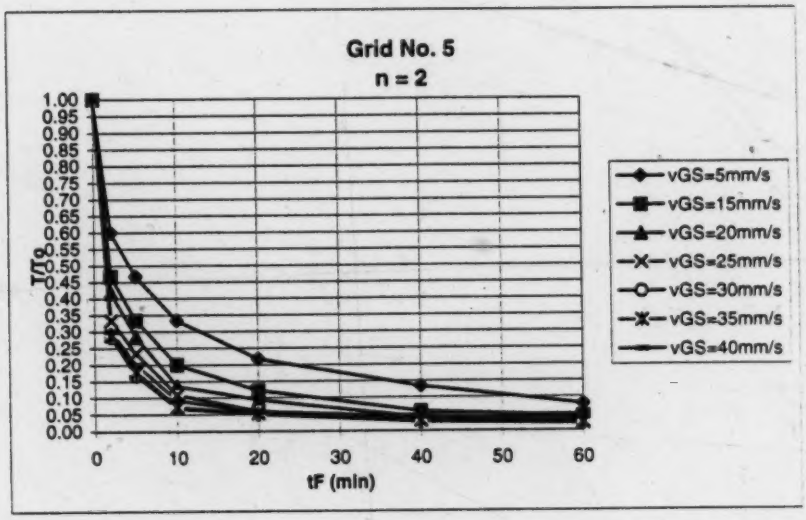
Grid No. 5
n = 2
1.00
0.95
0.90
0.85
0.80
0.75
0.70
0.65
0.60
0.55
0.50
0.45
0.40
0.35
0.30
0.25
0.20
0.15
0.10
0.05
0.00
J/J0
0
10
20
30
40
50
60
tF (min)
vGS=5mm/s
vGS=15mm/s
vGS=20mm/s
vGS=25mm/s
vGS=30mm/s
vGS=35mm/s
vGS=40mm/s

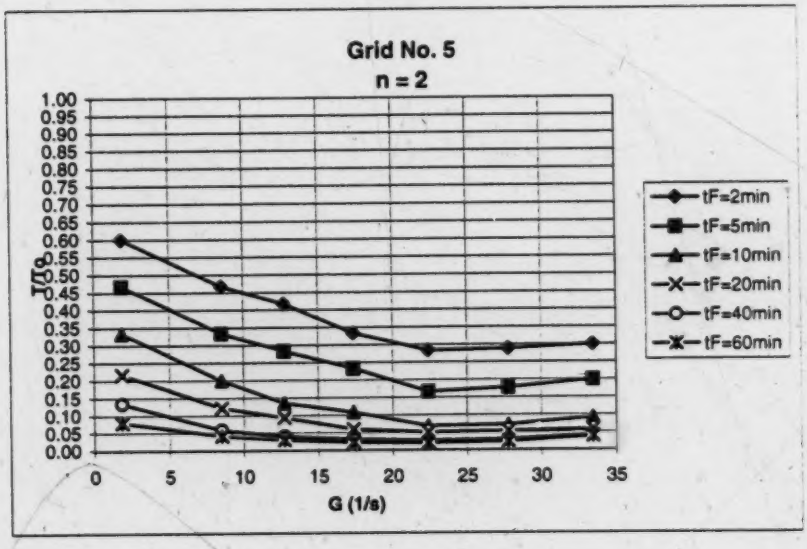
Grid No. 5
n = 2
1.00
0.95
0.90
0.85
0.80
0.75
0.70
0.65
0.60
0.55
0.50
0.45
0.40
0.35
0.30
0.25
0.20
0.15
0.10
0.05
0.00
J/J0
0
5
10
15
20
25
30
35
G (1/s)
tF=2min
tF=5min
tF=10min
tF=20min
tF=40min
tF=60min

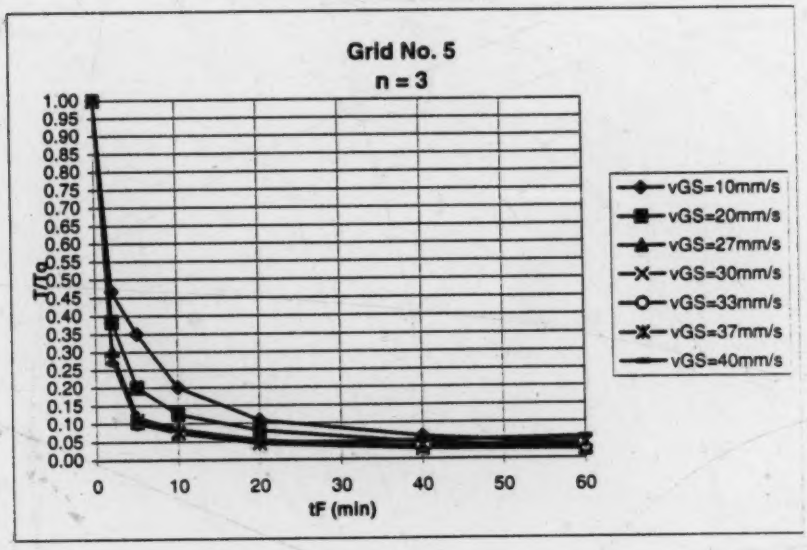
Grid No. 5
n = 3
I/I0
tF (min)
vGS=10mm/s
vGS=20mm/s
vGS=27mm/s
vGS=30mm/s
vGS=33mm/s
vGS=37mm/s
vGS=40mm/s

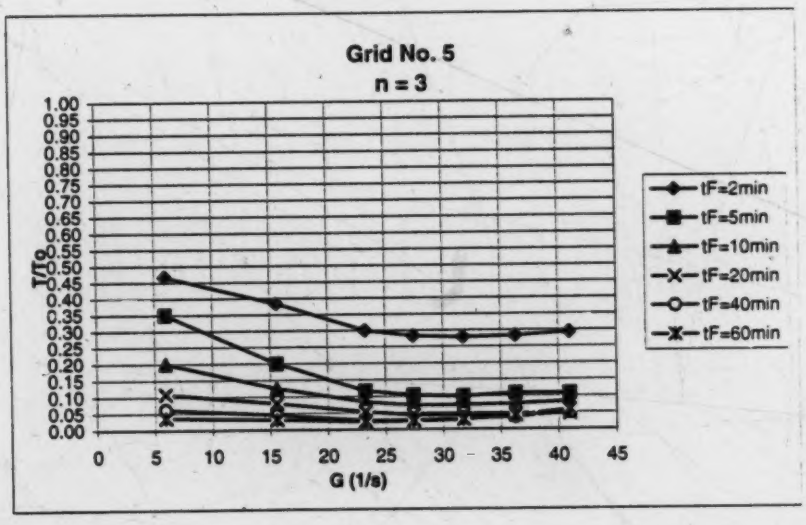
Grid No. 5
n = 3
I/I0
G (1/s)
tF=2min
tF=5min
tF=10min
tF=20min
tF=40min
tF=60min

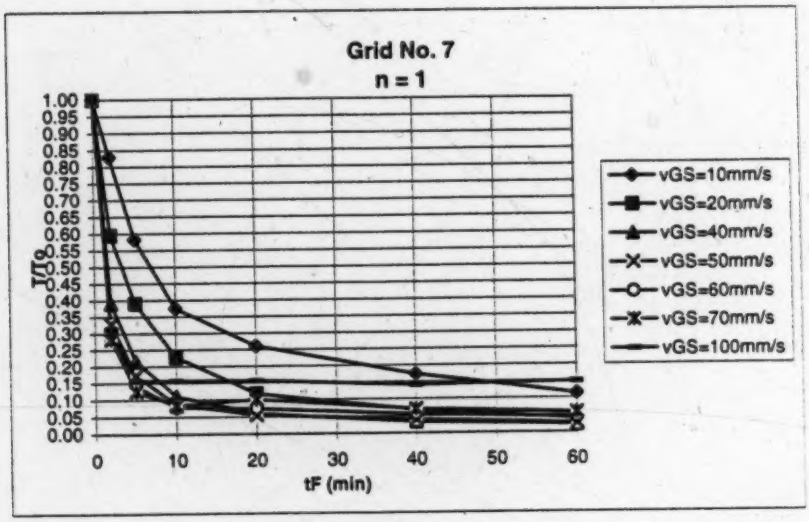
Grid No. 7
n = 1
T/T0
tF (min)
vGS=10mm/s
vGS=20mm/s
vGS=40mm/s
vGS=50mm/s
vGS=60mm/s
vGS=70mm/s
vGS=100mm/s

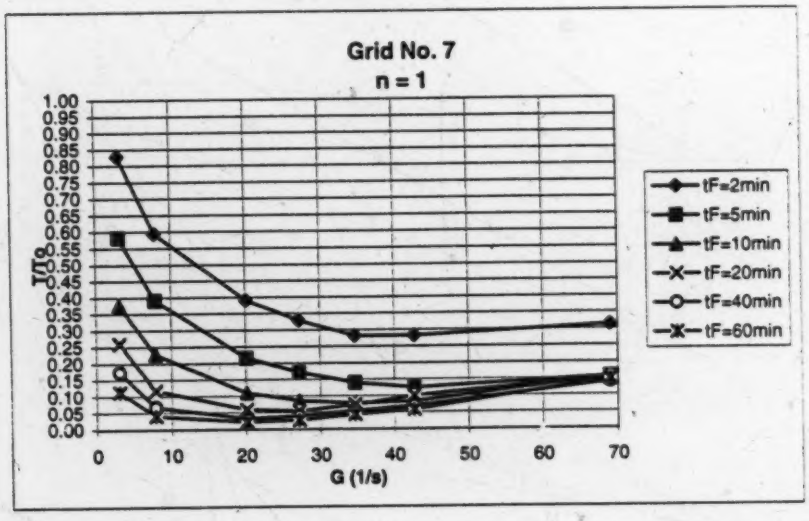
Grid No. 7
n = 1
T/T0
G (1/s)
tF=2min
tF=5min
tF=10min
tF=20min
tF=40min
tF=60min

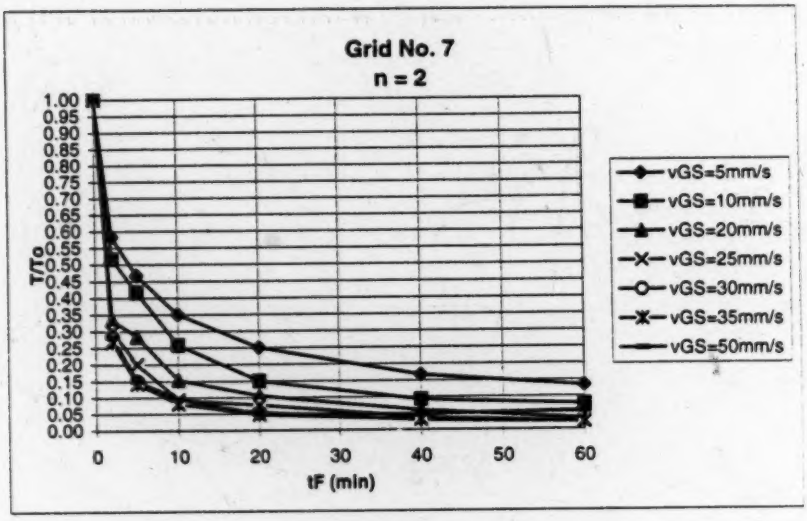
Grid No. 7
n = 2
T/T0
tF (min)
vGS=5mm/s
vGS=10mm/s
vGS=20mm/s
vGS=25mm/s
vGS=30mm/s
vGS=35mm/s
vGS=50mm/s

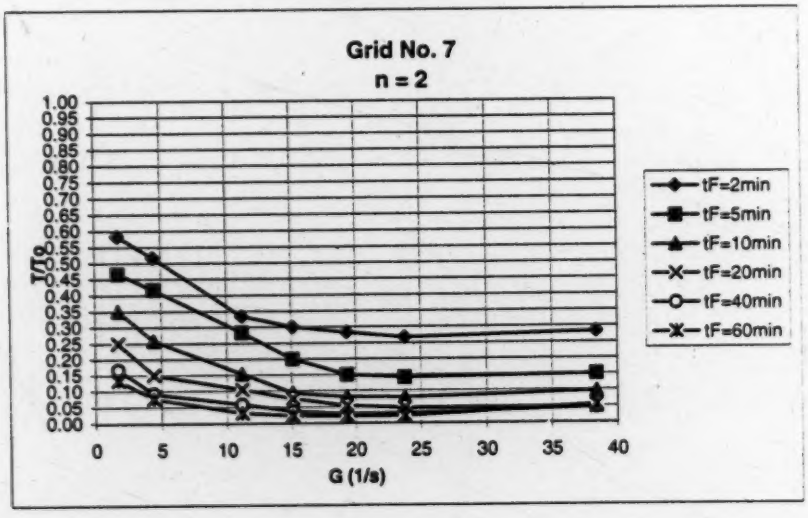
Grid No. 7
n = 2
T/T0
G (1/s)
tF=2min
tF=5min
tF=10min
tF=20min
tF=40min
tF=60min

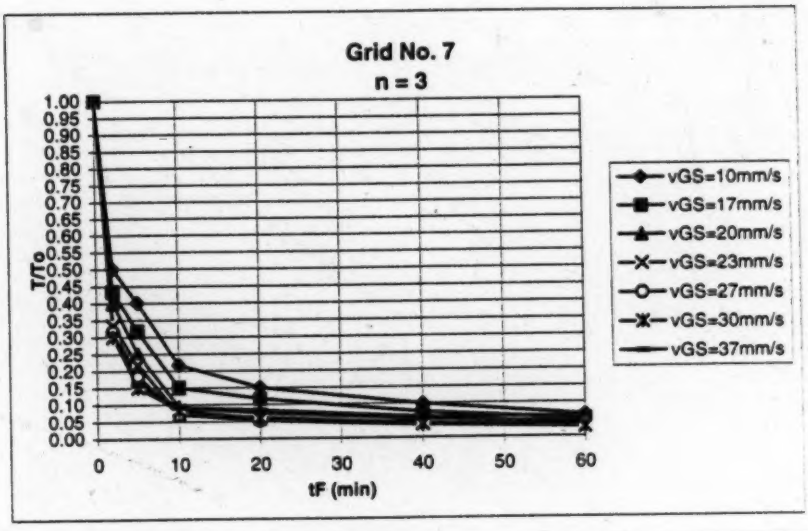
Grid No. 7
n = 3
T/To
tF (min)
vGS=10mm/s
vGS=17mm/s
vGS=20mm/s
vGS=23mm/s
vGS=27mm/s
vGS=30mm/s
vGS=37mm/s

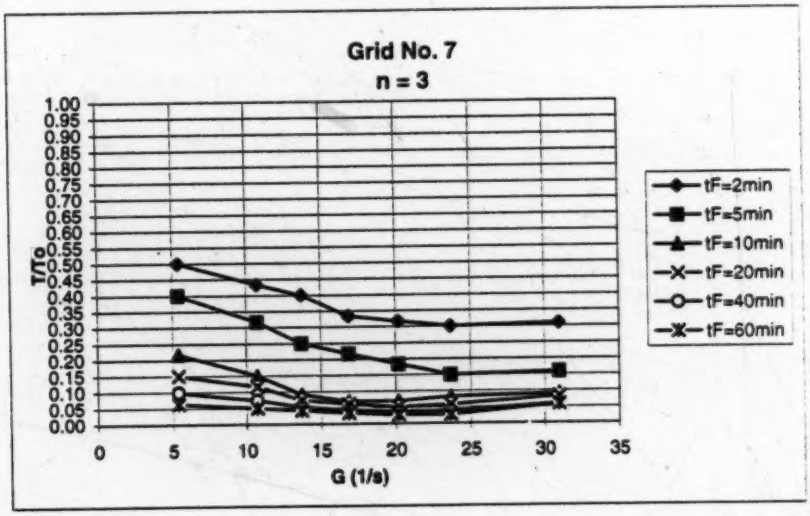
Grid No. 7
n = 3
T/To
G (1/s)
tF=2min
tF=5min
tF=10min
tF=20min
tF=40min
tF=60min

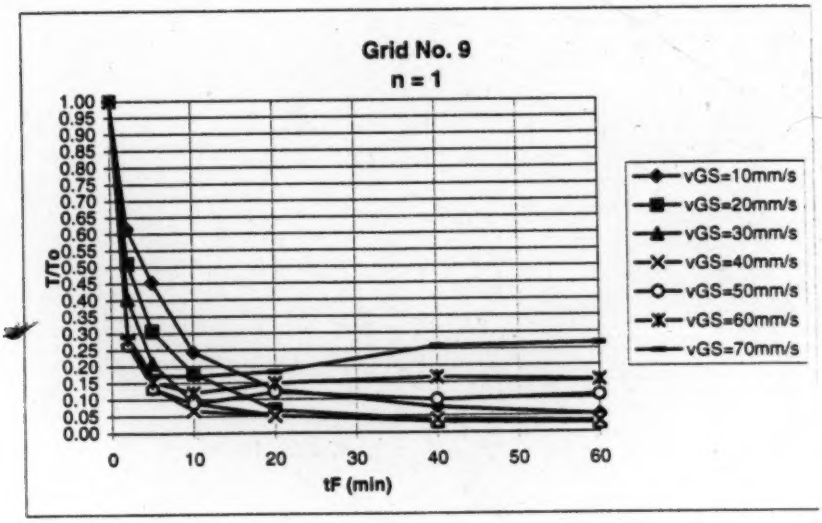
Grid No. 9
n = 1
T/To
tF (min)
vGS=10mm/s
vGS=20mm/s
vGS=30mm/s
vGS=40mm/s
vGS=50mm/s
vGS=60mm/s
vGS=70mm/s

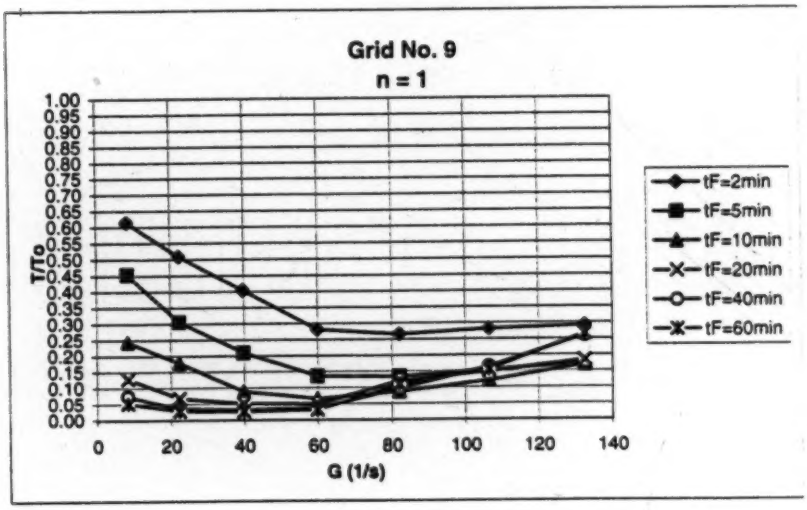
Grid No. 9
n = 1
T/To
G (1/s)
tF=2min
tF=5min
tF=10min
tF=20min
tF=40min
tF=60min

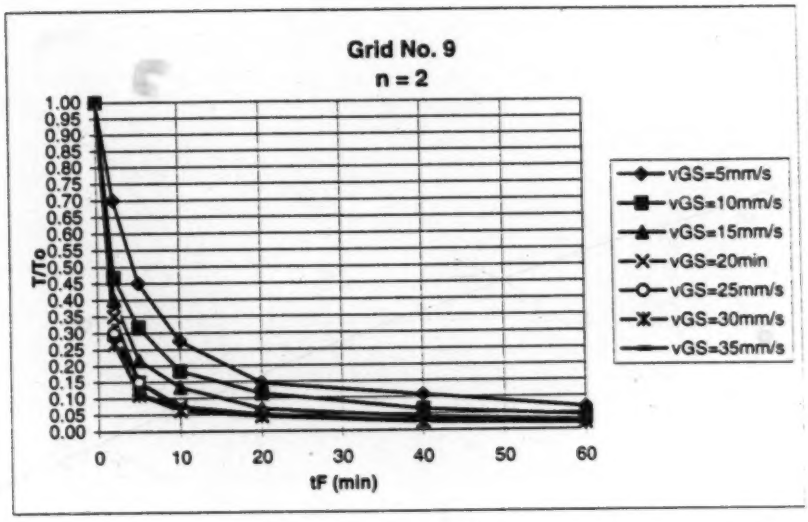
Grid No. 9
n = 2
T/To
tF (min)
vGS=5mm/s
vGS=10mm/s
vGS=15mm/s
vGS=20min
vGS=25mm/s
vGS=30mm/s
vGS=35mm/s

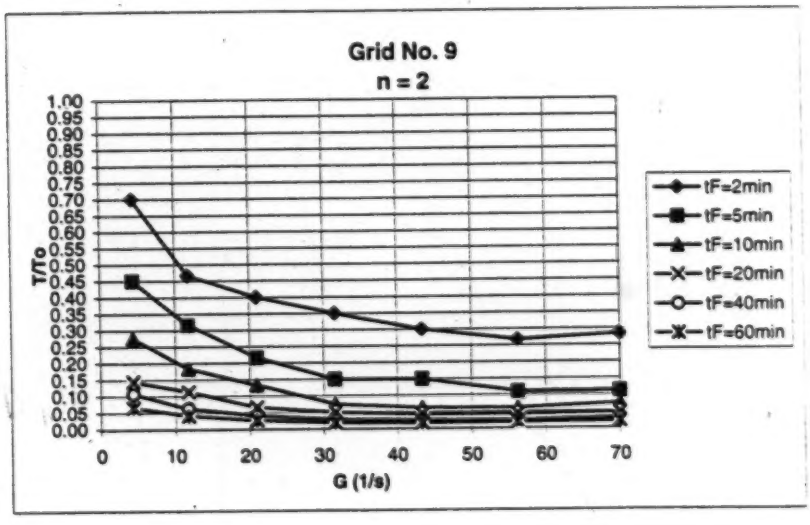
Grid No. 9
n = 2
T/To
G (1/s)
tF=2min
tF=5min
tF=10min
tF=20min
tF=40min
tF=60min

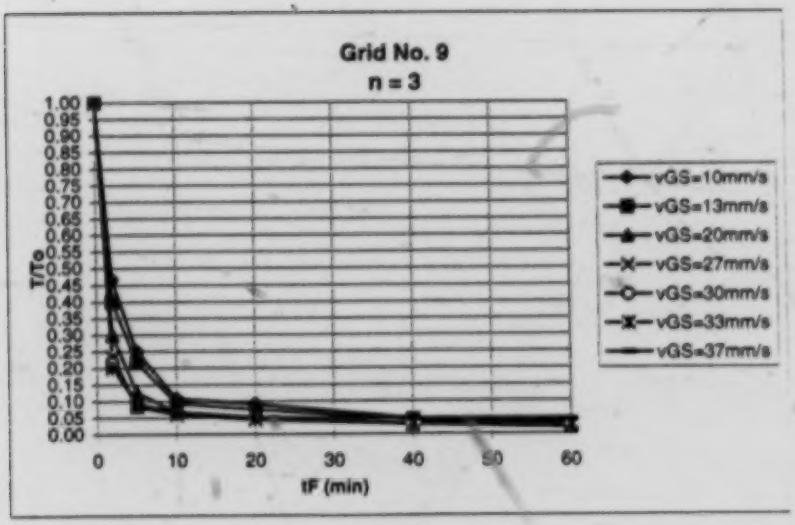
Grid No. 9
n = 3
T/To
tF (min)
vGS=10mm/s
vGS=13mm/s
vGS=20mm/s
vGS=27mm/s
vGS=30mm/s
vGS=33mm/s
vGS=37mm/s

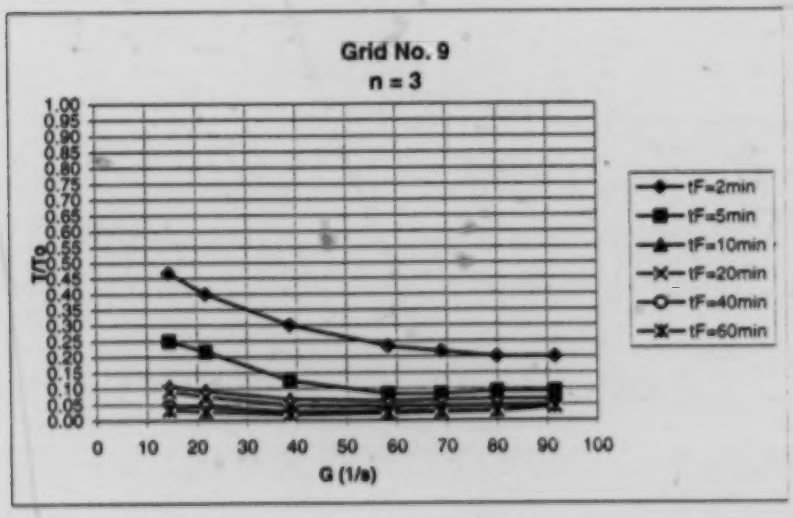
Grid No. 9
n = 3
T/To
G (1/s)
tF=2min
tF=5min
tF=10min
tF=20min
tF=40min
tF=60min

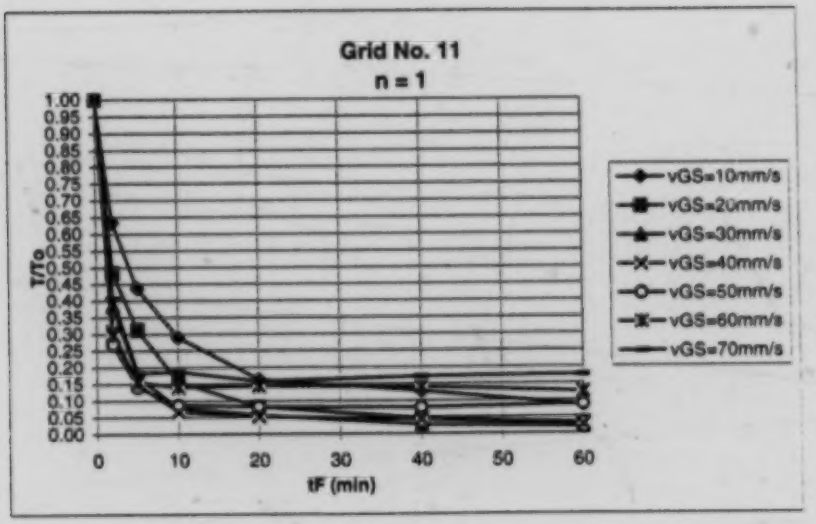
Grid No. 11
n = 1
T/To
tF (min)
vGS=10mm/s
vGS=20mm/s
vGS=30mm/s
vGS=40mm/s
vGS=50mm/s
vGS=60mm/s
vGS=70mm/s

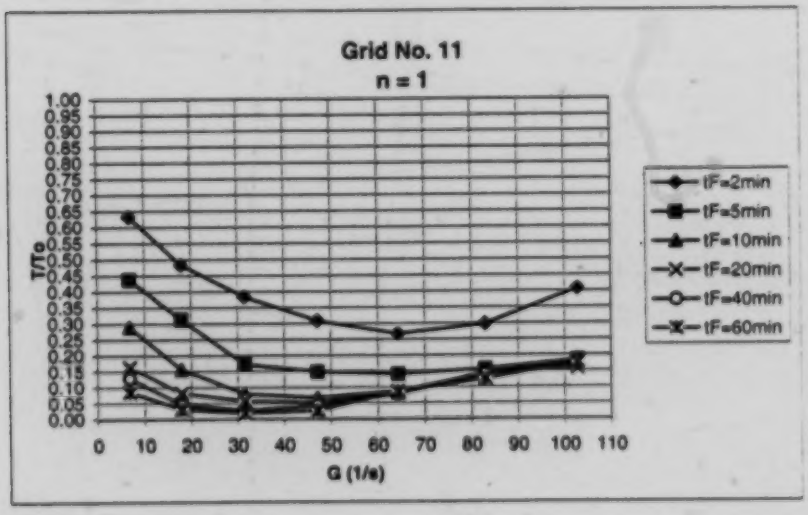
Grid No. 11
n = 1
T/To
G (1/s)
tF=2min
tF=5min
tF=10min
tF=20min
tF=40min
tF=60min

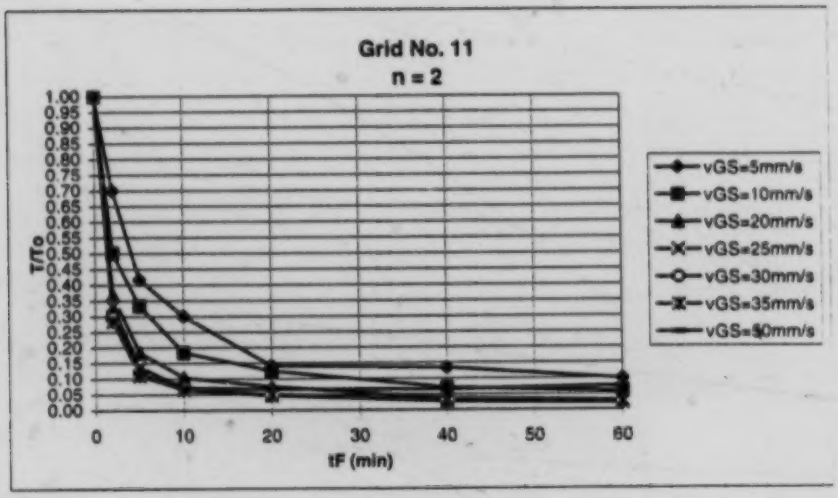
Grid No. 11
n = 2
T/To
tF (min)
vGS=5mm/s
vGS=10mm/s
vGS=20mm/s
vGS=25mm/s
vGS=30mm/s
vGS=35mm/s
vGS=40mm/s

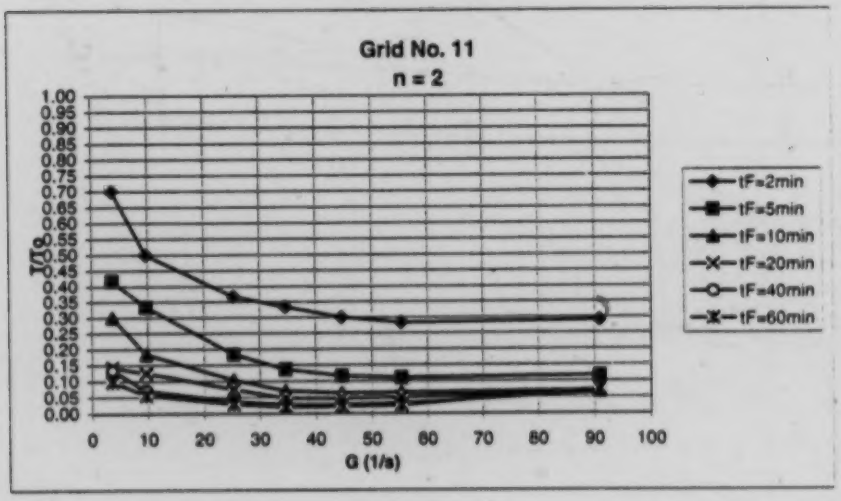
Grid No. 11
n = 2
T/To
G (1/s)
tF=2min
tF=5min
tF=10min
tF=20min
tF=40min
tF=60min

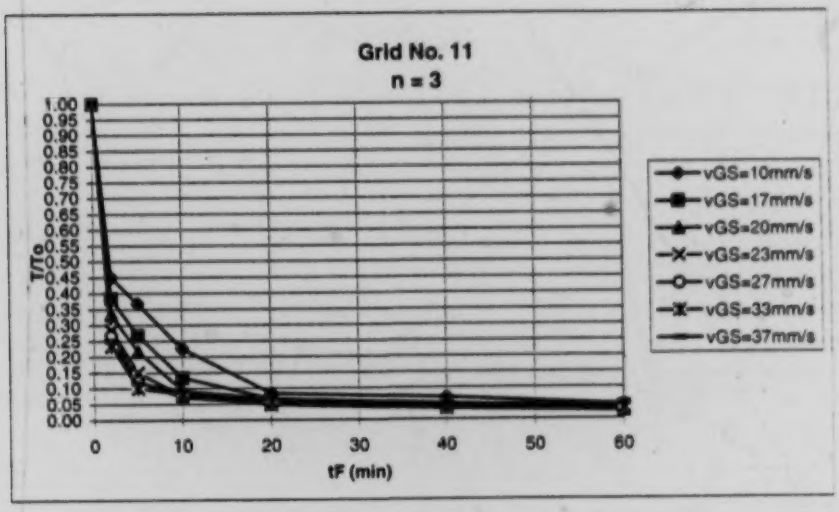
Grid No. 11
n = 3
T/To
tF (min)
vGS=10mm/s
vGS=17mm/s
vGS=20mm/s
vGS=23mm/s
vGS=27mm/s
vGS=33mm/s
vGS=37mm/s

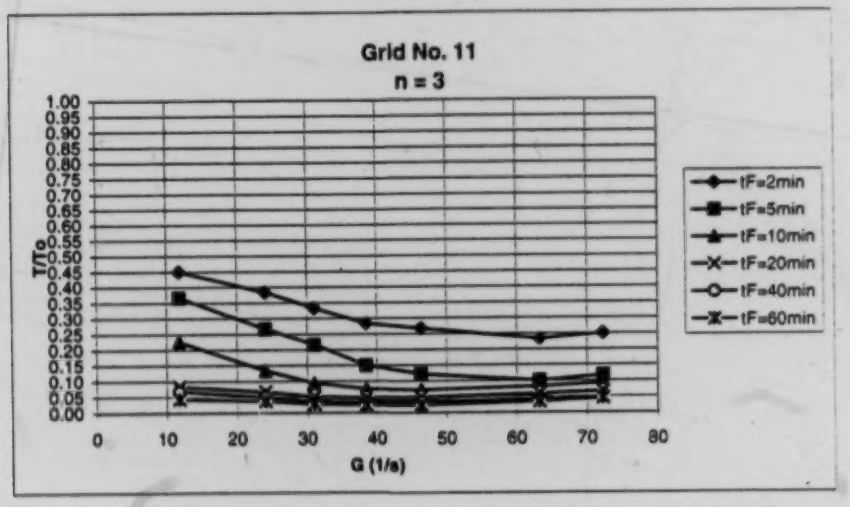
Grid No. 11
n = 3
T/To
G (1/s)
tF=2min
tF=5min
tF=10min
tF=20min
tF=40min
tF=60min

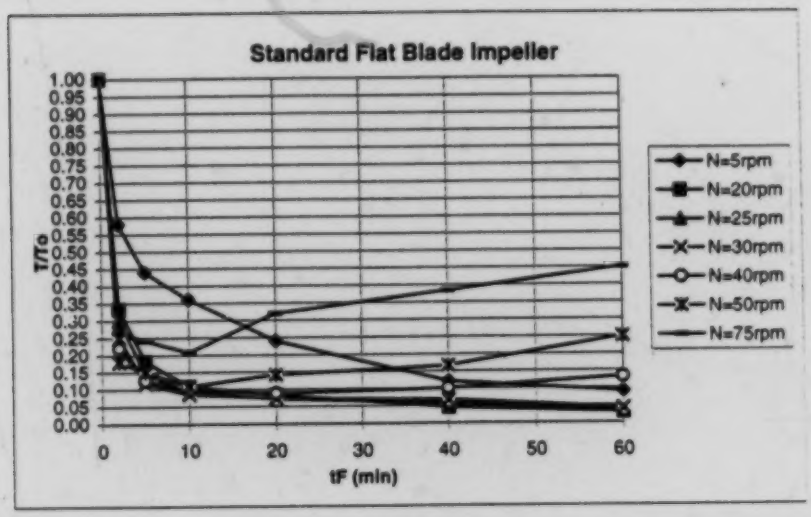
Standard Flat Blade Impeller
T/To
tF (min)
N=5rpm
N=20rpm
N=25rpm
N=30rpm
N=40rpm
N=50rpm
N=75rpm

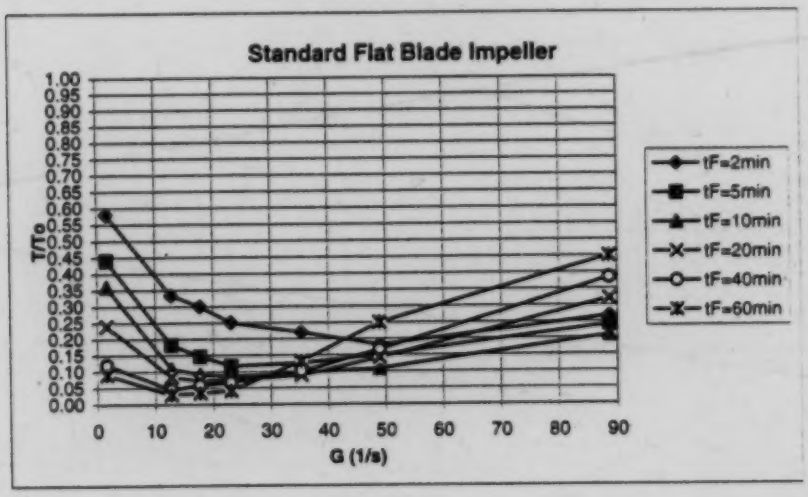
Standard Flat Blade Impeller
T/To
G (1/s)
tF=2min
tF=5min
tF=10min
tF=20min
tF=40min
tF=60min

APPENDIX 5:

Agglomeration and Erosion Rate Coefficients for All Grids and Impeller

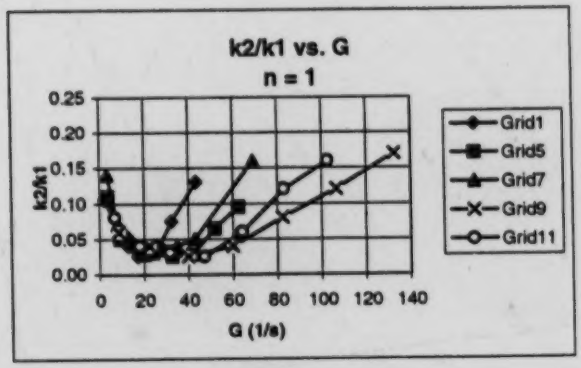
k2/k1 vs. G
n = 1
k2/k1
0.25
0.20
0.15
0.10
0.05
0.00
0
20
40
60
80
100
120
140
G (1/s)
Grid1
Grid5
Grid7
Grid9
Grid11

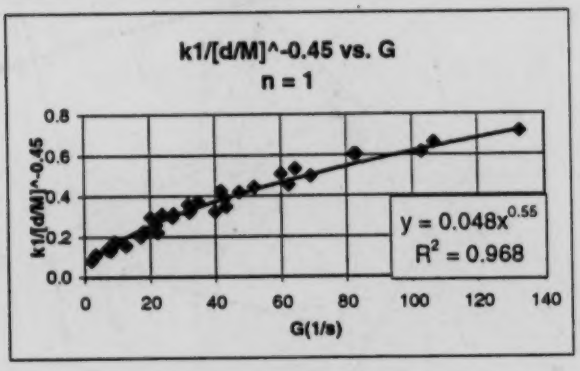
k1/[d/M]^-0.45 vs. G
n = 1
k1/[d/M]^-0.45
0.8
0.6
0.4
0.2
0.0
0
20
40
60
80
100
120
140
G(1/s)
y = 0.048x^0.55
R^2 = 0.968

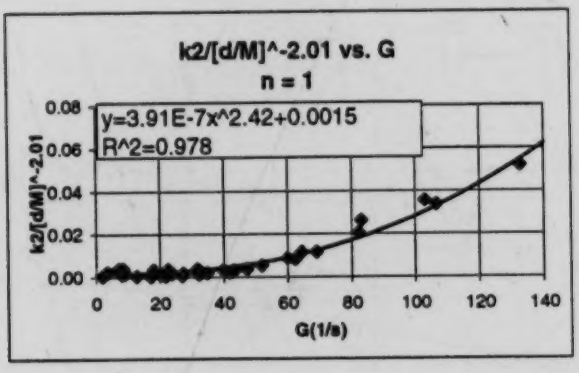
k2/[d/M]^-2.01 vs. G
n = 1
k2/[d/M]^-2.01
0.08
0.06
0.04
0.02
0.00
0
20
40
60
80
100
120
140
G(1/s)
y=3.91E-7x^2.42+0.0015
R^2=0.978

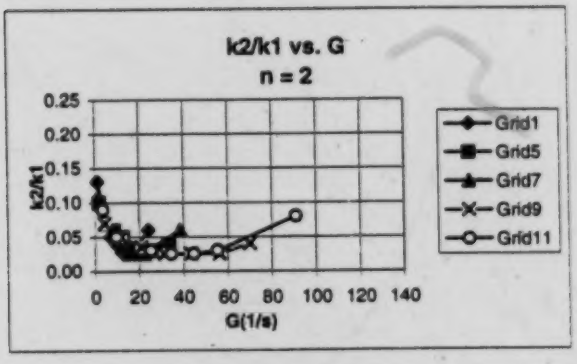
k2/k1 vs. G
n = 2
k2/k1
0.25
0.20
0.15
0.10
0.05
0.00
0
20
40
60
80
100
120
140
G(1/s)
Grid1
Grid5
Grid7
Grid9
Grid11

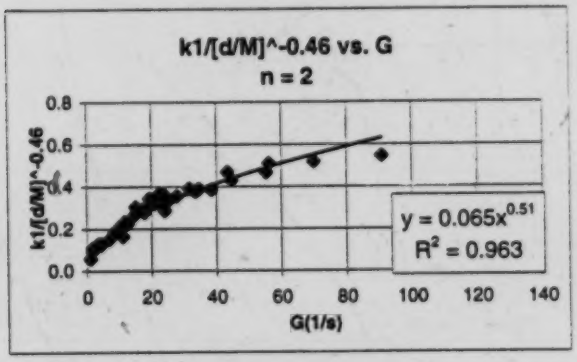
k1/[d/M]^-0.46 vs. G
n = 2
k1/[d/M]^-0.46
0.8
0.6
0.4
0.2
0.0
0
20
40
60
80
100
120
140
G(1/s)
y = 0.065x^0.51
R^2 = 0.963

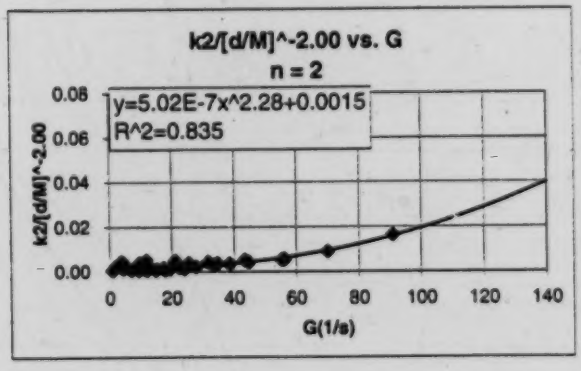
k2/[d/M]^-2.00 vs. G
n = 2
k2/[d/M]^-2.00
0.08
0.06
0.04
0.02
0.00
0
20
40
60
80
100
120
140
G(1/s)
y=5.02E-7x^2.28+0.0015
R^2=0.835

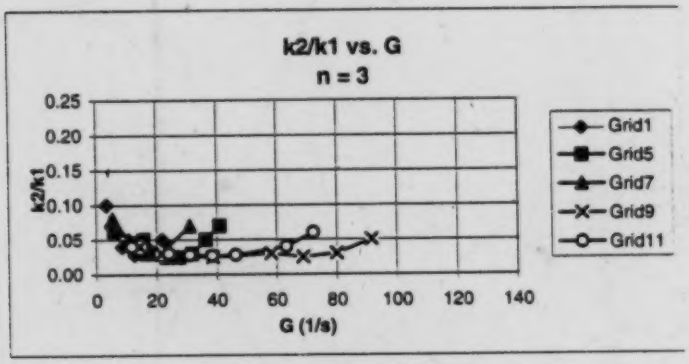
k2/k1 vs. G
n = 3
k2/k1
G (1/s)
Grid1
Grid5
Grid7
Grid9
Grid11

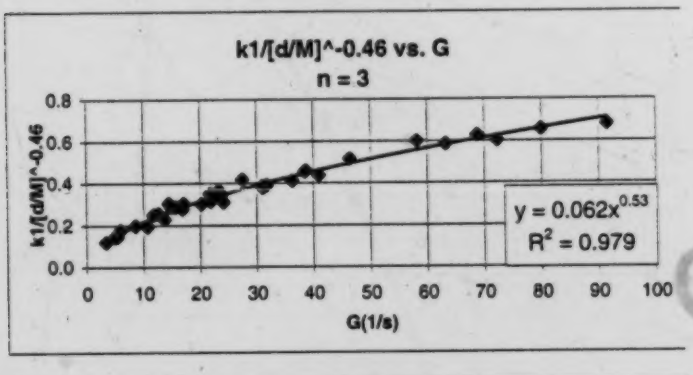
k1/[d/M]^-0.46 vs. G
n = 3
k1/(d/M)^-0.46
G(1/s)
y = 0.062x^0.53
R^2 = 0.979

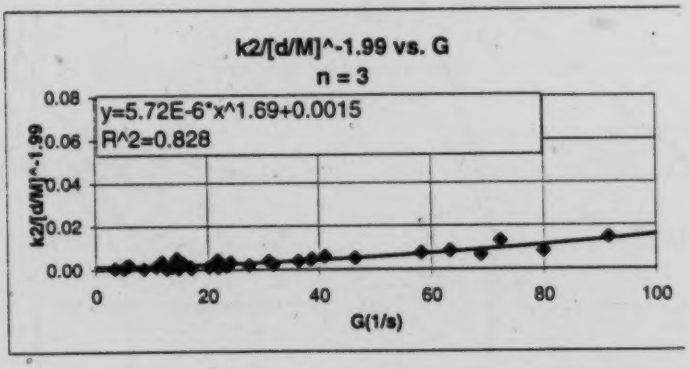
k2/[d/M]^-1.99 vs. G
n = 3
k2/(d/M)^-1.99
G(1/s)
y=5.72E-6*x^1.69+0.0015
R^2=0.828

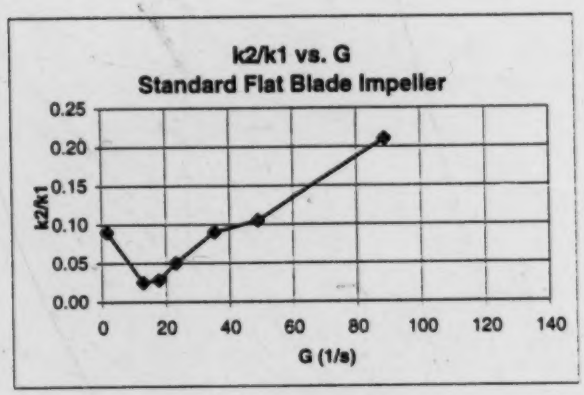
k2/k1 vs. G
Standard Flat Blade Impeller
k2/k1
0.25
0.20
0.15
0.10
0.05
0.00
0
20
40
60
80
100
120
140
G (1/s)

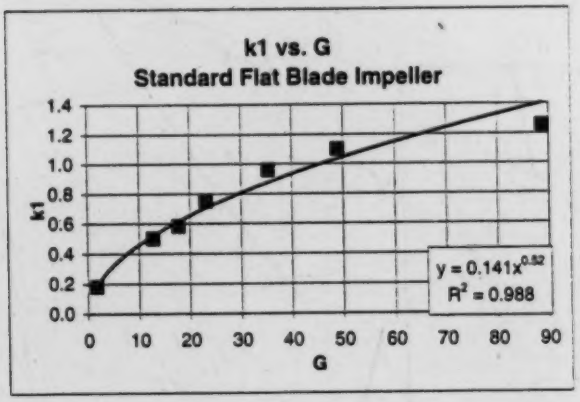
k1 vs. G
Standard Flat Blade Impeller
k1
1.4
1.2
1.0
0.8
0.6
0.4
0.2
0.0
0
10
20
30
40
50
60
70
80
90
G
y = 0.141x^0.52
R^2 = 0.988

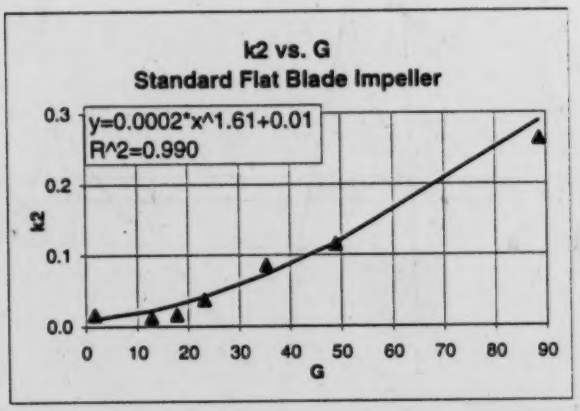
k2 vs. G
Standard Flat Blade Impeller
y=0.0002*x^1.61+0.01
R^2=0.990
k2
0.3
0.2
0.1
0.0
0
10
20
30
40
50
60
70
80
90
G